Evaluation of emerging diagnostic and therapeutic strategies in a tailored pig model for Duchenne muscular dystrophy

von Lina Marie Fonteyne

Inaugural-Dissertation zur Erlangung der Doktorwürde der Tierärztlichen Fakultät der Ludwig-Maximilians-Universität München

Evaluation of emerging diagnostic and therapeutic strategies in a tailored pig model for Duchenne muscular dystrophy

von

Lina Marie Fonteyne

aus Rotthalmünster

München 2020

Aus dem Veterinärwissenschaftlichen Department der Tierärztlichen Fakultät
der Ludwig-Maximilians-Universität München

Lehrstuhl für Molekulare Tierzucht und Biotechnologie

Arbeit angefertigt unter der Leitung von: Univ.-Prof. Dr. Eckhard Wolf

Mitbetreuung durch: Dr. Barbara Keßler

Gedruckt mit Genehmigung der Tierärztlichen Fakultät
der Ludwig-Maximilians-Universität München

Dekan:	Univ.-Prof. Dr. Reinhard K. Straubinger, Ph.D.
Berichterstatter:	Univ.-Prof. Dr. Eckhard Wolf
Korreferent/en:	Priv.-Doz. Dr. Matthias Eddicks
	Priv.-Doz. Dr. Sven Reese
	Univ.-Prof. Dr. Gerd Sutter
	Univ.-Prof. Dr. Rüdiger Wanke

Tag der Promotion: 25.07.2020

Für Kaspar, dem ich verdanke, dass ich dich kennengelernt habe.

TABLE OF CONTENTS

INDEX OF ABBREVIATIONS

µl	Microliters
2-DE	Two-dimensional gel electrophoresis
6-MWT	6-minute walking test
AA	Amino acid
AAV	Adeno-associated virus
ADP	Adenosine diphosphate
ALT	Alanine aminotransferase
aq. bidest.	Bidistilled water
AST	Aspartate aminotransferase
ATP	Adenosine triphosphate
BMD	Becker muscular dystrophy
bp	Base pair
BW	Body weight
CK	Creatine kinase
cLDLA	combined linkage disequilibrium and linkage analysis
CRISPR	Clustered regularly interspaced short palindromic repeats
CT	Computed tomography
d	day(s)
DCG	Dystrophin glycoprotein complex
DMD	Duchenne muscular dystrophy
DMD$^{Y/-}$	Male *DMD* knockout pig
DMD$^{+/-}$	Female *DMD* carrier pig
DNA	Deoxyribonucleic acid
ds	Double-stranded
ECG	Electrocardiography
ECM	Extracellular matrix
EF	Ejection fraction
ELISA	Enzyme-linked immunosorbent assay
EtOH	Ethanol
FF	Fat fraction
FFPE	Formalin-fixed, paraffin-embedded
gl acetic acid	glacial/ acetic acid

GRMD	Golden Retriever muscular dystrophy
GWAS	Genome-wide association study
h	Hour(s)
H.E.	Hematoxylin and eosin stain
HC	Healthy control(s)
i.m.	Intramuscular
i.v.	Intravenous
IHC	Immunohistochemistry
iPSC	Induced pluripotent stem cell
kDa	KiloDalton
KO	Knockout
LFQ	Label-free quantification
LoA	Loss of ambulation
LTBP	Latent TGFβ binding protein
LV	Left ventricular/ left ventricle
mdx	X chromosome-linked muscular dystrophy in mouse
min	Minute(s)
miRNA	Micro RNA
ml	Milliliter(s)
MRI	Magnetic resonance imaging
MRI-T_2	T2-weighted magnetic resonance imaging
mRNA	Messenger RNA
MRS	Magnetic resonance spectroscopy
MSOT	Multispectral optoacoustic tomography
NaOAc	Sodium acetate
NGS	Next generation sequencing
NMD	Neuromuscular diseases
NSSA	North star ambulatory assessment
nsSNP	Non-synonymous SNP
ORF	Open reading frame
PCR	Polymerase chain reaction
PMO	Phosphorodiamidate morpholino oligomer
PTC	Premature termination codon

QUS	Quantitative ultrasound
RIA	Radioimmunoassay
RNA	Ribonucleic acid
ROI	Region of interest
rpm	Rounds per minute
RUCT	Reflective ultrasound computed tomography
s	Second(s)
s.d.	Standard deviation
s.e.m.	Standard error of the mean
SNP	Single nucleotide polymorphism
SNV	Somatic short variants
SPP1	Secreted phosphoprotein 1
SRM	Selected reaction monitoring
Tris	Tris-(hydroxymethyl)-aminomethane
US	Ultrasound
UV	Ultra violet
vp	Viral particles
WT	Wild-type

I. INTRODUCTION

Duchenne muscular dystrophy (DMD) is the most prevalent heriditary neuromuscular disease in newborn boys (1:3500) (Emery, 1991; Ryder et al., 2017). It is characterized by severe and progressive generalized muscle degeneration and wasting, manifesting at an average age of 2.5 years (Ciafaloni et al., 2009), and leading to a total loss of ambulation latest at the age of 12 years (Blake et al., 2002). Affected individuals die within their 2nd to 3rd decade of life due to cardiorespiratory failure (Eagle et al., 2007; Passamano et al., 2012). DMD is triggered by a great variety of mutations, located within the dystrophin (*DMD*) gene, the largest gene in the human genome, located on the X-chromosome (Koenig et al., 1987; Monaco et al., 1986; Roberts et al., 1993). Mutations cause a loss of function of the muscle structure protein dystrophin, which is anchored as part of the dystrophin glycoprotein complex (DGC) to the sarcolemma (Nowak and Davies, 2004; Straub et al., 1992). Some mutations, however, lead to a low presence of truncated but partially functional dystrophin, which results in a milder form of the disease, the Becker muscular dystrophy (BMD) (Blake et al., 2002). Up to date, the most important therapeutic measures concerning the treatment of DMD are multidisciplinary care and glucocorticoid medication, aiming to relieve the symptoms and to slow down disease progression (Bello et al., 2015a; reviewed in Birnkrant et al., 2018b). Besides, for few disease-causing mutations, promising mutation-specific therapies intending to restore dystrophin expression have been developed within the past few years or are currently under investigation (National Library of Medicine, 2019; Ryan, 2014; Van Ruiten et al., 2017). Some recent molecular therapy approaches aim to permanentely restore dystrophin expression by editing the genome, converting DMD into the milder BMD (Long et al., 2016; Xu et al., 2016). Especially in therapeutic trials, the reliable assessment of disease progression is of prior importance. However, the availability of noninvasive, easy to use, sensitive diagnostic tools is limited, especially for young pediatric DMD patients. One of the primary used outcome measures for the assessment of physical capacity and the validation of therapeutic interventions, is the 6-minute walking test (6-MWT) (Bushby et al., 2014; McDonald et al., 2017; McDonald et al., 2010; Mendell et al., 2016). The diagnostic validity of this muscle function test is highly limited by its dependance on an active cooperation, the individual performance of the day (Geiger et al., 2007; McDonald et al., 2010) and, in general, of the ability to walk. For the development and validation of new therapeutic and diagnostic approaches, animal models mirroring the clinical picture of DMD are of need. However, the existing mammalian animal models have different genotypic or phenotypic characteristics limiting their applicability in biomedical research (McGreevy et al., 2015; Willmann et al., 2009). In comparison to other animals, the pig as omnivore shares a high number of similarities with humans (Aigner et al., 2010). Therefore, a genetically engineered DMD pig lacking *DMD* exon 52 (*DMD*Δ52) has been generated using somatic cell nuclear transfer (SCNT) and characterized at our institute (Klymiuk et al., 2013).

In this work, a female DMD carrier sow, generated by SCNT, was used to generate a stable DMD breeding herd. Different husbandry conditions to increase nursing efficiency were evaluated and *DMD* knockout pigs generated by breeding were characterized. A genome-wide combined linkage disequilibrium and linkage analysis (cLDLA), to identify potential genetic modifiers, which might influence phenotypic variations, was commenced. A new therapeutic approach, aiming at

permanently converting DMD into the milder BMD by restoring the *DMD* reading frame using adeno-associated viral vectors (AAV) to introduce CRISPR/Cas9 and two gRNAs targeting exon 51 flanking sequences, was applied to *DMD*Δ52 pigs. The restoration of internally truncated but functional dystrophin expression was assessed and improvement of muscle function was validated. Furthermore, a study using multispectral optoacoustic tomography (MSOT) to detect collagen in muscles of *DMD* knockout pigs was performed and the method was validated as new diagnostic biomarker in DMD.

Parts of this dissertation have been published:

Moretti A, Fonteyne L, Giesert F, Hoppmann P, Meier AB, Bozoglu T, Baehr A, Schneider CM, Sinnecker D, Klett K, Fröhlich T, Rahman FA, Haufe T, Sun S, Jurisch V, Kessler B, Hinkel R, Dirschinger R, Martens E, Jilek C, Graf A, Krebs S, Santamaria G, Kurome M, Zakhartchenko V, Campbell B, Voelse K, Wolf A, Ziegler T, Reichert S, Lee S, Flenkenthaler F, Dorn T, Jeremias I, Blum H, Dendorfer A, Schnieke A, Krause S, Walter MC, Klymiuk N, Laugwitz KL, Wolf E, Wurst W, Kupatt C. *Somatic gene editing ameliorates skeletal and cardiac muscle failure in pig and human models of Duchenne muscular dystrophy. Nature Medicine* 2020; 26(2):207-214.

Regensburger AP, Fonteyne LM, Jungert J, Wagner AL, Gerhalter T, Nagel AM, Heiss R, Flenkenthaler F, Qurashi M, Neurath MF, Klymiuk N, Kemter E, Frohlich T, Uder M, Woelfle J, Rascher W, Trollmann R, Wolf E, Waldner MJ, Knieling F. *Detection of collagens by multispectral optoacoustic tomography as an imaging biomarker for Duchenne muscular dystrophy. Nature Medicine* 2019; 25(12):1905-1915.

II. REVIEW OF THE LITERATURE

1. Duchenne muscular dystrophy

Duchenne muscular dystrophy (DMD) is the most prevalent hereditary neuromuscular disease in newborn boys (1:3500) (Emery, 1991). In newborn screening studies in the USA, the prevalence of DMD has been reported as 15.9 cases per 100,000 and in the UK as 19.5 cases per 100,000 live male births (reviewed in Ryder et al., 2017). The disorder is inherited in a X-linked recessive manner, therefore primarily boys are affected, whereas female carriers of the disease rarely manifest clinical symptoms (Moser and Emery, 1974).

DMD is caused by mutations in the *DMD* gene, which prevent the expression of the functional muscle structure protein dystrophin. Phenotypically, the lack of dystrophin results in progressive muscle damage and degeneration leading to muscle weakness and wasting. Following symptoms are a loss of ambulation (LoA), severe respiratory impairment and cardiomyopathy (Nigro et al., 1990; Nigro et al., 1995).

Currently, for most patients only symptomatic therapies are available, which aim to slow down disease progression but are no cure. However, for few disease-causing mutations, promising new therapies aiming at the restoration of dystrophin expression, were developed within the past few years or are currently under investigation. Moreover, life expectancy of affected patients has been fundamentally improved in the past decades due to multidisciplinary care. Nevertheless, as a consequence of cardiorespiratory complications, DMD still leads to an early death between the ages of 20 and 30 (Eagle et al., 2002; Eagle et al., 2007; Passamano et al., 2012).

1.1. Clinical features

DMD patients are clinically normal at birth, albeit serum creatine kinase (CK) levels, a blood serum marker for muscle damage, are already elevated (reviewed in Blake et al., 2002). The first clinical manifestations of DMD appear in early childhood at soonest one year of age (average at 2.5 years of age) (Ciafaloni et al., 2009). Caregivers, e.g. family members or other educators, might notice initial signs, such as clumsiness and a developmental delay (*e.g.*, children start walking later than usual). Nevertheless, symptoms usually are consciously recognized later, between two and five years of age, during toddler and preschool age (Ciafaloni et al., 2009), when children present a waddling gait and/or toe walking (reviewed in Birnkrant et al., 2018b; Verma et al., 2010). DMD patients at this stage also show a special manner to get up from a sitting in a standing posture, called Gowers' sign, which is typical for neuromuscular disorders (Gowers, 1879). The Gowers' sign description (Fig. 1) goes back on Dr. Gowers, who, in 1879, first published a definition of this special pattern of standing up (Gowers, 1879; Wallace and Newton, 1989).

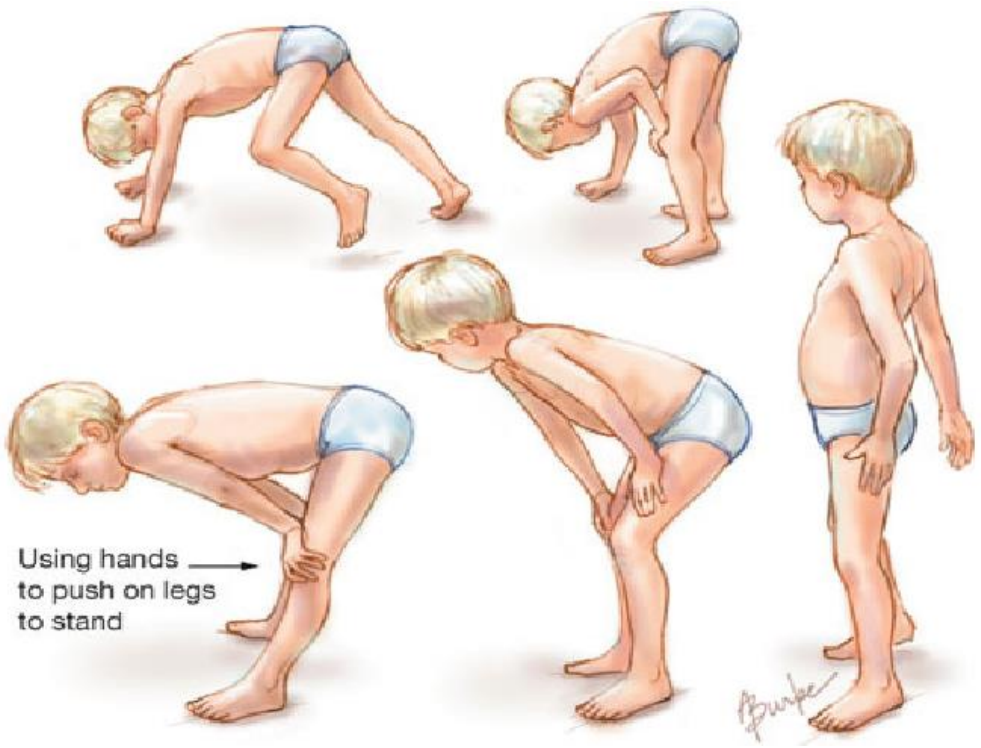

Figure 1: Gowers' sign. The Gowers' sign is a medical sign describing the typical way of getting from a sitting into a standing posture by "walking up the legs" with the hands. This behavioral pattern indicates muscle weakness in the lower limbs, hips and pelvic girdle (Asadi, 2017).

The first clinical stage is followed by a plateau phase, called the "honeymoon period" between the ages 5 and 8, where symptoms are often stabilized or even slightly improved (Brooke et al., 1983; Connolly et al., 2013). Subsequently, at the age of 7 to 8 years, a rapid clinical deterioration with a severe decline in functional ability and muscle strength starts (Brooke et al., 1983; Yiu and Kornberg, 2015). Patients show a severely labored gait and lose the ability to climb stairs, chairs or even toilet seats. In this stage, individuals with DMD may not be able to walk more than ten steps and are already dependent on physical assistance (Deutsche Duchenne Stiftung, 2017).

Calf pseudohypertrophy, Achilles heel contractures and tightening iliotibial bands on the one hand and an abnormal body posture on the other hand are most likely mutually dependent (Brooke et al., 1983). The chronic static positioning together with the inability to move the joints to their full extent, the muscle imbalances around the joints and the fibrotic changes cause joint contractures and a decreased muscle extensibility. These pathological changes exacerbate the symptoms and lead to severe deformity such as lordosis or scoliosis. Until the age of 12 years, most DMD patients already lose the ability to walk and become wheelchair bound. Limited upper-limb function follows at a later disease stage (reviewed in Birnkrant et al., 2018b; Verma et al., 2010).

Respiratory muscles (i.e. intercostal muscles and diaphragm) undergo similar pathological changes as other skeletal muscles. As a consequence of immobilization and muscle contractures, individuals with DMD develop a declined chest wall function leading to a reduced respiratory function and restricted breathing. Restricted breathing results in hypoventilation, first requiring assisted cough and

nocturnal ventilation and a full-time ventilation at later stages (reviewed in Birnkrant et al., 2018b; Verma et al., 2010).

The heart muscle, as a subtype of striated muscle, is likewise affected by the loss of dystrophin, causing myocardial fibrosis, dilated cardiomyopathy and arrhythmia (Nigro et al., 1990; Nigro et al., 1995; Silva et al., 2017). Even though an early involvement of the heart has been reported, cardiomyopathy in DMD patients is often asymptomatic, even at late stages. However, the development of a clinically apparent heart failure in DMD patients is latest present until the age of 18 (Nigro et al., 1990). In former times, the respiratory failure was the major reason for mortality in DMD. Nowadays, the cardiomyopathy is the main cause of death. This is due to the fact, that all other clinical features of the disease can be improved or cured by surgical or therapeutical means (Cheeran et al., 2017). Recognizing heart failure remains a challenge and requires a regular assessment of cardiac function (reviewed in Birnkrant et al., 2018b; Nigro et al., 1990; Van Ruiten et al., 2017).

Regarding mental capabilities, DMD patients might show a mild cognitive impairment, which indicates that the brain function is also abnormal in some individuals with DMD (reviewed in Blake and Kroger, 2000; Hinton et al., 2007; Prior and Bridgeman, 2005).

The gastrointestinal motor function also is shown to be markedly disturbed in several individuals with DMD (Lo Cascio et al., 2016). According to Kraus et al., in a cross-sectional prospective study, nearly 50% of patients are diagnosed with a functional obstipation (Kraus et al., 2016). However, there are only few case reports including histological examinations of the intestine, one showing smooth muscle fibrosis in the entire gastrointestinal tract (Leon et al., 1986). Another study hypothesizes a prolonged gastrointestinal transit time, but contrarily proves a normal gut transit (Kraus et al., 2018). Other nutritional complications are loss or gain of weight, low bone density, mandibular contracture, and swallowing dysfunction. These symptoms are partly attributed to long-term glucocorticoid treatment or calcium supplementation (reviewed in Birnkrant et al., 2018b; Kraus et al., 2016). However, the clinical context of gastrointestinal symptoms has not yet been fully elucidated.

Even though the awareness of DMD as important neuromuscular disease increased over the past years, these days there is still an average delay of 1 year, before boys are brought to a healthcare provider to evaluate the symptoms (Ciafaloni et al., 2009).

As women have two X-chromosomes, female carriers of DMD have one functional and one dysfunctional copy of the *DMD* gene. Therefore, they present a mosaic expression of dystrophin (Arahata et al., 1989), meaning that there is no total lack but a partial availability of dystrophin, compensating the loss. Nevertheless, there are some manifesting carriers showing symptoms, based on non-random X-chromosome inactivation (XCI) (Kamdar and Garry, 2016). Thus, clinical signs may vary from mild muscle weakness and cramps to DMD like severity (Moser and Emery, 1974; Soltanzadeh et al., 2010). However, affected female carriers do not mainly present with severe paralysis as seen in affected males, but primarily with symptoms of a cardiomyopathy, such as dilated cardiomyopathy, often seen as left-ventricle dilatation (Bushby et al., 1993; Hoogerwaard et al., 1999).

1.2. Becker muscular dystrophy

Becker muscular dystrophy (BMD) is a milder form of the neuromuscular disorder. The clinical course is similar to DMD but has a later onset of clinical manifestation and a much longer survival. BMD, equally to DMD, is caused by mutations in the *DMD* gene. The great majority of mutations on this gene locus result in a total loss of dystrophin leading to the manifestation of the severe disease type, DMD. However, mutations can also lead to a low presence of truncated but partially functional dystrophin, which results in the milder BMD disorder (reviewed in Blake et al., 2002).

In the past few years, new molecular therapy approaches took a major step in the direction of curing DMD by aiming to partially restore dystrophin, thus converting DMD into the milder BMD.

1.3. Structure of the *DMD* gene

The *DMD* gene is located on chromosome Xp21.2-p21.1 (OMIM#300377) (McKusick, 2002). With 2.5 million base pairs, it is the largest known gene in the human genome. Composed of 79 exons, it is transcribed into a full-length 14-kb mRNA (Roberts et al., 1993). The gene encodes dystrophin, a 427-kDa cytoskeletal protein. Dystrophin is predominantly expressed in skeletal and cardiac muscle and, with smaller amounts, in the brain.

Three independently regulated promoters are responsible for ensuring the expression of the full-length dystrophin: The B promoter (brain), the M promoter (muscle) and the P promoter (Purkinje cells), designated after the regions of their predominant activity. These promoters control the transcription of three different mRNAs, which share 78 same exons but contain unique first exons. The three resulting isoforms are designated Dp427 (B), Dp427 (M) and Dp427 (P) (Figure 2; reviewed in Blake et al., 2002).

Besides the promoters for these three long isoforms, there are four internal promoters, controlling the expression of truncated COOH-terminal dystrophin transcripts. To express their tissue-specificity, they are called R (retinal), (B3) brain-3, (S) Schwann cell and (G) general promoter. These promoters, which are distally located, use a unique first exon, splicing into exons 30, 45, 56 and 63, respectively. The generated protein products are referred to as Dp260 (R), Dp140 (B3), Dp116 (S) and Dp71 (G). These smaller proteins are ubiquitously expressed (reviewed in Blake et al., 2002; Muntoni et al., 2003). Dp71 (71kDa) is the most abundant transcript of the *DMD* gene in non-muscle tissue. It is expressed in several tissues such as brain, liver, kidney, lung and cardiac muscle, and ubiquitously expressed in most other tissues except for skeletal muscle (Austin et al., 1995; reviewed in Blake et al., 2002; Lederfein et al., 1992; Muntoni et al., 2003; Sarig et al., 1999). The other truncated isoforms are mainly expressed in the central and peripheral nervous system (reviewed in Blake et al., 2002). All in all, there are numerous isoforms and splice variants of mRNAs transcribed from the *DMD* gene in various tissues throughout the whole body (Austin et al., 1995; Feener et al., 1989).

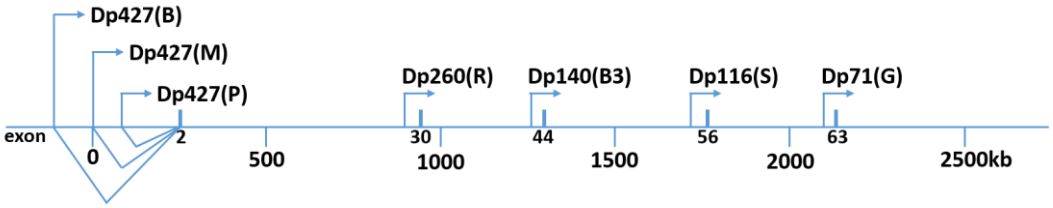

Figure 2: Schematic representation of the human *DMD* gene and the localization of the different promoter regions within the gene (adapted from Blake et al., 2002).

1.4. Dystrophin

Dystrophin, the product of the *DMD* gene, is a rod-shaped cytoplasmic muscle structure protein of about 150 nm length. It shares several features with the cytoskeletal protein spectrin and α-actinin (Koenig et al., 1988). Strongly anchored to the sarcolemma (the plasma membrane of cardiac and skeletal muscle), dystrophin connects the dystrophin glycoprotein complex (DGC) with the extracellular matrix (ECM) and the intracellular contractile apparatus (Campbell and Kahl, 1989; Rybakova et al., 2000; Straub et al., 1992). Figure 3 shows the DGC, an assembly of integral membrane proteins, and its localization in the sarcolemma.

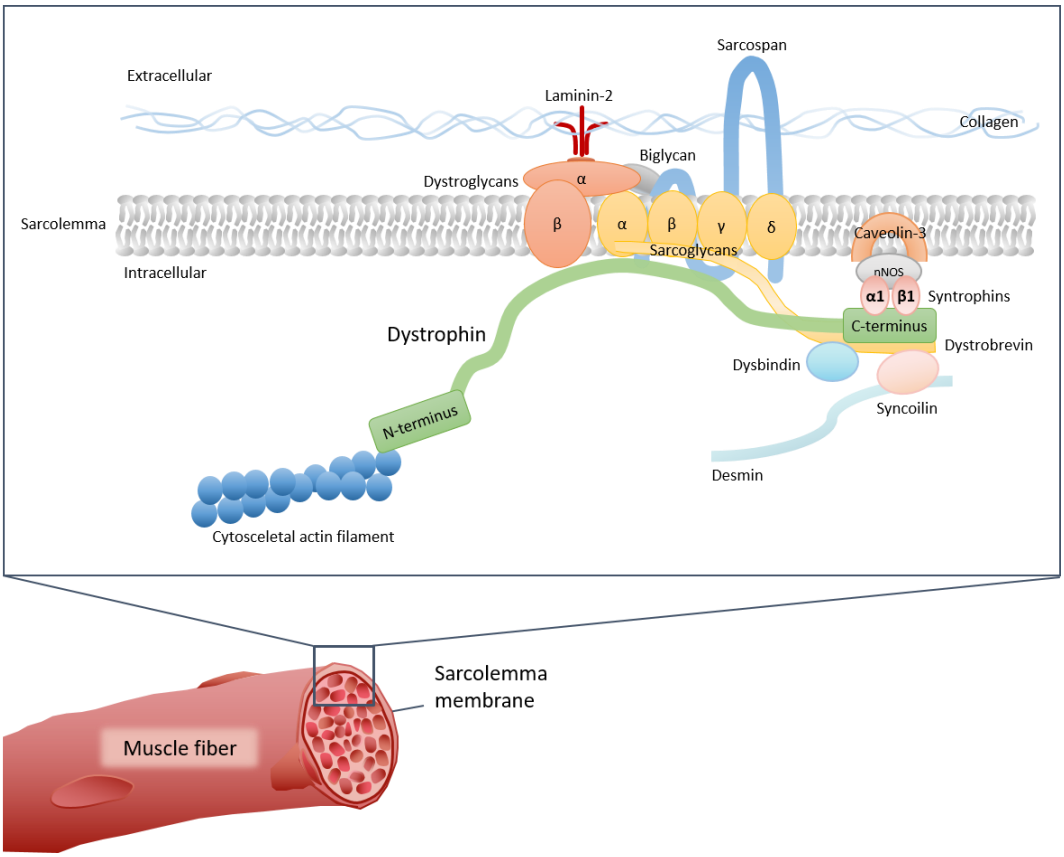

Figure 3: Schematic representation of the dystrophin glycoprotein complex (DGC). Dystrophin, localized to the periphery of striated muscles, is the membrane linker between the actin filaments and the external scaffold (adapted from Nowak and Davies, 2004).

Dystrophin can be separated into four domains. The 240 amino acid NH2-terminal domain (N-terminus) is identified as actin-binding site. A following rod-shaped domain is formed by a sequence of 25 triple-helical segments, which are similar to the repeat domains of spectrin. This rod domain and the N-terminus are part of the subsarcolemmal cytoskeleton. A third domain is a cysteine-rich segment. It is similar in part to the complete COOH domain of α-actinin in *Dictyostelium*. The last segment is a 420 amino acid COOH-terminal domain (C-terminus). It is located within or at the plasma membrane and links dystrophin to the integral membrane proteins (Koenig et al., 1988; Straub et al., 1992).

As shown in Figure 3, the main function of dystrophin is to be a transmembrane linker between actin and laminin in striated muscle cells (Campbell and Kahl, 1989; Ervasti and Campbell, 1993). Muscle fibers are protected from long-term contraction-induced damage and necrosis by the DGC stabilizing the sarcolemma (Rando, 2001; Straub and Campbell, 1997).

1.5. Mutations in the *DMD* gene

DMD, as well as BMD, can be the result of a spontaneous or an inherited mutation of the *DMD* gene. There is a great amount of independent mutations, varying in type, size and localization. Intragenic single- or multi-exon deletions build the majority of mutations. The frequency varies between 72%, according to Leiden DMD mutation database (Aartsma-Rus et al., 2006) and 60-65%, often mentioned in literature (Koenig et al., 1989; reviewed in Muntoni et al., 2003). Duplications of one or more exons are found in 5-15% of patients, depending on the sensitivity of the technique used. The remaining portion contains smaller deletions and insertions, or point mutations (reviewed in Aartsma-Rus et al., 2006; Abbs and Bobrow, 1992; Prior and Bridgeman, 2005).

Deletions in the *DMD* gene are found to be apparently nonrandom. There are two hotspot regions within the gene, where deletions are primarily located (Koenig et al., 1987). The first hotspot region is located towards the central portion of the gene. It includes exons 45-55. The endpoint where the mutation actually occurs, called genomic breakpoint, lies within intron 44. The second hotspot region lies within the 5´ portion of the *DMD* gene, including exons 2-19. The genomic breakpoints are most frequently found in the introns 2 and 7 but also expand towards the downstream introns (Beggs et al., 1990; Koenig et al., 1989; Muntoni et al., 2003; Prior and Bridgeman, 2005). The hotspot regions for deletions make the detection of these larger mutations comparatively straightforward (Prior and Bridgeman, 2005). Using a single multiplex polymerase chain reaction (PCR) technique, about 98% of deletions can be identified by the use of two multiplex reactions only (Beggs et al., 1990).

Point mutations are found evenly distributed among the *DMD* gene. They can cause frameshifts or affect splice sites, but they can also create missense codons or premature stop codons (reviewed in Roberts et al., 1994).

Generally, most mutations result in nonsense codons or frameshifts. A schematic explanation for an out-of-frame mutation is shown in Figure 4. A frameshift mutation is caused by the deletion or duplication of a number of nucleotides not divisible by three, which disrupts the open reading frame (ORF) (Monaco et al., 1988).

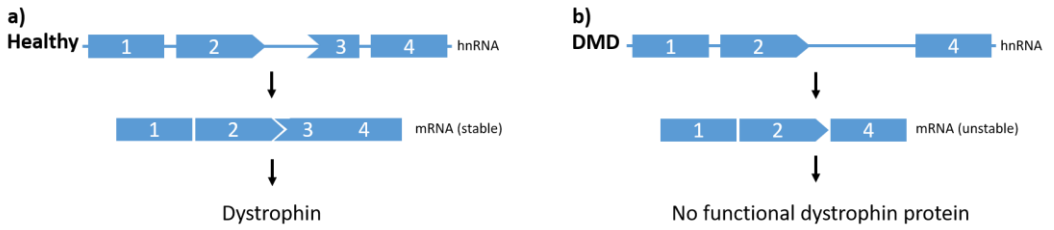

Figure 4: Schematic description of an out-of-frame mutation and its consequence on dystrophin expression. a) An intact exon intron sequence, resulting in a stable mRNA product after splicing. The mature mRNA is translated into functional dystrophin. b) Intragenic deletions lead to a disrupted ORF, thus to a frameshift. The result is either an unstable mRNA resulting in nonsense mediated mRNA decay, or a truncated nonfunctional dystrophin protein.

According to Monaco et al. (1988), the phenotypic difference between BMD and DMD can be explained by the type of mutation. The authors stated that deletion events in the genome, which maintain an ORF, result in the production of a truncated but semi functional dystrophin protein, leading to BMD. These kinds of mutations are called in-frame mutations. In contrast, an out-of-frame mutation is an intragenic deletion that cannot maintain the ORF and frameshifts after splicing of intron sequences. The translation either leads to an unstable mRNA product, causing mRNA degradation due to nonsense mediated mRNA decay, or the generation of a truncated nonfunctional dystrophin protein, with both translation pathways resulting in DMD.

In general, the milder BMD most commonly results from deletions or duplications that do not disrupt the ORF (Beggs et al., 1990). However, few deletions or duplications (9%) do not follow the reading-frame rule, stated by Monaco et al. In-frame mutations are also found in some DMD patients (Beggs et al., 1991; Koenig et al., 1989), whereas out-of-frame mutations are present in few BMD individuals (Aartsma-Rus et al., 2006).

Additionally, the phenotype, to some extent, is also determined by the size and location of the deletion (Arikawa-Hirasawa et al., 1995; Beggs et al., 1991; Fanin et al., 1996). Regarding the size, very large deletions, especially in particular regions, may result in a more severe phenotype (Beggs et al., 1991). Concerning the location of in-frame mutations the severity of the phenotype can be anticipated: It has been reported, that mutations in the N-terminal domain result in low levels of dystrophin and thus are classified as severe BMD or intermediate. An additional deletion of parts of, or of the whole central rod domain, give rise to DMD. Patients with deletions or duplications only in the proximal rod domain show primarily severe cramps and myalgia. Mutations in the central rod domain usually are associated with milder phenotypes, such as mild BMD, except if the deleted region becomes too large. Some BMD patients show deletions in the syntrophin binding domain, whereas mutations concerning the cysteine-rich domain result in DMD. Mutations in exon 74 or higher are found in BMD as well as in DMD patients (reviewed in Aartsma-Rus et al., 2006; Beggs et al., 1991). An intact C-terminal domain seems to be essential for the stability of dystrophin (Koenig et al., 1989).

Nevertheless, individuals with similar mutations show different phenotypes, suggesting epigenetic or environmental influence on the clinical expression. Thus, the severity of the phenotype cannot be certainly predicted by the size or type of

mutation (Beggs et al., 1991).

1.6. Pathomechanism

Dystrophin is a structural key component in muscle fibers. The main function of the DGC is to stabilize the plasma membrane. The loss of dystrophin in DMD patients results in delocalization of the dystrophin-associated proteins from the membrane (reviewed in Deconinck and Dan, 2007). This impairs the structural integrity of the muscle membrane resulting in fragile membranes. Mild exercise-induced muscle fiber damage is normal to occur even in healthy musculature (Petrof et al., 1993). However, in DMD patients the damage is greater. Regenerative processes aim to replace or repair lost or damaged muscle fibers, but repetitive greater damage exceeds the regenerative capacity of the muscles, due to limited number and ability of satellite cells. Therefore, normal mechanical stress in the musculature already leads to micro-lesions, followed by membrane leakage and muscle fiber damage (reviewed in Deconinck and Dan, 2007; Klingler et al., 2012; Petrof et al., 1993). The micro-lesions and resulting hyperosmotic stress lead to an increased sodium and calcium permeability.

The intracellularly increased sodium leads to depletion of ATP supply, as Na^+/K^+ pumps, normally regulating the electrolyte balance, cannot compensate the increased influx. Sodium, accompanied by water molecules, leads to cellular edema and necrosis (Klingler et al., 2012). Calcium, as a second messenger, is able to activate a cascade of inflammatory processes. With the disturbance of Ca^{2+}-homeostasis, various Ca^{2+}-dependent proteases, such as calpain, are activated, resulting in cell and membrane proteolysis and therefore cell death (Bodensteiner and Engel, 1978; reviewed in Deconinck and Dan, 2007; Klingler et al., 2012; Yeung et al., 2005). Calcium overload also results in oxidative stress (due to the production of reactive oxygen species), leading to an accumulation of acidic metabolites, such as lactic acid, mainly dissociated into La^- and H^+ at physiological pH. La^- increases the activity of collagen promoters. Procollagen mRNA production increases, leading finally to collagen synthesis. However, until now comparatively little attention has been paid to the actual role of fibrosis in DMD. As fibrosis in general is described as the exchange of normal tissue against scar tissue, indicating that fibrous connective tissue results from a reparative or reactive process, it is a general belief, that the increase of connective tissue in DMD is a secondary phenomenon. Fibrosis in DMD is generally seen as a compensatory replacement of the lost muscle tissue. Nevertheless, an endomysial tissue increase can already be observed long before any muscle fiber degradation appears, indicating that the fibrotic remodeling itself plays a major role in DMD. A co-determining role in the myofascial pathology is discussed, for example due to a possible negative effect of fibrosis on the nutrition of enclosed muscle cells (Klingler et al., 2012).

In histological examinations, muscle fibers are in process of regeneration, degeneration or are already necrotic. Degeneration and necrosis are followed by phagocytosis, with the presence of inflammatory cells (reviewed in Blake et al., 2002). Regenerating muscle cells histologically show larger and centrally placed myonuclei. The cytoplasm is RNA-rich, hence basophilic. The muscle fiber diameter decreases, leading to an increased variation of muscle fiber diameters (Bell and Conen, 1968; Bradley et al., 1972; Schmalbruch, 1984). Necrotic fibers are often seen in clusters, so called grouped necrosis. Necrotic tissue is gradually replaced by fatty and connective tissue (fibrosis), with the functional consequence of a decrease in the quantity of contractile tissue. These structural changes give rise

to the then clinically apparent pseudohypertrophy and contractures (reviewed in Blake et al., 2002; Wokke et al., 2014).

1.7. Modifier genes in DMD

Factors, independent from the pathogenic mutation, can influence the expressivity of Mendelian diseases (Bello et al., 2016). These factors are called modifier genes and are defined as genetic loci, which are able to positively or negatively influence the phenotype of a primary disease-causing mutation. As shown above, in DMD not a single, but several different causative mutations are present. As a result, it is hard to distinguish between the primary mutation, which is causative for the disease, and a secondary modifying locus (reviewed in Vo and McNally, 2015). Besides the genetic heterogeneity in DMD, the identification of modifier genes is complicated by the above-mentioned varying onset of clinical symptoms and different disease progression. Nonetheless, common symptoms can be observed and taken into account in regards to modifying gene loci. To identify these bases of variability in DMD is important for patient consultation, prognosis and an appropriate therapeutic approach (reviewed in Bello and Pegoraro, 2019). To date, several loci have been identified to be associated with variable DMD sub-phenotypes. In general, their influence may be reflected by the age of onset, the muscle groups which are affected, the severity or the progression of the disease (reviewed in Vo and McNally, 2015). Yet, the most commonly observed phenotypic variation in DMD patients, whose DMD mutations all prevent dystrophin expression, is the age at loss of ambulation (LoA) (Bello et al., 2016).

In this context a single nucleotide polymorphism (SNP) in the gene promoter of secreted phosphoprotein 1 (SPP1 or Osteopontin, encoded by the *SPP1* gene) has been described as potential genetic modifier in DMD patients (Bello et al., 2015b). Pegoraro et al. (2011) described this polymorphism, rs28357094, as significantly associated with disease progression (disease severity was defined by the age at LoA). The less common G allele (GT/GG genotype) was related to an earlier ambulatory loss of about one year. Thereby, the effect of the TT genotype is similar in magnitude to the therapeutic use of steroids (delaying LoA for about one year). At the age of 14, 20% of DMD patients with the TT genotype where shown to be still ambulatory, whereas none of the individuals with the GT/GG genotype were able to walk. The cause is, that the G allele variant decreases the promoter strength and consequently leads to a lower *SPP1* mRNA production. Many studies were done to explain the function of SPP1. Osteopontin, amongst others, plays a role in bone-remodeling, muscle repair, the maintenance or reconfiguration of tissue integrity during inflammation and immune function (Giacopelli et al., 2004; reviewed in Vo and McNally, 2015). Furthermore, *SPP1* is activated by transforming growth factor beta (TGFB) family members. There exist more than 30 TGFB family members, located in the ECM, which, for example, coordinate cell growth during development, regulate injury response, or are important for muscle health (Lamar et al., 2016; Taipale et al., 1994). Studies in double mutant mice, lacking both dystrophin and SPP1, revealed significant reduction in TGFB, fibrosis and inflammatory cell infiltration. Yet, due to its broad expression pattern, it is complicated to understand the means by which SPP1 exactly modifies DMD (Vetrone et al., 2009; reviewed in Vo and McNally, 2015). Moreover, the working group of van den Bergen et al. (2015) in their study disproved the significant association between *SPP1* rs28357094 SNP and LoA as they were unable to replicate the results in 336 genotyped patients.

Another important potential genetic modifier, also associated with the age at LoA in DMD patients, is latent TGFB binding protein 4 (LTBP4). Its function is to regulate, together with other latent TGFB binding proteins (LTBPs), the extracellular availability of latent TGFB (Lamar et al., 2016). Latent TGFB gets secreted as precursor and gets activated before the interaction with TGFB receptors on the cell surface (reviewed in Vo and McNally, 2015). LTBPs bind to inactivate TGFB in the ECM (Ceco et al., 2014). The importance of the regulating role of *LTBP4*, especially during development, is underlined by findings describing a multi-organ syndrome in humans with an recessive *LTBP4* loss (Urban et al., 2009). LTBP4 is primarily expressed in skeletal muscle, smooth muscle, heart and at a lower level in other tissues. In patients with DMD, four non-synonymous SNPs (nsSNPs) in *LTBP4* are associated with a prolonged ambulation (Giltay et al., 1997; Lamar et al., 2016). The four nsSNPs (rs2303729, rs1131620, rs10880 and rs1051303) form two major amino acid haplotypes: IAAM and VTTT (the names derive from the amino acids specified by these nsSNPs). From these two, a homozygous IAAM haplotype shows a significant association with a later LoA in several studies. Patients heterozygous or homozygous for VTTT showed an earlier ambulatory loss (Bello et al., 2015b; Flanigan et al., 2013; van den Bergen et al., 2015). LTBP4 containing the ameliorative haplotype IAAM, is able to alter TGFB binding or release. Consequently, TGFB signalling is reduced leading to decreased muscle fibrosis and benefiting muscle regeneration capacity (Flanigan et al., 2013). In line with these findings, *Ltbp4* was also identified to modify muscular dystrophy in mice. By differently targeting the *Ltbp4* gene, the outcomes in muscular dystrophy could be modified in both directions, a decreased fibrosis and improved muscle pathology, or increased proteolysis and fibrosis (Heydemann et al., 2009). To explore the function of LTBP4 in detail in skeletal muscle and, in particular, in muscular dystrophy, Lamar et al. (2016) generated mice, which overexpress the murine *Ltbp4* gene. The elevated levels of LTBP4 here led to increased muscle strength and, proportional to it, an increased muscle mass. Therefore, targeting LTBP4 is discussed as a therapeutic approach.

The two named genetic modifiers, *SPP1* and *LTBP4*, are the most researched polymorphic loci in DMD. They are both involved in molecular pathways, which regulate inflammation response to muscle injury, regeneration, and fibrosis (reviewed in Bello and Pegoraro, 2019). Several further, less investigated, possible genetic modifiers of the clinical phenotype in DMD have been discussed. Recently, in 2017, a common null polymorphism (R577X, rs1815739) in human *ACTN3* (encoding α-actinin-3) was shown to be significantly correlated to reduced muscle strength and a longer time in 10 m walking test in ambulatory patients with DMD. α-Actinin-3, an isoform of sarcomeric α-actinins, is only expressed in fast, glycolytic muscle fibers. In patients homozygous for the null polymorphism R577X, α-actinin-3 is completely absent (Hogarth et al., 2017). *ACTN3* is known as “the gene for speed”: an α-actinin-3 deficiency was already previously shown to be detrimental in elite athletes as well as in general population, reducing muscle power and sprint performance (reviewed in Bello and Pegoraro, 2019; Clarkson et al., 2005; Eynon et al., 2013; Moran et al., 2007). Bello et al. (2016) prioritized rs1883832 SNP in the untranslated region of *CD40*. CD40, also known as tumor necrosis factor receptor superfamily member 5 (TNFRSF5), is a co-stimulatory molecule for T cell polarization. The minor allele at rs1883832 reduces the expression of CD40. In the study of Bello et al., this was shown to be associated with an earlier LoA in a total of 660 DMD patients. Nevertheless, the precise role of *CD40* in muscular dystrophy is still poorly understood (reviewed in Bello and

Pegoraro, 2019). Another modifier locus, *THBS1*, was detected by Weiss et al. (2018). *THBS1* gene encodes thrombospondin-1 (THBS1), which activates TGFB signaling by directly interacting with LTBP4 in the ECM. Thus, it controls the bioavailability of TGFB. Furthermore it acts as inhibitor of pro-angiogenic nitric oxide signaling. Weiss et al. discussed a protective effect of the *THBS1* distal regulatory SNPs. Together with regulatory variants resulting in reduced expression of LTBP4, it was found to prolongate ambulation in patients with DMD. The working group of Davis et al. (2000) discussed myoferlin (MYOF) as possible modifier of muscular dystrophies after they found out, that a mouse model of DMD (*mdx* mouse) showed an upregulation of MYOF at the membrane of skeletal muscle. C2 domains, which are part of all ferlin family members, play a role in calcium-mediated membrane fusion events. Vieira et al. (2017) suggested phosphatidylinositol transfer protein α (PITPNA) as possible DMD modifier, referring to findings in two atypical DMD-dogs which demonstrated a strikingly mild dystrophic phenotype. This finding was pursued by knockdown of *PITPNA* gene in dystrophin-deficient sapje zebrafish and human DMD myogenic cells. Decreased expression of *PITPNA* led to increased expression of phosphorylated Akt (pAkt) and decreased phosphatase and tensin homolog (PTEN) levels. The muscle structure was ameliorated and survival was increased.

Although several genetic modifiers have been identified in DMD, the overall knowledge in this field is still initial. However, a detailed knowledge about modifier genes in DMD is important, since individual differences in disease progression complicate the interpretation of results of clinical trials (reviewed in Aartsma-Rus and Spitali, 2015). Most studies rely on hypothesis only, discovering candidate genes which are pre-specified genes of interest to find putative modifiers. Hence, most identified modifiers were already known to play a role in muscle health, with their pathways beeing already well established. Genome-wide association studies (GWAS) of polymorphisms influencing the muscle phenotype, however, scan the entire genome for common genetic variants. As hypothesis-free, unbiased approach GWAS would be necessary to identify also unexpected associations in DMD (reviewed in Bello and Pegoraro, 2019). To further increase the mapping precision of quantitative trait loci (QTL) a genome-wide combined linkage disequilibrium and linkage analysis (cLDLA) as fine mapping method can be conducted (Farnir et al., 2002). This method is based on the informative recombinations within gentoyped pedigrees as well as on informations given from historical recombinations of earlier, not genotyped generations (Meuwissen et al., 2002). For example, Muller et al. (2017) demonstrated that the haplotype-based genome-wide cLDLA can allow more precise mapping of QTL than the more commonly used SNP-based GWAS.

2. Animal models for DMD

There is a wide range of natural and engineered mammalian animal models reflecting the clinical aspects of DMD, including mouse, rat, rabbit, cat, monkey, dog and pig models. Tailored animal models are indespensable for the elucidation of DMD pathogenesis (reviewed in Nakamura and Takeda, 2011). The model organisms are of great importance for the development of new targeted therapies, aiming to prevent disease progression or to reverse pathological mechanisms (reviewed in Wells, 2018). Safety, as well as efficacy prediction of new therapeutic strategies requires reliable animal models mimicking the situation displayed in humans. Moreover, the discovery and validation of new biomarkers, indicating

physiological processes, pathological changes and the response to therapeutic treatment, plays a major role (Aigner et al., 2010).

2.1. Rodent models

The X Chromosome-Linked Muscular Dystrophy (*mdx*) in mouse (Bulfield et al., 1984) is the best known animal model for DMD. With more than 2800 published papers using the *mdx* mouse, it is the most widely utilized DMD model to date (reviewed in Wells, 2018). The model is a spontaneous mutant failing to produce dystrophin due to a mutation in exon 23 of the murine *Dmd* gene, which introduces a premature stop codon (Sicinski et al., 1989). This mouse model displays the biochemical processes and early stages of the disease, but yet it is not the best model organism in reflecting the clinical aspects of DMD. While exhibiting muscular dystrophy (Bulfield et al., 1984), the phenotype of *mdx* mice is much milder than in DMD patients. Obvious clinical signs of dystrophic musculature are completely missing (reviewed in Wells, 2018). Histological key features such as fibrosis and fatty deposits among muscle tissue, smaller number of myofibrils, insufficient regeneration process and severe degeneration in muscle fibers are only present in the diaphragm of *mdx* mice, but absent in every other muscle (Fukada et al., 2010). Last but not least, the life span of *mdx* mice is only slightly reduced (Chamberlain et al., 2007). A possible explanation for this milder phenotype might be that the mutation does not disturb the expression of four shorter isoforms, expressed from the *Dmd* gene through varying promoter usage (Araki et al., 1997). As the original B10-*mdx* mouse (C57BL/10 background) (Bulfield et al., 1984) is a weak model for DMD, it has been backcrossed onto several other genetic backgrounds. One resulting mouse line was the DBA/2J-*mdx* model, which is a backcross onto the DBA/2J mouse strain (reviewed in Wells, 2018). This model organism seems to worsen the dystrophic phenotype as desired and even reflects a cardiomyopathy. Unfortunately, the control DBA/2J mice show a similar myocardial pathology. Hence, the DBA/2J-*mdx* mouse is also a poor model for DMD (Hakim et al., 2017). Another tailored mouse model has been generated by Araki et al. (1997), disrupting exon 52 of the *Dmd* gene. This mutation is known to result in clinical DMD in humans. Nevertheless, the *mdx52* still shows limited, if at all, clinical signs of muscular dystrophy (reviewed in Wells, 2018). Perkins and Davies (2002) discussed, that throughout an increased expression of utrophin, an autosomal homologue of dystrophin, the loss of dystrophin in *mdx* mice could, at least in part, be compensated. Therefore, utrophin knockout (KO) mice were crossed with *mdx* mice (Deconinck et al., 1997). While these double-KO mice display a more severe dystrophic phenotype, they are obviously inappropriate as models for DMD, since DMD patients do not lack both, dystrophin and utrophin (reviewed in Wells, 2018). Altogether, there are several mouse models of DMD, but none of them appropriately mirrors the phenotype of DMD patients. A further disadvantage of the mouse as animal model can be seen in the small body size, imposing limitations on analysis, such as dose-finding in therapeutic trials of new treatments.

Two different rat models of DMD have been generated, both published in the year 2014. Larcher et al. (2014) engineered two lines of *Dmd*-mutant rats using transcription activator-like effector nucleases (TALENs) targeting exon 23 of the *Dmd* gene. The musculature of the Dmd^{mdx} rat lacks dystrophin and displays severe necrosis and regeneration, at a later stage it shows fibrosis and fatty infiltration. Clinically, muscle strength and spontaneous motor activity are impaired. Furthermore, Dmd^{mdx} rats show signs of dilated cardiomyopathy. Nakamura et al.

(2014) generated *Dmd*-mutated rats using a clustered regularly interspaced short palindromic repeats (CRISPR)/Cas system, targeting exon 3 and 16 in the rat *Dmd* gene simultaneously. Phenotypically this rat model shows similiar alterations as the *Dmd*^{mdx} rats, except for the heart, where a clear evidence of a functional cardiomyopathy is missing (reviewed in Wells, 2018). The two rat models of DMD seem to reflect the clinical aspects of DMD better that the mouse models.

2.2. Rabbit model

A novel animal model for DMD in the rabbit has been engineered and characterized by Sui et al. (2018). *DMD* knockout (KO) rabbits were generated by co-injection of Cas9 mRNA and sgRNA targeting exon 51 into zygotes of rabbits. This model exhibits a typical DMD phenotype, with impaired physical activity, muscle degeneration and fibrosis, and increased CK levels. Also functional alterations in the heart seem to be present in this model, indicating the development of cardiomyopathy. Nevertheless, this publication was the first introduction to this new animal model for DMD and it is not yet clear, if, for example, the reduction in activity, shown in this model, is sufficiently robust for accurate drug trials (reviewed in Wells, 2018).

2.3. Feline model

Progressive muscular dystrophy due to dystrophin-deficiency has been described to naturally occur in cats (Carpenter et al., 1989; Gaschen et al., 1999). The hypertrophic feline muscular dystrophy (HFMD) mainly results in muscle hypertrophy, predominantly observed in the tongue and diaphragm, leading to difficulties in eating and drinking. In histological examinations, degeneration and regeneration processes can be observed. Nevertheless, dystrophin in cats with HFMD is still faintly detectable in immunostaining of muscle fibers. About 10% of dystrophin, compared to normal dystrophin amounts, is detectible in Western blot analysis of skeletal muscle, showing that there is no total failure of dystrophin expression. Additionally, muscle fibers in HFMD cats do not show fibrotic alterations. Moreover, only a few cats suffer of cardiomyopathy. Histological changes in the heart are only present in some cases (Gaschen et al., 1999). All in all, dystrophin-deficient cats are not suitable as experimental models for human DMD (reviewed in Wells, 2018).

2.4. Nonhuman primate model

Chen et al. (2015) generated a dystrophin deficiency in rhesus monkeys. By using CRISPR/Cas9 for injection into fertilized oocytes, they targeted exon 4 and exon 46 in the monkey *DMD* gene, causing a frame shift of the coding sequences and thereby a termination of the full-length expression of dystrophin. The mutation results in a partial depletion of dystrophin and muscle degeneration. However, the CRISPR/Cas9 technology causes mosaic mutations, targeting only up to 87% of the dystrophin alleles, resulting in genetic and phenotypic variability. This again doesn’t comply with the mutations found in human DMD patients, which result in a total loss of dystrophin.

2.5. Canine models

The most famous homologue of DMD in dogs is the Golden Retriever Muscular Dystrophy (GRMD), also known as Canine X-linked Muscular Dystrophy (CXMD), which is the result of a spontaneous single base change in intron 6 leading to the skipping of exon 7 and therefore the termination of the dystrophin reading frame (Sharp et al., 1992). As well as DMD patients, GRMD dogs show myofiber degeneration with mineralization and fibrosis with fatty infiltration, altogether resulting in an atrophy of the musculature. Serum CK levels in affected dogs are elevated. The dog model also shows signs of cardiomyopathy (Sharp et al., 1992; Valentine et al., 1988). The mutation of the GRMD model has been introduced onto a Beagle background to enable a better handling due to a smaller body size. The phenotype of the resulting Beagle-based canine X-linked Muscular Dystrophy ($CXMD_J$) is roughly identical to the phenotype described in GRMD dogs (Shimatsu et al., 2005). Another canine model of DMD is the Cavalier King Charles Spaniel with dystrophin-deficient muscular dystrophy (CKCS-MD). It carries a missense mutation in the splice site of exon 50 in the canine dystrophin gene. The mutation gives rise to a single exon deletion (exon 50) in the mRNA, leading to a disrupted reading frame and the premature truncation of the gene product. While the phenotype of this dog model of DMD seems to resemble that of the two previously described dog models, GRMD and $CXMD_J$, the localization of the mutation is clinically more relevant. The region is also most commonly mutated in human DMD patients (Walmsley et al., 2010). There are many other dog breeds diagnosed with a muscular dystrophy due to a loss of dystrophin. Several of them have been used for the development of a dog model of DMD. Nevertheless, the big disadvantage of all these models is the high phenotypic dog-to-dog diversity described. These individual variations and the fact, that many DMD dogs die within the first 6 month of life, lead to difficulties in reaching the size of an experimental group and in showing clear statistically significant results (reviewed in Wells, 2018).

2.6. Pig models

Last but not least, in 2013, a tailored pig model of DMD has been generated in our working group. Klymiuk et al. (2013) established the large animal model by gene targeting, deleting *DMD* exon 52 in male pig cells. The region corresponding to human *DMD* exon 52 was replaced by a neomycin resistance cassette. DMD pigs were then generated by nuclear transfer. The introduced mutation reflects a frequent mutation in human DMD patients (Muntoni et al., 2003). DMD pigs lack dystrophin and exhibit progressive muscle weakness, impaired mobility and disturbances in locomotion due to dystrophic changes of skeletal musculature. Histological examination of the DMD pig muscle tissue reflects the structural changes seen in DMD patients. These findings include excessive variation of muscle fiber diameters, internalized central nuclei indicating regeneration processes, cell infiltration, necrosis of muscle fibers and interstitial fibrosis. The DMD pig shows an accelerated strong muscle phenotype and disease progression, leading to muscle structure changes already in newborn piglets. Furthermore, serum CK levels are severely elevated. Most likely due to respiratory failure, the maximum life span of DMD pigs is around 3 month of age (Klymiuk et al., 2013). Therefore, male DMD pigs do not reach sexual maturity. To overcome this drawback, in cooperation with the working group of Matsunari we generated unique chimeric boars, comprising mutant cells which harbor the lethal *DMD* mutation and normal cells. These

chimeric boars, containing DMD $X^{KO}Y$ germ cells, show a milder impairment of respiratory and motor function. The model indicates, that muscle dysfunction, at least partly, can be cured by normal cells. However, most importantly, the chimeric boars are able to reach adulthood. The design of such chimeric DMD $X^{KO}Y$ boars as effective system to produce tailored DMD pigs, will have a great impact on the establishment of next-generation theraphies, such as gene editing and gene therapy, cell-transplantation therapy and medication aiming at exon-skipping (Matsunari et al., 2018).

Summarizing the advantages and disadvantages of the different animal models for DMD it becomes apparent that, except for the pig, all models are far from humans with regard to genetics, anatomy and physiology. Most models of DMD are not able to reliably reflect the patients' situation and therefore are not stable in predicting efficiency and safety of new therapies or devices. This is an obstacle to the extrapolation and interpretation of treatment effects from animal to human (reviewed in Aigner et al., 2010; Echigoya et al., 2016). Pigs, unlike the other named animals, are omnivores, as well as humans. They show a huge number of similarities in anatomy, physiology, pathology and metabolism (reviewed in Aigner et al., 2010). The cardiovascular and immune, as well as respiratory and skeletal muscle system of pigs and humans closely resemble each other. Therefore, generally one can say, that pigs as large animal model for DMD are supporting translational medicine by bridging the gap between proof-of-concept trials in mice and clinical studies in DMD patients (Klymiuk et al., 2016).

3. Diagnostic approaches in DMD

As already mentioned above, diagnosis of DMD is regularly delayed. The first clinical symptoms are noted at a mean age of 2.5 years with a first evaluation by a care provider at a mean age of 3.6 years. In many cases the initial consultation of a pediatrician doesn't result in diagnostic testing, but in referral to occupational, physical or speech therapy or programs for development stimulation (Ciafaloni et al., 2009). Immediate referral to a specialist for neuromuscular problems, who requests genetic analysis of the *DMD* gene, would avoid the diagnostic delay (reviewed in Birnkrant et al., 2018b). To date, definite diagnosis of DMD disease is made at a mean age of 4.9 years (Ciafaloni et al., 2009). Early diagnosis of the disease and sensitive monitoring of disease progression are necessary for most of the current therapeutic approaches, such as corticosteroid treatment, which aim to intervene before severe and irreparable muscle damage have taken place (reviewed in Ciafaloni et al., 2009).

Family history in many cases gives a first hint for the diagnosis of DMD, as approximately 1 in 3 DMD cases (about 30%) stem from spontaneous *de novo* mutations in the *DMD* gene (reviewed in Aartsma-Rus et al., 2016; reviewed in Ciafaloni et al., 2009). Therefore it is carefully analyzed before further diagnosis in patients presenting any suspicion of abnormal muscular function (reviewed in Birnkrant et al., 2018b).

3.1. Genetic testing

DMD diagnosis is verified by genetic testing. A correct diagnosis is important for providing proper care and support to patients and for further family planning. Moreover, mutation-specific therapy approaches require clear and exact

localization of the underlying mutation (reviewed in Aartsma-Rus et al., 2016).

Dystrophin gene deletion or duplication analysis is the initial confirmatory DNA analysis done in individuals with suspected DMD. It is the most labor- and cost-efficient way, since approximately 65% of the DMD causing mutations are single- or multi-exon deletions or duplications in the dystrophin gene, as shown above (reviewed in Aartsma-Rus et al., 2016; reviewed in Birnkrant et al., 2018b). Chamberlain et al. (1988) established a multiplex PCR kit, containing primers for 9 exons to detect 80% of deletions in the *DMD* gene. Two years later, Beggs et al. (1990) presented primers for 9 additional exons. In conjunction the Chamberlain and Beggs multiplex PCR kit is able to detect 97% of all deletions. However, multiplex PCR is no longer recommended for the genetic diagnosis of DMD, but is still used in many laboratories, since the method is cheap. Aartsma-Rus et al. (2016) even recommends re-analysis of historic cases identified with multiplex PCR. The detection of duplications is more technically and laborious demanding. Although causing DMD in 5-8% of patients, these mutations were not routinely screened, until a multiplex ligation-dependent probe amplification (MLPA) assay had been designed. To date MLPA is the most reliable and suitable method, simultaneously screening all 79 exons of the *DMD* gene for both, deletions and duplications (reviewed in Aartsma-Rus et al., 2016; reviewed in Birnkrant et al., 2018b). It is a cheap and simple assay offering a high ease of use (Lalic et al., 2005). Although MLPA is proposed as the screening method of choice for detecting rearrangements in the *DMD* gene, ambiguous MLPA amplification products can occur. These uncertain products should absolutely be verified by other methods, as they might result from small mutations which partially disturb MLPA amplification (Okizuka et al., 2009; Sansovic et al., 2013). Alternatively to MLPA, comparative genomic hybridisation array (array CGH) can be used to detect relative abundance of each exon of the *DMD* gene (reviewed in Aartsma-Rus et al., 2016). MLPA and array CGH are both able to identify the boundaries of a deletion or duplication and hence might indicate, whether the mutation results in a disruption of the reading frame or not. As explained before, this is important to predict disease progression (reviewed in Aartsma-Rus et al., 2016).

If the screening for deletions or duplications is negative, whole dystrophin gene analysis is the next step to analyse for the remaining mutation types able to cause DMD (reviewed in Birnkrant et al., 2018b). These mutations, as stated above, include point mutations and smaller deletions, duplications or insertions. Therefore, Sanger sequencing can be used to identify individual exons. Sanger sequencing is more expensive and labor-intensive than MLPA or array CGH. A better alternative to this method, however, are next-generation sequencing (NGS) techniques, which in the future might even be able to replace MLPA, array CGH and Sanger sequencing. NGS has a high sensitivity and specificity and is able to identify various types of mutations, including novel mutations not identified before, such es novel partial deletions (Okubo et al., 2016; Wang et al., 2014; Wei et al., 2014). However, NGS until now is cost- and labor-intensive. In some cases, genetic testing does not confirm the clinical diagnosis. The reason for this can be mutations located within an intronic region, which are harder to detect. This is the case in about 0.5% of reported mutations. Even if such mutations are identified by NGS, it is still questionable whether they cause an alteration on the RNA level. Hence, subsequent RNA analysis need to be done (reviewed in Aartsma-Rus et al., 2016).

3.2. Examination of muscle biopsies

Finally, if a clear identification of the DMD causing mutation by genetic analysis is not possible at all, the presence of dystrophin protein in skeletal muscle can be tested. This is done by staining cross-sections of a muscle biopsy with immunohistochemical (IHC) techniques or by analysing muscle protein extract by western blot (immunoblotting) (reviewed in Birnkrant et al., 2018b; Magrath et al., 2018). Hereby it can be tested, if any dystrophin is produced or not (reviewed in Muntoni et al., 2003). Furthermore, histological examinations in individuals with DMD can give a clear picture of the degree of severity of the dystrophic process. Therefore, cross-sections of muscle tissue are stained with haematoxylin and eosin (HE). In the preclinical stage typical alterations in muscle tissue are active necrosis, phagocytosis and regenerative activity. With increasing age, the degree of variation in fiber size diameter increases, as well as phagocytosis, whereas regeneration processes decline (Bradley et al., 1972). Special staining methods, such as Masson Trichrome (MT) and Sirius Red (SR), allow the detection of fibrosis, which is discussed to be a significant co-determining factor for myofascial pathology. An increase of collagenous connective tissue might have a negative effect on the nutrition of the enclosed muscle cells (Klingler et al., 2012).

Muscle biopsies are not only of use with regard to histological examinations and gel-based quantitative proteomics. Although two-dimensional polyacrylamide gel electrophoresis (2-DE) up to date remains the method of choice and is widely applied (Abdallah et al., 2012), gene expression profiles from muscle biopsies can also be generated by other methods. Expression microarrays for example, can identify components with possible important control functions or unexpected involvement in regulatory or pathological pathways in muscle (Bakay et al., 2002; Haslett et al., 2003). Even more effective, however, are holistic proteome analyses by mass spectrometry (MS). MS as a gel-free quantitative technique enables profiling of proteins with a high throughput rate, thus providing high precision in quantification of proteins (Abdallah et al., 2012). Several MS-based gene expression studies in animal models for DMD emphasize the increasing importance of these holistic proteome studies.

A 2-DE and MS of hindlimb muscles of *mdx* compared to WT mice identified differently abundant proteins (Ge et al., 2003). Investigation of *mdx* mice at different ages revealed age-dependent changes of the muscle proteome (Ge et al., 2004). Several subsequent proteome studies in the *mdx* mouse investigated age-related changes in other muscles, such as the tibialis anterior muscle or diaphragm and proteome differences between different muscle groups (Carberry et al., 2013; Carberry et al., 2012a, b). In the GRMD dog model a quantitative proteomic study, using isotope-coded affinity tag (ICAT) profiling analyzed by MS, indicated that a central hallmark of muscular dystrophy in dogs is a defective energy metabolism, providing new insights into molecular pathology of DMD (Guevel et al., 2011). In the tailored pig model of DMD generated by our institute (Klymiuk et al., 2013), a proteome analysis revealed the extent of proteome changes in DMD muscle compared to WT. Analysis of 2-day-old versus 3-month-old DMD and WT pigs showed that proteome changes increase markedly with age. This reflects the progression of early pathological changes in this model (Frohlich et al., 2016). Carr et al. (2017) incorporated the different existing MS-based proteomic datasets of dystrophin-deficient tissue. The authors used proteome datasets of the *mdx* mouse, the GRMD dog and the dystrophin-deficient pig. Since in DMD patients proteome studies of skeletal muscle are still missing, they performed the intersection of data

of studies using blood and urine of DMD patients. The muscle proteome differs between species, individuals and muscles. However, the absence of dystrophin has a profound impact on the muscle proteome. The identification of differentially expressed proteins in DMD might unveil the molecular pathophysiology, leading to novel therapeutic targets or possible biomarkers to monitor disease progression.

Biopsy procedure, however, involves an invasive surgical intervention. It requires general anesthesia with special precautions in DMD boys in comparison to healthy individuals. Risks are mainly perioperative cardiac and respiratory complications due to anesthesia, but also rhabdomyolysis. Up to date, little is known about the short- and long-term consequences of muscle biopsy excision (Hayes et al., 2008; Verhaart et al., 2019). Therefore, this method indeed is a last necessary step for a reliable diagnosis, but an inappropriate tool concerning clinical trials.

3.3. Muscular function tests

Since up to now primary outcome measures are based on quantitative and manual muscle examinations and timed function tests, it is of current interest to develop classification systems and simplified scales to assess the functional abilities of DMD patients (Kim et al., 2018). Multidisciplinary rehabilitation assessment includes muscular function tests for the evaluation of mobility and disease progression.

In most early studies in children with neuromuscular diseases (NMD) in general, the muscle strength was measured and assessed. One example of this is the Brooke Scale (Brooke et al., 1981; Stuberg and Metcalf, 1988). Already in 1982, a scale especially devised for boys with DMD, called the Hammersmith Motor Ability Scale (HMAS) was developed (Scott et al., 1982). Used within a clinical setting, this test is satisfactory. However, validity and reliability have never been determined. Moreover, the test has been developed before the broad application of corticosteroids, thus excludes the detection of an improvement following treatment (Scott et al., 2012).

The more recent studies focus on functional scales. There are several general scales which can be utilized for the assessment of different NMD, such as the Gross Motor Function Measure (GMFM) and the Motor Function Measure (MFM) (Berard et al., 2005; Mazzone et al., 2010; Russell et al., 1989). Other scales are specifically designed to evaluate aspects of function in certain cohorts. The Hammersmith Functional Motor Scale (HFMS) for spinal muscular atrophy (SMA) types 2 and 3 in children, for example monitors the clinical progress and tests the motoric abilities in children with limited mobility (Main et al., 2003). An expanded version of this test evaluates the ambulatory patients in this certain cohort (O'Hagen et al., 2007). The test was further expanded to assess children with non-ambulant SMA using the Modified Hammersmith Functional Motor Scale (MHFMS) (Krosschell et al., 2006). This test especially is useful in young children (younger than 30 months) and thus may also be beneficial in young DMD boys (Connolly et al., 2013; Krosschell et al., 2011). As young DMD patients are an especially challenging population, another test, the Bayley III infant motor scale, which normally is used to test motor delay in the first years of life, has been validated and demonstrated as useful in very young DMD boys. The Bayley III test allows to study motor function in children less than 6 months old (Connolly et al., 2013). Another currently relevant functional scale, particularly designed for the evaluation of disease progression in ambulant DMD boys, is the North Star Ambulatory Assessment

(NSAA). This test of Scott et al. (2012) is an adaption of the HMAS for DMD boys developed in 1982. The NSAA contains important disease milestones, already previously used in DMD boys, such as getting from sitting to standing, timed rising from the floor or the 10 m timed walk/run test. Furthermore, it includes new items that allow the detection of possible improvement due to treatment, such as running and hopping – aspects of function which usually are not observed in untreated DMD boys. NSAA performance takes only approximately 10 minutes to complete, has a high test-retest ability and a good intra- and inter-rater reliability. Last but not least, it is practical, requiring only minimal equipment for standardization. The NSAA is designated as reliable test and actual gold standard to score DMD motor ability (Cacchiarelli et al., 2011; De Sanctis et al., 2015).

A simple but regularly applied global assessment of the endurance and ability to walk, as well as of the evaluation of functional mobility in DMD patients is the 6-minute walking test (6-MWT) (Pane et al., 2014). It describes the distance walked over a period of 6 minutes. The 6-MWT is used to assess functional capacity in several different diseases (McDonald et al., 2010). For the measurement of walking skills at baseline, functional capacity and assessment of disease progression it is useful in DMD patients. Furthermore, it is regularly used as additional evaluation method for muscle function in clinical trials of DMD therapies (Goemans et al., 2011; Pane et al., 2014). The 6-MWT is simple to apply, accurate, well-tolerated and reproducible (Anonymous 2002). Pane et al. (2014) refers to the 6-MWT as the primary outcome measure in most of clinical trials of DMD. However, since DMD patients fall frequently, safety, feasibility and accuracy of this test might be compromised (McDonald et al., 2010).

The NSAA and timed functional tests have a high reliability and validity. They are foundational clinical assessments of muscle function in the ambulatory period of DMD patients and thus should be done every 6 months (reviewed in Birnkrant et al., 2018b).

A new Comprehensive Functional Scale for DMD (CFSD) and accompanying Ambulatory Functional Classification System for DMD (AFCSD) have been developed based on other previously published classification systems. The CFSD only, already consists of 21 items and 78 sub-items (Kim et al., 2018). This new functional assessment was established in 2018. It appears as rather complex evaluation scale, and might thus be not practical in use. To date only preliminary evaluation of CFSD and AFCSD exist.

There are several functional tests to assess muscular function in DMD patients. First of all, the great number of different functional scales might complicate the comparison of the results of different clinical trials. Moreover, lack of understanding and motivation, especially in young children, may affect the performance outcome (Geiger et al., 2007). Cognitive impairment and behavioral challenges in some individuals with DMD can additionally exacerbate the potential problems of functional tests (Hinton et al., 2007). Last but not least, muscular function tests are only feasible in ambulant DMD patients, excluding the evaluation of disease progression in non-ambulatory individuals with DMD. However, non-ambulant patients make up the majority of the patients, since the average age at loss of ambulation is about 10.5 years and the median survival of the patients is 30 years (Straub et al., 2016).

3.4. Biomarkers in DMD

A biomarker is defined as "a characteristic that is objectively measured and evaluated as an indicator of normal biological processes, pathogenic processes, or pharmacologic response to therapeutic intervention" by the Biomarkers Definitions Working Group of the National Institutes of Health (NIH) (Anonymous 2001). This definition includes prognostic, as well as diagnostic biomarkers, and biomarkers, that indicate the response to a therapeutic agent (reviewed in Aartsma-Rus and Spitali, 2015). In DMD there are several different kinds of biomarkers which aim to quantify disease pathology and progression. Biofluid markers, found in serum, urine and saliva, occur due to passive protein leakage or an active release of proteins in the circulatory system. Primary tissue markers are compounds of the dystrophin glycoprotein complex. Secondary muscle tissue markers are for example cellular stress proteins, metabolite transporters and mitochondrial enzymes. Last but not least, there are several noninvasive imaging biomarkers (reviewed in Dowling et al., 2019).

3.4.1. Biomarkers in body fluids

3.4.1.1. CK, AST, ALT, LDH in blood serum

An elevation of blood serum creatine kinase (CK) level counts as important indicator for DMD. CK plays a major role in tissues with fluctuating energy demands, like brain and muscle (Schlattner et al., 2006). It catalyzes the reversible reaction of creatine and adenosine triphosphate (ATP) forming phosphocreatine and adenosine diphosphate (ADP) (reviewed in Wallimann et al., 1992). There exist mitochondrial and cytosolic CK isoenzymes. The elevation of circulating cytosolic CK isoforms in serum is tissue-specific. The circulating isoform CK-BB rises after brain damage, CK-MB after acute myocardial infarction. The myofibrillar CK-MM is present in skeletal muscle, its elevation in serum indicates muscle damage (Ebashi et al., 1959; Koch et al., 2014; Schlattner et al., 2006). In the case of muscle injury, cell membrane permeability increases, allowing CK-MM to leak into interstitial fluids. This results in elevated circulating CK-MM in blood serum. The quantification of serum CK levels is low in cost and an easy to apply measurement method (Ciafaloni et al., 2009; Koch et al., 2014). CK-MM hence is routinely measured and proposed as best biomarker for skeletal muscle damage in general (reviewed in Koch et al., 2014; McLeish and Kenyon, 2005).

CK in newborn infants with DMD is already severely increased. As a result, the routine measurement is discussed as potential newborn screening method for DMD (Zellweger and Antonik, 1975). However, it has to be noted, that there are several other causes for a CK elevation, such as other hereditary forms of muscular dystrophy, injuries or traumas, recent bacterial or viral infections, hypothyroidism or drugs. Even though CK under the named differential diagnoses rarely approaches the levels found in DMD patients, false positive diagnosis need to be seriously taken into account and should be avoided (reviewed in Verma et al., 2010). A single-tier newborn screening, only based on increased CK levels at birth, as it was introduced in many countries, therefore strictly requires a re-testing at around 6-8 weeks of age (reviewed in Mendell and Lloyd-Puryear, 2013). A lasting CK elevation is an indicator but still no prove for the disease. Diagnosis of DMD needs to be confirmed by further methods, such as genetic testing (reviewed in Birnkrant et al., 2018b). Last but not least, since only limited data on the impact of an early diagnosis and an early initiation of therapy in DMD exist, so far there are restrictions of regular

screenings for DMD in newborns (Kemper and Wake, 2007).

Not only newborn screening benefits from CK as diagnostic marker in DMD. Using CK as indicative measurement in children displaying early clinical symptoms of DMD is recommended but yet underutilized (Ciafaloni et al., 2009). Typically, in patients with DMD, CK levels are severely elevated, ranging between 5000 and 150 000 IU/L (normal <200 IU/L) (reviewed in Verma et al., 2010). Regular measurements show a CK peak between 1 and 6 years of age and a decrease with age due to the replacement of muscle tissue by connective and fatty tissue (Zatz et al., 1991). Elevated CK levels consequently indicate a floride, i.e. active, state of the disease. Thus, as CK elevation is directly associated with muscle damage, the parameter can also be utilized as biomarker in therapeutic trials. However, it is discussed to be of little use here, as a decline of CK can stand for both, the reduction of CK-leakage due to the success of a therapeutic approach or a further decrease of muscle quality (reviewed in Aartsma-Rus and Spitali, 2015; Jensen et al., 2017).

Interestingly, in 1972 observations of an individual with DMD already showed, that CK levels may vary between different measurement timepoints, sometimes being only mildly increased and years after being elevated severely (Bradley et al., 1972). A reason for varying CK levels could be hemolysis due to the procedure of blood collection. Perovic and Dolcic (2019) in their study examined the influence of hemolysis on clinical chemistry parameters, and described a hemolysis interference for CK. For CK-MB even clinically significant differences were detected (Koch et al., 2014). Other reasons for varying serum CK levels are, for example, seasonal and an intra- and interindividual variation (Nicholson et al., 1985; Percy et al., 1982). Summarizing, CK evaluation as indicator for DMD, as informative biomarker about the clinical course of the disease, or as diagnostic biomarker in therapeutic trials is reasonable. Nevertheless, for a reliable clinical assessment CK has always to be considered together with several other clinical parameters.

Serum analysis of DMD patients will not only reveal the presence of elevated CK. Persistently elevated serum activities of transaminases, i.e., aspartate aminotransferase (AST) and alanine aminotransferase (ALT), together with a negative diagnostic workup for a hepatic dysfunction (e.g. gamma GT is not elevated), can also be indicative for DMD and should be considered, although the reason for this is so far unexplained (reviewed in Aartsma-Rus et al., 2016; Birnkrant et al., 2018b; Verma et al., 2010). Less commonly, DMD is considered due to increased serum enzyme concentration of lactate dehydrogenase (LDH) (reviewed in Birnkrant et al., 2018b).

3.4.1.2. Emerging DMD biomarkers in blood

There is an entire list of emerging biomarkers in body fluids, which are found to be altered in DMD patients and animal models for DMD compared to healthy controls (HC).

Concerning the coagulation cascade, in serum a peptide of coagulation factor XIIIa was for example identified as discriminator between dystrophin-deficient *mdx* mice and wild-type (WT) controls (Alagaratnam et al., 2008). Several more up- and down-regulated factors in plasma samples of *mdx* compared with WT mice were identified. Among these is fibrinogen, another important factor in the coagulation cascade. It was shown to be increased in abundance in dystrophic mice (Colussi et al., 2010) as well as in DMD patients (Hathout et al., 2014; Nadarajah et al., 2012). Moreover, fibrinogen was shown to be accumulated in dystrophic muscles of DMD

patients and *mdx* mice, and it was speculated to promote inflammation and to be linked to the formation of fibrotic tissue (Vidal et al., 2008).

Concerning serum lipids, significantly higher triglycerides, phospholipids, free cholesterol, cholesterol esters and total cholesterol concentrations were measured in DMD patients compared to healthy controls (HC) (Srivastava et al., 2010).

Another discussed serum biomarker for DMD is fibronectin, a glycoprotein. Fibronectin is a major component of the ECM. Significantly increased levels in DMD patients compared to age-matched healthy subjects are found (Cynthia Martin et al., 2014).

Matrix metalloproteinase-9 (MMP-9) is another potential serum biomarker in individuals with DMD. Longitudinal studies in DMD patients on corticosteroid treatment showed that MMP-9 levels were significantly elevated in older, non-ambulatory patients. Moreover, MMP-9 was shown to increase significantly with age. It is therefore discussed as biomarker for the assessment of disease progression (Hathout et al., 2014; Nadarajah et al., 2011). However, studies in patients on corticosteroid treatment did not allow the discrimination of effects derived from aging or the influence of the therapy on MMP-9 (Zocevic et al., 2015).

In a new proteome profiling study of individuals with DMD not yet treated with glucocorticoids, compared to HC, 107 elevated and 70 decreased proteins were identified in serum. Elevated proteins mainly were of muscle origin and cell adhesion proteins, but also ECM and pro-inflammatory proteins. Proteins that were found to be decreased, are mainly involved in cell adhesion processes, cell differentiation or have to do with growth factors. Interestingly, subsequent treatment of the same cohort with glucocorticoids allowed to examine the impact of therapy on the detected serum biomarkers. 17 proteins, associated with DMD, were shown to normalize under treatment. 80 proteins, not associated with DMD, were shown to be up- or downregulated after treatment, illustrating a broader effect of glucocorticoids (Hathout et al., 2019). These results are important, since most current therapies and therapy trials in DMD patients contain glucocorticoid treatment (reviewed in Aartsma-Rus and Spitali, 2015).

Several other elevated proteins, mainly of muscle origin, were identified in serum of DMD patients. Among these were for example myofibrillar proteins, such as titin (connectin) and myosin, glycolytic enzymes, such as aldolase, transport proteins, as for example fatty acid binding protein and myoglobin and others, like CK-MM (Hathout et al., 2014).

Another important group of potential biomarkers for the diagnosis of DMD in early stages, and the analyses of progression and treatment, are microRNAs (miRNAs). miRNAs are small non-coding RNAs, which function in the post-transcriptional regulation of gene-expression in a sequence specific manner by inducing mRNA degradation or translational repression. In the control of skeletal muscle and cardiac development, several essential miRNA families were identified. miRNAs are known to control in part regenerative myogenesis, and the differentiation, maintenance and repair of muscle (reviewed in Hrach and Mangone, 2019). Due to muscle cell damage specific muscle-miRNAs (dystromiRs) leak into the bloodstream. Thus, dystromiRs are extracellular dystrophy-associated miRNAs, whose levels correlate with the severity of the disease. Up to now, several miRNAs were found to be up- or downregulated in DMD patients or animal models for DMD compared to healthy controls (Becker et al., 2016; Cacchiarelli et al., 2011;

Catapano et al., 2018; Llano-Diez et al., 2017; Mitchell et al., 2008; Zaharieva et al., 2013).

3.4.1.3. Emerging DMD biomarkers in urine

Since taking blood samples still is minimally invasive, some recent studies focused on potential urine-accessible metabolites as biomarkers associated with DMD. Urine can be collected easily, on multiple time-points and noninvasively (reviewed in Dowling et al., 2019; Thangarajh et al., 2019). Titin, which is already named above as a serum biomarker, was also detectable in urine of DMD patients (Matsuo et al., 2019; Rouillon et al., 2014). Equally, the L-arginine/nitric oxide pathway (L-Arg/NO), which regulates endothelial function and was found to be impaired in DMD patients, was reported to be affected in urine (and plasma) of individuals with DMD (Horster et al., 2015). A major PGD_2 metabolite, tetranor-PGDM, was observed to be elevated in urine of DMD patients. Even longitudinal changes were detectable, as the metabolite was found to increase further with age. This supported the hypothesis, that prostaglandin D_2 (PGD_2)-mediated inflammation is involved in the DMD pathology (reviewed in Aartsma-Rus and Spitali, 2015; Nakagawa et al., 2013; Takeshita et al., 2018). Several further studies of candidate biomarkers in urine of DMD patients exist (Catapano et al., 2018; Rouillon et al., 2018). However, until now none of these urine biomarkers reached practical implementation.

3.4.2. Noninvasive imaging biomarker in DMD

Until now, clinical trials generally rely on measures of muscle function and strength (Zaidman et al., 2017). However, noninvasive imaging modalities are valuable clinical and research tools for monitoring disease progression in DMD. Imaging biomarkers can be used for cardiac and respiratory assessment, but also for monitoring progressive alterations in muscle over time.

3.4.2.1. Echocardiography and Holter monitoring

Echocardiography (ECG) allows the monitoring of cardiac dysfunction in DMD patients (reviewed in Birnkrant et al., 2018b; Cheeran et al., 2017; Silva et al., 2007). As noninvasive imaging method for cardiac assessment it is recommended for young patients (before the age of 6-7 years) as it is well tolerated and does not require anesthesia. By ECG, the ejection fraction (EF) and cavity dimensions can be noted, thus enabling the detection of left ventricular dysfunction or dilated cardiomyopathy (Barison et al., 2009; reviewed in Birnkrant et al., 2018a). In the late non-ambulatory stage of DMD patients, it is recommended to include periodic 24 h Holter monitoring in surveillance (reviewed in Birnkrant et al., 2018a).

3.4.2.2. Quantitative ultrasound assessment

Fatty infiltration as well as increased interstitial fibrous tissue among dystrophic skeletal muscle of DMD boys results in an increased echo intensity in standard ultrasound B-mode imaging (Pillen et al., 2009; Reimers et al., 1993). The echo intensity, also known as the grey value of the image, is determined by the amount of returning echoes per square area. The changes in echo intensity can be quantified by two different methods: by quantitative backscatter analysis (QBA) the amplitudes of the sound-waves, which are scattered back from the tissue, are directly measured during imaging procedure; the backscattered amplitudes can also be analyzed after the imaging process, after compression into greyscale levels

(GSL) received from the images. Both methods are shown to perform similarly (Rutkove et al., 2014; Shklyar et al., 2015; Zaidman et al., 2017). Skeletal muscle echogenicity can visually be graded, for example by the Heckmatt scale, ranging from normal (grade I) to very strong muscle echo and complete loss of bone echo (grade IV) (Heckmatt et al., 1982).

Quantitative ultrasound (QUS) was shown to identify differences earlier than simple functional measures, such as the 6-MWT and supine-to-stand test (Rutkove et al., 2014; Zaidman et al., 2017). A near-significant association between QUS and the NSAA functional scale was demonstrated (Rutkove et al., 2014). Moreover, QUS was stated to detect disease progression in DMD (Zaidman et al., 2017). QUS is a noninvasive and painless imaging modality, demanding low effort. As it does not require anesthesia, it is especially useful in the assessment of skeletal muscle in young children with DMD.

3.4.2.3. Magnetic resonance imaging and spectroscopy

One of the preferred approaches to noninvasively diagnose disease pathology and progression in individuals with DMD is magnetic resonance imaging (MRI). MRI benefits of a high soft tissue contrast with exquisite detail and provides volumetric information. It avoids harmful ionizing radiation, unlike for example computed tomography (CT) or x-ray and is therefore generally applicable to pediatric patients (Magrath et al., 2018).

With regard to cardiac assessment in individuals with DMD, cardiovascular magnetic resonance imaging (CMR) is the noninvasive imaging method of choice for assessing cardiac dysfunction and evaluating the degree of cardiomyopathy (reviewed in Birnkrant et al., 2018a; Cheeran et al., 2017; Magrath et al., 2018). CMR provides higher sensitivity compared to ECG and is recommended already at early ages (Buddhe et al., 2016). It enables to detect the earliest signs of cardiomyopathy, long before the onset of clinical symptoms (Magrath et al., 2018). A typical cardiac MRI protocol, to assess cardiac function and morphologic changes in DMD patients, incorporates several different techniques: black-blood imaging for the evaluation of thoracic and cardiovascular anatomy, dynamic (cine) white-blood imaging (balanced steady-state free precession) for the assessment of global and regional cardiac function, contrast enhanced perfusion imaging and late gadolinium enhancement (LGE) for the assessment of myocardial fibrosis (Silva et al., 2007). As a result, CMR allows to note early heart failure symptoms, such as tissue degeneration and myocardial structural changes (e.g. myocardial fibrosis and fibrofatty involvement), just as myocardial function and regional wall motion abnormalities (normal/ mild or severe hypokinesia/ akinesia, dyskinesia). Cardiac mass, left ventricular (LV) remodeling and wall thickening as well as abnormal chamber dimensions can be assessed. End systolic and end diastolic time frames can be identified, allowing for example to detect depressed LV ejection fraction (LVEF) (Barison et al., 2009; reviewed in Birnkrant et al., 2018a; Magrath et al., 2018; Silva et al., 2007). There are several alternative MRI methods to assess cardiovascular function in DMD. Pre- (native) and postcontrast parametric "spin-lattice" relaxation time (T1-weighted mapping) (Bell and Jones) techniques, for example, are emerging cardiac biomarkers for early myocardial microstructural remodeling (such as diffuse fibrosis), enabling to estimate extracellular volume fraction. However, these methods assist ancillary to the named standard biomarkers, but are not widely used (Magrath et al., 2018). One reason for this is, that for

implementing T1 mapping in clinical routine, the characteristic range of normal T1 values at a particular magnetic field strength must be established to identify deviations from the normal range (Bottomley et al., 1984). Apart from magnetic field strength, a plethora of factors influence T1 time values, such as protocol parameters, motion, sequence design and scanner adjustments. Altogether, these factors highly reduce comparability between different sites over time. A further limitation in the comparability of T1 times between different study sites is, that analysis of parametric T1 maps often uses relatively restricted in-house developed tools, early-stage commercial packages, or manufacturer prototypes. Therefore, highly adaptable and robust tools for standardized T1 quantification and map presentation are desirable. Furthermore, analysis is not standardized and often based on expert knowledge (reviewed in Messroghli et al., 2017).

Since current clinical trials mostly rely on ambulatory endpoints (e.g. muscular function tests), thereby excluding non-ambulatory patients, MRI and magnetic resonance spectroscopy (MRS) are emerging techniques providing promising biomarkers for muscle quality or primary outcome measures for all DMD patients. MRS is capable to measure the concentrations of different chemical components within tissues and is based on the same physical principles as MRI. As DMD muscles show compositional and structural changes, these approaches can be used to assess the following: alterations of the maximal muscle cross-sectional area (mCSA), muscle damage, inflammation and edema and, at a later stage of the disease, fat infiltration and fibro-fatty replacement (Forbes et al., 2013; Mathur et al., 2010). The visualisation of these pathologic changes depends on different specialized imaging protocols, which provide quantitative outcome measures (Straub et al., 2016). mCSA, for example, can be measured using longitudinal relaxation time (T_1) weighted MRI (Mathur et al., 2010). High sensitivity for detecting DMD disease pathology and progression was shown for two quantitative MR measures: transverse relaxation time (T_2) weighted magnetic resonance measures (MRI-T_2) and intramuscular fat fraction (FF) (Willcocks et al., 2016). Both methods are most commonly used in (multicenter) clinical trials to assess disease severity, activity and progression by MRI (Barnard et al., 2018; Forbes et al., 2013; Forbes et al., 2014; Willcocks et al., 2016). FF can for example be measured by 3-point chemical shift-encoded (Dixon) MRI or proton MRS (^{1}H-MRS). With ^{1}H-MRS the separation of water and lipid signal is possible. For a more targeted evaluation of inflammation and damage in muscle tissue, $^1H_20$ T_2 can be used. FF is not only shown to correlate with disease progression but also with the outcome of functional tests (Willcocks et al., 2016). However, there are several limitations to these methods indicating, that other MRI variables need to be established. As $^1H_20$ T_2 primarily detects inflammation and damage, it is not suitable for tracking disease progression in terms of fibrosis. Consistent with its sensitivity to inflammation, $^1H_20$ T_2 is highly responsive to corticosteroid therapy and might thus be more appropriate for clinical trials with anti-inflammatory therapeutics (Arpan et al., 2014). In MRI-T_2, water T_2 changes are nonspecific due to the sensitivity to edema, inflammation, necrosis and fibrosis on the one hand, and lipid on the other hand (Straub et al., 2016). Moreover, MRI-T_2 is influenced by treatment with corticosteroids. In addition, the measurement of FF has poor prognostic value, since there is a high inter- and intrasubject variability (Gerhalter et al., 2019). Furthermore, adipose infiltration of muscles tissue has a very heterogeneous distribution in DMD patients (Chrzanowski et al., 2017; Hooijmans et al., 2017).

A relatively new emerging MRI protocol is ^{23}Na MRI, to calculate total sodium

concentration (TSC) and intracellular-weighted ^{23}Na signal (ICwS) in muscle tissue. As intracellular sodium concentration is shown to increase severely due to loss of dystrophin and resulting muscle cell damage, ^{23}Na MRI is a more promising tool for informations about early pathological changes (Gerhalter et al., 2019; Glemser et al., 2017), but its capability is highly restricted to a limited number of specialized ultra high-field MRI sites worldwide and it is not established in the clinical routine.

Even if MRI exams may become shorter and simpler and the acceptance for younger patients improves (reviewed in Magrath et al., 2018), very young children are usually not able to cooperate for MRI procedure, such as breath holding for periods of 5 to 20 seconds for cardiac MRI. Thus, MRI in patients younger than 6-7 years requires anesthesia, harboring specific risk for DMD patients. Hence, these procedures are typically avoided in early live periods, when they are not tolerated (Birnkrant et al., 2018a).

3.4.2.4. Other noninvasive imaging modalities

When DMD patients, at a later stage of the disease, complain about cardiac rhythm disturbances, event monitors, recording for a longer period of time, can additionally be indicated for cardiac surveillance (reviewed in Birnkrant et al., 2018a).

Another noninvasive imaging tool to assess muscle condition in DMD patients is electrical impedance myography (EIM). The method is based on applied low-electric alternating current, dissipating as it travels through a substance (here: muscle), and thereby producing a measurable voltage (reviewed in Rutkove, 2009). Localized impedance changes indicate underlying muscle structure alterations. EIM is painless and requires low effort (Rutkove et al., 2014). However, there are only few studies about EIM in DMD and many questions to the mechanism remain open. Thus EIM still needs to be refined (reviewed in Rutkove, 2009).

An emerging tool to assess clinical anisotropy for monitoring muscle degeneration in DMD is Viscoelastic Response (VisR) ultrasound. The extent of anisotropy is given by the ratios of VisR relative viscosity (RV) or relative elasticity (RE). RE and RV are measured with parallel versus perpendicular to muscle fiber alignment oriented asymmetric radiation force. VisR ultrasound shows significantly higher RE and RV anisotropy ratios in rectus femoris muscle of DMD patients compared to HV. However, even if VisR ultrasound is stated to reflect changes in viscous and elastic anisotropy associated with muscle degeneration, investigations in other muscle groups do not exactly reflect these results. Furthermore, to date, only a pilot *in vivo* clinical feasibility study exists (Moore et al., 2018).

Concerning the appearance of gastrointestinal symptoms, such as constipation and gastro-oesophageal reflux, a scintigraphic gastric emptying scan, to assess gastric emptying time, can be useful (Birnkrant et al., 2018b).

4. Multidisciplinary treatment and emerging therapies for DMD

DMD disease requires exhaustive clinical multidisciplinary management. Up to date, despite corticosteroid treatment, there exists no effective therapy for DMD. However, several genetic approaches have been made in the last few years (reviewed in Guiraud and Davies, 2017).

4.1. Multidisciplinary treatment for DMD

A main aspect of multidisciplinary care in DMD patients is the treatment with glucocorticoids. Glucocorticoids, as anti-inflammatory and immunosuppressant drugs, slow down muscle deterioration. This causes prolongation of ambulation (estimated 3-year median delay of LoA), prevention of scoliosis surgery and maintained respiratory and upper limb function (reviewed in Bello et al., 2015a; Birnkrant et al., 2018b). Prednisone and prednisolone, typical representatives for synthetic glucocorticoids, however, show significant adverse effects in long-term treatment. Side effects include, in order of frequency, weight gain, adrenal suppression and insulin resistance (cushingoid appearance), growth retardation, behavioral changes, bone morbidity, cataracts, and skin abnormalities (Bello et al., 2015a; Hoffman et al., 2019). These effects are in particular problematic in very young and elderly patients (Hoffman et al., 2019). However, glucocorticoid initiation in younger children with DMD, not yet affected from significant physical decline, was shown to be especially beneficial (Merlini et al., 2012). Deflazacort, a synthetic corticosteroid with labelled indication especially for DMD, showed a greater effect on extending the preservation of independent ambulation than prednisone/prednisolone treatment. However, the same adverse effects as for prednisone or prednisolone were observed for deflazacort, with the sole difference of less weight gain (Bello et al., 2015a). A novel synthetic steroid for treatment of DMD is vamorolone. Vamorolone seems to optimize the anti-inflammatory effect, traditional for steroids. Of importance, suspectibility to bone morbidity, adrenal suppression and insulin resistance appeared to be less pronounced for vamorolone relative to other published trials of glucocorticoid treatment (Hoffman et al., 2019).

Another important aspect in the multidisciplinary care for DMD patients at all ages is physiotherapy to prevent contractures and deformity. Postural correction, as well as orthotic intervention and splinting, are necessary at later stages of the disease. To further improve quality of life and to extend the overall lifespan, physical aids, such as wheelchairs and medical devices for assisted respiration are used. Rarely, orthopaedic surgery, such as posterior spinal fusion, is required (reviewed in Birnkrant et al., 2018b; Hrach and Mangone, 2019).

As soon as any signs of heart failure are detectable, or latest at the age of 10 years, specific treatment should be initiated for patients with DMD (reviewed in Birnkrant et al., 2018b). Cardiovascular medication regimes vary in individuals with DMD and show different efficiency at treating the DMD associated cardiomyopathy (Cheeran et al., 2017). As first-line therapy, patients in young adulthood receive angiotensin-converting enzyme (ACE) inhibitors or angiotensin II receptor blockers (ARBs) (reviewed in Birnkrant et al., 2018a; Cheeran et al., 2017). Only about a third of DMD patients receive β-blockers. Few DMD patients are on other guideline-directed medications for heart failure, such as diuretic therapy and mineralocorticoid receptor antagonists. Additionally, steroid therapy is suggested to delay the progression of cardiomyopathy and therefore, to improve the overall survival (reviewed in Cheeran et al., 2017; Verma et al., 2010).

Gastrointestinal and nutritional management is indispensable for DMD patients with complications, such as weight loss or gain, swallowing dysfunction, mandibular contracture, constipation or low bone density. The management includes general nutrition plans, nutrient supplementation (e.g. 25-hydroxy-vitamin D, multivitamin or mineral supplement), as well as daily intake of osmotic laxatives (e.g. polyethylene glycol, or lactulose) (Birnkrant et al., 2018b).

4.2. Emerging treatments for DMD

Considerable progress, concerning the treatment of DMD, has been made in the past years in genetic approaches. There is a full list of treatment trials for DMD, which changes continually. An update on the ongoing trials is available at the WHO International Clinical Trials Registry Platform or at ClinicalTrials.gov (reviewed in Birnkrant et al., 2018b).

4.2.1. Cell therapy

Muscle precursor cells of one genotype are able to fuse with host muscle fibers of another genotype and then to express the donor genes (Partridge et al., 1989). Based on this, the transplantation of myoblasts of healthy donors into skeletal muscle of DMD patients, with the main goal to create a pool of dystrophin competent satellite cells, is one therapeutic approach studied for treatment of DMD (Bajek et al., 2015; Sun et al., 2019). Partridge et al. (1989) showed, that transplantation of normal muscle precursor cells in skeletal muscle of dystrophic *mdx* mice induces dystrophin expression. In a DMD patient, intramuscular cell transplantation of normal muscle precursor cells even showed long-term expression of donor derived dystrophin (Skuk et al., 2007). However, several other studies in DMD patients state that there is either no or only low expression of donor derived dystrophin (Karpati, 1991; Mendell et al., 1995) and that there are no functional improvements, except for one study (Huard et al., 1992). Compared to myoblasts, muscle stem cells, with their regenerative ability and their capacity to renew themselves, have a strong therapeutic advantage (Sun et al., 2019). Stem cell transplantation, using muscle satellite cells transduced with micro-dystrophin, was shown to regenerate *mdx* dystrophic muscles (Ikemoto et al., 2007). The transplantation of a single mouse muscle fiber, containing only few or even a single satellite cell, in mouse likewise showed better engraftment than myoblast transplantation (Collins et al., 2005; Sacco et al., 2008). In addition, experiments of transplanting human satellite cells into immunocompromised *mdx* mice led to a stable engraftment (Garcia et al., 2018). Equally, stem cell transplantation using bone marrow stromal cells showed potential as therapeutic agent (Dezawa et al., 2005). A recent study analyzed the effect of intracoronary allogeneic cardiosphere-derived cells (CAP-1002) administered by global intracoronary infusion in hearts of DMD patients with substantial myocardial fibrosis. Cell therapy here showed signals of efficacy on cardiac as well as on upper limb function (Taylor et al., 2019).

Up to date, several subsequent studies focus on stem cell-based therapies for DMD. However, there are many safety concerns and practical limitations (such as for example the small number of satellite cells that can be isolated from a muscle biopsy), which so far prevent the clinical application of human satellite cells. Another disadvantage of cell therapy is the low dissemination rate of satellite cells and the high rate of death among satellite cells after transplantation. Furthermore, systemic administration with the goal to reach all skeletal muscles including, for example, diaphragm, leads to the aggregation of satellite cells as microthrombi in small vessels, instead of the colonization of muscle tissue (Sun et al., 2019). The transplantation of allogeneic cells also requires posttransplantational immunosuppression to prevent rejection of the cells (Bajek et al., 2015).

4.2.2. Ribosomal read-through of premature termination codons

In 11% of individuals with DMD, a nonsense point mutation generates a premature termination codon (PTC) within the protein coding region of the mRNA. The PTC stalls translation, leading to an unstable and nonfunctional truncated dystrophin protein product (Bladen et al., 2015). By altering the RNA confirmation and hence reducing the codon-anticodon accuracy, aminoglycoside antibiotics, such as gentamicin, enable the read-through of PTCs by promoting the insertion of alternative amino acids at the position of the mutated codon. Thereby, dystrophin synthesis increases. However, aminoglycosides also have severe adverse effects when used long-term or at high dosage, such as renal and otic toxicity (reviewed in Guiraud and Davies, 2017; Linde and Kerem, 2008). PTC124, a new small organic molecule without antibiotic characteristics, was shown to read through disease-causing PTCs without displaying the severe side effects observed for aminoglycosides. It furthermore does not affect intended termination due to the stop codon localized at the end of the coding sequence (Linde and Kerem, 2008). Due to these properties, PTC124 is a promising genetic treat for DMD patients with the causal mutation being a nonsense mutation leading to premature termination of translation (Bushby et al., 2014; McDonald et al., 2017). PTC124 with the trade name translarna, in 2014, under its former name ataluren, gained approval by the European Commission for use in the European Union, as the first mutation-specific therapy in DMD (Ryan, 2014).

4.2.3. Utrophin modulators

Another therapeutic approach in DMD is the upregulation of the expression of the protein utrophin. Utrophin, a member of the spectrin superfamiliy, shares 80% homology with dystrophin, thus is an autosomal homologue of the protein. It is normally highly expressed during embryogenesis and is later progressively substituted at the sarcolemma by dystrophin. In adult muscle, utrophin can be found at neuromuscular and myotendinous junctions. The great structural and functional similarities between the two proteins allow for using utrophin as surrogate for dystrophin (reviewed in Guiraud and Davies, 2017; reviewed in Perkins and Davies, 2002; Song et al., 2019). As already stated above, in dystrophin-deficient *mdx* mice, the upregulation of utrophin is discussed to prevent the expression of the severe DMD phenotype. This thesis is supported by the generation of the utrophin null-*mdx* double knockout mice, which exhibit a severe dystrophic phenotype, lethal within several weeks after birth (reviewed in Perkins and Davies, 2002). Altogether, this gives rise to the approach of utrophin-derived therapies to treat dystrophin deficiency in DMD patients (Goyenvalle et al., 2011). In different animal models, such as the GRMD dog and the *mdx* mouse, a miniaturized utrophin encoding synthetic transgene was shown to be highly functional acting as surrogate to compensate the loss of dystrophin. Miniaturized utrophin was able to prevent most of the detrimental physiological and histological aspects, such as necrosis of muscle fibers and mononuclear cell infiltrates. Unfortunately, limitations to this method are set by the achievable adeno-associated viral (AAV) vector dose (Song et al., 2019). Ezutromid (SMT C1100), an utrophin modulator, was shown to reduce degeneration of musculature, leading to an improved muscle function in the *mdx* mouse (reviewed in Guiraud et al., 2015). Subsequently, first in pediatric clinical trials with SMT C1100 have been completed, reporting tolerability and safety for this agent (reviewed in Guiraud and Davies, 2017; Ricotti et al., 2016). There are other utrophin modulators, such as heregulin and resveratrol, aiming to upregulate

utrophin by modulating the utrophin promoter. However, these drugs were reported to be efficient in the *mdx* mouse, but clinical trials for DMD are still missing (Moorwood et al., 2011).

4.2.4. Delivery of mini- or microdystrophin via AAV vectors

Adeno-associated viruses (AAV) as vectors are not only capable to deliver miniaturized utrophin, but also used to deliver mini- and microdystrophin systems, thereby restoring dystrophin in DMD patients. In general, AAV vectors have clear benefits compared to other vector systems, e.g. they display non-pathogenicity and only minimal immunogenicity and they show an extensive tissue and cell tropism (e.g. muscle cells amongst others count as the most efficient targets), accompanied by site-specific integration and long-term persistence (reviewed in Athanasopoulos et al., 2000; Athanasopoulos et al., 2004). In mice, AAV vectors are shown to mediate high long-term transgene expression in muscle fibers (Fisher et al., 1997). However, a disadvantage is the size of the AAV genome (<5 kb), limiting the packaging volume and therefore the transgene capacity (reviewed in Athanasopoulos et al., 2004). To overcome this obstacle, dystrophin protein is reduced to its essential components. A rod-truncated micro-dystrophin is shown to ameliorate the dystrophic phenotype of *mdx* mice (Sakamoto et al., 2002; Yoshimura et al., 2004). As one approach, systemic in utero AAV delivery of micro-dystrophin in *mdx* mice to reach the dystrophin deficient fetuses, shows dystrophin-expressing muscle-fibers and a significant improvement of the dystrophic phenotype at 9 weeks after birth (Koppanati et al., 2010). In the GRMD dog, localized and systemic delivery of recombinant AAV vectors expressing a canine microdystrophin was shown to restore dystrophin expression, stabilizing the clinical symptoms (Le Guiner et al., 2017). Trials of AAV micro-dystrophin therapies in human DMD patients are partly completed or currently running (National Library of Medicine, 2019). So far, small adverse events were manageable and the treatment results in neuromuscular and respiratory function improvements (reviewed in Duan, 2018). However, a steep setback is a recently reported vector-dose-dependent severe immunotoxicity of AAV vectors in non-human primates and piglets (Hinderer et al., 2018). Concerning this, careful clinical monitoring and early laboratory evaluations for signs of toxicity is indispensable (Hinderer et al., 2018). Moreover, further studies in large animal models to cautiously approach non-toxic levels are essential.

4.2.5. Exon skipping by antisense oligonucleotides targeting RNA

In DMD, most mutations disrupt the ORF, whereas mutations where the ORF remains intact, lead to the synthesis of truncated dystrophin, resulting in the milder BMD. This less severe form of the disease exemplifies, that an internally deleted dystrophin can be functional. The spectrin-like rod domain, for example, in which most of the DMD causing mutations occur, is largely dispensable. Thus, splicing around a here located mutation can lead to the production of a truncated but functional dystrophin (Lu et al., 2003). Antisense oligonucleotide (AON)-mediated exon skipping aims to correct the ORF, and hence to restore the synthesis of partly functional dystrophin (Sharp et al., 2011). It thus converts an out-of-frame mutation in an in-frame mutation, inducing a BMD phenotype (Aartsma-Rus et al., 2009).

AONs are synthetic single-strand DNAs or RNAs with a length of 20 to 25 bases. The sequences are designed in a way, that they recognize and bind to a complementary sequence in the target RNA and modulate premature mRNA

splicing (reviewed in Nakamura and Takeda, 2009) by hiding specific exons from the splicing process or from translation. This leads to skipping of the target exon and thereby restoration of the ORF (Aartsma-Rus et al., 2009). The AONs 2′-O-methyl phosphorothionate AO (2OMeAO) and phosphorodiamidate morpholino oligomer (PMO) are most frequently used. To enhance their pharmaceutical properties, they differ from each other in chemical modifications of the oligonucleotides (reviewed in Nakamura and Takeda, 2009). PMO is largely unmetabolized, charge-neutral, and not linked to hepatotoxicity, immune or platelet activation. It thus provides properties, necessary for safety and tolerability (Mendell et al., 2016).

The approach is mutation specific. Nevertheless, as shown above, most deletions cluster in hotspot regions, allowing that AON-mediated skipping of a small number of exons is applicable to a relatively large number of patients. In theory, exon-skipping mediated by AONs, amounts to 83% of all DMD mutations, including deletions, small mutations and duplications (Aartsma-Rus et al., 2009). The therapeutic approach has been extensively tested in DMD mouse models, (Aoki et al., 2012; Sharp et al., 2011), in dog models of DMD (Mcclorey et al., 2006; Yokota et al., 2009), and has already been translated into clinical trials (Goemans et al., 2011; Van Deutekom et al., 2007). Eteplirsen is a PMO, designed to skip exon 51 in the *DMD* gene (Mendell et al., 2016). Exon 51 skipping restores the ORF of 13% of DMD patients. This is the largest targetable group of all individuals with DMD (Aartsma-Rus et al., 2009). In 2016, eteplirsen, with the trade name Exondys 51 (Sarepta Therapeutics), reached approval by the U.S. Food and Drug Administration (FDA) (Syed, 2016). Patients, treated with eteplirsen over a longer period of time, show no or only rare signs or symptoms of renal or hepatic toxicity, which is attributed to the chemistry of PMO (Mendell et al., 2016). Effects on cardiac muscle, however, have not been reported yet (reviewed in Guiraud and Davies, 2017). There are several ongoing or already completed trials of other exon skipping therapies, such as golodirsen (SRP-4053), amenable to exon 53 skipping, PRO045, designed to skip exon 45, or PRO044, designed for exon 33 skipping (National Library of Medicine, 2019; Van Ruiten et al., 2017). Nevertheless, as AONs target RNA, so far they are only able to cause very small, temporary increases of dystrophin. As a consequence, exon skipping drugs based on AONs require regular systemic application and it is not yet clear if the levels of restored dystrophin in patients are sufficient to affect the course of the disease (Muntoni and Wood, 2011).

4.2.6. Somatic gene editing

Better than exon-skipping on the level of RNA is a permanent gene correction. There are different genome editing tools, i.e. transcription activator-like effector nucleases (TALEN), zinc-finger nucleases (ZFN) or Cas9 endonuclease associated to clustered regularly interspaced short palindromic repeats (CRISPR/Cas9) (Gaj et al., 2013). Among these, the emerging CRISPR/Cas9 technology, first published by Jinek et al. (2012), which originally provides bacteria and archaea immunity to viruses, represents the most promising, simple and versatile RNA-directed tool for introducing double-stranded (ds) breaks into the DNA. The CRISPR/Cas9 enzyme mechanism in bacteria and archaea operates as adaptive defense system using antisense RNAs of past viral invasions as memory signatures. Cas9, as a CRISPR-associated endonuclease, uses a guiding sequence within a RNA duplex for the formation of base pairs with targeted DNA sequences. Thereby the endonuclease is able to introduce a site-specific DNA ds break (Doudna and Charpentier, 2014). In

January 2016, the emerging importance of CRISPR/Cas9 as preferred gene editing tool in DMD was stressed by two publications, published parallely. CRISPR-mediated genome editing was shown to restore the dystrophin expression in dystrophin deficient *mdx* mice. An intact *Dmd* ORF was restored by skipping the mutant *Dmd* exon 23. The gene editing components were delivered by adeno-associated viral vectors. Long et al. (2016) were able to show dystrophin expression in varying degrees not only in skeletal but also in cardiac muscle. In Xu et al. (2016), dystrophin expression in the transduced muscles was restored to about 50%. In 2018, the proof of concept was confirmed in a large animal model for DMD, a small group (n = 4) of deltaE50-dogs. The CRISPR/Cas9 system and the sgRNAs targeting a mutation specific region were delivered by adeno-associated virus serotype 9 (AAV9). Amoasii et al. (2018) were able to restore dystrophin expression levels ranging from 3 to 90% of normal. Cardiac muscle showed a dystrophin expression of up to 93% of normal.

CRISPR/Cas9 to date is the most powerful and promising method to heal inherited or from de novo gene mutation deriving diseases, such as DMD, by correcting the mutations responsible for the disease (Long et al., 2016).

III. ANIMALS, MATERIAL AND METHODS

1. Animals

In this work animals were produced by breeding from a herd of heterozygous female *DMD*$^{+/-}$ pigs inseminated with sperm of wild-type boars. One single German Landrace and Swabian-Hall mix sow with a heterozygous *DMD* exon 52 deletion (*DMD*Δ52) was used to establish the breeding herd. Following Mendelian inheritance, litters comprised male and female wild-type piglets (WT), heterozygous *DMD*Δ52 carrier pigs (*DMD*$^{+/-}$) and male *DMD*Δ52 knockout pigs (*DMD*$^{Y/-}$). As DMD is an X-chromosomal disease, the male offspring of a female carrier (*DMD*$^{+/-}$), receiving the X-chromosome with the mutated *DMD*, still have a Y-chromosome not carrying a *DMD* allele. Therefore, in the following, *DMD* knockout pigs are referred to as *DMD*$^{Y/-}$.

All animal experiments were carried out according either to the German Animal Welfare Act with permission by the Regierung von Oberbayern (55.2-1-54-2532-163-2014 and 02-16-137).

2. Material

2.1. Devices

Agarose gel elecrophoresis chamber	OWL Inc., USA
Artificial wet nurse unit	HCP-Technology, Notrup
AT-FS708 switch	Allied Telesis Inc., USA
BE400 incubator	Memmert, Schwabach
Benchtop 96 Tube working rack	Stratagene, USA
Centrifuge 5424 R	Eppendorf, Hamburg
Centrifuge 5430 R	Eppendorf, Hamburg
Centrifuge Rotina 380 R	Hettich Lab Technology, Tuttlingen
Daewoo KOC-154K microwave	Daewoo, South Korea
Excelsior AS A82310100	Thermo Scientific, USA
FiveEasy pH meter F20	Mettler-Toledo, USA
FreeStyle Freedom Lite blood glucose meter	Abbott Laboratories, USA
Grant JB Nova water bath	Grant Instruments, UK
Heating plate with magnetic stirrer RH basic	IKA-Werke, Staufen im Breisgau
HLC Cooling-ThermoMixer MKR 13	Ditabis, Pforzheim

IKA MS1 Minishaker Vortexer	IKA-Werke, Staufen im Breisgau
Incubator	Kendro Laboratory Products, Hanau
IndigoVision 9000 Encoder	IndigoVision Inc., UK
inoLab® pH meter 7110	WTW, Weilheim
Labcycler thermocycler	SensoQuest, Göttingen
Lax Disco Box	Lax Stalleinrichtung, Geldern
Leica DM IL LED Inverse microscope	Leica Microsystems, Wetzlar
MS-196VUT microwave	LG Electronics, South Korea
MSOT Acuity Echo protoype imaging system	iThera Medical, Munich
Pipettes (1000 µL, 200 µL, 100 µl, 20 µL, 10 µL, 2 µL)	Gilson Inc., USA
Platform Scale Kern und Sohn	Kern und Sohn, Balingen
Power Pac 300 gel electrophoresis unit	BioRad, Munich
Power Station 300 gel electrophoresis unit	Labnet International, USA
Precision balanace Chyo MJ-3000	YMC Co. Ltd., Japan
Precision balance Kern PCB 3500-2	Kern und Sohn, Balingen
RH Basic magnetic stirrer with heating	IKA, Staufen
Rotary microtome Microm HM 325	Thermo Scientific, USA
Rotilabo® mini centrifuge	Carl Roth, Karlsruhe
SANTEC color camera VTC-E220IRP	Santec, Ahrensburg
Select vortexer	Select BioProducts, USA
SimpliNano spectrophotometer	Thermo Scientific, USA
Smart Weigh GLS50 instecho	Better Basics, USA
TES 99 modular paraffin embedding system	Medite, Burgdorf
Thermo-Shaker TS-100	BioSan, Lettland
Tilting table Rocky®	Froebel Laboratory Technology, Lindau
Tissue cool plate COP 30	Medite, Burgdorf
Tissue float bath 1052	GFL, Burgwedel
UVP GelStudio PLUS	Analytik Jena, Jena
Zeiss Axiovert 200 M	Zeiss, Oberkochen

2.2. Chemicals

Acetic Acid (glacial)	Carl Roth, Karlsruhe
Agarose Universal	Bio&SELL, Nuremberg
Bromphenolblue Sodium Salt	Carl Roth, Karlsruhe
di-Sodium hydrogen phosphate, ≥ 99%, water free	Carl Roth, Karlsruhe
EDTA (Ethylenediaminetetraacetic acid)	Roth, Karlsruhe
Eosin Y (yellowish) powder (C.l. 45380)	Merck, Darmstadt
Ethanol Rotipuran® 99.8%	Carl Roth, Karlsruhe
Formaldehyde 37%	Carl Roth, Karlsruhe
GelRed® Nucleic Acid Gel Stain	Biotium, USA
Histokitt	Karl Hecht, Sondheim/ Rhön
Hydrochloric acid 25%	VWR, USA
Hydrogen chloride 37%	Carl Roth, Karlsruhe
Hydrogen peroxide 35% pure, stabilised	Carl Roth, Karlsruhe
Mayer's Hemalum Solution	Merck, Darmstadt
Methanol	Carl Roth, Karlsruhe
NaOH (Sodium hydroxide 2N)	Roth, Karlsruhe
Roti Histofix 4%	Carl Roth, Karlsruhe
Sodium chloride Emsure®	Merck, Darmstadt
Sodium dihydrogen phosphate monohydrate ≥ 98%	Carl Roth, Karlsruhe
Sodium hydroxide 2 mol / l (2 N) in aqueous solution, AVS TITRINORM	VWR, USA
Tissue Tek O.C.T.™ Compound	Sakura, Staufen
Tris (Tris-(hydroxymethyl)-aminomethane)	Roth, Karlsruhe
TRIS PUFFERAN® ≥ 99%	Carl Roth, Karlsruhe
Tri-Sodium- citrate 2-hydrate	Carl Roth, Karlsruhe
Tween®20	Sigma-Aldrich, Steinheim
Xylene	VWR, USA

2.3. Consumables

Cellstar® tubes (15 ml, 50 ml)	Greiner BioOne, Austria
Cover slips for histology	Carl Roth, Karlsruhe

Disposable plastic pipettes	Greiner BioOne, Austria
Disposable scalpel #21	Henry Schein, Munich
Embedding molds premium	Medite, Burgdorf
Feather® microtome blades S35	pfm medical, Cologne
FreeStyle Freedom Lite Blood glucose Test Strips	Abbott Laboratories, USA
Glass pasteurpipettes	Brand, Wertheim
K3E Monovette®	Sarstedt, Nümbrecht
LH Monovette®	Sarstedt, Nümbrecht
Microscope slides Marienfeld Superior™	Marienfeld Superior, Lauda-Königshofen
Microscope slides Star Frost®	Engelbrecht, Edermünde
NitriSense nitrile gloves	Süd-Laborbedarf, Gauting
Parafilm® M	Carl Roth, Karlsruhe
PCR reaction tubes (0.2ml)	Brand, Wertheim
Petri dish 94×16	Greiner BioOne, Austria
Pipet tips with filter	Greiner BioOne, Austria
Pipet tips	Eppendorf, Hamburg
Qualitative filter paper, grade 303, folded filter	VWR, USA
SafeGrip® latex gloves	SLG, Munich
Safe-Lock reaction tubes (1.5 ml, 2 ml)	Eppendorf, Hamburg
Serum Monovette®	Sarstedt, Nümbrecht
Tissue-Tek® Cryomold® (25 mm × 20 mm × 5 mm and 15 mm × 15 mm × 5 mm)	Sakura, Staufen
Uni-link embedding cassettes	Engelbrecht, Edermünde

2.4. Enzymes, oligonucleotides and antibodies

HotStarTaq DNA Polymerase	Qiagen, Hilden

Oligonucleotides

Oligonucleotides were manufactured by Thermo Scientific, USA.

DMDqf1	5´-TGC ACA ATG CTG GAG AAC CTC A-3´
DMDqfr1	5´-GTT CTG GCT TCT TGA TTG CTG G-3´
neoPf	5´-CAG CTG TGC TCG ACG TTG TC-3´
neoSr	5´-GAA GAA CTC GTC AAG AAG GCG ATA G-3´

Primary antibodies

Monoclonal mouse anti-DYS1 (Rod domain, no. NCL-DYS1; clone no. Dy4/6D3)	Leica Biosystems, Wetzlar

Secondary antibodies

Biotinylated goat anti-mouse IgG (no. 115-065-146)	Jackson ImmunoResearch, USA

2.5. Buffers and solutions

Unless indicated otherwise, water, deionized in a Easypure® II ultrapure water system (Werner, Leverkusen) or a Milli-RO 60 Plus device (Merck Millipore, USA), and termed as aqua bidest was used as solvent.

Buffers and solutions for PCR and agarose gels

DNA loading buffer (10×)
10% glycerol in aqua bidest.
Add 1 spatula tip of bromophenolblue.
Add 0.5 M NaOH until the colour turns blue.
Stored in aliquots at 4°C.

dNTP-mix
2 mM dATP, dCTP, dGTP, dTTP mixed in aqua bidest.
Stored in aliquots at -20°C.

GeneRuler^{TM} 1 kb DNA molecular weight standard
100 µl GeneRuler^{TM} 1 kb DNA molecular weight standard.
100 µl 6× loading dye.
400 µl aqua bidest.
Stored in aliquots at -20°C.

TAE buffer (50×)
242 g 2 M Tris,
100 ml 0.5 M EDTA (pH8.0),
57 ml gl acetic acid,
add 1000 ml aqua bidest.
Buffer was filtered, autoclaved and stored at room temperature. Before usage the buffer solution was diluted to single concentration with aqua bidest.

Buffers and solutions for DNA isolation

10 mM Tris/HCl, pH 8.0
10 mM Tris
Adjust pH to 8.0 with HCl.

Buffers and solutions for fixation and immunological detection

Phosphate-Buffer
40 g Sodium dihydrogen phosphate monohydrate
65 g di-Sodium hydrogen phosphate
mixed and dissolved in 1000 ml aqua bidest.

4% Formalin solution
100 ml Phosphate Buffer
100 ml Formaldehyde 37%
mixed in 800 ml aqua dest.

Eosin 1%
10 g Eosin Y powder
dissolved in 1000 ml aqua bidest, 80°C.
Cooled down to room temperature.
Add 1.5 ml gl acetic acid.
Filtrate the solution through a 5-13 µm filter.
Stored in darkness, at room temperature.
Note: Solutions stored over an extended period can be refreshed with gl acetic acid.

HCl 25%
675 ml hydrogen chloride 37%
mixd with 325 ml aqua bidest.

EtOH 70%
700 ml EtOH 100%
mixed in 300 ml aqua bidest.

EtOH 96%
960 ml EtOH 100%
mixed in 40 ml aqua bidest.

HCl-EtOH stock solution
1500 ml Ethanol 96%
mixed in 357 ml aqua bidest.
Add 14.2 ml HCl 25%.

0.5% HCl-EtOH solution
100 ml HCl-EtOH stock solution.
Add 100 ml 70% EtOH.

10 mM Sodium citrate buffer pH 6.0 for IHC
2.94g Tri-sodium-citrate 2-hydrate,
mixed in 1000 ml aqua bidest.
Adjust pH to 6.0 with HCl 25%.
Add 0.5 ml Tween 20.
Stored at room temperature for a maxium of 3 months.
For extended storage, store at 4°C.

10× TBS buffer for IHC
83.33 g NaCl
60.57 g Tris
Ad 1000 ml aq. bidest.
Adjusted to pH 7.6 using HCl 25%.
Concentrated stock solution of buffer was autoclaved.
The TBS stock was diluted to single concentration with aq. bidest. before use:
100 ml TBS stock
mixed in 900 ml aqua bidest.

2.6. Kits

DNeasy® Blood & Tissue Kit (250)	Qiagen, Hilden
HotStarTaq *Plus* DNA Polymerase	Qiagen, Hilden
ImmPACT™ DAB Peroxidase (HRP) Substrate	Vetor Laboratories, Biozol, Eching
nexttec™ Genomic DNA IsolationKit	Nexttec, Leverkusen
SK-4105	Vector Laboratories, USA
Vectastain® Elite ABC-Peroxidase Kit	Vetor Laboratories, Biozol, Eching

2.7. Other reagents

Buffer AE	Qiagen, Hilden
dNTP Set (100 mM)	Thermo Scientific, USA
Gene Ruler™ 1 kb DNA Ladder	Thermo Scientific, USA
Goat Serum	MP Biomedicals, USA
PCR Buffer 10 ×	Qiagen, Hilden

2.8. Software

ASReml	VSNi, Hemel Hempstead, UK
cLabs software v.2.66	iThera Medical, München
IndigoVision control center software v.3.19.5	IndigoVision Inc., UK
Leica Application Suite v.4.4.0	Leica Microsystems, Wetzlar
AxioVision V 4..10 or newer	Zeiss, Oberkochen
PathZoom LiveView	
Microsoft office Suite 2016 Standard	Microsoft, USA
Graphad Prism v.5.04 or newer	GraphPad Software, USA
UVP Software VisionWorks™ LS	Thermo Scientific, USA
ViewMSOT software v.3.8	iThera Medical, München

2.9. Drugs and supplementary feed

astoral® Pet Lax	almapharm, Wildpoldsried
Atropine sulfate (0.5 g/ 1 ml) (monohydrate)	B. Braun, Melsungen
Azaperone (Stresnil®)	Elanco, USA
Bonimal SB PowerMilk with blood plasma	Bonimal, Munich

Bromhexidinhydrochloride powder (Bisolvon®)	Boehringer Ingelheim, Ingelheim am Rhein
Buscopan®	Boehringer Ingelheim, Ingelheim am Rhein
Cloprostenol as sodium salt (Estrumate®)	MSD, USA
Embutramid, Mebezonium, Tetracain (T61®)	Intervet, Unterschleißheim
Fentadon (50 µg/ 1 ml)	Dechra, Aulendorf
Glucose solution 20%	B. Braun, Melsungen
HS Cat Laxative	Henry Schein, USA
Ketamine hydrochloride (Ursotamin® 10%)	Serumwerk Bernburg, Bernburg
Lactulose AL Syrup	Aluid Pharma, Laichingen
Oxytocin 10 IE/ml	cp-pharma, Burgdorf
Potassium choride 7.45%	B. Braun, Melsungen
Propofol 2% (20 mg/ 1 ml) MCT Fresenius	Fresenius Kabi, Bad Homburg
Stomach tube 80 cm × 4 mm	Henry Schein, USA
Ursoferran® (200 mg/ 1ml)	Serumwerk Bernburg, Bernburg
Xylazine	Serumwerk Bernburg,Bernburg

3. Methods

3.1. Animal generation

Generation of the *DMD*Δ52 founder sow

The exon 52 deletion of the porcine *DMD* gene was generated by the working group of Nikolai Klymiuk of our institute, according to Klymiuk et al. (2013), as described in Moretti et al. (2020). In summary, the targeting bacterial artificial chromosome CH242-9G11 was modified to carry instead of exon 52 a neomycin selection cassette. Subsequently, the modified BAC was nucleofected into a female primary kidney cell line (PKCf). Single cell clones were generated, according to Richter et al. (2012). From a batch of each cell clone genomic DNA was isolated. In order to screen for correctly targeted cell clones with a heterozygous deletion of *DMD* exon 52, the copy number of the *DMD* exon 52 was compared to the number of copies of two reference loci within the *POU5F1* and the *NANOG* genes (Klymiuk et al., 2013). Of 258 screened cell clones, 9 cell clones were identified to have one intact and one modified allele. For the generation of *DMD*Δ52 carrier sows, the cell clones with the heterozygous deletion of *DMD* exon 52 were used for somatic cell nuclear transfer (SCNT), carried out by Prof. Dr. Valeri Zakhartchenko, Dr. Mayuko Kurome, Dr. Barbara Keßler and Tuna Güngör of our institute. A total of 14 transfers of SCNT embryos to synchronized recipients were performed, resulting in

3 litters and 4 live piglets with the heterozygous *DMD*Δ52 (*DMD*$^{+/-}$) genotype. Only one animal could be raised to adulthood: clone #3040, the founder sow of the DMD breeding herd.

Generation of male *DMD*$^{Y/-}$ piglet clones

Furthermore, male *DMD*$^{Y/-}$ clones were generated by SCNT as decribed by Klymiuk et al. (2013).

3.2. Genotyping of piglets

Isolation of genomic DNA from tail biopsies

For the isolation of genomic DNA tail biopsies were obtained from individual piglets within 24 h after birth and stored at -20 °C until further processing. Genomic DNA was isolated with the nexttec™ Genomic DNA Isolation Kit for Tissues and Cells, according to the manufactorer's instructions. A very small amount of tissue (3-4 pieces with an approximate diameter of 0.5 mm) was incubated in a 1.5-ml reaction tube with 303 µl lysis buffer mix, using a thermomixer attuned to 60 °C and 1200 rpm for at least 30 min. Each sample additionally containted 3 µl DTT to increase the DNA yield and to ensure proper lysis of the tissue. After the tissue samples were dissolved, 120 µl of the lysate was purified on an equilibrated nexttec™ cleaning column. The eluate, containing the purified DNA, was subsequently used for PCR.

PCR

Two different sets of primers were used to detect the intact (WT) and the mutant sequence. The presence of the wildtype *DMD* allele, containing exon 52, was detected by the specific primer pair DMDqf1 and DMDqfr1. The neomycin selection cassette, replacing *DMD* exon 52, was detected by the primer pair neoPf and neoSr. All PCR components were mixed on wet ice to a final volume of 20 µl in 0.2 ml PCR reaction tubes. Previously isolated genomic DNA of WT (#5142) and *DMD*$^{Y/-}$ (#5143) piglets served as controls. As non-template control aq. dest. was used. Table 1 and 2 below list the details for master mix composition and PCR condition.

Table 1: Master mix composition for genotyping PCR.

aq. dest.	14 µl
dNTPs (2 mM)	2 µl
10× PCR Buffer	2 µl
Primer f (10 µM)	0.4 µl
Primer r (10 µM)	0.4 µl
Taq Polymerase (5U/µl)	0.2 µl
DNA template	1 µl

Table 2: Cycler protocol for genotyping PCR.

Denaturation	95 °C	5 min	
Denaturation	95 °C	30 s	35×
Annealing	62 °C	30 s	
Elongation	72 °C	30 s	
Final elongation	72 °C	5 min	
Termination	4 °C	5 min	

Agarose gel electrophoresis

After completion of PCR amplification, the presence of amplified DNA was proven by agarose gel electrophoresis. A 1.0% agarose gel was prepared, heating 1 g Universal Agarose per 100 ml 1 × TAE buffer solution in a microwave, panning from time to time, until total dissolution of the agarose. After cooling down the agarose gel to 50-60 °C, it was poured into a gel electrophoresis chamber, then left to settle. To each 20 µl PCR sample, 2.5 µl of a 1:250 mixture of GelRed® and DNA loading buffer (10×) (GR:BPB 1:250) was added. 1 × TAE buffer was used to fill the gel electrophoresis chamber. The samples as well as 6 µl GeneRuler™ 1 kb DNA molecular weight standard mixed with 2.5 µl of GR:BPB 1:250 were loaded into individual gel slots. DNA fragments were seperated according to their size by applying an electric current to the gel electrophoresis chamber. Afterwards, the DNA fragments were visualized under UV light. PCR products were analyzed in relation to the DNA molecular weight standard.

3.3. Rearing of *DMD*$^{Y/-}$ piglets

Rearing of the *DMD*$^{Y/-}$ piglets required birth monitoring and subsequent intense nursing during the first days of life, including supplementary feeding. A reduced general condition of newborn *DMD*$^{Y/-}$ piglets, due to a severe DMD phenotype, may lead to increased losses of animals resulting from severe energy deficit and/or crushing by the sow. To increase survival chances, different rearing conditions for suckling *DMD*$^{Y/-}$ piglets were validated. In the described breeding systems, straddling piglets received anti-straddle cuffs until independent standing and walking, if not described otherwise. Furthermore, all piglets received an intramuscular iron supplementation of 1 ml Ursoferran® 200 mg/ml on day 5 of life.

Motherless rearing in an artificial rearing unit

First, motherless rearing in an artificial rearing unit for piglets was studied. To allow colostrum intake, piglets remained with the sow during the first 12 h of life under supervision by a veterinarian. After these 12 h, the piglets were separated from the mother and transferred into an artificial rearing unit, the Lax Disco Box. The unit was equipped with slatted floor, constant access to fresh water and an automatic temperature regulation were provided. Supplementary milk was manually mixed and replaced every 8 h. Piglets were trained to independently drink milk substitute out of an installed drinking trough. In case piglets were not able to drink independently, they received milk substitute orally via a syringe. The supplementary milk was fed for the normal suckling period of 4 weeks, with slowly reducing the amount to none. After the first week of life, dry piglet feed was

supplemented progressively. After weaning, piglets were rehoused in barn compartments, equipped with heating lamps. During the whole rearing period piglets had *ad libitum* access to food and water.

48 h supervised suckling at the sows' teats

To reduce losses due to cruhsing by the sow, all *DMD*$^{Y/-}$ piglets were separated from the sow right after birth by a disconnecting device for the first 48 h of life. Suckling at the sows' teats only took place under the supervision by a veterinarian at approximately every 2 h. No further supportive actions were provided.

5 d intense nursing

During the first 5 days after birth *DMD*$^{Y/-}$ piglets were left with the sow and intense nursing by a veterinarian, as explained in the following, was ensured:

In a first approach, drinking at the sows' teats was taught to piglets, which were not able to suckle without support. Soonest 24 h after birth, weak *DMD*$^{Y/-}$ piglets were trained to drink milk substitute (Bonimal SB PowerMilk with blood plasma, Bonimal, Munich) independently out of a drinking trough, which was replaced after every 8 h. If independent milk intake out of the trough was not possible, adjuvant tube-feeding of a maximum of 20 ml milk substitute was offered. Pale *DMD*$^{Y/-}$ piglets received 0.5 ml Ursoferran® 200 mg/ml i.m. injected ahead of schedule, followed by the regular 1 ml Ursoferran® 200 mg/ml i.m. injection on day 5 of life. Birth weight was documented and weight was subsequently controlled every 24 h for the first 5 days of life. In case of strongly reduced general condition and severe weight loss, 10 ml glucose solution 20% was injected intraperitoneally (i.p.), and heat supply, to support the increase of body temperature, was provided. After the first week of life, dry piglet feed was supplemented. Additional milk subsitute feeding was maintained for the normal suckling period of 4 weeks, with slowly reducing the amount to none.

In a second approach all piglets appearing weak right after birth (before the completion of genotyping), received adjuvant tube-feeding of frozen stored and reheated colostrum to ensure sufficient colostrum intake and to avoid energy deficiency. Drinking at the sows' teats was taught to the piglets, which were not able to suckle without support. Venous blood for blood glucose measurement was gained by puncturing the lateral ear vein. Glucose levels were measured using a FreeStyle Freedom Lite blood glucose meter. If the blood glucose level of a *DMD*$^{Y/-}$ piglet was low compared to a WT piglet, adjuvant tube-feeding of frozen stored and reheated colostrum was provided to the individual animal. In case of severe energy deficiency and strongly reduced general condition, 10 ml glucose solution 20% was injected i.p., and heat supply was provided. Straddling piglets received anti-straddle cuffs, which were enhanced by supportive taping, and manual physiotherapy was applied to stimulate circulation, to prevent contructions and to strengthen the muscles. The individual birth weight was documented and weight was subsequently controlled every 24 h for the first 5 days of life. If the weight loss within 24 h exceeded 50 g, adjuvant tube-feeding of a maximum of 20 ml freshly retrieved breast milk and/or milk substitute at approximately every 5-8 h was continued during the first 2-3 days of life, depending on the general condition of the individual animal. After 24 h of life, all *DMD*$^{Y/-}$ piglets were trained to independently drink milk substitute out of a drinking trough, replaced every 8 h. Pale *DMD*$^{Y/-}$ piglets received 0.5 ml Ursoferran® 200 mg/ml i.m. ahead of schedule, followed by the

regular 1 ml Ursoferran® 200 mg/ml i.m. on day 5 of life. Additional milk subsitute feeding was maintained for the normal suckling period of 4 weeks, with slowly reducing the amount to none. After the first week of life, dry piglet feed was supplemented. In a further approach, the rearing conditions in later litters were extended by an automatic wet-nursing unit (HCP Technology, Notrup), providing freshly mixed supplementary milk every hour, automatically calculating the necessary milk amout per day. In a last experimental approach, piglets noted with increasing abdominal girth and loss of appetite at the same time, received laxatives and digestion-aiding nutritional supplements.

3.4. Blood collection and clinical chemistry

Blood samples of *DMD*$^{Y/-}$, *DMD*$^{+/-}$ and WT pigs were taken with Serum Monovettes®. Animals had free access to food and water before blood collection. Blood was collected from the jugular vein. After clotting at room temperature for 30 min, serum was separated by centrifugation at 1.800 rcf for 10-20 min at 4 °C. The blood serum was transferred into 1.5 reaction tubes and stored at –80 °C until further processing. Serum samples for creatine kinase (CK) measurement did not exceed a storage period of 6 months until further processing. CK values were determined by the Clinic for Swine LMU Munich, Oberschleißheim.

CK analysis

For the characterization of the DMD breeding herd (VI. 3), CK values were monitored over a longer time period. Therefore, blood of *DMD*$^{Y/-}$, *DMD*$^{+/-}$ and WT pigs was collected in the first, second, third and fourth week of life, and at the second and third month of life, and CK levels were determined subsequently.

In the therapeutic trial (IV.5.), CK levels were analysed as biomarker for the severity of the disease. Therefore, blood was collected before application of the therapeutic agent and right before euthanasia, and CK levels were determined. Longitudinal CK measurement was not feasible due to the occurrence of sudden cardiac death in some *DMD*$^{Y/-}$ pigs.

3.5. Necropsy

All animals were euthanised at a predetermined timepoint, or if the state of health necessitated euthanasia. Generally, for euthanasia, pigs were sedated with Ursotamin® at a dosage of 20 mg ketamine/kg body weight (BW) in combination with Stresnil® (2 mg Azaperone/kg BW), applicated intramuscularly (i.m.). To deepen anesthesia, Ursotamin® (20 mg ketamine/kg BW) in combination with xylazine (1 mg/kg BW) was injected intraveniously (i.v.). Animals were euthanised with an i.v. or intracardial (i.c.) application of T61® in a dosage of 1 ml/10 kg BW. Animals used in the therapeutic trial (IV.3.) were presedated with an i.m. application of Ursotamin® (20 mg ketamine/kg BW) in combination with Stresnil® (2 mg Azaperone/kg BW) and atropine sulfate (0.025 mg/kg BW). To deepen and maintain anesthesia during veterinary-accompanied transportation and subsequent examination of the individual animal, Propofol (1.5-4.4 mg/kg BW/h, depending on the effect) was applied intravenously. Fentanyl was administered i.v. as bolus (0.5-1 ml) before surgery or euthanasia. Animals were euthanised with an i.c. overdose of potassium chloride (30-60 mg/kg BW, depending on the effect), generating an atrioventricular block and cardiac arrest.

Post-mortem examination for cLDLA study

Necropsy of the animals included in the genome-wide cLDLA (IV.4.) contained the macroscopic evaluation of the severity of musular dystrophy, apparent as macroscopically visible white striated muscle bundles, exemplarily shown in Figure 5, and laparatomy.

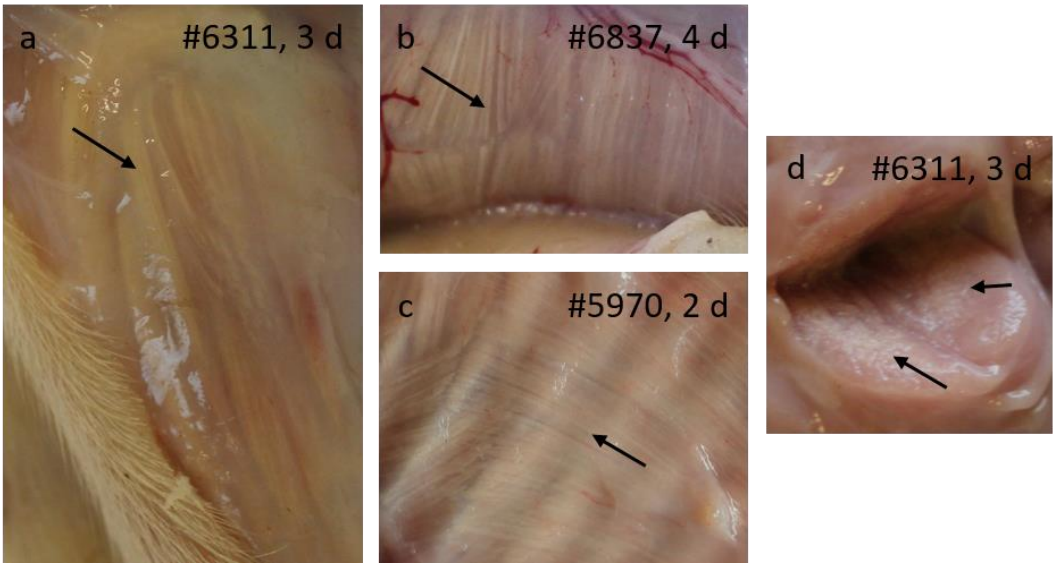

Figure 5: Exemplary presentation of macroscopically striated muscle phenotype of short-term surviving *DMD*$^{Y/-}$ piglets. a, Extensor muscles of the lower arm of piglet #6311 on day 3 after birth. **b**, Mylohyoid muscle of piglet #6837 on day 4 after birth. **c**, Latissimus dorsi muscle of piglet #5970 on day 2 after birth. **d**, Cut surface of triceps brachii muscle of piglet #6311. Arrows: macroscopically striated muscle bundles.

Necropsy done for somatic gene therapy trial

Of the animals included in the therapeutic trial (IV.5.), tissue specimens of different organs (lung, liver, spleen and kidney) were taken following a systematic sampling protocol. A proportion of the obtained tissue specimens was fixed in 4% formalin solution and processed as described below for staining. Another part of the tissue samples was cut into pieces of desired sizes, placed into tissue tek cryo molds, surrounded with Tissue Tek® O.C.T.™ compound and shock frozen on dry ice. Samples embedded in Tissue Tek® O.C.T.™ compound were stored at -80 °C. Furthermore, around 10 small pieces of approximately 3 mm × 3 mm × 3 mm of each tissue specimen were cut, shock frozen on dry ice and transferred into 1.5-ml reaction tubes for storage at -80 °C. The whole heart of each animal was sampled following a systematic sampling protocol. Tissue samples were obtained and stored as described above. Tissue specimens of different skeletal muscles (masseter, longissimus dorsi, triceps brachii, biceps femoris, lower limb muscles and diaphragm) were taken. Importantly, for the i.m. treated animals skeletal muscles of both sides (treated and non-treated) of the body were sampled. Tissue samples were obtained and stored as described above.

Necropsy done for diagnostic trial, validating MSOT

From all animals including the four anatomical regions previously imaged with the MSOT imaging system for validation as an imaging biomarker (IV.6.) representative tissue biopsies were taken. A schematic description of the anatomical regions is shown in Figure 6. One proportion of the obtained tissue specimens was fixed in 4% formalin solution and processed as described below for staining. The other part of the tissue samples was cut in around 10 small pieces of approximately 3 mm × 3 mm × 3 mm, shock frozen on dry ice and transferred into 1.5 ml reaction tubes for storage at -80 °C.

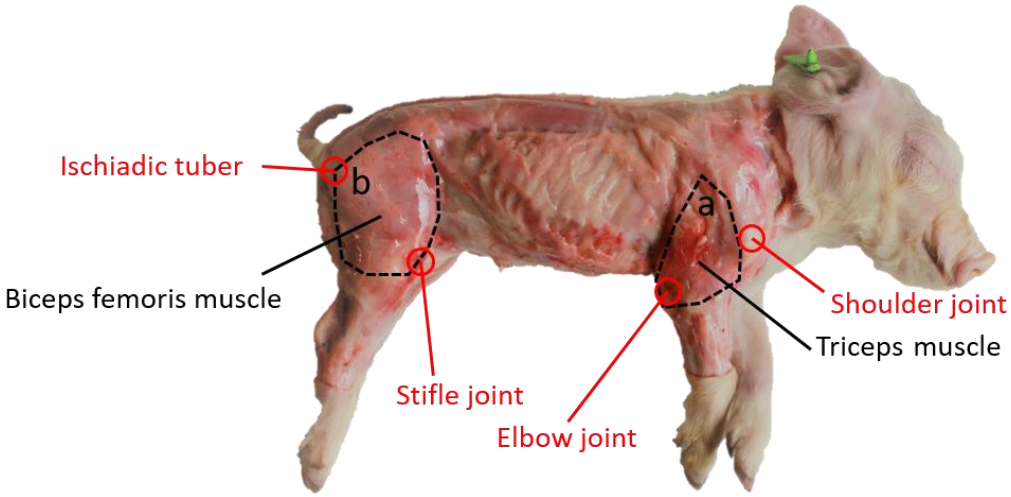

Figure 6: Schematic overview over the tissue specimens taken at MSOT necropsy. Tissue samples were extracted of both body sides, since both sides were imaged with MSOT imaging system. **a**, As palpable landmarks of the upper arm, elbow and shoulder joint were used to locate piglet muscles before imaging. The area between the shoulder and elbow joint, mainly containing the triceps femoris muscle, was taken at necropsy. **b**, For the thigh, the ischiadic tuber and the stifle joint were used. Tissue specimens were taken in the area between the two landmarks, mainly containing biceps femoris muscle.

3.6. Tissue preparation

Formalin fixation and paraffin embedding

For formalin-fixed, paraffin-embedded (FFPE) sampling, harvested tissue samples were directly transferred into 4% formalin solution for a maxium of 24 h for pre-fixation. Subsequently, tissue was cut into desired sizes, placed into embedding cassettes, and fixed further in 4% formalin solution for another 6 h at maximum. After fixation, tissue underwent automated processing in the Thermo Scientific Excelsior, as described in Table 3.

Table 3: Tissue processing in Scientific Excelsior.

Dehydration	Ethanol 70%	2 × 1.5 h
	Ethanol 90%	1.5 h
	Ethanol 90%	1 h
	Ethanol 100%	2 × 1 h
Intermedium	Xylol	3 × 1 h
Infiltration	Paraffin	2 × 1.75 h
	Paraffin	2 h

In the following, the paraffin-impregnated tissue samples were paraffin embedded with the TES 99 modular paraffin embedding system. With a Rotary microtome Microm HM 325 sections of about 4 µm were cut and mounted on microscope slides Star Frost® for immunohistochemistry stain (IHC) or on microscope slides Marienfeld Superior™ for hematoxylin and eosin stain (H.E.). Sections were stored at 37 °C until staining.

Tissue fixation for cryo-conservation

Three different methods for cryo-conservation of tissue specimens were applied, depending on further processing. For expression data analysis, homogenous tissue specimens were cut into pieces of approximately 3 mm × 3 mm × 3 mm, frozen on dry ice, and stored in 1.5 ml reaction tubes on –80 °C. For staining of cryosections, obtained tissue samples were cut into pieces of approximately 10 mm × 5 mm × 2 mm before embedding in the correct orientation in OCT compound and snap-freezing on dry ice. This conservation method should not interfere with antigenicity of epitopes and should lead to better conservation of tissue morphology than FFPE tissue.

3.7. Staining methods

Hematoxylin and eosin stain

H.E. staining results in blue dyed nuclei and pink to red dyed cytoplasm. It was used to visualize cellular and tissue structure detail. H.E. staining was performed on slices of FFPE tissue, mounted on Marienfeld Superior™ microscope slides. It was applied following a standard H.E. protocol as shown in Table 4. After the clearing the tissue slice in the last step, the tissue was mounted with Histokitt mounting medium. All steps were performed at room temperature.

Table 4: Standard H.E. protocol.

Dewaxing	Xylol	20 min
Rehydration	EtOH 100%	2 × 2 min
	EtOH 96%	2 × 2 min
	EtOH 70%	2 min
Washing	Aqua bidest.	2 min
Staining	Mayer's Hemalum	5 min
Rinsing	Floating tap water, warm	5 min
Differentiation	0.5% HCl-EtOH solution	1-2 × 1 s
Rinsing	Floating tap water, warm	5 min
Counterstaining	Eosin 1%	2 min
Washing	Aqua bidest.	2-3 × 1 s
Dehydration	EtOH 70%	2 min
Dehydration	EtOH 96%	2 × 2 min
Clearing	EtOH 100%	2 × 2 min
	Xylol	≥ 5 min

H.E. staining for the diagnostic trial (IV.6.) was performed by the Department of Pediatrics and Adolescent Medicine, University Hospital Erlangen, FAU Erlangen-Nuremberg, according to the laboratory protocols.

Masson Trichrome, Sirius Red, Von Kossa staining

For Masson trichrome (MT), Sirius Red (SR) and Von Kossa staining tissue samples were fixed in 4% formalin solution and subsequently embedded in paraffin as described above. MT and SR staining of skeletal muscle sections for the diagnostic trial (IV.6.) as well as analyses of the collagen content of these sections was performed by the Department of Pediatrics and Adolescent Medicine, University Hospital Erlangen, FAU Erlangen-Nuremberg, as described in Regensburger et al. (2019). Therefore, the MT and SR stained sections were photographed using an AXIO Scope.A1 (Carl Zeiss, Oberkochen) and the AXIO Vs40 software (v.4.8.10, Carl Zeiss, Oberkochen) at 10 × magnification. TIF images were split into three channels (red, blue and green) and the red and green channels were used for collagen quantification. Therefore, the respective positive-stained areas were calculated as a fraction of the whole image.

For the characterization of the DMD breeding herd (IV.3.) cutting of 4 µm sections and staining with MT, SR and Von Kossa was performed by the paraffin laboratory of the Institute for Veterinary Pathology, LMU Munich.

Immunohistochemical staining

Immunostaining of muscle sections of *DMD*$^{Y/-}$ pigs compared to WT littermates was performed using monoclonal mouse anti-DYS1 as primary antibody, reacting with the rod domain (between amino acids 1181 and 1388) of human dystrophin, with cross-reactivity to porcine dystrophin. As secondary antibody biotinylated goat anti-mouse IgG was used. In detail, for immunohistochemical staining (IHC) staining, all tissue sections were mounted on Star Frost® microscope slides and

stored at 37 °C before further processing. All steps were performed at room temperature, if not indicated otherwise. Dilutions of H_2O_2, normal serum and antibodies were prepared with TBS buffer. In a first step, FFPE tissue sections were deparaffinized and rehydrated through a descending alcohol row, according to Table 5. In Table 6, an overview over the workflow of the used IHC protocol is given.

Table 5: Dewaxing and rehydration of FFPE tissue sections.

Dewaxing	Xylol	20 min
Rehydration	EtOH 100%	2 × 2 min
	EtOH 96%	2 × 2 min
	EtOH 70%	2 min
Washing	Aqua bidest.	2 × 2 min

Table 6: IHC protocol for dystrophin detection.

	Procedure	**Agent**	**Conditions**
STEP 1	Heat induced antigen-retrieval	10 mM Citrate buffer pH 6.0 + 0.05% Tween	800 W until boiling, then subboiling (320 W) for 15 min
STEP 2	Cooling		30 min
STEP 3	Washing	1 × TBS buffer	10 min
STEP 4	Blocking of endogenous peroxidase activity	1% H_20_2	15 min
STEP 5	Washing	1 × TBS buffer	10 min
STEP 6	Blocking in normal serum	5% NS goat	1 h
STEP 7	Primary antibody		4 °C over night
STEP 8	Washing	1 × TBS buffer	10 min
STEP 9	Secondary antibody		1 h
STEP 10	Washing	1 × TBS buffer	10 min
STEP 11	Detection	Avidin-biotin-complex	30 min
STEP 12	Washing	1 × TBS buffer	10 min
STEP 13	Substrate	DAB	
STEP 14	Rinsing	Floating tap water	5 min
STEP 15	Counterstaining	Meyer's Hemalum	
STEP 16	Rinsing	Floating tap water	5 min

Heat induced antigen-retrieval (HIAR), to restore hidden antigen sites, was performed by heating the tissue sections mounted on Star Frost® microscope slides in a microwave at subboiling temparature for 15 min, with 10 mM sodium citrate

buffer as agent, applied to break the protein cross-links, which were formed during formalin fixation. After cooling down for 30 min, endogenous peroxidase activity was blocked with 1% H_2O_2 for 15 minutes. Following a 10 min washing step in 1 × TBS buffer, 5% normal goat serum was used for blocking non-specific antibody binding. Primary antibody was NCL-DYS1 (dilution 1:20; overnight at 4 °C), secondary antibody was biotinylated AffiniPure goat anti-mouse IgG (dilution 1:250, 1 h at room temperature). For the detection of dystrophin in striated muscles, the Vectastain Elite ABC HRP Kit with 3.3-diaminobenzidine tetrahydrochloride dihydrate (DAB) as chromogen (brown color) was used. Meyer's Hemalum was applied as counterstain.

Immunofluorescence staining

Concerning the somatic gene editing therapy study (IV.5.), described and published by Moretti et al. (2020), immunofluorescence (IF) staining was applied for the visualization of dystrophin in striated muscles. The staining process, imaging and analyses of the stained samples, were performed by Tarik Bozoglu of the Clinic and Policlinic for Internal Medicine I, Klinikum Rechts der Isar, TU Munich. As primary antibody against dystrophin, Leica NCL-DYS2 (1:25, Novocastra) was used. The IF staining protocol, as described in Dorn et al. (2018), was used. For imaging of the stained samples, inverted and confocal laser scanning microscopes were used (DMI6000B and TCS Sp8, Leica Microsystems, Wetzlar).

3.8. Total protein and total collagen quantification

Total collagen (hydroxyproline) quantification was calculated in relation to total protein content to confirm MSOT collagen signal (IV.6.). All analyses were performed by the Department of Pediatrics and Adolescent Medicine, University Hospital Erlangen, FAU Erlangen-Nuremberg. In brief, a Total Protein Assay and a Total Collagen Assay (both QuickZyme Biosciences, Leiden) were performed according to the manufacturer's instructions. Per muscle, five FFPE muscle tissue sections of 10 µm were analyzed, as described in Regensburger et al. (2019).

3.9. Proteomic experiments

Sample preparation for proteomic experiments

Tissue samples were homogenized using an ultrasonic device (Sonoplus GM3200 with BR30 cup booster, Bandelin, Berlin) in 8 M urea/0.4 M NH_4HCO_3 (15 µl/mg frozen tissue). Protein concentrations were measured photometrically using the Pierce 660 nm Protein Assay (Thermo Scientific, USA). The lysates were analyzed either by selected reaction monitoring or by a holistic proteome analysis.

Selected reaction monitoring

Selected reaction monitoring (SRM) was performed in cooperation with Thomas Fröhlich and Florian Flenkenthaler, Gene Center - Laboratory for Functional Genome Analysis (LAFUGA), LMU Munich, as described in Moretti et al. (2020) and explained in the following:

In detail, samples containing 100 µg of total protein were diluted with equal volumes of 2-fold sample buffer (0.125 M Tris-HCl pH 6.8, 4% SDS, 20% glycerol, 10% β-mercaptoethanol, 0.002% bromophenol blue) and separated on a 4–20% Mini-PROTEAN® TGX™ precast gel (Bio-Rad, Hercules, USA). After Coomassie staining (Roti-Blue, Carl Roth, Karlsruhe), the gel slices with proteins >250 kDa were excised, de-stained using 50% acetonitrile (ACN) in 50 mM NH_4HCO_3 and subjected to in-gel digestion. For reduction, the gel pieces were incubated in a reduction solution of 45 mM dithioerythritol (DTE) dissolved in 50 mM NH_4HCO_3 for 30 min at 55°C. By incubating the gel slices in 100 mM iodoacetamide (IAA) dissolved in 50 mM NH_4HCO_3 in the dark for 30 min at room temperature, the alkylation of sulfhydryl (–SH) groups was achieved. Prior to digestion, 50 fmol of the synthetic heavy peptides (JPT, Berlin) were spiked in. Using 70 ng Lys-C (FUJIFILM Wako Chemicals Europe, Neuss), a first digestion step for 4 h at 37°C was performed. A second digestion step was carried out using 70 ng porcine trypsin (Promega, Fitchburg, WI, USA) overnight at 37°C. Subsequently, extraction of peptides was performed utilizing 70% ACN.

Before mass spectrometry, samples were dried using a SpeedVac vacuum concentrator. The SRM runs were carried out using a nanoACQUITY UPLC® system (Waters Corporation, USA), which is coupled to a triple-quadrupole linear ion trap mass spectrometer (QTRAP 5500, AB SCIEX, USA). The tryptic peptides were transferred to a trap column (PepMap100 C18, 5 µm, 300 µm i.d. × 5 mm, Thermo Scientific, USA) with a flow rate of 10 µl/min. A reversed-phase C^{18} nano-LC column (ReproSil-Pur 120 C18-AQ, 1.9 µm, 75 µm i.d. ×15 cm, Dr. Maisch HPLC, Ammerbuch) separated the tryptic peptides at 280 nl/min. As consecutive linear gradients 1-5% B (0.1% formic acid in acetonitrile) in 1 min, 5–35% B in 45 min and 35-85% B in 5 min were used. Three transitions were measured for every peptide.

To increase the sensitivity and specificity of the approach, proteins > 250 kDa were enriched using 1D-SDS-PAGE. Proteins within the corresponding gel slice were digested using LysC and Trypsin. The resulting peptides were separated by liquid chromatography and detected by a mass spectrometer. A triple-quadrupole analyzer was used with the first quadrupole (Q1) selecting the targeted precursor peptide and transferring it to the second quadrupole (Q2), where it undergoes collision-induced dissociation (CID).

For an accurate absolute quantification, internal standards, consisting of synthetic peptides labeled with ^{13}C/ ^{15}N (so called heavy peptides), were spiked into the sample. Since the „heavy peptide" is chemically identical to the corresponding endogenous peptide, it shows identical behavior, concerning chromatography and ionization. Therefore, the "heavy" and the corresponding endogenous peptide both coelute from the chromatography column, but can be detected individually by the mass spectrometer due to their difference in molecular weight. The coelution of the synthetic internal standard and the endogenous peptide proves the specificity of the signal and further allows the accurate absolute quantification of the target protein. For dystrophin quantification, the two peptides NILSEFQR (Dystrophin AA 2207-2214) and LSALQPQIER (Dystrophin AA 876-885) as well as corresponding heavy internal standard peptides were used.

Holistic proteome analysis

Beside targeted approaches, the combination of liquid chromatography and tandem-mass spectrometry (LC-MS/MS) allows the quantitative comparison of proteomes. Since LC-MS/MS can more effectively be performed at the peptide level, the proteins were cleaved by LysC and trypsin in a first step. Subsequently, during the LC-MS/MS run, the mass spectrometer measured the masses as well as the intensities of the peptides eluting from the chromatography system. Since beside pure peptide molecular weights, structural information is mandatory for the peptide identification, ions of individual peptides were fragmented and a second mass spectrum of the peptide fragments (a so-called MS/MS or MS^2 spectrum) was acquired. Using latest high-performance mass spectrometers, such an analysis allows the identification and quantification of thousands of proteins.

Holistic proteome analyses for the therapeutic trial (IV.5.) as well as for the diagnostic trial (IV.6.) were performed in cooperation with Thomas Fröhlich and Florian Flenkenthaler, Gene Center - LAFUGA, LMU Munich, as described in Moretti et al. (2020) and Regensburger et al. (2019). The detailed procedure was as follows: Using 8 M Urea/ 0.4 M NH_4HCO_3, the lysates' protein concentration was adjusted to a concentration of 2.3 µg/µl. Using DTE at a final concentration of 5 mM, 250 µg of total protein was reduced for 30 min at 37°C. Cysteines were alkylated with iodoacetamide (final concentration 15 mM) at room temperature for 30 min in the dark. Adding 2.5 µg LysC (FUJIFILM Wako Pure Chemicals, Osaka, Japan), digestion of the proteins for 4 h at 37 °C was carried out. Samples were diluted with water to 1 M urea and a second digestion step overnight with 5 µg porcine trypsin (Promega, USA) at 37°C was carried out. 1.5 µg of tryptic peptides were seperated on an Ultimate 3000 nano-LC system (Thermo Scientific, USA). A 50-cm column (Column: PepMap RSLC C18, 75 µm x 50 cm, 2 µm particles, Thermo Scientific, USA) was used for separation. A 160 min gradient from 5% solvent A (0.1% formic acid in water) to 25% solvent B (0.1% formic acid in acetonitrile) was followed by a 10 min gradient from 25% to 40% solvent B. Using an online coupled Q Exactive HF-X mass spectrometer (Thermo Scientific, USA) the identification of the tryptic peptides was performed with a top 15 data dependent method. For protein identification (false discovery rate < 1%) and label-free quantification the obtained spectra were analyzed using the porcine subset of the NCBI refseq database combined with the MaxQuant software platform (V1.6.1).

3.10. Combined linkage disequilibrium and linkage analysis (cLDLA)

DNA isolation for cLDLA

For the isolation of genomic DNA from freshly docked tails of newborn piglets for the GWAS, the DNasy® Blood & Tissue Kit was employed. Therefore, the tail biospsies were cut into little pieces (3-4 pieces with an approximate diameter of 0.5 mm). Afterwards, the manufacturer's instructions for the treatment of tissue were performed. No optional steps to increase DNA yield were implemented. DNA concentration was measured at 260 nm using the SimpliNano spectrophotometer. DNA purity was examined by measuring 260 nm/280 nm and 260 nm/230 nm ratios. The DNA samples were diluted to a concentration of 70 ng/µl using 10 mM Tris buffer, pH 8.0. In cases of a DNA concentration lower than 70 ng/µl, high-salt precipitation was performed. Therefore, 20 µl NaOAc 3M were added to the 200 µl DNA sample, diluted in buffer AE. Afterwards, 500 µl 100% EtOH were added.

Subsequently, the sample was incubated at -80 °C for 30 min. After centrifugation at 13.000 rpm for 30 min at 4 °C, the supernatant was removed with a pipette and the pellet was washed in 500 µl 70% EtOH. The sample was stored at 4 °C overnight. Afterwards, the sample was centrifuged at fullspeed for 3 min. The supernatant was removed with a pipette and the pellet was left to air-dry at room temperature for 6 min. The pellet was resuspended in 32 µl of buffer AE. DNA concentration was measured again and DNA was diluted to a concentration of 70 ng/µl as described previously.

The SNP genotyping was performed by the working group of Doris Seichter, TZF Poing-Grub, using the PorcineSNP60 (Illumina, USA).

Study criteria

A subset of male *DMD*$^{Y/-}$ pigs, based on the following criteria, was selected for SNP genotyping: 1.) Phenotype observed as continuous trait was abbreviated as PhContinous and was coded as "length of life in days"; 2.) Phenotype observed as discrete trait was abbreviated as PhDiscrete and coded as category 1 if *DMD*$^{Y/-}$pigs "died within 2-9 days of life" and as category 2 if *DMD*$^{Y/-}$pigs "died within ≥ 10 days of life". The selected subset consisted of n = 52 male *DMD*$^{Y/-}$pigs (for further details see section IV.4.1.). Markers of PorcineSNP60 chip were remapped to the *Sus scrofa* reference genome assembly Sscrofa11.1 (Genome - Assembly - NCBI). The data was analyzed by Ivica Međugorac, Population Genomics Group, Department of Veterinary Science, Faculty of Veterinary Medicine, LMU Munich, Martinsried, as described in Gehrke et al. (2020). In brief, markers with a call rate per marker < 0.9, minor allele frequency (MAF) of < 0.025 and with unknown position were excluded during quality control. Missing genotypes were imputed and haplotypes reconstructed using the software BEAGLE 5 (Browning et al., 2018). The genome-wide quantitative trait loci (QTL) mapping was performed using a combined linkage disequilibrium and linkage analysis (cLDLA) approach, as described in Medugorac et al. (2017). In brief, first a genomic relationship matrix (G) (Powell et al., 2010) was estimated. To correct for potential polygenic effects and population structure in the model of the subsequent QTL mapping its inverse (G^{-1}) was applied. For sliding windows consisting of 40 SNPs identical by descent (IBD) probabilities for pairs of haplotypes (Meuwissen and Goddard, 2001) were estimated. The estimated IBD probabilities were than summarized into a diplotype relationship matrix (DRM). The computation of a DRM is performed similarly to the additive genotype relationship matrix (GRM) (Lee and Van der Werf, 2006). cLDLA mapping of PhContinous and PhDiscrete coded phenotype was performed using a procedure similar to that reported in (Meuwissen et al., 2002), considering random QTL and polygenic effects. In the middle of each of the sliding windows of 40 SNPs a variance component analysis was performed using the ASReml package (https://www.vsni.co.uk/downloads/asreml/release3/UserGuide.pdf) and a mixed linear model as already described in and adopted from Medugorac et al. (2017) and Gehrke et al. (2020).

The cLDLA mapping was performed in two runs: first, the DMD phenotype was considered as continuous variable (PhContinous), i.e. "length of life in days", in a second run the DMD phenotype was considered as discrete variable (PhDiscrete), i.e. group 1, including all piglets "death within 0-9 days of life" and group 2, including all piglets "death within ≥ 10 days of life". cLDLA mapping was only performed for male affected *DMD*$^{Y/-}$ pigs. Genotyping and haplotyping of parental

animals was performed as well, with the results not directly involved in the cLDLA mapping.

The parental genotypes included female *DMD*$^{+/-}$ mother sows and WT boars. SNP-genotypes of the WT sires were provided by Martin Heudecker (EGZH, Poing-Grub) and Kay-Uwe Götz (ITZ, Poing-Grub). Haplotyping of *DMD*$^{Y/-}$ pigs in trios (sire-dam-offspring) ensured high quality haplotypes for the cLDLA mapping.

3.11. Therapeutic approach

Somatic gene editing approach

As described in Moretti et al. (2020), adeno-associated viral vectors, serotype 9, coated with PAMAM-G2 nanoparticles and carrying an intein-split Cas9 and a pair of guide RNAs, targeting exon 51 flanking sequences (G2-AAV9-Cas9-gE51), were used to introduce somatic gene editing in *DMD*$^{Y/-}$ piglets. Therefore, the intein-split Cas9 and gRNAs were established by the working group of Wolfgang Wurst of the Institute of Developmental Genetics, Helmholtz-Centre and Munich School of Life Sciences Weihenstephan, TU Munich, Freising. The AAV9-vectors were generated and raised by Tarik Bozoglu, Tilman Ziegler and Anja Wolf, and G2-optimization *in vitro* and *in vivo* was introduced by Seungmin Lee, Tilman Ziegler, members of the Clinic and Policlinic for Internal Medicine I, Klinikum Rechts der Isar, TU Munich, and DZHK, Munich Heart Alliance, and Manfred Ogris, MMCT Laboratory of Macromolecular Cancer Therapeutics, Department of Pharmaceutical Chemistry, University of Vienna, Vienna, Austria.

As therapeutic approach, AAV9-Cas9-gE51 was tested as a somatic gene editing agent. In brief, as described above, *DMD*$^{Y/-}$ piglets lack exon 52 (*DMD*Δ52), with the frameshift mutation resulting in an unstable mRNA leading to nonsense-mediated mRNA decay and therefore a total loss of dystrophin. G2-AAV9-Cas9-gE51 was aimed to restore the open reading frame as shown in Figure 7, introducing the expession of an internally truncated, but partially functional, dystophin protein, thus converting the Duchenne muscular dystrophy into the milder Becker muscular dystrophy.

Figure 7: Schematic description of the somatic gene editing approach in *DMD*Δ52 pigs. The treatment aims to achieve a corrected reading frame (ΔE51-52) by Cas9-mediated excision of exon 51 (adapted from Moretti et al., 2020).

Conduction of the pig transduction

Whenever possible, matched pairs (siblings treated or untreated) with equally distributed birthweights were choosen for the experimental study. During 96 h after the injection of G2-AAV9-Cas9-gE51, piglets were seperated in metabolism cages for the collection and safe disposal of all excrements. General condition of all animals was monitored and scored daily throughout the entire duration of the study. Animals injected i.m. received pain-relieving agents before application of the therapeutic agent and on two consecutive days.

In a first proof-of-principle study, with the aim to show local dystrophin expression and functional improvement of skeletal muscle fibers, n = 6 *DMD*$^{Y/-}$ piglets, at day 14 after birth, received unilateral i.m. injections of 200 µl each (100 µl of each virus subsequently) at a total of 15 injection sites (6 × upper arm, 9 × thigh). Of both Cas9-intein-halfs (N-Cas9 and C-Cas9), 2.5×10^{13} vector genomes (vg) / kg BW were injected. The muscular part of the contralateral side of the body served as untreated control. For a further experimental set-up, with the aim to also achive diaphragm and heart muscle additionally to skeletal muscle, *DMD*$^{Y/-}$ piglets received either low-dose ($1\text{-}5 \times 10^{13}$ coated virus particles (vp)/ kg BW for each, N-Cas9 and C-Cas9) or high-dose (2×10^{14} vp / kg BW for each strain) G2-AAV9-Cas9-gE51 i.v. injections, applied into the ear vein. Intravenously injected animals received G2-AAV9-Cas9-gE51 not before weaning from the mother, due to the potential presence of colostral antibodies against AAV.

The duration of the experiment varied between the individual animals, on the basis of the following reasons: studies were terminated due to animal protection regulations (DMD characteristic physical deterioration, e.g. stridor, tachypnea or exhaustion), or *DMD*$^{Y/-}$ pigs succumbed to sudden cardiac death, occurring at rest or following environmental stressors (e.g. dominant behavior of siblings, trapping, transportation, or anaesthetic induction). To overcome these obstacles, pigs to be euthanized at a predetermined time point, received anaesthetic introduction directly followed by intubation, ensuring sufficient oxygen supply.

Off-target anaysis

The analysis to detect undesired off-target effects triggered by CRISPR/Cas9 was performed by the research unit Genomics of LAFUGA, Gene Center Munich, LMU Munich, using a targeted and a holistic approach, as described in Moretti et al. (2020).

Concerning the targeted sequencing approach, potential off-targets were predicted using the CRISPOR and the CHOPCHOP web tool (Labun et al., 2019). For intron 50 and 51 gRNA, the top five predicted off-targets were amplified by PCR, performed by Florian Giesert, Institute of Developmental Genetics, Helmholtz-Centre and Munich School of Life Sciences Weihenstephan, TU Munich, Freising. Therefore, genomic DNA from muscle tissue of n = 1 WT pig, n = 2 i.m. treated pigs and n = 1 i.v. treated pig, was used. For each reaction, 400 ng of genomic DNA was utilized. The PCR products were analyzed subsequently, using next-generation sequencing (NGS). Therefore, NGS libraries of the PCR-products were created. The sequencing of these libraries was performed in paired-end mode, with a read length of 100 nucleotides, using the HiSeq® 1500 system (Illumina, USA) and the received sequences were compared to the original PCR-products, respectively. The Bioconductor package CrispRVariants was used for data analysis (Lindsay et al., 2016).

As holistic approach, genome wide sequencing of human *DMD*Δ52 induced Pluripotent Stem Cells (iPSCs) and an isogenic edited *DMD*Δ51-52 iPSC clone was applied. The reads were sequenced in paired-end mode, with a read length of 100 bases, using a HiSeq® sequencer (Illumina, USA). Applying the GATK somatic SNV + INDEL pipeline (Van der Auwera et al., 2013), insertions or deletions of bases (INDELs) and single nucleotide variants (SNVs) in each sample were called and filtered for variants specific to the edited *DMD*Δ51-52 iPSC clone. Subsequently, a minimal Levenshtein distance analysis was applied to clarify, if the

identified variants represented off-target effects due to the use of CRISPR/Cas9, or randomly occurring variants, due to the clonal expansion of the edited *DMD*Δ51-52 iPSCs. Therefore, two gRNAs were aligned in a sliding window, which covered 25 base pairs (bp) upstream and 25 bp downstream of each variant position. The alignment with the smallest distance, i.e. the smallest number of mismatches with which a gRNA could have bound and cause an off-target effect, was determined.

3.12. Movement and gait analysis

To assess functional muscle parameters as biomarker for the clinical course of the disease was indispensible for the evaluation of the somatic gene editing approach achieved by G2-AAV9-Cas9-gE51 (IV.5.). Due to sudden arrhythmia-induced death as difficulty in working with the *DMD*$^{Y/-}$-pig model, performing treadmill tests to assess muscle strength and endurance was not feasible. Therefore, a video surveillance system was installed, allowing to observe the animals at any time of a day, on seven days a week (24/7).

Video surveillance

Digital night and day vision infrared cameras provided a 24/7 video surveillance of the pigs. Each stable compartment contained one camera, allowing an overview over the whole sector. Clear distinction of the observed animals was possible either by individual coat patterns, tags with animal marker pens, colored ear tags, or by great variation in body sizes within the compared couple. On site, a control room served for monitoring all cameras. Camera signals were digitalized by encoders of the type IndigoVision 9000. Encoders were connected to a computer via an AT-FS708 switch, as represented schematically in Figure 8. The evaluation of the videos was performed using the IndigoVision control center software (v.3.19.5).

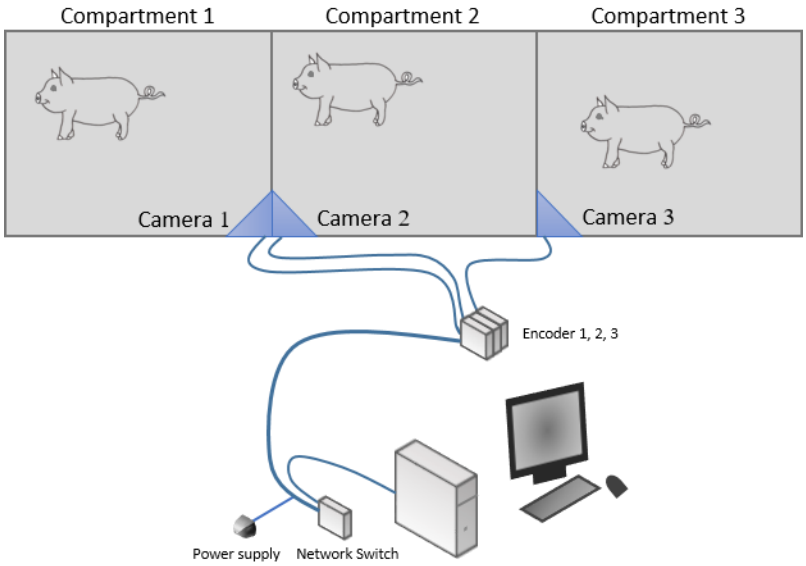

Figure 8: Schematic representation of the monitoring unit for 24/7 video surveillance of pigs.

Evaluation of behavioral patterns

For analysing behavioral patterns, two behavioral observation methods were used, according to Martin et al. (1993). Instantaneous sampling was used to record the state of an individual animal at predetermined time intervals. Therefore, the animals were observed over a total period of 24 h and the behavioral information at every 5th min was assessed. Only the instant moment (measured down to the centisecond) was graded. However, to ensure reliability, the seconds before and after grading were involved in the evaluation. Continous recording allowed the observation of total activity and total resting time in 24 hours. For this purpose, only two states, upright and lying posture, were measured to the second. Subsequently, the duration of standing and lying postures, as well as the frequency for these events, were evaluated.

3.13. Multispectral optoacoustic tomography

MSOT imaging was performed with the MSOT Acuity Echo prototype imaging system (iThera Medical) as described in Regensburger et al. (2019). In brief, MSOT is based on a photoacoustic effect. Using a 25-Hz pulsed Nd:YAG laser, the system induces thermoelastic expansion of endogenous absorbers in the examined tissue, allowing the detection of resulting pressure waves, which can be subsequently identified by spectral unmixing. Thus, it enables the visualization and quantification of different endogenous chromophores, such as hemoglobin, melanin and oxygen saturation. Illumination in the near- and extended near-infrared rages (exNIR) from 680-1.100 nm enables the visualization and quantification of lipids and collagens.

A 2D concave handheld detector (4-MHz center frequency, 256 transducer elements) enables cross-sectional imaging. It provides a spatial resolution of < 150 µm and a field of view of 30 mm. For anatomic guidance during examination, the device is combined with a reflective ultrasound computed tomography (RUCT) unit. With a 3D hemispherical handheld detector (8-MHz center frequency, 256 transducer elements), isotropic volumetric optoacoustic imaging is provided. This detector offers a spatial resolution of 100 µm and a field of view of 15 mm.

Study design

At the time point of imaging, genotypes of all animals were already determined. The investigator and persons carrying out analysis, however, were blinded to the genotypes. To ensure a stress-free handling during imaging procedure, piglets underwent a daily training from birth onwards. Only WT piglets were sedated with midazolam, administered intranasally, if required. To reduce interfering signals, skin-locations, in the regions to be examined, were shaved cautiously shortly before imaging procedure. During imaging, the piglets were hold gently. To improve the level of comfort during imaging, piglets were placed on a heat cushion, whenever necessary. Warmed transparent ultrasound gel (AQUASONIC clear, Parker Laboratories, USA) was used for optimal coupling between the MSOT detector and the skin.

In a first step, a proof-of-concept study was performed in the DMD pig model, scanning newborn WT and *DMD*$^{Y/-}$ piglets. Therefore, standardized 2D MSOT transverse imaging was applied to the muscles of the upper arm (triceps brachii) and the thigh (biceps femoris). In a subsequent longitudinal study, WT and *DMD*$^{Y/-}$ piglets underwent standardized 2D transversal and 3D scanning of bilateral upper

arm and thigh muscles. Here, MSOT imaging was performed on a total of 4 successive time points: days 1/2 (week 1), days 8/9 (week 2), days 15/16 (week 3) and days 22/ 23 (week 4) of life.

In a second step, the approach was applied to pediatric patients and correlation of MSOT collagen signal to magnetic resonance imaging and patients' functional status was investigated (not shown).

3.14. Exclusion criteria for individual *DMD*$^{Y/-}$ piglets from the studies

Concerning the GWAS to investigate phenotype variability in *DMD*$^{Y/-}$ piglets, all stillbirths, crushed piglets and animals, which died due to an infectious disease or due to questionable reasons were excluded from the analysis. Concerning the therapeutic approach, aiming at somatic gene editing, *DMD*$^{Y/-}$ piglets, which died during the first week of life (d 0-6), were excluded from the study. For the diagnostic approach, using the MSOT device to detect collagens, all alive piglets were included in the study.

3.15. Statistics

In all results, differences between groups were considered as significant at $P < 0.05$. *P*-values were presented as: *: $P < 0.05$; **: $P < 0.01$; ***: $P < 0.001$; ****: $P < 0.0001$.

In chapter IV. 1.-3. results are presented as mean±s.e.m. Two experimental groups (WT vs. *DMD*$^{Y/-}$) were compared using independent samples *t*-test. Kaplan-Meier survival curves were used in Fig. GraphPad Prism v.5.04 was used for statistical analyses.

In chapter IV.4. in the middle of each of the sliding windows of 40 SNPs a variance component analysis was performed using the ASReml package (VSNi, Hemel Hempstead, UK) and a mixed linear model as already described in and adopted from Medugorac et al. (2017) and Gehrke et al. (2020).

In chapter IV.5.-6., concerning selection reacted monitoring (SRM), chromatograms were evaluated using Analyst V 1.5.1. (AB SCIEX, USA). Regarding holistic proteome analysis principal component analysis, hierarchical clustering, and Student's t-test were calculated with Perseus (V 1.5.3.2), part of the MaxQuant proteomics software package.

In chapter IV.5., results are presented as mean±s.e.m., unless indicated otherwise. If more than two experimental groups were compared, one-way analysis of variance (ANOVA) was applied and whenever a significant effect was obtained multiple comparison tests between the groups were performed, using the Bonferroni procedure (parametric). The SPSS statistical program (version 25) was used for statistical analyses in IV.5.2. GraphPad Prism v.5.04 was used for statistical analyses in IV.5.3.

In chapter IV.6., continous variables were presented as mean±s.d. Categorial variables were presented as numbers and percentages. For testing the normal distribution, Shapiro-Wilk test was used before inferential analysis. Two experimental groups (WT vs. *DMD*$^{Y/-}$) were compared using independent samples *t*-test. Welch's correction was applied in cases of unequal variance in independent samples *t*-test. A Mann-Whitney *U*-test was applied for comparison of independent samples if the assumption of normal distribution was violated. To compare

longitudinal 3D MSOT collagen signals, Tukey's honest significant difference (HSD) test following a two-way ANOVA, including time points and piglet group, was performed. For the comparison of longitudinal 2D MSOT collagen signals, post hoc Tukey's HSD following a mixed-effects model were applied (with fixed effects: time points and piglet group, and random effect: piglet), due to missing values in week 1. All scans of WT and *DMD*$^{Y/-}$ in each week were compared using independent samples *t*-test. Welch's correction was applied in cases of unequal variance in independent samples *t*-test. A Mann-Whitney *U*-test was chosen for comparison of independent samples if the assumption of normal distribution was violated. Correlations are given by the Spearman correlation coefficient (r_s), two-tailed test. GraphPad Prism v.7.00 or newer was used for statistical analyses.

IV. RESULTS

1. Animal generation by a DMD breeding herd

A total of 29 litters were generated by the DMD breeding herd, consisting of 9 *DMD*$^{+/-}$ sows, at the Lehr- und Versuchsgut, LMU Munich, Oberschleißheim. The *DMD*$^{+/-}$ founder animal #3040, born in 2014, generated a total of 10 litters. As shown in Table 7, n = 5 F1-sows (#5153, 3 litters; #5381, 3 litters; #5382, 4 litters; #5383, 4 litters; #6314, 1 litter) and n = 3 F2-sows (#6225, 1 litter; #6243, 1 litter; #6245, 2 litters), were used to complete the DMD breeding herd.

Table 7: *DMD*$^{Y/-}$ pigs generated breeding.

year	litters	sow	date	DMD$^{Y/-}$	still births	death d0-6	thereof crushed d0-6	possibly crushed d 0-6
2015	1	#3040	08.06.2015	5	0	0	0	0
	1	#3040	28.01.2016	3	0	0	0	0
	1	#3040	29.06.2016	5	1	2	1	0
2016	1	#3040	09.12.2016	0	0	0	0	0
	1	#3040	29.06.2017	1	0	1	1	0
	1	#5153	18.10.2017	5	0	5	1	0
	1	#5383	17.11.2017	6	0	4	0	0
2017	1	#3040	30.11.2017	3	0	1	1	0
	1	#5381	16.01.2018	2	0	2	0	0
	1	#5382	09.03.2018	9	2	4	1	0
	1	#5153	16.03.2018	5	0	4	1	2
	1	#5383	12.04.2018	2	0	0	0	0
	1	#3040	03.05.2018	5	0	2	1	0
	1	#5381	14.06.2018	0	0	0	0	0
	1	#5382	03.08.2018	4	0	3	0	0
	1	#5153	09.08.2018	3	0	2	0	1
	1	#5383	06.09.2018	3	0	3	0	2
	1	#3040	03.10.2018	1	0	1	0	0
2018	1	#5381	08.11.2018	2	0	0	0	0
	1	#3040	28.02.2019	3	1	0	0	0
	1	#5382	27.03.2019	3	0	0	0	0
	1	#6243	13.06.2019	3	0	2	1	0
	1	#6245	19.06.2019	3	0	1	0	0
	1	#3040	25.07.2019	2	1	0	0	0
	1	#5382	22.08.2019	6	1	3	0	0
	1	#6225	02.09.2019	1	0	1	0	0
	1	#5383	08.10.2019	2	0	0	0	0
	1	#6245	09.11.2019	7	0	2	0	0
2019	1	#6314	01.12.2019	3	0	1	0	0
total	29			97	6	44	8	5

Sows were inseminated with sperm of WT boars of Bayern Genetik, Poing-Grub. In total, n = 97 affected *DMD*$^{Y/-}$ piglets were produced by breeding. The *DMD*$^{Y/-}$

phenotype was confirmed by PCR analysis of DNA isolated from individual tail biopsies, with the primer pair 5´-TGC ACA ATG CTG GAG AAC CTC A-3´ and 5´-GTT CTG GCT TCT TGA TTG CTG G-3´ detecting the intact *DMD* allele and a second primer pair 5´-CAG CTG TGC TCG ACG TTG TC-3´ and 5´-GAA GAA CTC GTC AAG AAG GCG ATA G-3´ detecting the mutated (*DMD*Δ52) allele by the neomycin selection cassette. Of all *DMD*$^{Y/-}$ piglets generated by breeding, n = 6 piglets were still born and n = 13 piglets were crushed by the sow (n = 8 crush secured, n= 5 possibly crushed). Another n = 44 animals died within the first week of life (d 0-6), equivalent to 50.55% survivors of day 6 of life.

2. Validation of different rearing conditions for *DMD*$^{Y/-}$ piglets

For the validation of the different husbandry conditions for rearing, a total of 27 litters was considered, as shown in Table 8.

Table 8: Color coding for the 4 different husbandry conditions applied for a total of 27 litters. Litters highlighted in **orange** indicate motherless nursing of *DMD*$^{Y/-}$ piglets in an artificial rearing unit. Litters highlighted in **pink** indicate 48 h supervised suckling at the sows' teats. Litters highlighted in **green** indicate 5 d intense nursing (first approach) and in **dark blue** 5 d intense nursing (second approach). The litters colored in **light blue** indicate 5 d intense nursing (second approach) combined with a further experimental approach (explained in IV.3.).

year	litters	sow	date	DMD$^{Y/-}$	still births	death d0-6	thereof crushed d0-6	possibly crushed d 0-6
	1	ET 220	19.05.2017	4	1	2	1	0
	1	#3040	29.06.2017	1	0	1	1	0
	1	ET 228	24.07.2017	4	3	0	0	0
	1	#5153	18.10.2017	5	0	5	1	0
	1	#5383	17.11.2017	6	0	4	0	0
2017	1	#3040	30.11.2017	3	0	1	1	0
	1	#5381	16.01.2018	2	0	2	0	0
	1	#5382	09.03.2018	9	2	4	1	0
	1	#5153	16.03.2018	5	0	4	1	2
	1	#5383	12.04.2018	2	0	0	0	0
	1	#3040	03.05.2018	5	0	2	1	0
	1	#5381	14.06.2018	0	0	0	0	0
	1	#5382	03.08.2018	4	0	3	0	0
	1	#5153	09.08.2018	3	0	2	0	1
	1	#5383	06.09.2018	3	0	3	0	2
	1	#3040	03.10.2018	1	0	1	0	0
2018	1	#5381	08.11.2018	2	0	0	0	0
	1	#3040	28.02.2019	3	1	0	0	0
	1	#5382	27.03.2019	3	0	0	0	0
	1	#6243	13.06.2019	3	0	2	1	0
	1	#6245	19.06.2019	3	0	1	0	0
	1	#3040	25.07.2019	2	1	0	0	0
	1	#5382	22.08.2019	6	1	3	0	0
	1	#6225	02.09.2019	1	0	1	0	0
	1	#5383	08.10.2019	2	0	0	0	0
	1	#6245	09.11.2019	7	0	2	0	0
2019	1	#6314	01.12.2019	3	0	1	0	0
total	27			92	9	44	8	5

Artificial rearing unit

n = 5 litters, resulting in n = 12 alive *DMD*$^{Y/-}$ piglets, were nursed in an artificial rearing unit, the Lax Disco Box. Despite supervision by a veterinarian, n = 3 piglets were crushed by the sow during birth or during the first 12 h of suckling at the sows' teats. Another n = 7 *DMD*$^{Y/-}$ piglets died or had to be euthanized due to poor general condition or the inability of drinking milk substitute by themselves. Only 17% of all animals (equivalent to n = 2 out of n = 12 *DMD*$^{Y/-}$ piglets) survived the suckling period, as shown in Figure 10a.

48 h of supervised suckling at the sows' teats

Due to the low efficiency of rearing *DMD*$^{Y/-}$ piglets in an artificial rearing unit, as a second nursing approach, 48 h of supervised suckling at the sows' teats was evaluated. The main intention was to increase the colostrum and breast milk intake. After 48 h of supervised suckling, no further supplementation or nursing was provided and piglets were left alone with the sow. Under these conditions, the survival success increased to 44% (equivalent to n = 7 out of n = 16 *DMD*$^{Y/-}$ piglets), as shown in Figure 10b. These results indicated, that colostrum intake over a longer time period and the further nutrition with natural mother milk instead of milk replacers, plays a major role in survival of *DMD*$^{Y/-}$ piglets. In total, n = 3 litters, resulting in n = 16 alive *DMD*$^{Y/-}$ piglets, underwent the named breeding conditions, of which n = 3 animals were crushed by the sow during birth or supervised suckling.

In the first two named approaches, n = 16 out of n = 28 alive *DMD*$^{Y/-}$ piglets showed severe loss of body weight within the first 1-3 days after birth, combined with a complex of symptoms, appearing as lateral positioning, rowing with the four limbs, salivation and, in part, nystagmus. A meningitis infection with *Staphylococcus aureus* was suspected at first. Therefore, n = 3 animals (n = 1 WT and n = 2 *DMD*$^{Y/-}$) were examined in the Institute for Veterinary Pathology, LMU Munich, where a meningitis infection could be ruled out. For all animals, appearing with the described symptoms, every attempt to retrieve a normal general condition failed and piglets had to be euthanized immediately. To evaluate a putative link between the described complex of symptoms and hypoglycemia, which might be caused by an insufficient milk intake due to suckling problems, a special focus was drawn on macroscopic examination of head muscles. As displayed in Figure 9, facial muscles used for suckling motions, neck muscles important for keeping the head upright, and forelimb muscles, enabling standing posture and forward pressure, showed white striated bundles of muscles, indicating a severe DMD phenotype.

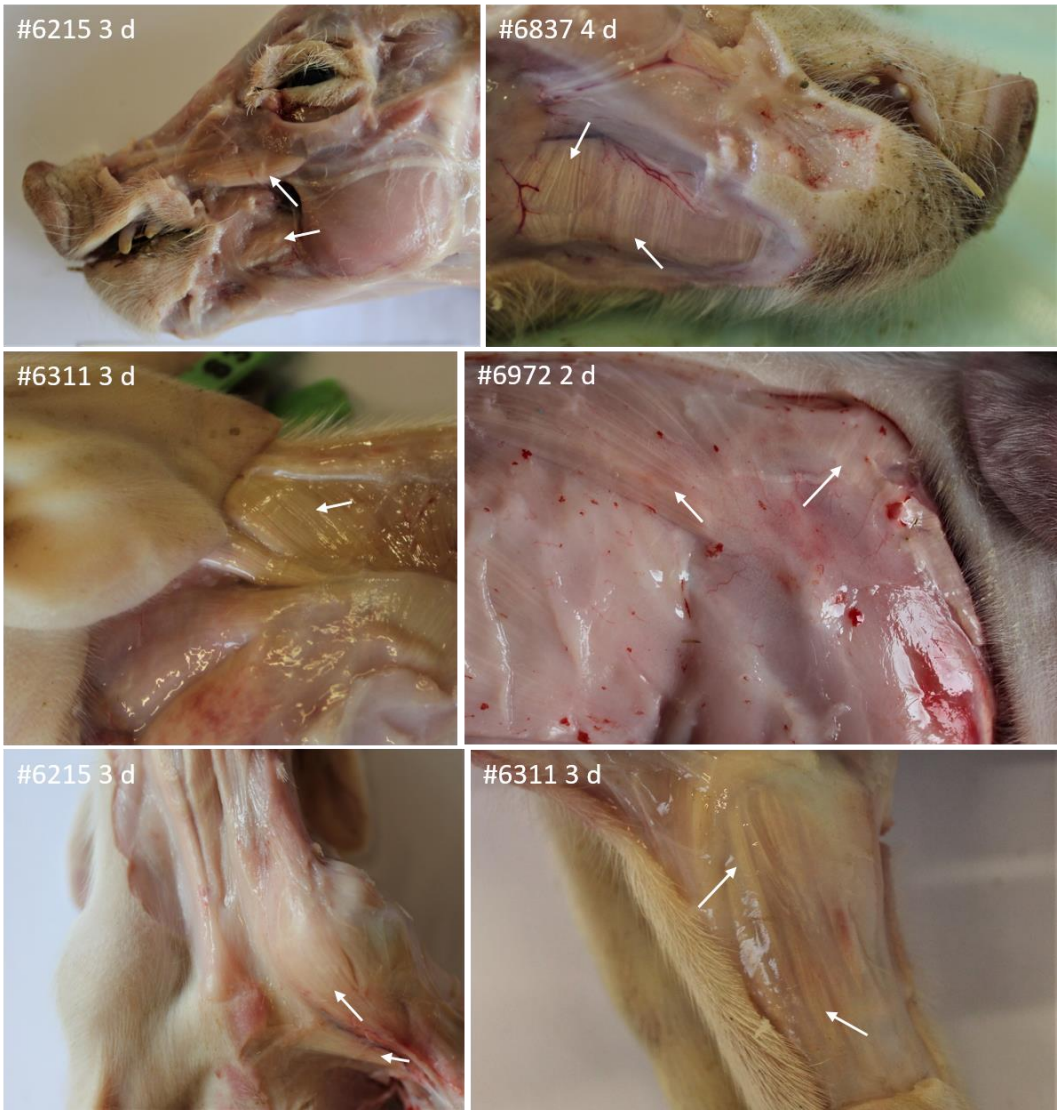

Figure 9: Representative pictures of muscles of short-term surviving *DMD*$^{Y/-}$ piglets. All shown muscle areas are important for the positioning at the sows' teats and the suction process. Facial and neck muscles, as well as muscles of the forelegs show paleness when compared to healthy musculature. Furthermore, a different amount of bundles of muscles appearing with a white striated pattern were observed. **Upper row:** *DMD*$^{Y/-}$ piglet #6215 shows pale depressor rostri and depressor labii muscles; DMD$^{Y/-}$ piglet #6215 shows a pale mylohyoid muscle. **Middle row**: *DMD*$^{Y/-}$ piglet #6311 shows a pale trapezius muscle, equally as *DMD*$^{Y/-}$ piglet #6972. **Bottom row:** *DMD*$^{Y/-}$ piglet #6215 shows pale cleidobrachialis and pectoralis muscles, *DMD*$^{Y/-}$ piglet #6311 shows pale extensor muscles of the lower arm. Pale and white striated muscle bundles were always observed in conjunction with a severe DMD phenotype.

5 days of intense nursing

Due to the results above, two further approaches for nursing *DMD*$^{Y/-}$ piglets were developed. In a first attempt, the main goal was to avoid energy deficiency, particularly dangerous within the first 24 h after birth. The first approach was applied for 7 litters (n = 23 *DMD*$^{Y/-}$ piglets). 35% of *DMD*$^{Y/-}$ piglets (equivalent to n = 8 out of n = 23 *DMD*$^{Y/-}$) survived day 6 of life utilizing this rearing approach,

as shown in Figure 10c.

The second approach was applied for a total of n = 9 litters (n = 23 alive born *DMD*$^{Y/-}$ piglets). It was extended by hedging colostrum intake and subsequently upgraded by further parameters. To varify if colostrum intake was sufficient, the blood glucose levels of weak appearing *DMD*$^{Y/-}$ piglets (n = 17 newborn *DMD*$^{Y/-}$ piglets) was measured.

A glucose level lower than 50 mmol/l (present in n = 7 newborn *DMD*$^{Y/-}$ piglets) was considered as threshold to initiate supplementary gastric tube feeding of frozen stored and reheated colostrum. Using this advanced approach of 5 days of intense nursing, 70% (equivalent to n = 16 out of n = 23 *DMD*$^{Y/-}$ piglets) survived day 6, as shown in Figure 10d.

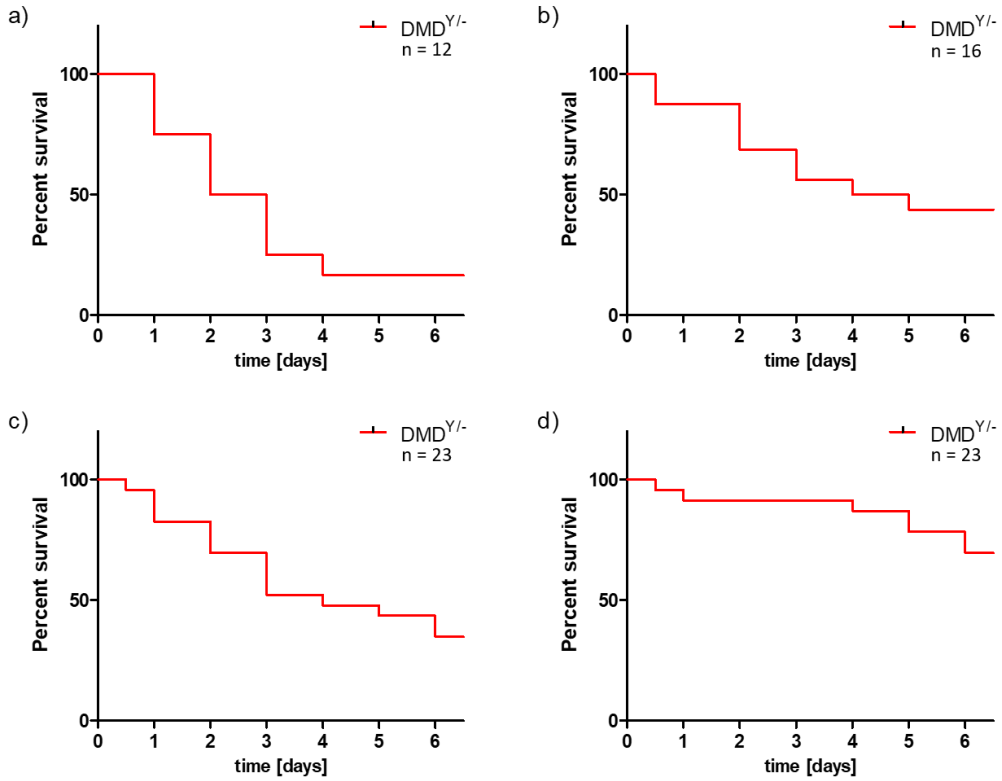

Figure 10: Kaplan-Meier survival curve of all alive born *DMD*$^{Y/-}$ pigs reared under four different nursing conditions. a, Survival of *DMD*$^{Y/-}$ piglets in the artificial rearing unit (motherless rearing). Only 17% of all alive born *DMD*$^{Y/-}$ piglets survived day 6 of life. **b**, Survival of alive born *DMD*$^{Y/-}$ piglets under conditions of 48 h supervised suckling at the sows' teats with 44% surviving day 6 of life. **c**, 5 days intense nursing, approach 1, shows similar effectiveness as 48 h supervised suckling at the sows' teats. 35% survived day 6 of life. **d**, 5 days intense nursing, approach 2, was the most successful rearing condition with 70% of alive born *DMD*$^{Y/-}$ piglets surviving day 6 of life.

Survival of *DMD*$^{Y/-}$ piglets severely increased within the improvement of rearing conditions, highlighting the importance of specially adapted nursing in the DMD pig model.

The impact of supplementary milk substitute feeding 24 h after birth on the body weight of *DMD*$^{Y/-}$ piglets

The severe loss of body weight in *DMD*$^{Y/-}$ piglets within the first 24 h of life could be compensated by the supportive administration of milk substitute from 24 h after birth onwards. The effect of this milk supply on body weight of *DMD*$^{Y/-}$ piglets is shown in Figure 11. The data is generated from the husbandry system "5 d intense nursing" only. Due to insufficient breast milk intake resulting of an inability to suckle well at the sows's teats, as shown above, nearly none of the *DMD*$^{Y/-}$ piglets which did not learn to drink milk substitute out of a piglet drinking trough were able to survive. This indicates, that for affected *DMD*$^{Y/-}$ piglets suckling at the sows's teats is not sufficient for generating and maintaining sufficient energy reserves.

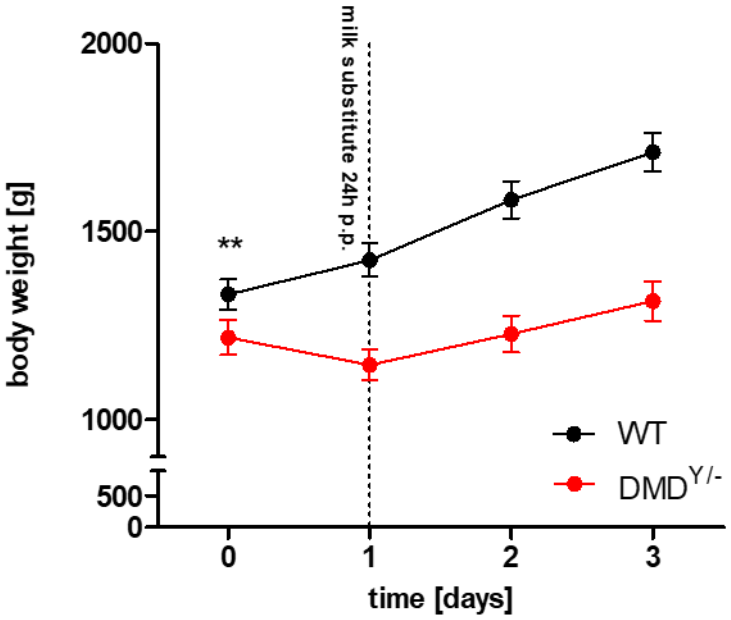

Figure 11: Impact of supplementary milk substitute feeding 24 h after birth on the body weight of *DMD*$^{Y/-}$ piglets. Newborn *DMD*$^{Y/-}$ piglets show a significantly reduced birth weight when compared to male WT littermates. A further severe loss of body weight within the first 24 h, as observed in most *DMD*$^{Y/-}$ piglets, can be partly compensated the supplementary feeding of milk substitute.

3. Phenotypic characteristics of *DMD*$^{Y/-}$ pigs generated by breeding

3.1. Immunohistochemical staining of dystrophin

Skeletal muscle of WT animals exhibited a clear dystrophin staining (Figure 12). In contrast, no dystrophin signal was detected in skeletal muscle sections of *DMD*$^{Y/-}$ pigs, with exception of single isolated revertant (dystrophin positive) fibers (not shown).

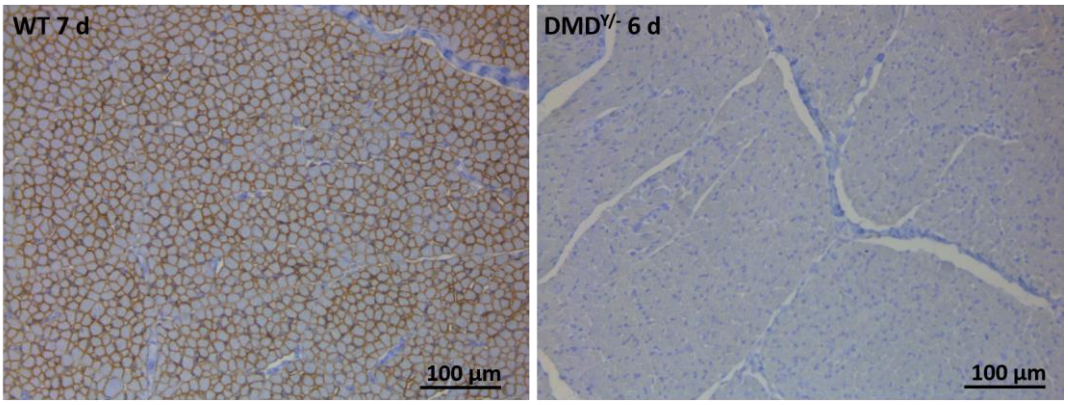

Figure 12: Representative skeletal muscle samples of a WT and a *DMD*$^{Y/-}$ pig stained immunohistochemically for dystrophin. Compared to WT controls no dystrophin is detectable in the skeletal muscle sections of *DMD*$^{Y/-}$ pigs. This finding reflects the situation found in human DMD patients. Dystrophin: brown color.

3.2. Creatine kinase levels

CK levels of a total of n = 89 pigs (n = 25 WT, n = 35 *DMD*$^{+/-}$ and n = 29 *DMD*$^{Y/-}$) were measured at different timepoints. A CK level ≤ 2000 U/l was considered to be normal. As shown in Figure 13, CK levels in week 1 of life were already severely elevated in *DMD*$^{Y/-}$ piglets compared to their WT littermates (42956±29020 U/l versus 274±59 U/l). Female *DMD*$^{+/-}$ carrier did not show an elevation of CK in week 1 of life (602±273 U/l), whereas between week 2 and 11 of life a mild elevation of CK (3771±1080 U/l) was observed for this group. CK levels of *DMD*$^{Y/-}$ piglets compared to their WT littermates continued to be severely elevated between week 2 and week 11 of life (54041±9058 U/l versus 1513±259 U/l).

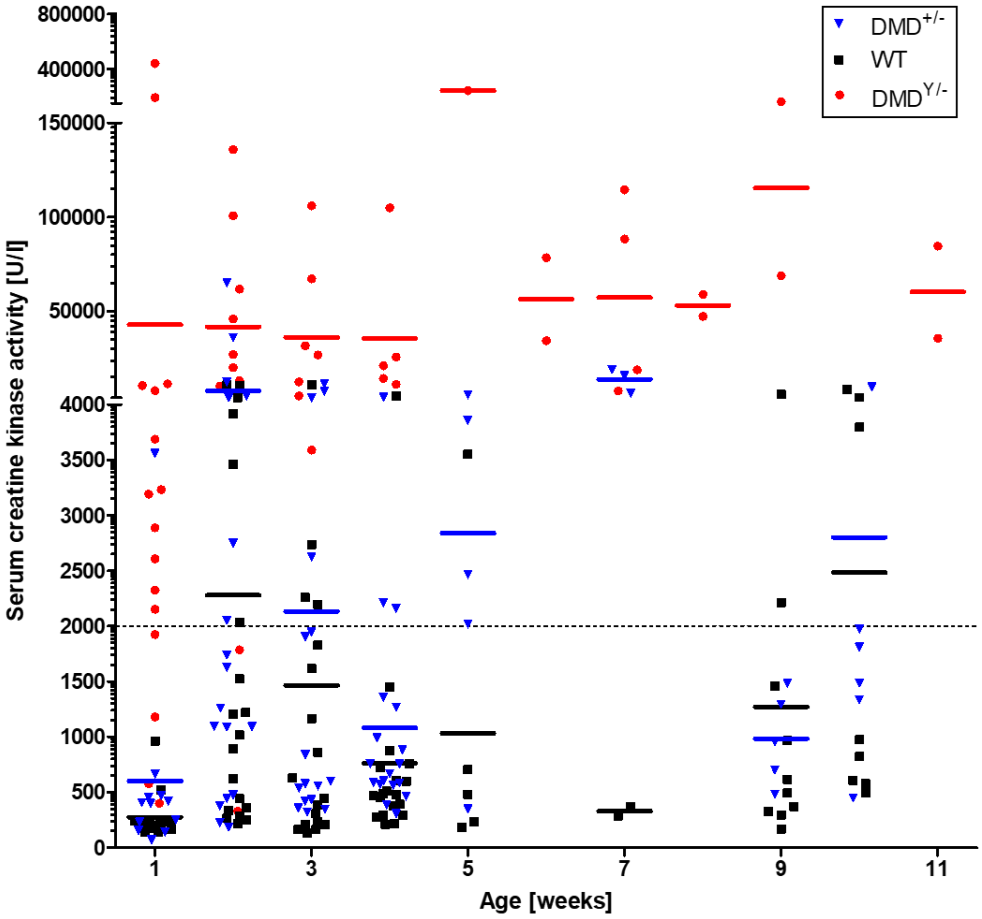

Figure 13: Comparison of creatine kinase levels. CK measuements of n = 89 pigs (n = 25 WT, n = 35 *DMD*$^{+/-}$ and n = 29 *DMD*$^{Y/-}$) are shown. Threshold: CK ≤ 2000 U/l is considered as normal.

3.3. Body weight of *DMD*$^{Y/-}$ compared to WT pigs

Newborn *DMD*$^{Y/-}$ piglets (n = 51) showed a significantly (p = 0.0091) lower birthweight, compared to male WT littermates (n = 54), however with a large variance of values ranging between 612 and 1766 g for *DMD*$^{Y/-}$ piglets and between 640 and 2240 g for male WT littermates (Figure 11). Subsequently, nearly all newborn *DMD*$^{Y/-}$ piglets showed a severe loss of body weight within the first 24 h of life, with a mean loss of 69.8±10.5 g (n = 47 *DMD*$^{Y/-}$ piglets). In comparison to male WT piglets (n = 45) that gained 90.9±12.9 g within the first 24 h of life, the loss of body weight in *DMD*$^{Y/-}$ piglets was highly significant (Figure 14, Insert). Figure 14 exemplarily shows the external appearance of 4-day-old *DMD*$^{Y/-}$ piglets (marked in blue) compared to male WT littermates. In Figure 16 an adolescent *DMD*$^{Y/-}$ pig compared to an age-matched female *DMD*$^{+/-}$ littermate is shown. *DMD*$^{Y/-}$ pigs show a reduced body size as well as generalized muscle atrophy compared to WT or *DMD*$^{+/-}$ littermates.

Figure 14: Representative pictures of 4-day-old *DMD*$^{Y/-}$ piglets (blue marked) and a male WT littermate. *DMD*$^{Y/-}$ piglets appear thinner and weaker, compared to age-matched WT animals.

From day 2 onwards, *DMD*$^{Y/-}$ piglets started to gain body weight (as displayed in detail in Fig. 11). However, body weight increase always stayed below the body weight levels of male WT littermates, as shown in Figure 15.

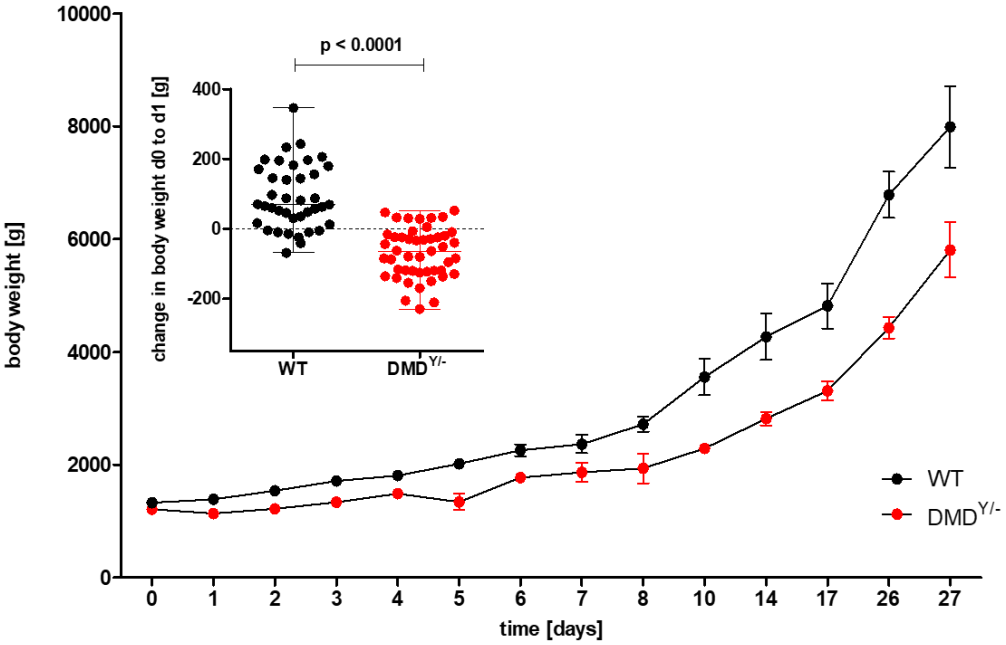

Figure 15: Comparison of body weight of *DMD*$^{Y/-}$ and male WT littermates in the first 27 days of life. The first 5 time points display body weight values of n ≥ 16 pigs for each genotype (max. n = 48, min. n = 16). From day 5 onwards time points display body weight values of n ≥ 5 for each genotype. Not all animals could be weighed at exactly the same time points, therefore raw data were adjusted to defined ages by linear interpolation. **Insert** shows the change in body weight from birth to 24 h after birth of *DMD*$^{Y/-}$ (n = 47) and male WT littermates (n = 39). Compared to male WT littermates, *DMD*$^{Y/-}$ piglets show a highly significant weight loss within the first 24 hours of life.

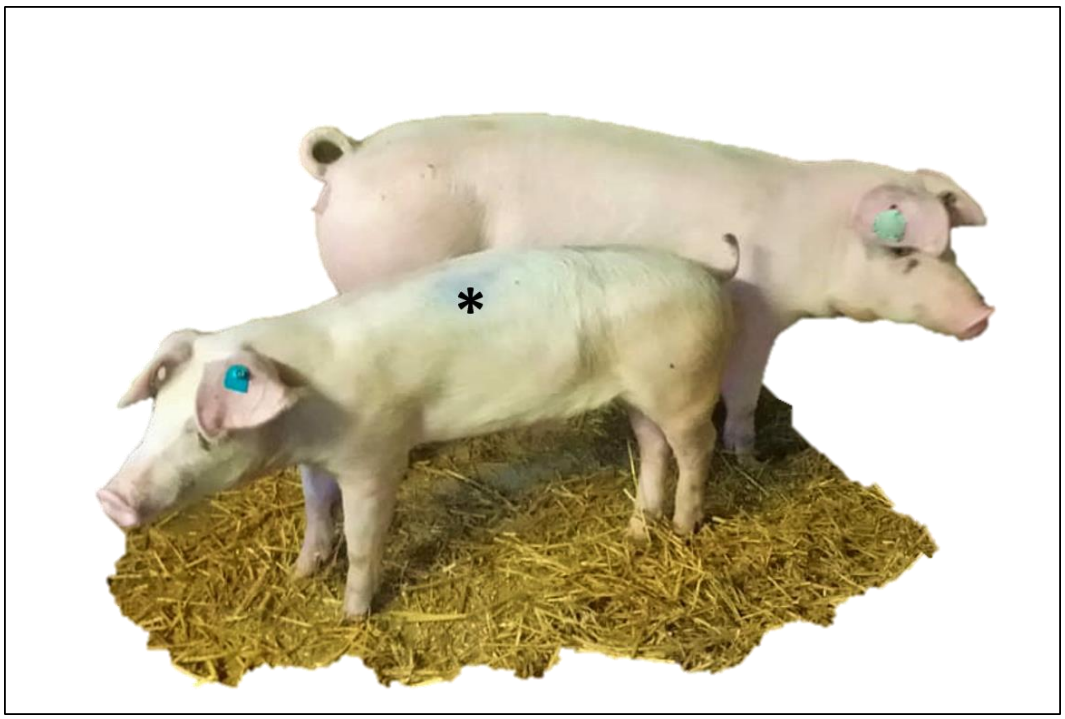

Figure 16: Representative picture of an adolecent male *DMD*$^{Y/-}$ pig and a female *DMD*$^{+/-}$ littermate. *DMD*$^{Y/-}$ pigs show a reduced body size as well as generalized muscle atrophy compared to WT or *DMD*$^{+/-}$ littermates. Foreground: *DMD*$^{Y/-}$ pig (black asterisk); background: *DMD*$^{+/-}$ pig; age of pigs shown: 126 days of life.

3.4. High mortality of *DMD*$^{Y/-}$ pigs generated by breeding

As indicated above, *DMD*$^{Y/-}$ pigs generated by breeding displayed a high mortality. Of a total of n = 97 *DMD*$^{Y/-}$ animals, n = 44 animals died within the first week of life (d 0-6), in the further referred to as "short-term surviving *DMD*$^{Y/-}$ piglets". 51% of all *DMD*$^{Y/-}$ pigs survived day 6 of life (in the further referred to as "long-term surviving *DMD*$^{Y/-}$ piglets"). 36% of all *DMD*$^{Y/-}$ piglets survived day 50 of life. Results are presented in a Kaplan-Meier survival curve, Figure 17. To prevent competition at the sows' teats between affected *DMD*$^{Y/-}$ and WT piglets, WT littermates were removed from the individual litters as soon as possible. Therefore, a Kaplan-Meier survival curve comparing survival of *DMD*$^{Y/-}$ and WT pigs was only feasible for the first 7 days of life (Insert Fig. 17).

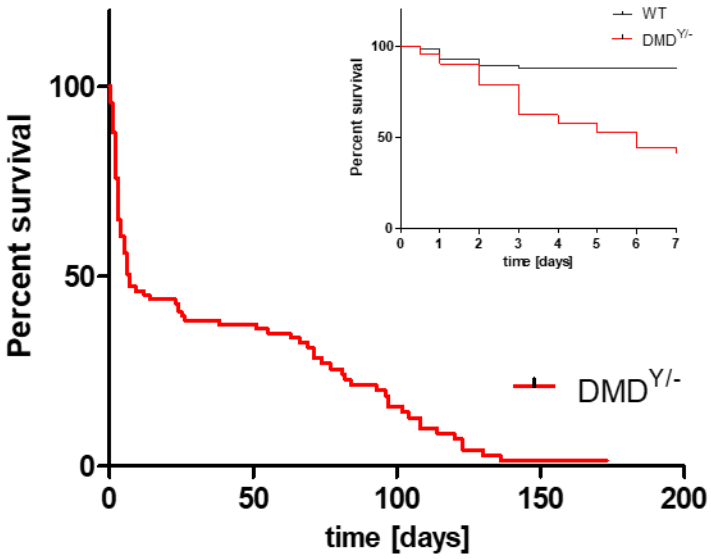

Figure 17: Kaplan-Meier survival curve for all n = 91 alive born *DMD*$^{Y/-}$ piglets, produced by breeding. Only one animal survived 173 days of life (#6790). **Insert** shows the neonatal death rate in week 1 of life of *DMD*$^{Y/-}$ piglets compared to male wild-type littermates (WT) (n = 61 *DMD*$^{Y/-}$, n = 56 male WT).

In week 1 of life, *DMD*$^{Y/-}$ piglets mainly had to be euthanized due to hypoglycemia, severely reduced general condition, the inability to drink independently, severe contractures and/ or muscle alterations or gastrointestinal symptoms. Adolescent *DMD*$^{Y/-}$ pigs died either due to sudden cardiac death, observed in several *DMD*$^{Y/-}$ pigs by analysing 24 h video surveillance data of the animals, or had to be euthanized due to severe physical deterioration (exhaustion, stridor or tachypnea) following the animal protection regulation.

3.5. Gross anatomical findings in short-term surviving *DMD*$^{Y/-}$ piglets

The majority, but not all short-term surviving *DMD*$^{Y/-}$ piglets (death during day 0 to day 6 of life) showed macroscopic muscle alterations in form of white discoloration at least in some muscle bundles of the intercostal muscles (Fig. 18), the neck muscles or the fore limb muscles, with the triceps brachii muscle being most frequently affected. Long-term surviving *DMD*$^{Y/-}$ pigs (surviving week 1 of life and longer) only rarely showed macroscopic muscle alterations, with the masseter being most frequently affected in these animals.

Figure 18: Macroscopic alterations of striated muscles in a 2-day-old *DMD*$^{Y/-}$ piglet. The picture section shows the white striped pattern observed in different muscle groups, here shown for the intercostal respiratory musculature.

3.6. Muscle histology of short- and long-term surviving *DMD*$^{Y/-}$ pigs

Histological findings in skeletal muscle of short-term surviving *DMD*$^{Y/-}$ piglets

Histology of skeletal muscles was performed at the paraffin laboratory of the Institute for Veterinary Pathology, LMU Munich. As shown in Figure 19a, skeletal muscle of 3-day-old WT pigles exhibited healthy striated muscle fibers with peripherically located nuclei and homogeneously stained cytoplasm. In contrast, in skeletal muscle of short-term surviving 3-day-old *DMD*$^{Y/-}$ piglets some muscle fibers had centrally located nuclei (Fig. 19b-c). In addition, skeletal muscles exhibited increased interstitial fibrosis and numerous foci with lymphohistiocytic infiltrations (Fig. 19b and d). Furthermore, several local foci with calcifications were observed in skeletal muscles of 3-day-old *DMD*$^{Y/-}$ piglets, which might explain the above mentioned macroscopic white striated pattern (Fig. 19b, e, f).

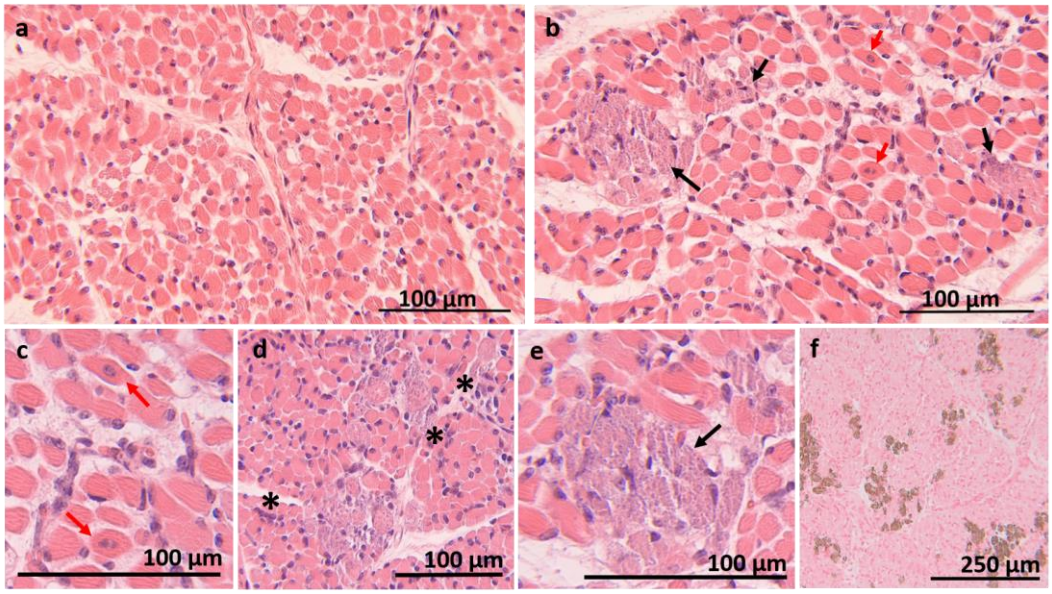

Figure 19: Histomorphological analysis of the triceps brachii muscle of a 3-day-old WT control pig (a) and a 3-day-old *DMD*$^{Y/-}$ littermate (b-f). Short-term surviving *DMD*$^{Y/-}$ pig shows local foci with calcifications (black arrows), centralized nuclei (red arrows) and lymphohistiocytic infiltrates (asterisks). Staining: **a-e**: H.E., **f**: Von Kossa.

An increased amount of collagenous connective tissue fibers was found in skeletal muscle tissue of short-term surviving *DMD*$^{Y/-}$ piglets compared to WT littermates (Fig. 20).

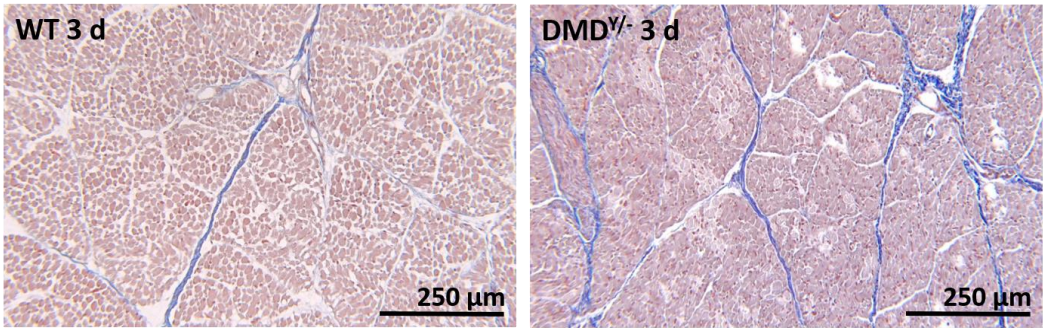

Figure 20: Representative images of skeletal muscle (triceps brachii) of 3-day-old WT and *DMD*$^{Y/-}$ piglets. Skeletal muscles of short-term surviving *DMD*$^{Y/-}$ piglets exhibited increased interstitial fibrosis. Staining: Masson Trichrome.

Histological findings in skeletal muscle of long-term surviving *DMD*$^{Y/-}$ piglets

Long-term surviving *DMD*$^{Y/-}$ pigs did not exhibit the macroscopic white striated muscle alterations as seen in young *DMD*$^{Y/-}$ piglets, except for mild to moderate white striping of masseter muscle found in some long-term surviving animals. Histologic examinations of triceps brachii muscle of long-surviving *DMD*$^{Y/-}$ pigs (> 84 d) revealed muscle fibers of varying diameters, in part angular shaped fibers. Several muscle fibers contained centralized nuclei or were round shaped and hypereosinophilic stained in H.E. staining, consistent with muscle fiber hypertrophy and degeneration. Endo- and perimysial tissue focally appeared with

moderate to marked lymphohistiocytic infiltrates occasionally surrounding and invading athrophic and necrotic myofibers, indicating myophagocytosis (Fig. 21). Interstitial fibrosis was highly apparent (Fig. 22a), whereas fatty replacement (Fig. 21d) was only occasionally present. Focal calcifications as seen in newborn *DMD*$^{Y/-}$ piglets were not observed (Fig. 22b).

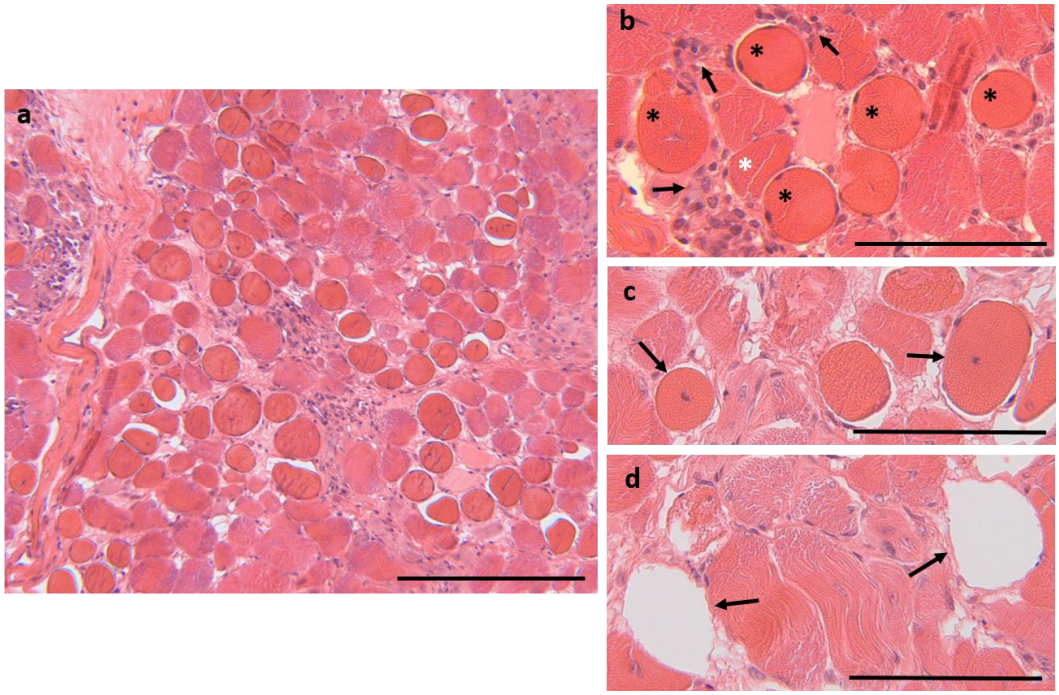

Figure 21: Histomorphology of triceps brachii muscle of long-term surviving *DMD*$^{Y/-}$ pigs. a, Overview of transverse sections reveal muscle fibers of varying diameters, hypercellularity with lymphohistiocytic infiltrates, muscle fiber hypertrophy and cell degeneration. **b**, Hypertrophic rounded fibers (black asteriks), angular shaped fibers (white asterisks), lymphohistiocytic infiltrates in endo- and perimysial tissue (arrows). **c**, Centrally located nuclei (arrows). **d**, Focal fatty replacement (arrows). Staining: H.E., scale bars: **a**: 250 µm, **b-d**: 100 µm. Age of pigs shown: 15th week of life.

In skeletal muscle of long-term surviving *DMD*$^{Y/-}$ piglets collagenous connective tissue was highly increased (Fig. 22a), whereas no calcium deposits were detected (Fig. 22b).

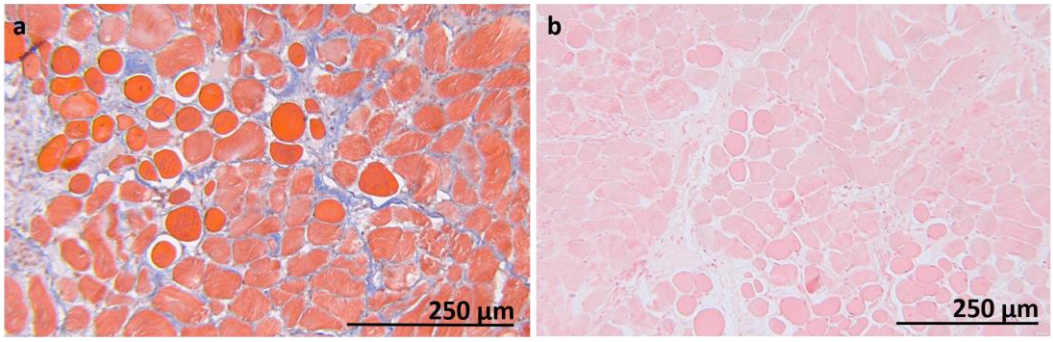

Figure 22: Representative histological sections of triceps brachii muscle of long-term surviving *DMD*$^{Y/-}$ pigs. Staining: **a**: Masson Trichrome, **b**: Von Kossa (brown color: calcium deposits). Age of pigs shown: 15th week of life.

In conclusion, the observed alterations in skeletal muscle of newborn and adolecent *DMD*$^{Y/-}$ pigs both illustrate severe muscular dystrophy, including muscle degeneration and regeneration processes. However, skeletal muscles of *DMD*$^{Y/-}$ piglets which died during week one (d 0-6) of life, in general appeared to be more severily affected by focal calcium deposits, whereas in skeletal muscle of adolecent *DMD*$^{Y/-}$ pigs the subsequent replacement of muscle tissue by fatty and connective tissue, reflecting the conditions in human DMD patients, was more prominent.

3.7. Gastrointestinal alterations in *DMD*$^{Y/-}$ piglets

DMD$^{Y/-}$ pigs of the short-surviving group died or where euthanized due to different reasons, as described above. A severely reduced general condition of newborn *DMD*$^{Y/-}$ piglets was often consistent with reduced blood glucose levels (a glucose level below 50 mmol/l was set as threshold to induce supplementary gastric tube feeding). Therefore, within the last applied rearing approach glucose levels were measured in all weak appearing newborn *DMD*$^{Y/-}$ piglets (n = 24 analyzed). However, few newborn *DMD*$^{Y/-}$ piglets (n = 2; 8% of newborn *DMD*$^{Y/-}$ piglets analyzed) exhibited acute poor general condition in combination with an abnormally high blood glucose level (up to 237 mmol/l). Other *DMD*$^{Y/-}$ animals were registered with difficulties in defecation (repeated strain to eliminate feaces) and increasing abdominal girth and, at later stages, anorexia. One *DMD*$^{Y/-}$ animal had to be euthanized due to increased abdominal girth combined with abdominal edema and ascites (detected by ultrasound scan). In total n = 11 *DMD*$^{Y/-}$ piglets (out of 28 *DMD*$^{Y/-}$ piglets resulting of n = 9 litters) were registered presenting at least one of the described symptoms. Therefore, necropsy of animals euthanized after showing either one or more of the described conditions, was extended by macroscopic evaluation of the entire gastrointestinal tract. Accumulation of gas and ingesta in the jejunum and large intestine, consistent with an obstipation, and dark coloration of the intestinal wall, consistent with an infarction of the intestinal wall, were observed, as exemplarily shown in Figure 23. In case of complete ileus, present in n = 2 animals, the intestinal wall already showed porosity, and the subsequent part of the intestine was empty. A submucosal rupture site was mainly found at the peak of the ascending large intestine (colon ascendens), anatomically presenting a 180° curve (Fig. 23c).

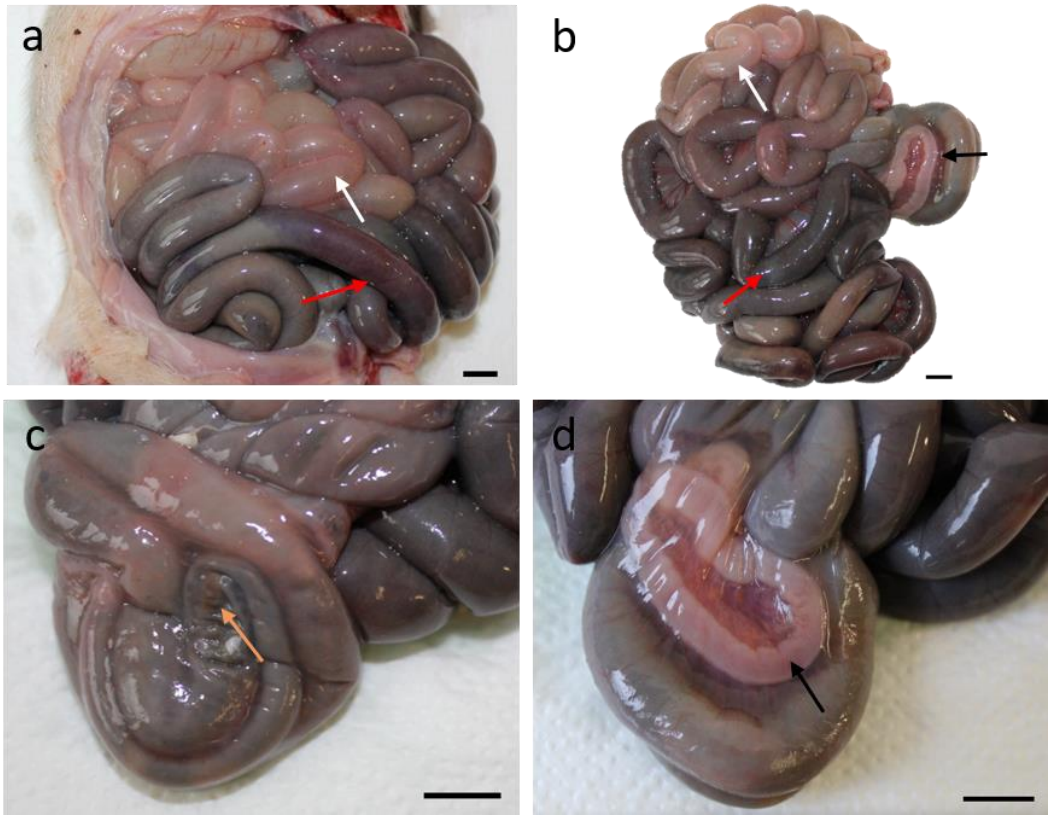

Figure 23: Macroscopic findings in a 6-day-old *DMD*$^{Y/-}$ piglet, presenting symptoms of a gastrointestinal phenotype. *DMD*$^{Y/-}$ piglet #6836 was found lying in lateral position with the legs tightened to the body and an increased abdominal girth. The animal was immediately euthanized and examined. **a**, Opening of the abdominal cavity shows dilated intestinal loops. **b**, Extracted intestine. **c**, Peak of the ascending large intestine with porous site. **d**, Descending large intestine subsequent to the obstructed part of the intestine, presenting as empty intestine section. White arrows: accumulation of gas; red arrows: infarction of the intestinal wall; black arrows: completely empty intestine, subsequent to ileus site; orange arrow: porous intestine site. Scale bars: **a-d:** 1 cm.

In some few animals, ascites and fibrinous layers in the abdominal cavity consistent with a peritonitis were present, indicating an already longer-lasting, clinically undetected, process.

Initial histologial studies of *DMD*$^{Y/-}$ piglets with gastrointestinal phenotype, performed by Christian Loch at the Institute for Veterinary Pathology, LMU Munich, indicate a putative increased amount of Type I collagen fibers, exemplarily shown in Figure 24. However, more research on this topic is needed and currently in work.

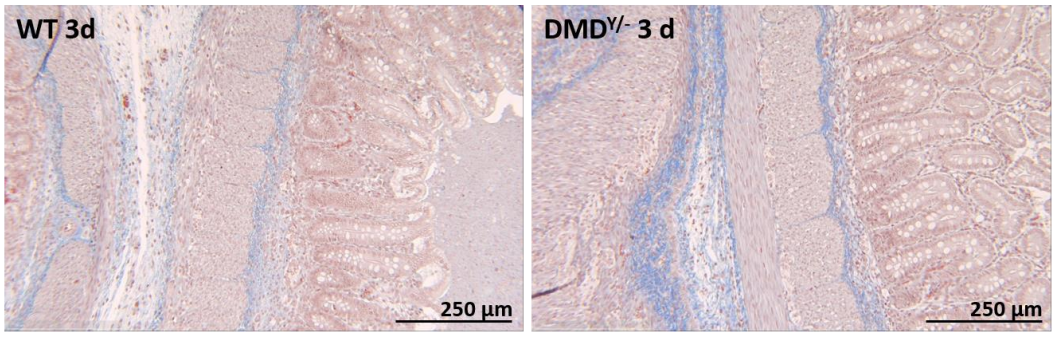

Figure 24: Representative histological images of colon ascendens of a 3-day-old *DMD*$^{Y/-}$ compared to an age-matched WT littermate. Staining: Masson Trichrome.

On the basis of the gastrointestinal findings, all *DMD*$^{Y/-}$piglets of litters, in which one or more animals showed gastrointestinal symptoms, received laxatives and digestion-aiding nutritional supplements from day 1 after birth onwards. In total, this medication was applied for n = 7 *DMD*$^{Y/-}$ piglets (out of 2 litters, colored in light blue in VI.2. Table 8). Of these, 86% (equivalent to n = 6 *DMD*$^{Y/-}$ animals) survived day 62 of life, indicating an effect of laxatives and digestion-aiding nutrients on the DMD phenotype in *DMD*$^{Y/-}$ pigs.

4. Identification of potential modifier loci in the *DMD*$^{Y/-}$ pig

It is known that the severity and manifestation of the DMD phenotype in human DMD patients can be strongly influenced by modifier genes. In human individuals with DMD, the most common phenotypic variation is the age at loss of ambulation (Bello et al., 2016). However, most studies rely on hypothesis, thus investigate only pre-specified candidate genes of interest. As already implied in the previous sections, the phenotypic characteristics in our *DMD*$^{Y/-}$ pigs generated by breeding varied. Therefore, modifier genes, which might influence the manifestation and severity of the phenotype in the *DMD*$^{Y/-}$ pig were studied. To identify candidate loci influencing the DMD phenotype, a genome wide combined linkage disequilibrium and linkage analysis (cLDLA) mapping study, scanning the entire genome for common genetic variations by detecting known single nucleotide polimorphisms (SNPs), was commenced.

4.1. Selection of survival time as study criteria for SNP genotyping

In total n = 97 *DMD*$^{Y/-}$ pigs were generated by breeding. As as shown in Table 9, all genotypes (WT male, WT female, *DMD*$^{Y/-}$ and *DMD*$^{+/-}$) were inherited equally following Mendelian segregation.

Table 9: Overview of all animals generated by breeding.

Sow	Boar	Birthdate	WT male	WT female	DMD$^{Y/-}$	DMD$^{+/-}$	Total
#3040	Tenor	08.06.2015	5	4	5	3	17
#3040	Tenor	28.01.2016	3	2	3	7	15
#3040	Eposo	29.06.2016	6	4	5	4	19
#3040	Rabatz	09.12.2016	4	0	0	3	7
#3040	Eposo	29.06.2017	1	1	1	1	4
#3040	Costa	30.11.2017	2	2	3	3	10
#3040	Costa	03.05.2018	5	4	5	0	14
#3040	Costa	03.10.2018	2	2	1	3	8
#3040	Costa	28.02.2019	1	5	3	1	10
#3040	Cor	25.07.2019	5	2	2	6	15
#5153	Isomer	18.10.2017	1	6	5	5	17
#5153	Casanova	16.03.2018	1	2	5	4	12
#5153	Boletto	09.08.2018	7	4	3	2	16
#5381	Costa	16.01.2018	4	1	2	5	12
#5381	Costa	14.06.2018	5	0	0	0	5
#5381	Costa	08.11.2018	3	3	2	6	14
#5382	Isomer	09.03.2018	4	4	9	3	20
#5382	Boletto	03.08.2018	1	6	4	7	18
#5382	Costa	27.03.2019	4	8	3	1	16
#5382	Cossa	22.08.2019	5	1	6	6	18
#5383	Costa	17.11.2017	1	4	6	3	14
#5383	Costa	12.04.2018	4	2	2	4	12
#5383	Casanova	06.09.2018	3	5	3	5	16
#5383	Cor	08.10.2019	3	2	2	7	14
#6225	Cor	02.09.2019	0	1	1	2	4
#6243	Cor	13.06.2019	5	3	3	3	14
#6245	Rabart	19.06.2019	3	4	3	3	13
#6245	Rabart	09.11.2019	2	3	7	4	16
#6314	Rabart	01.12.2019	4	3	3	3	13
Total			94	88	97	104	383
%			**24,54**	**22,98**	**25,33**	**27,15**	**100**

Among the phenotypic parameters determined in *DMD*$^{Y/-}$ pigs, survival time appeared to be the best defined and unbiased parameter for a genome-wide cLDLA mapping study. To avoid assignment erros, all still births and short-term survivors, which were crushed or possibly crushed by the sow or died due to an uncertain reason (e.g. infection), had to be excluded from the genome-wide cLDLA mapping study. Consequently, only a subset of n = 52 male *DMD*$^{Y/-}$ animals could be integrated.

Partial pedigrees of all DMD litters were created, showing only the *DMD*$^{Y/-}$ decendants. A color-coding helped to distinguish at first sight between short-term survivors (death within day 0-9 of life) and a long-term survivors (death after ≥ 10 days of life; Fig. 25-31).

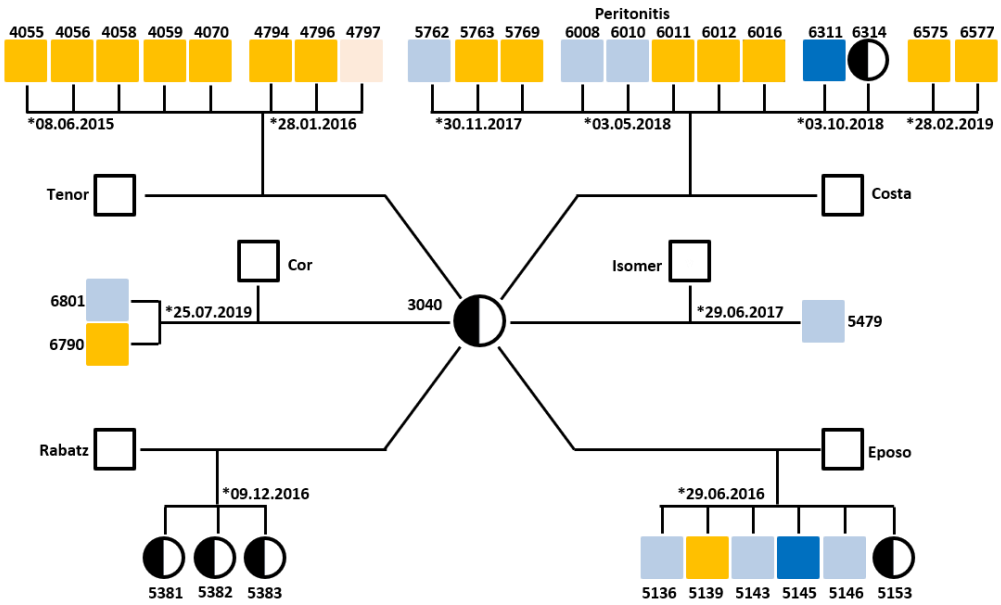

Figure 25: Partial pedigree of founder sow #3040 (black semi-marked circle, middle). Breeding boars are indicated in blank black squares. For each litter only *DMD*$^{Y/-}$ decendants (colored squares) and *DMD*$^{+/-}$ pigs used to expand the breeding herd (black semi-marked circles) are shown. Symbols: **Light blue squares:** either still born, crushed or possibly crushed short-term survivors (d 0-9 of life) excluded from the GWAS; **dark blue squares:** short-term survivers (d 0-9 of life) included in the GWAS, which most likely died due to a severe DMD phenotype; **Light orange squares:** long-term survivors (≥ 10 d of life) excluded from the GWAS (here: no DNA available); **dark orange squares:** long-term survivors (≥ 10 days of life) included in the GWAS.

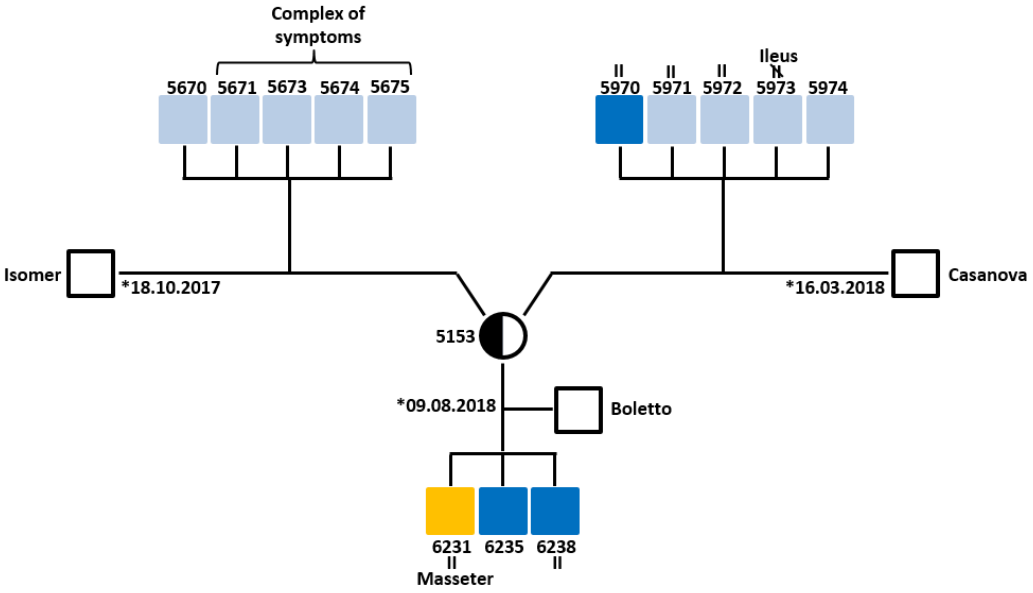

Figure 26: Partial pedigree of F1 sow #5153 (black semi-marked circle). Symbols: **light blue squares:** either still born, crushed or possibly crushed short-term survivors (d 0-9 of life) excluded from the GWAS; **dark blue squares:** short-term survivers (d 0-9 of life) included in the GWAS, which most likely died due to a severe DMD phenotype; **light orange squares:** long-term survivors (≥ 10 d of life) excluded from the GWAS (here: no DNA availible); **dark orange squares:** long-term survivors (≥ 10 days of life) included in the GWAS; **II:** macroscopic white striated muscle bundles (if "**Masseter**": only masseter muscle was white striated); **~~II~~:** no macroscopic white striated muscle bundles found; **complex of symtoms:** in part observed lateral positioning, rowing with the four limbs, salivation and, nystagmus (described in IV.2.).

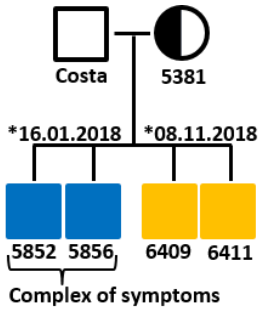

Figure 27: Partial pedigree of F1 sow #5381 (black semi-marked circle). Symbols: **dark blue squares:** short-term survivers (d 0-9 of life) included in the GWAS, which most likely died due to a severe DMD phenotype; **dark orange squares:** long-term survivors (≥ 10 days of life) included in the GWAS; **complex of symtoms:** in part observed lateral positioning, rowing with the four limbs, salivation and nystagmus (described in IV.2.).

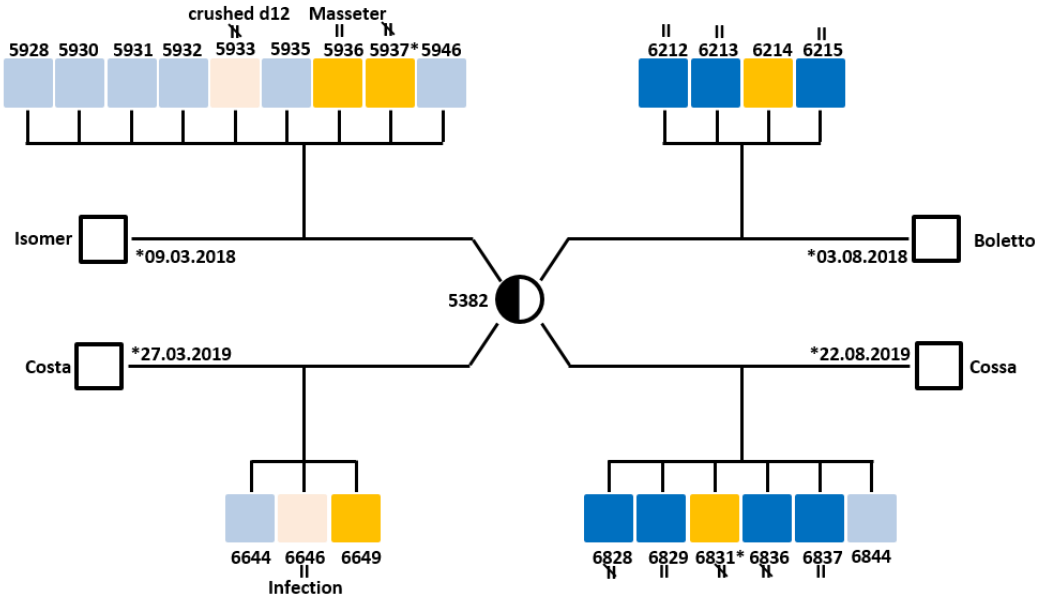

Figure 28: Partial pedigree of F1 sow #5382 (black semi-marked circle). Symbols: **Light blue squares:** either still born, crushed or possibly crushed short-term survivors (d 0-9 of life) excluded from the GWAS; **dark blue squares:** short-term survivers (d 0-9 of life) included in the GWAS, which most likely died due to a severe DMD phenotype; **Light orange squares:** long-term survivors (≥ 10 d of life) excluded from the GWAS (here: crushed at 12 days of life, or infection); **dark orange squares:** long-term survivors (≥ 10 days of life) included in the GWAS; **II:** macroscopic white striated muscle bundles (if "**Masseter**": only masseter muscle was white striated); **~~II~~:** no macroscopic white striated muscle bundles found.

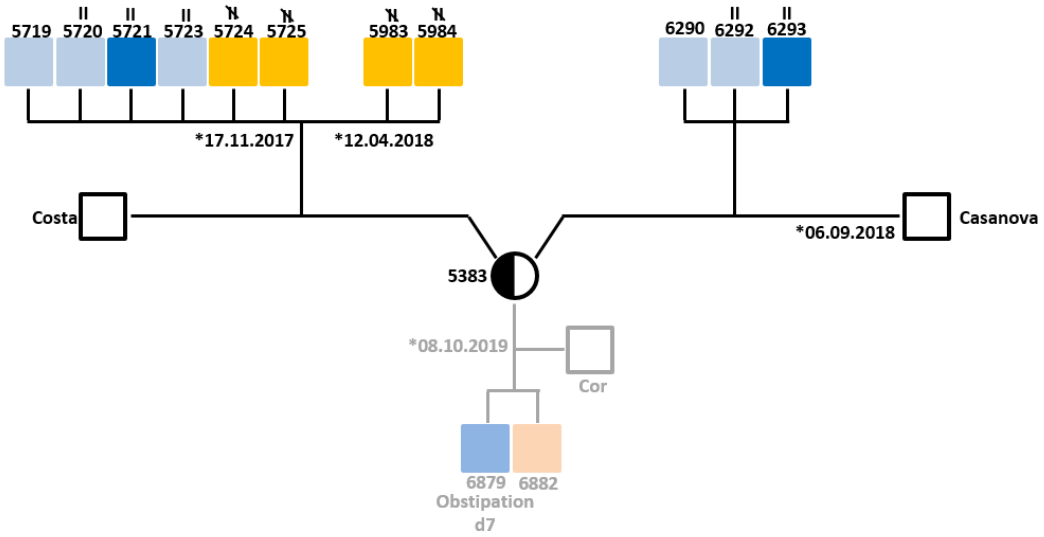

Figure 29: Partial pedigree of F1 sow #5383 (black semi-marked circle). Symbols: **Light blue squares:** either still born, crushed or possibly crushed short-term survivors (d 0-9 of life) excluded from the GWAS; **dark blue squares:** short-term survivers (d 0-9 of life) included in the GWAS, which most likely died due to a severe DMD phenotype; **Light orange squares:** long-term survivors (≥ 10 d of life) excluded from the GWAS (here: crushed at 12 days of life, or infection); **dark orange squares:** long-term survivors (≥ 10 days of life) included in the GWAS; **II:** macroscopic white striated muscle bundles; **~~II:~~** no macroscopic white striated muscle bundles found. **Gray shaded litter**: excluded from SNP genotyping, due to the questionable effect of laxatives on survival of *DMD*$^{Y/-}$ pigs.

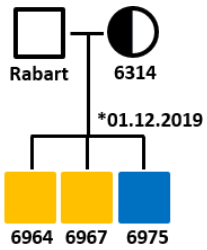

Figure 30: Partial pedigree of F1 sow #6314 (black semi-marked circle). Symbols: **dark blue squares:** short-term survivers (d 0-9 of life) included in the GWAS, which most likely died due to a severe DMD phenotype; **dark orange squares:** long-term survivors (≥ 10 days of life) included in the GWAS.

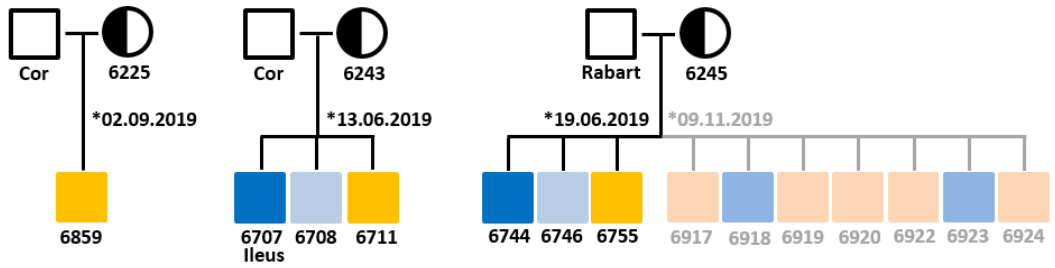

Figure 31: Partial pedigree of F2 sows #6225, #6243 and #6245 (black semi-marked circles Symbols: **Light blue squares:** either still born, crushed or possibly crushed short-term survivors (d 0-9 of life) excluded from the GWAS; **dark blue squares:** short-term survivers (d 0-9 of life) included in the GWAS, which most likely died due to a severe DMD phenotype; **dark orange squares:** long-term survivors (≥ 10 days of life) included in the GWAS; **gray shaded litter**: excluded from SNP genotyping, due to the questionable effect of laxatives on survival of *DMD*$^{Y/-}$ pigs.

4.2. Identification of candidate regions within the genome of *DMD*$^{Y/-}$ pigs

DNA was isolated from all *DMD*$^{+/-}$ sows and male *DMD*$^{Y/-}$ offspring. The purified DNA was subsequently employed for a genome wide cLDLA mapping. SNP-genotypes of the WT sires were provided.

Male *DMD*$^{Y/-}$ animals were analysed according to two different criteria: PhContinous categorized "length of life in days", and PhDiscrete categorized phenotype 1 as short-term survivors (death within 2-9 days of life) and phenotype 2 as long-term survivors (death within ≥ 10 days of life). Using PhDiscrete as cirterion, n = 19 animals were rated as short-term survivors and n = 33 as long-term survivors.

Positions with significant likelihood ratio test (LRT)-values

A likelihood ratio test (LRT) was calculated at each SNP interval midpoint. Using PhDiscrete phenotype coding, an LRT peak suggesting linkage between underlying haplotypes and observed phenotype, was estimated on chromosome 7 (19.8 Mb) with estimated LRT-value of 12.0. Using PhContinous phenotype coding, a QTL was estimated on chromosome 1 (at 46.6 Mb) with an indicative LRT peak of 12.2. Nevertheless, chromosome 1 in total revealed a noisy LRT pattern, relativizing the probability of this locus. Another QTL was estimated on chromosome 8 (109.7 Mb) with an estimated LRT-value of 12.6. For both criterions further indicative LRT-values have been found on other chromosomes, however, not revealing marked peaks. On 17 chromosomes (chrom. 2, 3, 4, 5, 6, 10, 11, 12, 13, 14, 15, 16, 17, 18, 19, 20) an evenly low, homogeneous pattern of LRT values was observable, making these chromosomes unlikely to contain modifying loci influencing the survival phenotype of *DMD*$^{Y/-}$ pigs. The results for all chromosomes are shown in Figure 32, with chromosome 8 selected as example to illustrate a candidate for a potential modifying locus.

Summarizing, using PhContinous and PhDiscrete as criteria, so far no genome-wide significant QTL responsible for the variable survival phenotype of *DMD*$^{Y/-}$ pigs could be identified. However, with a continously increasing number of animals

included in the study, the LRT curves became smoother and less peaked. On some chromosomes indicative values were observed. Thus, a higher number of animals and, eventually, a more explicit classification system, might reveal a clearer picture.

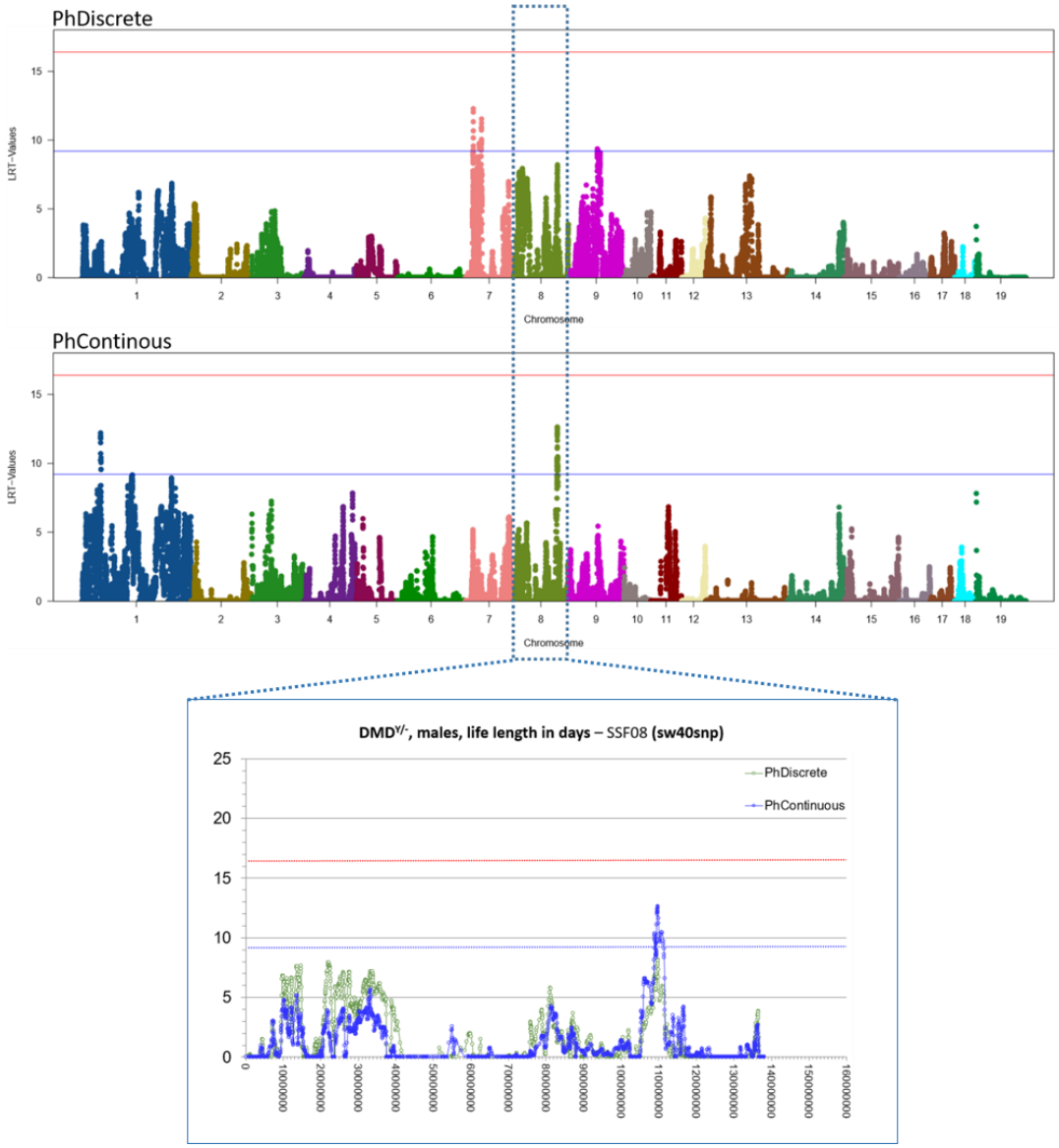

Figure 32: Manhattan plot used to display candidate regions suggesting modifying loci with influence on survival time of *DMD*$^{Y/-}$ pigs. Results of the cLDLA for *DMD*$^{Y/-}$ pigs with sliding window of 40 SNPs are displayed. The pig chromosomes are presented on the x-axis. On the y-axis, the calculated likelihood ratio test (LRT)-values are shown. The blue horizontal line marks the chromosome-wide (i.e. indicative), the red horizontal line the genome-wide significance threshold. PhDiscrete categories phenotype 1 as short-term survivors (death within 2-9 days of life) and phenotype 2 as long-term survivors (death within ≥ 10 days of life). PhContinous categories "length of life in days". In total, n = 52 *DMD*$^{Y/-}$ decendants were included in the GWAS. For PhDiscrete n = 19 *DMD*$^{Y/-}$ animals were rated as phenotype 1 and n = 33 as phenotype 2. **Insert:** Chromosome 8 was selected as example to illustrate a candidate for a potential modifying locus.

5. Somatic gene editing ameliorates muscle failure in the DMD pig

In a therapeutic trial in *DMD*$^{Y/-}$ pigs, somatic gene editing to restore the open reading frame (ORF) of the *DMD* gene was performed, analysed and validated. The aim of the therapeutic approach was to excise exon 51 in *DMD*Δ52 pigs after self-assembly of both intein-carrying Cas9 halves, and thereby to restore the ORF, which leads to the expression of an internally truncated but largely functional dystrophin protein. It thus aims at converting Duchenne muscular dystrophy into the milder Becker muscular dystrophy. The complete results are published in Moretti et al. (2020).

Transduction of *DMD*$^{Y/-}$ pigs with G2-AAV9-Cas9-gE51

For the therapeutic trial, a total of n = 25 *DMD*$^{Y/-}$ pigs were used. Of these, n = 6 animals served as untreated controls, n = 6 animals received local i.m. injections in the fore- and hindlimb of the right side of the body and n = 13 animals received systemic i.v. injection of G2-AAV9-Cas9-gE51. Of the i.v. injected *DMD*$^{Y/-}$ pigs n = 6 animals received a low dose (1-5 × 10^{13} vp/kg BW), wheras n = 7 animals received a high dose (2 × 10^{14} vp/kg BW) of G2-AAV9-Cas9-gE51.

5.1. Dystrophin expression in skeletal muscle of treated *DMD*$^{Y/-}$ pigs

In a first *in vivo* approach in the *DMD*$^{Y/-}$ pig, the expression of internally truncated stable dystrophin was assessed after local application of AAV9-Cas9-gE51Cas9. Therefore, 10- to 14-day-old *DMD*$^{Y/-}$ pigs were injected unilaterally into their fore- and hindlimb muscles with AAV9-Cas9-gE51 in doses of 2 × 10^{13} viral particles (vp) per kg BW. 6 weeks after AAV9-Cas9-gE51 transduction, pigs were euthanized and histologic analysis was performed, revealing the restoration of membrane-localized dystrophin in the treated muscle sites. Low dystrophin levels at the contralateral limbs could be detected. As might be expected, vital organs such as diaphragm and heart were not affected by i.m. limb injection. Therefore, dystrophin expression in these organs was aimed at by systemic application of AAV9-Cas9-gE51. For this approach, AAV9-Cas9-gE51 was coated with G2-PAMAM nanoparticles for the enhancement of myotropism of the viral vectors. A first low-dose approach (1-5 × 10^{13} vp/kg BW) with G2-AAV9-Cas9-gE51 revealed only sporadic transduction of skeletal muscle specimens. A second approach using high-doses (2 × 10^{14} vp/kg BW) of G2-AAV9-Cas9-gE51 enabled the expression of dystrophin in skeletal muscles, as well as in diaphragm and heart.

All results were confirmed at the genomic (successful elimination of exon 51) and transcript level (the expression of a *DMD*Δ51-52 transcript) (not shown). Immunofluorescence analysis visualized the expression of dystrophin in striated muscles. Targeted absolute quantification of dystrophin in skeletal muscle of treated *DMD*$^{Y/-}$ pigs by selected reaction monitoring (SRM) likewise proved the expression of dystrophin. In a holistic proteome analysis, an insight on the effect of DMD treatment on the skeletal muscle proteome of *DMD*$^{Y/-}$ pigs was provided. Analyses of 24 h behavioral observations of WT, treated and untreated *DMD*$^{Y/-}$ pigs substantiated the effectiveness of DMD treatment. Furthermore, two different approaches to analyze potential intracellular off-target effects were applied.

Immunofluorescence analysis for the visualization of dystrophin expression in skeletal muscle

Immunofluorescent staining, performed by Tarik Bozoglu of the Clinic and Policlinic for Internal Medicine I, Klinikum Rechts der Isar, TU Munich, visualized the results explained above. Dystrophin expression was observed in the locally treated muscle sites of i.m. injected *DMD*$^{Y/-}$ pigs. A wide spread expression of dystrophin was visible in all considered muscles of systemically high-dose treated *DMD*$^{Y/-}$ pigs. In muscles of systemically low-dose treated *DMD*$^{Y/-}$ animals nearly no dystrophin expression was detectable (Figure 33).

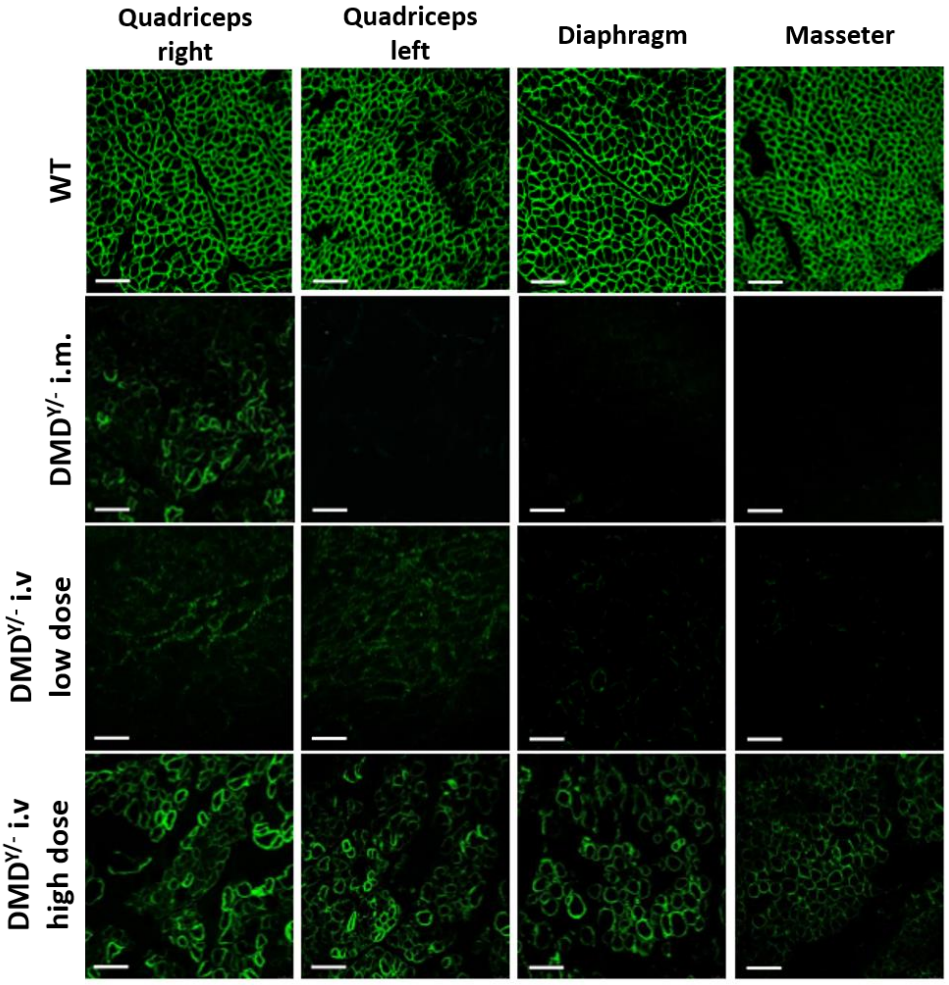

Figure 33: Representative immunofluorescence (IF) analysis. IF staining was applied for the visualization of dystrophin in striated muscles (quadriceps muscle, diaphragm and masseter) of WT, i.m. treated *DMD*$^{Y/-}$ (Quadriceps right = treated side, Quadriceps left = non-treated side) and i.v. treated *DMD*$^{Y/-}$ pigs (low- and high-dose). Scale bars indicate 200 µm (adapted from Moretti et al., 2020).

Targeted absolute quantification of dystrophin in skeletal muscle of treated *DMD*$^{Y/-}$ pigs by selected reaction monitoring analysis

Targeted absolute quantification of dystrophin in skeletal muscle by selected reaction monitoring (SRM) analysis likewise confirmed the expression of dystrophin. The approach was performed in cooperation with Thomas Fröhlich and

Florian Flenkenthaler, Gene Center - LAFUGA, LMU Munich.

SRM analysis of representative samples from indicated skeletal muscles of i.m. treated or high-dose i.v. treated *DMD*$^{Y/-}$ pigs confirmed the expression of dystrophin in either the injected muscle sites (i.m. treated) or analyzed muscle sites (high-dose i.v. treated). As shown in Figure 34, the quantification of dystrophin expression revealed highly variable dystrophin levels between different muscle specimens, varying from < 1% up to 62% (of WT dystrophin level) in i.m. treated and from < 1% up to 38% (of WT dystrophin level) in high-dose i.v. treated *DMD*$^{Y/-}$ pigs. However, different analytical methods (genomic analysis, transcriptomic analysis) of the same muscle specimens revealed similar results, indicating varying distribution of the pair of intein-split Cas9 and gRNA-encoding virus particles from the application site.

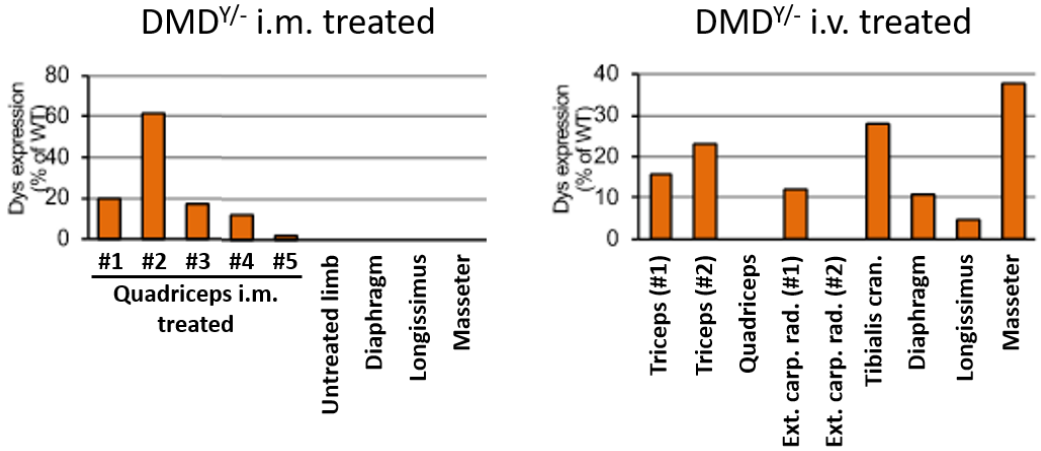

Figure 34: Representative results of mass spectrometry-based (SRM) dystrophin quantification. Dystrophin quantity of samples of indicated skeletal muscles of i.m. treated (n = 2) and high-dose i.v. treated (n = 3) *DMD*$^{Y/-}$ pigs are shown. Dystrophin expression levels are shown in % of WT. Expression data of i.m. treated *DMD*$^{Y/-}$ pigs reveals highly variable dystrophin expression in different muscle specimens of locally treated quadriceps muscle, whereas untreated muscle shows a total lack of dystrophin. Variable levels of dystrophin expression can also be observed in different muscle samples of i.v. high-dose treated *DMD*$^{Y/-}$ animals, in part reaching nearly 40% of WT (adapted from Moretti et al., 2020).

Holistic proteome analysis provides insights into the effect of DMD treatment on the skeletal muscle proteome of *DMD*$^{Y/-}$ pigs

Holistic proteome analysis was performed in cooperation with Thomas Fröhlich and Florian Flenkenthaler, Gene Center - LAFUGA, LMU Munich. In total 2414 different proteins were identified. Of label-free, normalized quantification intensity values for skeletal muscle specimens of WT, i.m. treated and untreated *DMD*$^{Y/-}$ pigs, unsupervised hierarchical clustering (Fig. 35a) and a principal component analysis (Fig. 35b) were performed. Except for triceps #1 (i.m. treated *DMD*$^{Y/-}$), the samples clustered into 3 groups according to genotype (WT vs. DMD) and treatment (DMD i.m. treated vs. DMD untreated). The proteome pattern of triceps#1 (i.m. treated *DMD*$^{Y/-}$), which was the sample showing the highest dystrophin recovery, was even more shifted towards the WT proteome, indicating that DMD treatment had a clear effect to normalise the skeletal muscle proteome of

DMD$^{Y/-}$ pigs.

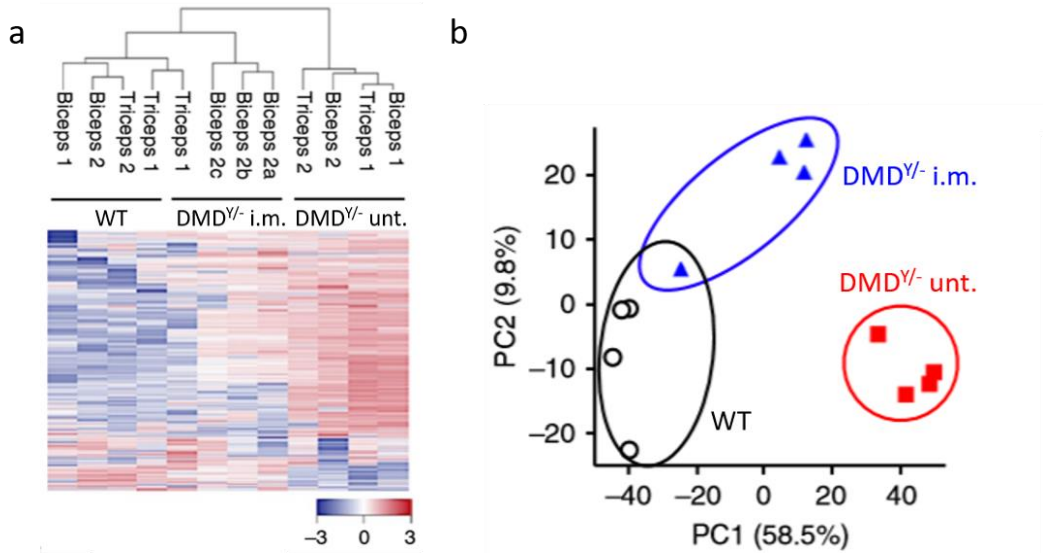

Figure 35: Holistic proteome analysis to validate the effect of DMD treatment on the skeletal muscle proteome of *DMD*$^{Y/-}$ pigs. a, Unsupervised hierarchical clustering of label-free quantification (LFQ) values for skeletal muscle specimens of WT, i.m. treated and untreated *DMD*$^{Y/-}$ pigs. Z-score-normalized expression values for the different proteins are color coded. **b**, For principal component analysis, proteins were isolated from the same triceps and biceps muscle samples from WT, i.m. treated and untreated *DMD*$^{Y/-}$ pigs (n = 2 per group) as used in **a**. Each symbol is equivalent to an individual sample (n = 4 samples per group). The proportion of variance explained by each component is shown (adapted from Moretti et al., 2020).

5.2. Creatine kinase levels decreased in high-dose treated *DMD*$^{Y/-}$ pigs

Serum creatine kinase (CK) levels of *DMD*$^{Y/-}$ animals were measured at two timepoints: between week 1-3 of life (before treatment), and at the day of termination of the experiment. However, blood collection before treatment was not possible in all *DMD*$^{Y/-}$ animals due to individual high suspectibility to stress. Concerning CK values at termination of the experiment, only plausible values could be used for analysis. Implausbility of values included for example death due to external stressors (e.g. transportation, harrassment by littermates), unobserved death and a resulting long timespan between death and blood collection, or obvious severe hemolysis. Consequently, only selected CK values were analyzable, reducing the statistic validity. However, of n = 4 WT, n = 3 untreated *DMD*$^{Y/-}$, n = 4 i.m. injected *DMD*$^{Y/-}$ and n = 3 i.v. high-dose i.v. treated *DMD*$^{Y/-}$ pigs the evaluation of CK values was feasible. CK levels of WT animals were low as expected (below the threshold of 2000 U/l). A derease of CK levels in i.v. high-dose treated *DMD*$^{Y/-}$ compared to untreated or i.m. treated *DMD*$^{Y/-}$ animals was observable. The results are shown in Figure 36.

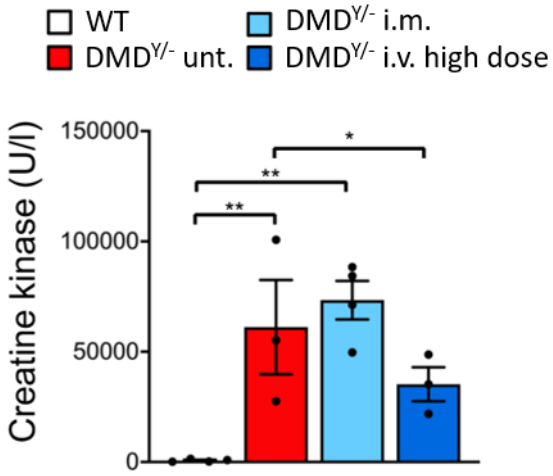

Figure 36: Serum creatine kinase (CK) values. CK levels of n = 4 WT, n = 3 untreated *DMD*$^{Y/-}$, n = 4 i.m. injected *DMD*$^{Y/-}$ and n = 3 i.v. high-dose i.v. treated *DMD*$^{Y/-}$ pigs are shown. Statistics: one-way ANOVA with Bonferroni's multiple comparison test, results are presented as mean±s.e.m. (adapted from Moretti et al., 2020).

5.3. Functional muscle improvement due to somatic gene editing

To validate the effect of DMD treatment on muscle function as biomarker for the clinical course of the disease, locomotion had to be assessed in WT, treated and untreated *DMD*$^{Y/-}$ pigs. Therefore, different approaches, such as treadmill tests and supervision with step counters, were examined. Due to the occurrence of sudden arrhythmia-induced death of *DMD*$^{Y/-}$ pigs in low stress situations (e.g. handling such as weighing and blood taking, veterinary accompanied transportation, or ranking order fights between littermates), the performance of treadmill tests was not feasible. Step-counters to objectively monitor activity and resting periods and to compare the numbers of steps were likewise figured out to be inappropriate when used for pigs kept in groups, as littermates damaged the detectors affixed to the hind limbs.

Therefore, a video surveillance system was installed monitoring the animals 24 hours on seven days a week (24/7) and the obtained video data was analysed with regard to motion patterns and activity. As major advantage when compared to treadmill tests, video surveillance did not require interaction with the animals, facilitating a random and objective evaluation. Furthermore, a current lack of motivation of the individual animal or a reluctance to move did not influence analyses, as always 24 hours at a time were evaluated. As further benefit, errors of assessment due to interaction triggered behavioral changes were avoided. Furthermore, analyses could be repeated to avoid errors of observation.

As stated in Klymiuk et al. (2013), dystrophin-deficient pigs exhibit striking muscle weakness, occurring as reduced mobility in comparison with age-matched WT controls. To validate the effect of DMD treatment by somatic gene editing on muscle function, the activity of age-matched WT, treated and untreated *DMD*$^{Y/-}$ pigs was evaluated and compared. Therefore, a total of n = 12 animals (n = 4 male

WT pigs, n = 2 untreated *DMD*$^{Y/-}$, n = 2 i.m. injected *DMD*$^{Y/-}$ pigs, n = 4 high dose i.v. injected *DMD*$^{Y/-}$ pigs), were analyzed due to their behavior and activity on day 64 of life (64.4±3.5 days). As i.m. injection of G2-AAV9-Cas9-gE51 was attributed exclusively to the muscles of one side of the body, and no behavioral changes or functional impairment was expected in these animals when compared to untreated *DMD*$^{Y/-}$ pigs, all i.m. treated *DMD*$^{Y/-}$ and untreated *DMD*$^{Y/-}$ animals were considered as one group, in the further designated as *DMD*$^{Y/-}$ untreated.

As shown in Figure 37a, untreated *DMD*$^{Y/-}$ pigs showed a significantly decreased standing time (270±29 min/24 h) when compared to male age-matched WT littermates (429.3±33.5 min/24 h), consistent with premature fatigue. In high dose i.v. treated *DMD*$^{Y/-}$ pigs, the total duration of standing events was significantly ($p<0.05$) increased (388.8±20.7 min/24 h). Additionally, the average duration of standing events in untreated *DMD*$^{Y/-}$ pigs (3.05±0.69 min) was as a trend shorter than in WT pigs (5.97±1.19 min), but increased after high dose i.v. treatment (5.89±1.08 min). However, these differences were not statistically significant (Fig. 37b).

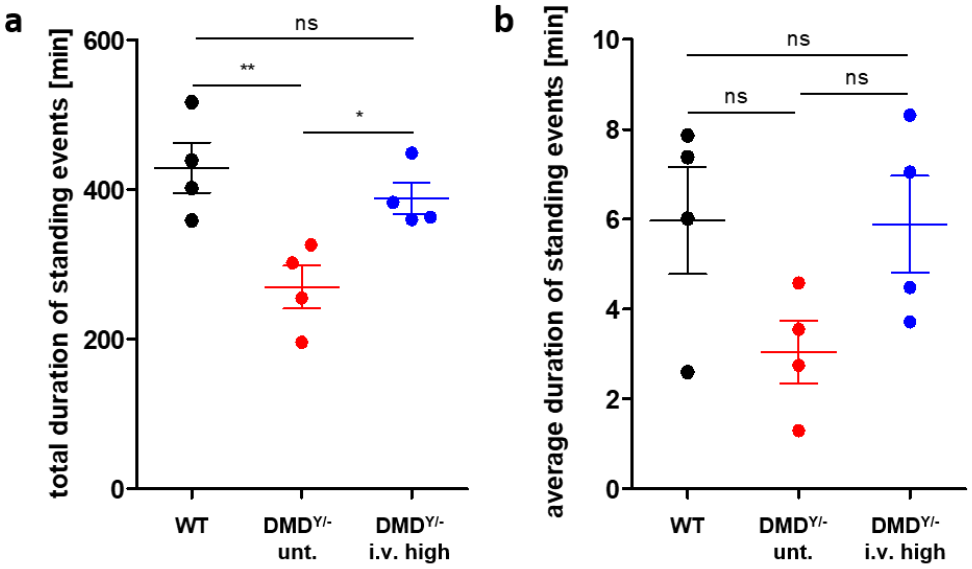

Figure 37: Continuous recording of motion patterns. Quantification of **a**, total and **b**, average duration of standing events per pig, performed for n = 4 WT, n = 4 *DMD*$^{Y/-}$ untreated and n = 4 *DMD*$^{Y/-}$ high dose i.v. treated pigs on day 64.4±3.5 of life. Statistics: one-way ANOVA with Bonferroni's multiple comparison test, results are presented as mean±s.e.m.

To highlight the above described impression of an increased duration of standing periods observed in high dose i.v. treated *DMD*$^{Y/-}$ animals, timelines of the 24 h video monitoring were generated, showing the frequency of adopting an upright posture. Figure 38 exemplarily shows timelines for a WT, an untreated and a high dose i.v. treated *DMD*$^{Y/-}$ pig.

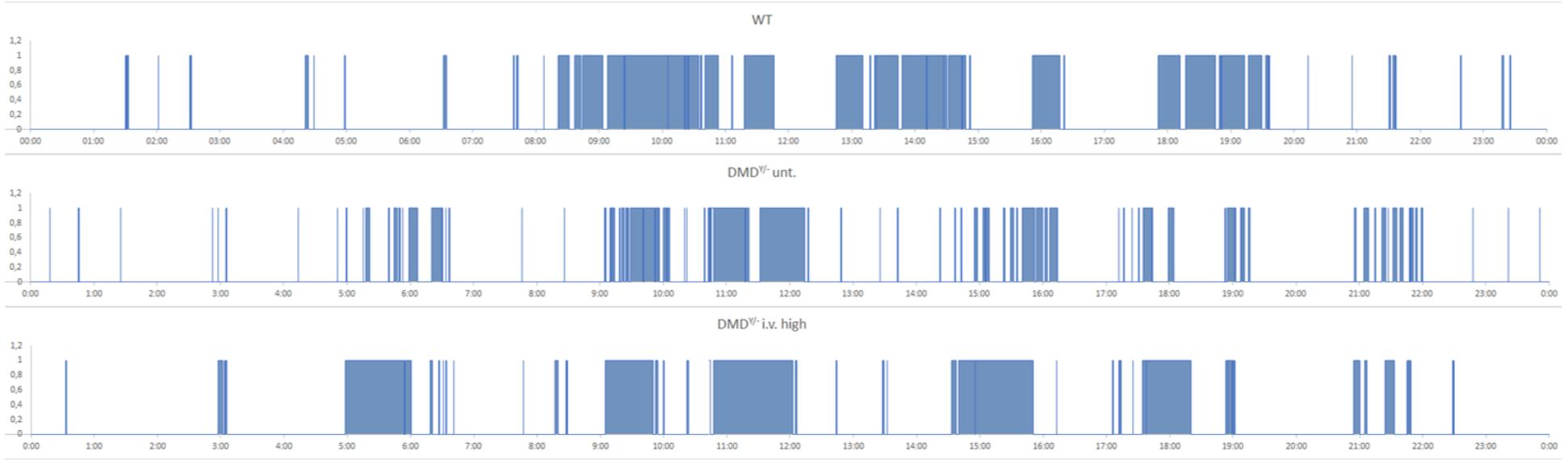

Figure 38: Representative timelines for 24 h video monitoring. 24-hour timelines of n = 1 WT, n = 1 untreated *DMD*$^{Y/-}$ and n = 1 high dose i.v. treated *DMD*$^{Y/-}$ pig are shown. Standing in upright posture is marked in blue color compared to lying or sitting posture. Generated timelines stress the impression of an increased standing duration in high dose i.v. treated *DMD*$^{Y/-}$ compared to untreated *DMD*$^{Y/-}$ pigs. However, no significant differences were found between WT, untreated *DMD*$^{Y/-}$ and high dose i.v. treated *DMD*$^{Y/-}$ pigs.

With instantaneous sampling the instant picture of every fifth minute (measured down to the centisecond) within 24 hours was evaluated in regards to activity versus lying or sitting posture. The number of activity events within 24 h significantly ($p < 0.05$) decreased in untreated *DMD*$^{Y/-}$ pigs (54.3±7.5 activity events/24 h) compared to WT pigs (82.8±7.7 activity events/24 h). High dose i.v. treatment increased the activity of *DMD*$^{Y/-}$ pigs almost to WT levels (76.5±4.0 activity events/24 h). In Figure 39 data for all n = 12 animals (n = 4 WT, n = 2 *DMD*$^{Y/-}$ i.m., n = 2 *DMD*$^{Y/-}$ untreated, n = 4 *DMD*$^{Y/-}$ high dose i.v. treated) is shown. Here, *DMD*$^{Y/-}$ untreated and *DMD*$^{Y/-}$ i.m. treated pigs are again splitted into two groups, as a difference in the number of activity events between these two groups was observed.

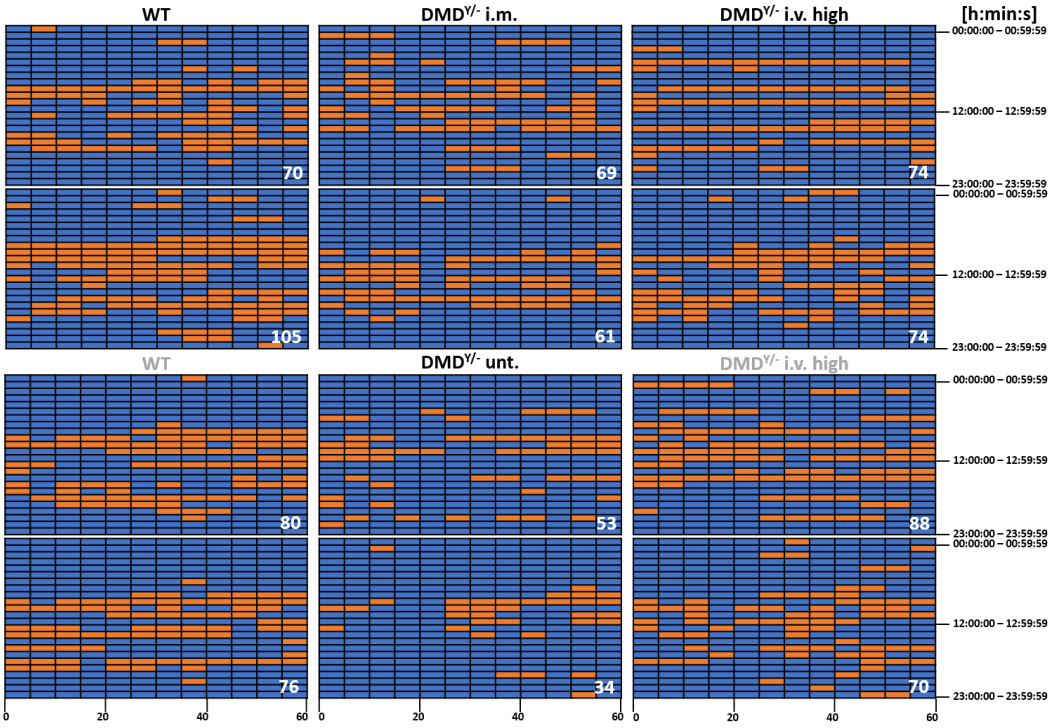

Figure 39: Instantaneous sampling of activity profiles. n = 12 pigs (n = 4 WT, n = 2 *DMD*$^{Y/-}$ i.m., n = 2 *DMD*$^{Y/-}$ untreated, n = 4 *DMD*$^{Y/-}$ high dose i.v. treated) were analysed. Activity versus lying or sitting posture was evaluated at every fith minute in 24 hours. Every box shows the activity pattern of one animal in 24 hours. Activity is coloured in orange, lying or sitting posture is colored in blue. White numbers in the boxes represent the sum of activity events counted for each box (i.e. animal).

During evaluation of the surveillance material, several additional individual behavior patterns were detected, such as pattering of the hind limbs, maintaining a sitting posture over an extended period, getting up over a sitting posture instead of immediate rising or eating in lying posture. Pattering of the hind limbs was observed for n = 2 animals (n = 1 i.m. treated *DMD*$^{Y/-}$ and n = 1 high dose i.v. treated *DMD*$^{Y/-}$ pig). However, for the high dose i.v. treated *DMD*$^{Y/-}$ animal the behavior was observed only one time in 24 h, compared to 7 times in 24 h for the i.m. treated *DMD*$^{Y/-}$ animal. n = 1 i.m. treated *DMD*$^{Y/-}$ pig showed positioning of the hind limbs in cranial direction during standing, leading to a frequent sliding away of the hind limbs. The same animal showed pattering of the hind limbs and eating in lying posture. For n = 7 animals (n = 2 WT, n = 1 untreated *DMD*$^{Y/-}$, n = 2 i.m. treated

DMD$^{Y/-}$ and n = 2 high dose i.v. *DMD*$^{Y/-}$) getting up over a sitting posture or the maintainance of a sitting posture over an extended period was observed. As animals of all groups showed this behavior it was approved as normal individual behavior. However, one untreated and one i.m. treated *DMD*$^{Y/-}$ pig showed severely prolonged sitting periods at nearly every getting up. n = 1 untreated *DMD*$^{Y/-}$ animal showed breathing through the mouth, consistent with stenotic breathing or limited respiratory function. For n = 3 pigs (n = 1 untreated, n = 1 i.m. treated and n = 1 high dose i.v. treated *DMD*$^{Y/-}$) eating in lying posture was observed.

5.4. Off-target analysis

As described in Moretti et al. (2020), two approaches were used to detect possible off-target effects triggered by the treatment with G2-AAV9-Cas9-gE51. First, targeted sequencing was used to detect mutations at the most likely predicted off-targets. Second, whole genome sequencing was performed as holistic approach to detect further potential off-target mutations.

Regarding the first approach, no mutations were found in the five most likely predicted sites for off-target effects. In the treated samples, no concordant alterations were found for the insertions or deletions of bases (INDELs) in the target regions. The observed mean alteration frequency of 0.01% (SD±0.3) ranged within the background error level of the DNA sequencer (0.1%).

By whole-genome sequencing in isogenic human DMDΔ51-52 iPSCs compared to the parental human DMDΔ52 iPSC line, a total of 88 INDELs and 769 single nucleotide variants (SNVs) were identified. The performed minimal Levenshtein distance analysis, calculating the smallest number of mismatches between one of the two DMD-E51 gRNAs and a putative off-target mutation site revealed that at least 7 operations (insertions, deletions or base exchanges) around a variant were required to match a gRNA (Figure 40), indicating that the identified INDELS and SNVs do not represent off-target effects of CRISPR-Cas treatment.

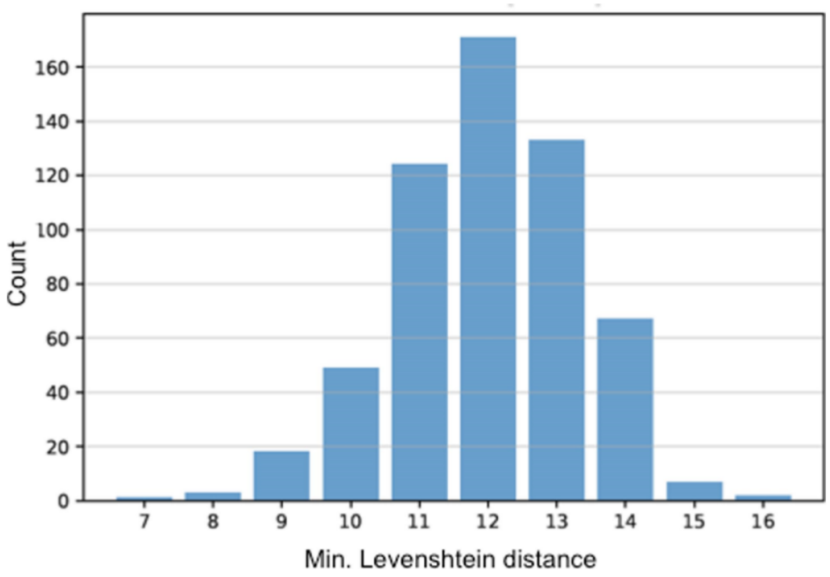

Figure 40: Minimal Levenshtein distance. The Levenshtein distance is the minimum number of mismatches (here: 7 mismatches) between a gRNA and a putative off-target mutation site. As no variants with <7 mismatches were found, the identified INDELS and SNVs cannot be considered as off-target effects of G2-AAV9-Cas9-gE51 treatment.

6. Multispectral optoacoustic tomography detects collagens in skeletal muscle

As dystrophic muscle tissue is gradually replaced by connective and fatty tissue, MSOT was validated as new noninvasive *in vivo* diagnostic imaging biomarker to assess the degree of muscle deterioration, apparent as fibrotic muscular transformation in DMD patients (Klingler et al., 2012). Therefore, the feasibility of the MSOT technology was first demonstrated in the DMD pig model, and later applied to pediatric patients. The complete results are published in Regensburger et al. (2019).

In the proof-of-concept study MSOT imaging of n = 17 piglets (n = 10 WT and n = 7 *DMD*$^{Y/-}$) was performed within 1-3 days after birth. In the longitudinal study, n = 11 piglets (n = 6 WT and n = 5 *DMD*$^{Y/-}$) underwent MSOT imaging at 4 time-points (week 1, week 2, week 3, week 4).

In the second step, applying the approach to pediatric patients (not shown), MSOT collagen signal was shown to highly correlate to the patients' functional status. When comparing MSOT imaging to magnetic resonance imaging, MSOT was found to provide additional information on molecular features.

All analysis of MSOT signals, as well as the bioanalytical analyses of collagen and protein content of individual muscle specimens and analysis of stained histologic slices of individual skeletal muscles were performed by the Department of Pediatrics and Adolescent Medicine, University Hospital Erlangen, FAU Erlangen Nuremberg, Erlangen.

6.1. Proof-of-principle study for collagen detection in *DMD*$^{Y/-}$ pigs

Collagen detection in *DMD*$^{Y/-}$ pigs by MSOT in single measurement

As described in Regensburger et al. (2019), in the proof-of-concept study a total of n = 58 scans (n = 34 in WT and n = 24 in *DMD*$^{Y/-}$ piglets) were acquired from independent muscle regions of n = 17 animals (n = 10 WT and n = 7 *DMD*$^{Y/-}$piglets) within day 1-3 of life. For every scan, a region of interest (ROI) was drawn within the assessed muscle, using ultra-sound guidance, exemplarily shown in Figure 41.

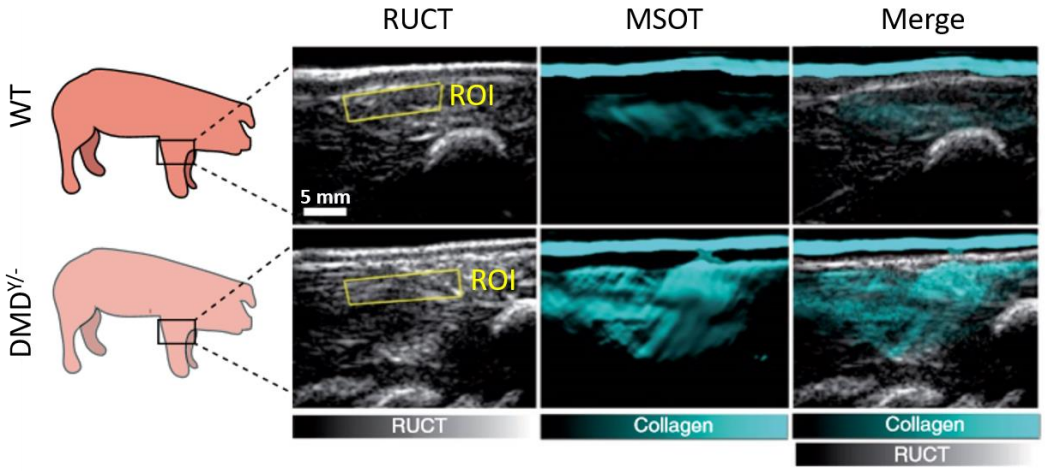

Figure 41: Representative presentation of skeletal muscle images from WT and *DMD*$^{Y/-}$ piglets, generated by MSOT imaging. ROIs are determined in the reflective ultrasound computed tomography (RUCT) image, which is used to anatomically guide the investigator. After spectral unmixing of the optoacoustic signals, qualitative differences of collagen signals between WT and *DMD*$^{Y/-}$ are visible (turquoise). In the merged RUCT/MSOT image, the collagen distribution within the muscle is visualized (adapted from Regensburger et al., 2019).

For the collagen$_{mean/max}$ signal, a significant difference was observed, when all independent muscle regions were compared between the two groups (n = 34 WT / n = 24 *DMD*$^{Y/-}$), as shown in Figure 42a-b (collagen$_{mean}$ = 14.41±2.66 a.u. versus 23.14±3.87 a.u. and collagen$_{max}$ = 27.68±2.72 a.u. compared to 41.05±7.43 a.u). When comparing 2d MSOT collagen$_{mean/max}$ signal per animal between groups (n = 10 WT and n = 7 *DMD*$^{Y/-}$ piglets), likewise a highly significant difference was observed between MSOT signals of the two groups, as shown in Figue 42c-d (collagen$_{mean}$ = 14.23±1.96 a.u. compared to 22.67±3.59 a.u. and collagen$_{max}$ = 27.70±1.67 a.u. versus 41.01±5.16 a.u.). For oxygenated, deoxygenated and total hemoglobin no differences in MSOT signal levels were observed (P > 0.05) (not shown).

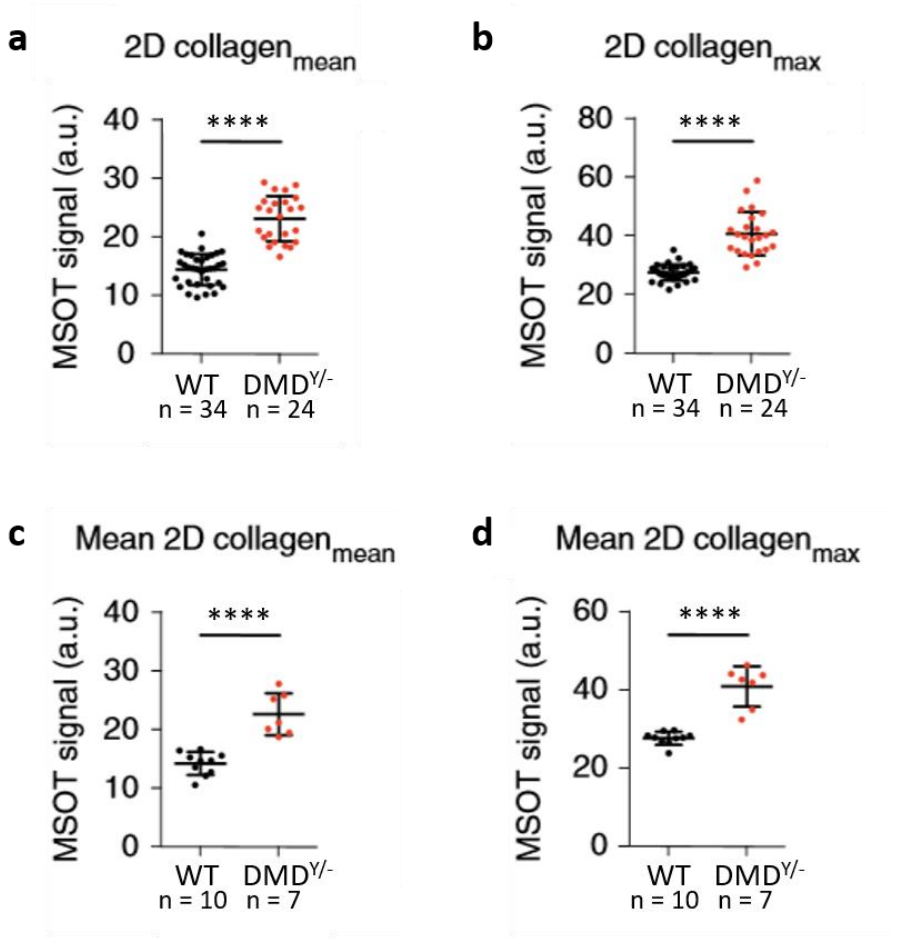

Figure 42: Diagrams represent the MSOT collagen signals from WT and *DMD*$^{Y/-}$ piglets generated within the proof-of-concept study. MSOT collagen signals are shown in arbitrary units (a.u.). **a-b**, 2D MSOT collagen$_{mean/max}$ signal, with each filled circle representing one MSOT signal per independet skeletal muscle region (n = 34 scans in WT and n = 24 scans in *DMD*$^{Y/-}$ piglets). **c-d**, Comparison of 2D MSOT collagen$_{mean/max}$ signal per animal between groups (n = 10 WT and n = 7 *DMD*$^{Y/-}$ piglets). Each filled circle represents the mean MSOT signal of an independent animal. Statistics: Two-tailed independent samples t-test, Welch's correction in cases of unequal variances, Mann-Whitney U-test if assumption of normal distribution was violated. Data are shown as mean±s.d. (adapted from Regensburger et al., 2019).

Receiver operator characteristic analysis

To distinguish between muscles from WT and *DMD*$^{Y/-}$ piglets, an exploratory receiver operator characteristic (ROC) analysis was performed (Figure 43), plotting the true-positive rate (sensitivity) against the false-positive rate (specificity). For the obtained 2D collagen$_{mean/max}$ signals the area under the curve (AUC), giving the discriminatory abilities of the method, with the respective 95% CI were calculated. MSOT-derived imaging parameters showed an excellent ability to distinguish healthy (WT) from diseased muscles (*DMD*$^{Y/-}$).

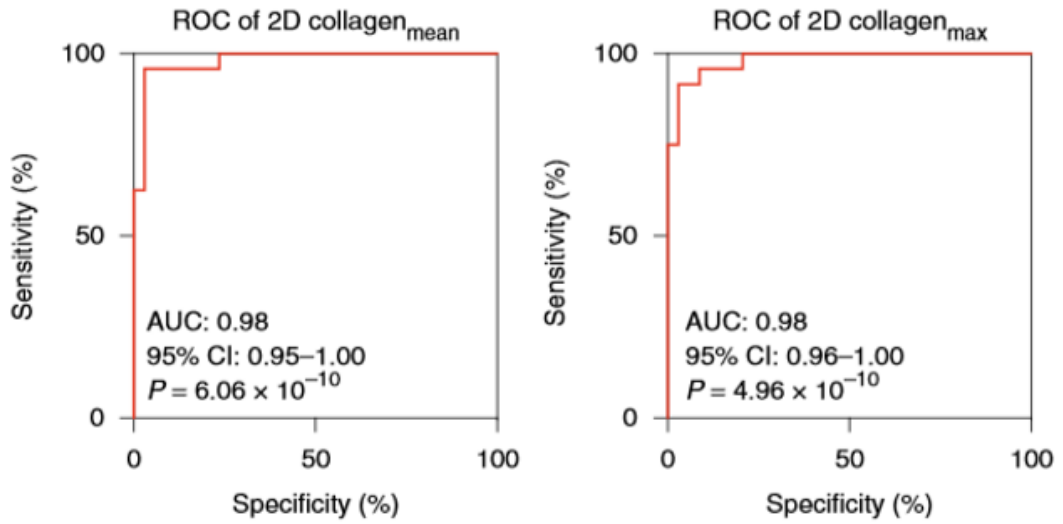

Figure 43: Receiver operating characteristic (ROC) curve. The area under the curve (AUC) and 95% confidence inerval (CI) show the ability of MSOT collagen signals to distinguish between healty (WT) and diseased muscles (*DMD*$^{Y/-}$). Analyses were performed using data from n = 58 independent muscle regions (n =34 WT, n = 24 *DMD*$^{Y/-}$) of n = 17 independent animals (n = 10 WT and n = 7 *DMD*$^{Y/-}$ piglets). ROC analysis showed a high specificity and a high sensitivity for collagen$_{mean/max,}$ indicating that the collagen signals detected by the MSOT technology show a high ability to distinguish between muscles of WT and *DMD*$^{Y/-}$ pigs (adapted from Regensburger et al., 2019).

Histologic examination reveals severly increased collagen content in skeletal muscle of *DMD*$^{Y/-}$ piglets

By H.E. staining, disrupted muscular structure was observed in the previously scanned muscle regions of *DMD*$^{Y/-}$ piglets. DYS1 immunohistochemistry confirmed the total loss of dystrophin in *DMD*$^{Y/-}$ piglets. Masson Trichrome (MT) and Sirius red (SR) staining revealed an increased collagen content in skeletal muscle of *DMD*$^{Y/-}$ compared to WT piglets (Figure 44a). Quantitation of collagen in MT and SR stained histological sections of skeletal muscle of WT and *DMD*$^{Y/-}$ piglets confirmed the increased collagen content in skeletal muscle of *DMD*$^{Y/-}$ piglets (Figure 44b).

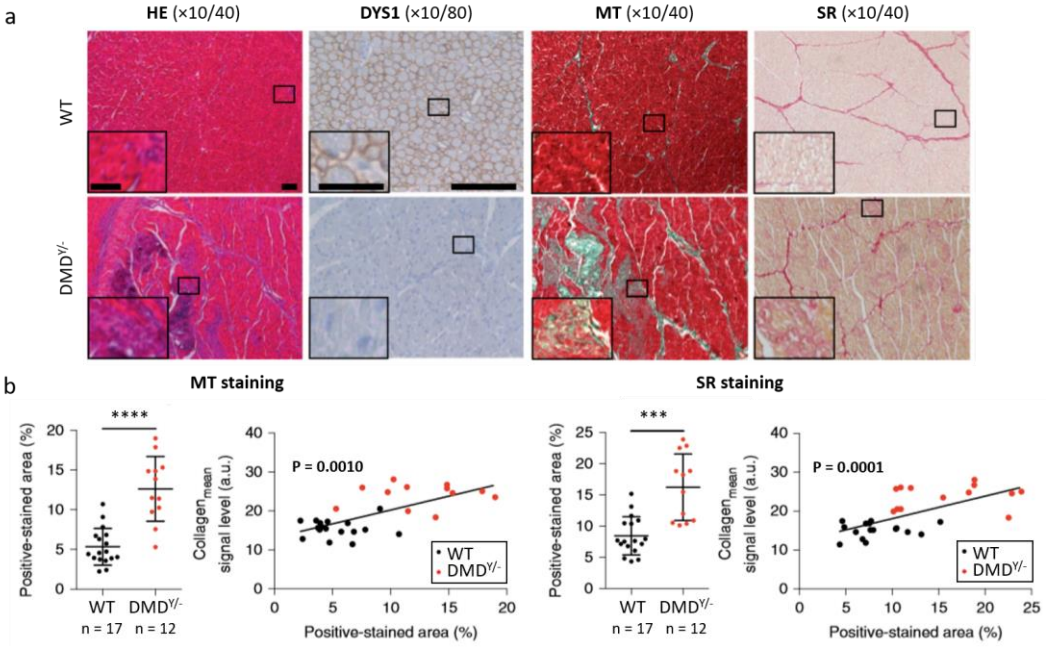

Figure 44: Histological examinations reflect the increase of collagen in skeletal muscle of *DMD*$^{Y/-}$ piglets. a, Representative skeletal muscle samples of the previously imaged regions from WT (upper row) and *DMD*$^{Y/-}$ piglets stained with HE, DYS1 immunohistochemistry, MT and SR. Scale bars: 100 µm in main micrographs, 50 µm in inserts. **b**, Quantitation of collagen in MT and SR stained histological sections of skeletal muscle of WT and *DMD*$^{Y/-}$ piglets and correlations between the MSOT collagen signals and positively stained collagen areas (MT: r_s= 0.58; SR: r_s=0.65) are shown. Statistics: Two-tailed independent samples t-test, Welch's correction in cases of unequal variances, Mann-Whitney U-test if assumption of normal distribution was violated. Data are shown as mean±s.d. Correlations are given by the Spearman correlation coefficient (r_s), two-tailed test. Black lines display linear regression (adapted from Regensburger et al., 2019).

6.2. Quantitative visualization of disease progression in *DMD*$^{Y/-}$ pigs

In a subsequent longitudinal study in the *DMD*$^{Y/-}$ pig, the feasibility of MSOT for the *in vivo* monitoring of disease progression was conducted as described in (Regensburger et al., 2019). Therefore, n = 11 male piglets (n = 6 WT and n = 5 *DMD*$^{Y/-}$) were used, of which n = 1 WT piglet was excluded after the first imaging, to generate an identical group size. The imaging was performed in week 1 (days 1 or 2), week 2 (days 8 or 9), week 3 (day 15 or 16) and week 4 (days 22 or 23) of life to quantitatively visualize the early-stage progression of the disease. n = 5 animals (n = 3 WT and n = 2 *DMD*$^{Y/-}$) completed the full experimental protocol and were euthanized after fulfillment of all four MSOT imaging sessions (at day 24 and day 26 of life). n = 3 *DMD*$^{Y/-}$ piglets died or had to be euthanized prematurely (at day 5, day 6 and day 7 of life), and thus n = 2 corresponding age-matched WT piglets were sacrificed (at day 5 and 6 of life).

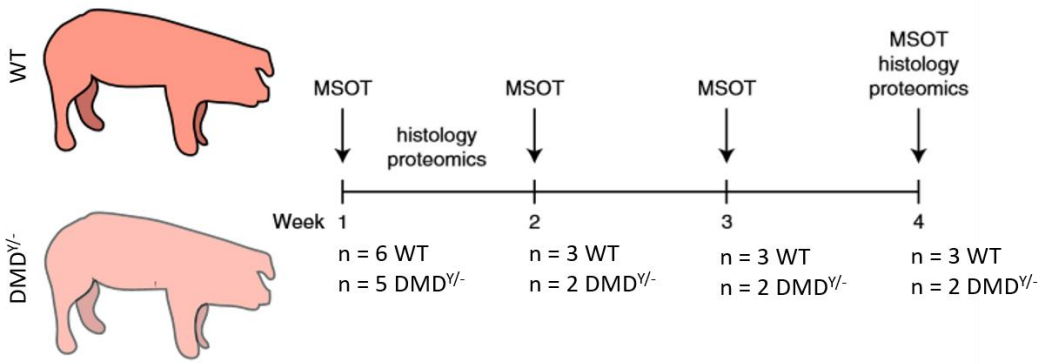

Figure 45: Longitudinal MSOT study to quantitatively visualize early-stage disease progression in *DMD*$^{Y/-}$ piglets. Imaging sessions were performed in week 1, 2, 3 and 4 of life. Initially, n = 11 animals (n = 6 WT and n = 5 *DMD*$^{Y/-}$) were used for MSOT imaging. N = 3 *DMD*$^{Y/-}$ died or were euthanized in week 1 of life, thus n = 2 age-matched WT piglets were sacrificed as controls. N = 5 piglets (n = 3 WT and n = 2 *DMD*$^{Y/-}$) completed the full experimental protocol (adapted from Regensburger et al., 2019).

In week 1, n = 44 independent muscles (biceps femoris and triceps muscle, both bilaterally; equivalent to n = 24 WT and n = 20 *DMD*$^{Y/-}$) were imaged. Throughout the whole 4-week experiment, n = 20 independent muscles (n = 12 WT and n = 8 *DMD*$^{Y/-}$) were investigated.

By *in vivo* MSOT imaging over time visible tissue changes consistent with increased fibrotic transformation of the skeletal muscle tissue were observed in the *DMD*$^{Y/-}$ cohort, as exemplarily shown in Figure 46a. Likewise as in the previous proof-of-principle study, a significant MSOT collagen$_{mean/max}$ signal difference was found for both, 2D and 3D MSOT imaging, in all independent muscle regions of WT and *DMD*$^{Y/-}$ for all imaging timepoints of the study. For the remaining n = 5 animals (n = 3 WT and n = 2 *DMD*$^{Y/-}$), imaged at every time point of the 4-week experiment, a steady increase in collagen signals (2D and 3D MSOT) over the time was observed only in independent muscle regions of *DMD*$^{Y/-}$ piglets (Figure 46b).

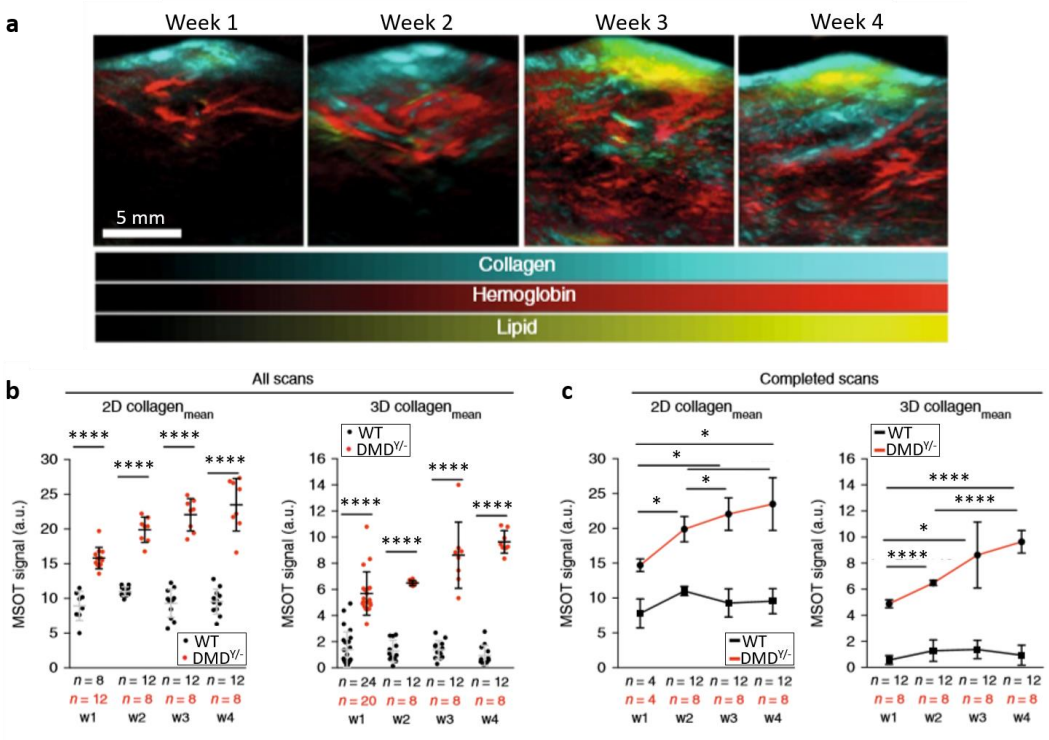

Figure 46: Early-stage disease progression quantitatively visualized over time by MSOT imaging. a, Representative 3D MSOT images of one *DMD*$^{Y/-}$ piglet for all 4 imaging timepoints. Color coded maps show mean collagen in turquoise, total hemoglobin in red and lipid in yellow. **b-c**, 2D and 3D MSOT collagen$_{mean}$ signals in muscles of WT and *DMD*$^{Y/-}$ are quantified over time. **b**, MSOT signals of independent muscles of all WT and *DMD*$^{Y/-}$ animals were compared to each other at all four time points (w1-w4), with each filled circle representing one MSOT signal per independent muscle region. Data are shown as mean±s.d. **c**, MSOT signals of independent muscles of the WT and *DMD*$^{Y/-}$ animals surviving over the whole 4-week experiment were compared to each other at all four time points (w1-w4), with each filled circle/ square representing mean±s.d. MSOT signals of independent muscle regions over the course of the study. Statistics: Two-tailed independent samples t-test (Welch's correction in case of unequal variance), Mann-Whitney U-test if the assumption of normal distribution was violated, Bonferroni-Holm adjustment to control type I error due to four comparisons (w1-4) for each parameter (adapted from Regensburger et al., 2019).

At the time of the last imaging (week 4), clearly evident differences between the WT and the *DMD*$^{Y/-}$ cohort were found *in vivo* and *ex vivo*, both macroscopically and histologically, as exemplarily shown in Figure 47a. Using histological and bioanalytical collagen quantification, within 4 weeks increased collagen deposition of up to 248% (from baseline) for MT staining (10.40±5.41 in week 1 to 25.80±7.93 in week 4, $p = 4.94 \times 10^{-5}$) and 170% (from baseline) for SR staining (19.59±5.40 in week 1 to 33.30±5.71 in week 4, $p = 3.63 \times 10^{-5}$) were observed in the *DMD*$^{Y/-}$ cohort (Fig. 47b). The content of total collagen (TC) per total protein (TP) increased by up to 139% (77.57±38.80 TC/TP µl/mg in week 1 to 107.80±42.02 TC/TP µl/mg in week 4, p = 0.12) (Figure 47c).

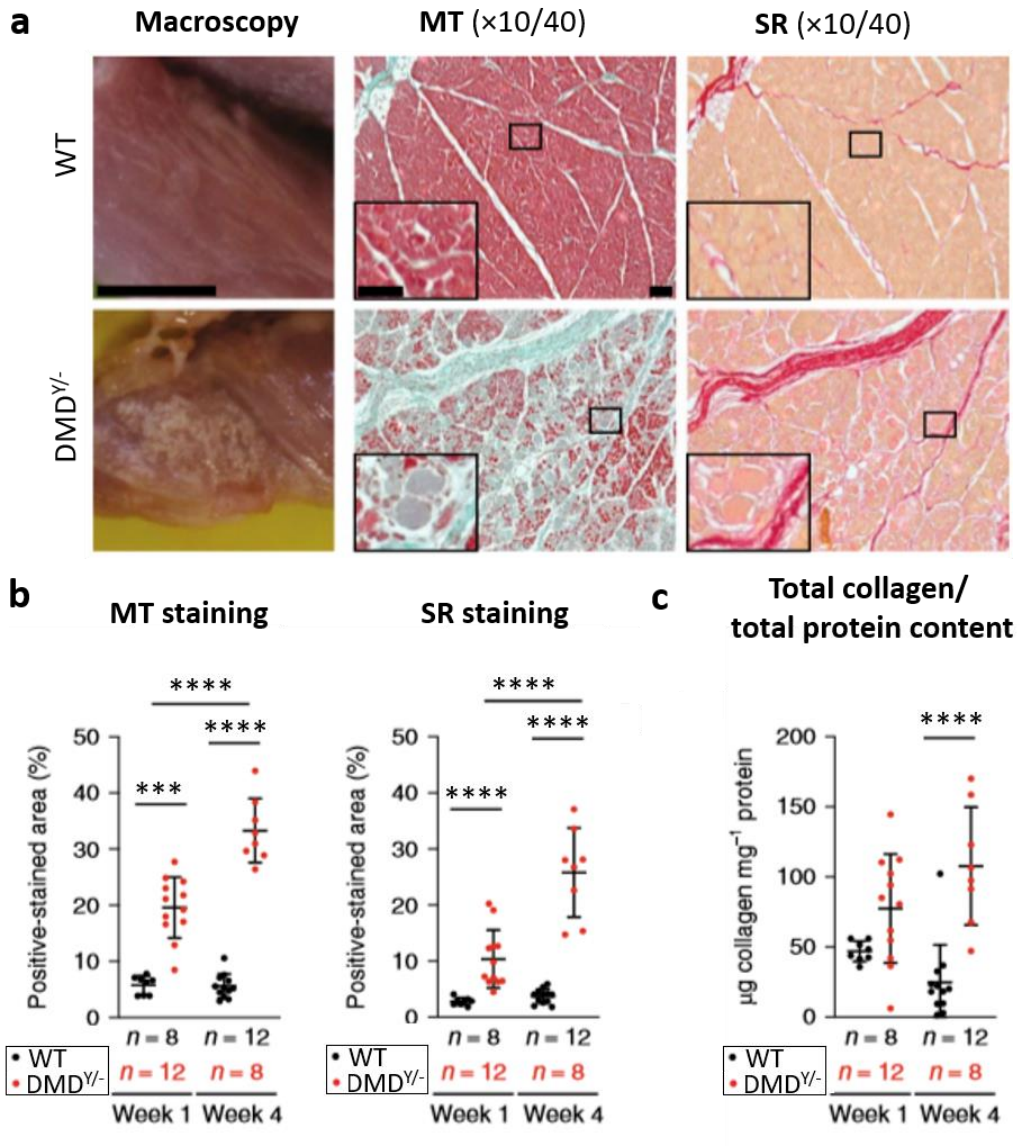

Figure 47: Histologic examinations reflect the increase of collagen in skeletal muscle of *DMD*$^{Y/-}$ piglets visualized over time by MSOT imaging. a, Macroscopic and histologic alterations in skeletal muscle of 4-week-old WT (upper row) and *DMD*$^{Y/-}$ pigs. Scale bars: 1 cm in macroscopic images, 100 µm in main histological images, and 50 µm in inserts. **b**, Quantification of areas stained positive for collagen by MT and SR staining of muscles of 1-week and 4-week-old WT and *DMD*$^{Y/-}$ piglets. **c**, Quantitation of total collagen abundance in WT and *DMD*$^{Y/-}$ piglets. Statistics: Two-tailed independent samples t-test, Welch's correction in cases of unequal variances, Mann-Whitney U-test if assumption of normal distribution was violated. Data are shown as mean±s.d. (adapted from Regensburger et al., 2019).

6.3. Quantitative proteome analysis confirms muscular fibrosis and the potential origin of MSOT signals

To confirm muscular fibrosis in *DMD*$^{Y/-}$ pigs as the potential origin of MSOT signals, quantitative proteome analysis was performed in cooperation with Thomas Fröhlich and Florian Flenkenthaler of the Gene Center - LAFUGA, LMU Munich. Therefore, n = 16 shock-frozen independent muscle samples (n = 8 WT, n = 8 *DMD*$^{Y/-}$) of n = 8 independent piglets (n = 4 WT and n = 4 *DMD*$^{Y/-}$) were analyzed. Thereby, a total of 2820 different proteins was identified.

In a principal component analysis and an unsupervised hierarchical clustering of LFQ values for biceps femoris and triceps brachii muscle specimens of 1-week and 4-week-old WT and *DMD*$^{Y/-}$ piglets the proteomes separated exactly according to the genotype and the age (Fig. 48). When comparing the collagens of of the both genotypes, collagen VI was found to be already enriched in 1-week-old *DMD*$^{Y/-}$ piglets, whereas in 4-week-old *DMD*$^{Y/-}$ piglets, besides the most abundant collagen VI, also the collagens III and XIV were increased.

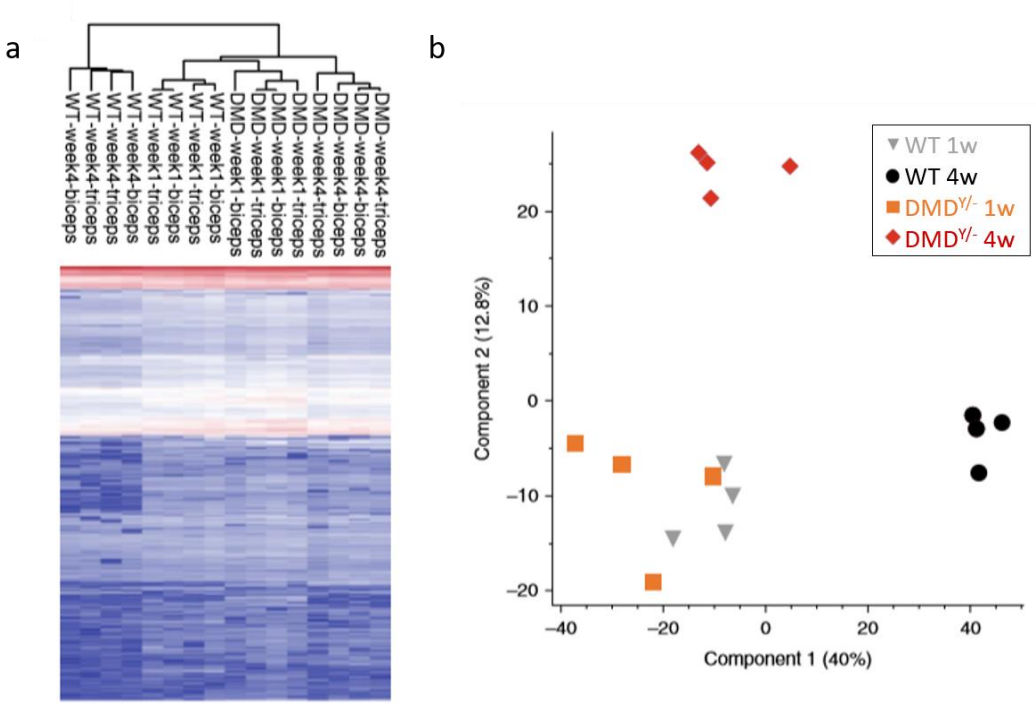

Figure 48: Holistic proteome analysis of skeletal muscle tissue from 1- and 4-week-old WT and *DMD*$^{Y/-}$ piglets, previously imaged by MSOT. a, Unsupervised hierarchical clustering of LFQ values for previously imaged triceps brachii and biceps femoris muscle specimens of 1- and 4-week-old WT and *DMD*$^{Y/-}$ piglets. Z-score-normalized expression values for the different proteins are color coded. **b**, Principal component anaysis, with each symbol equivalent to an individual sample (n = 4 samples per group) (adapted from Regensburger et al., 2019).

V. DISCUSSION

DMD is a severe progressive muscular wasting disease, which leads to premature death of the affected patients (Blake et al., 2002). Even though there is considerable progress concerning the therapy of DMD and many genetic approaches have been tested in the past few years (reviewed in Birnkrant et al., 2018b) there is no cure for the most frequent mutations triggering the disease. Moreover, diagnostic tools to assess disease progression in DMD are still initial. Most clinical trials rely on measures of muscle function and strength only (Zaidman et al., 2017). Especially in young pediatric DMD patients, noninvasive *in vivo* imaging modalities to monitor disease progression are of need. Animal models play a major role in the establishment of new treatments and the discovery and validation of new biomarkers (Aigner et al., 2010). However, in the case of DMD, the existing animal models display advantages but also several limitations, depending on the study question (McGreevy et al., 2015). Pigs as animal models have been proven to be appropriate with regard to various applications in the field of biomedical research (Aigner et al., 2010). Therefore, a tailored DMD pig model, lacking exon 52 in the *DMD* gene (*DMD*Δ52), has been generated at our institute (Klymiuk et al., 2013). In this work we aimed to establish a stable DMD breeding herd to obtain large animal numbers, first for the development of a new therapeutic approach aiming at somatic gene editing, and second for the validation of a new noninvasive *in vivo* imaging biomarker for DMD.

The DMD pig generated by breeding as adequate animal model for DMD

In this work, a total of n = 97 affected *DMD*$^{Y/-}$ piglets were produced by breeding over a period of approximately four years. The *DMD*$^{Y/-}$ genotype was confirmed by PCR analysis of DNA isolated from individual tail biopsies, with one primer pair detecting the intact *DMD* allele and a second primer pair detecting the mutated (*DMD*Δ52) allele by neomycin selection cassette. All genotypes (WT male, WT female, *DMD*$^{Y/-}$ and *DMD*$^{+/-}$) were inherited equally following Mendelian laws.

As rearing of *DMD*$^{Y/-}$ piglets was highly complicated by a reduced general conditon of newborn affected animals, different rearing conditions for the period of suckling were established and evaluated. Moreover we took a closer look at the cause of the reduced general condition present in most of the newborn *DMD*$^{Y/-}$ piglets. *DMD*$^{Y/-}$ pigs generated by breeding were characterized with regard to expression of dystrophin, creatine kinase levels, body weight, mortality, macroscopic and histologic phenotypic characteristics of skeletal muscle, macroscopic and histologic gastrointestinal alterations and muscle function.

All DMD models which are severely affected by the disease, such as double-knockout mice (either utrophin/dystrophin or integrin/dystrophin) or different dystrophin-deficient dog breeds, are difficult to generate and to care for (Ambrosio et al., 2009; McGreevy et al., 2015). Therefore, in our DMD pig breeding herd, we evaluated different rearing conditions with regard to survival chances. In all cases, rearing of affected *DMD*$^{Y/-}$ piglets required birth monitoring and intense nursing during the first days of life. A reduced general condition of newborn *DMD*$^{Y/-}$ piglets by reason of a severe premature expression of the DMD phenotype, led to increased losses of animals due to severe energy deficit and/or crushing by the sow. To reduce losses caused by crushing, the separation of the piglets from the sow after 12 h of

supervised suckling at the sows' teats and subsequent motherless rearing in an artificial rearing unit was evaluated. With 83% the mortality in this approach was quite high. As the preweaning mortality is highly associated with colostrum intake even in healthy newborn piglets (Declerck et al., 2016), the colostrum intake was seen as crucial factor and suckling at the sows' teats was prolonged in subsequent rearing approaches. Thus, in a second approach "48 h of supervised suckling at the sows' teats" was evaluated. With 56% *DMD*$^{Y/-}$ piglets surviving this approach, a definite advance was achieved. In a third and fourth approach, rearing conditions were further improved step by step, with the main focus on supervision of the individual energy demand and individual colostrum supplementation. A generally satisfactory decrease of mortality down to 30% was achieved within the last rearing approach.

When characterizing *DMD*$^{Y/-}$ pigs generated by breeding, a high accordance of phenotypic characteristics compared to human DMD patients was found. A comparison of disease severity and development and expression of the phenotype in dystrophin deficient mice, dogs, pigs and humans is shown in Table 10.

Table 10: Comparison of phenotypic characteristics and disease severity in dystrophin deficient mice, dogs, pigs and humans (adapted from Duan, 2015; and McGreevy et al., 2015).

Disease Phenotype				
	mdx-Mice	**Dogs**	**Pigs**	**Humans**
Body weight at birth	= normal	= normal	< normal	= normal
Grown-up body weight	≥ normal	< normal	< normal	< normal
Disease progression	mild, non-progressive	severe, progressive	severe, progressive	severe, progressive
"Honeymoon" Period	no (mild, non-progressive phenotype)	at 6-10 months of age	n.d.	between 5-8 years of age, symptoms are often stabilized or even slightly
Loss in ambulation	rare	rare	no, but progressive activity decrease	Wheelchair-bound by early teenage
Life span	= 75% of normal (≈ 22 months of age)	= 25% of normal (≈ 3 years of age)	see Kaplan-Meier curve (≈ 4 month of age)	= 25% of normal (≈ 20 years of age)

Neonatal death	rare	15-30% within 2 weeks after birth (likely due to diaphragm failure)	49.45% within 1 week after birth	rare
Age at first symptoms	≥ 15 months	birth to 3 months	birth (reduced general condition) to latest 1 month (reduced weight gain)	2-4 years
Muscle wasting	minimal until ≥ 15 months	progressive	progressive	progressive
Limb weakness	n.d.	2 to 3 months of age	yes, partly (see IV.5.3.)	≈ 3 years
Creatine kinase (CK)	severely elevated [4]	severely elevated [5]	severely elevated	severely elevated
Respiratory Dysfunction	no[7]	severe, progressive[3]	partly, severe & progressive (see IV.5.3)	moderate to severe, progressive
Gastrointestinal impairment	decreased intestinal transit and fecal output[1]	detected (dysphagia, salivation and mega-esophagus)[2]	partly detected (severe & progressive obstipation)	markedly disturbed in several individuals[8]
ECG abnormalities	frequent	frequent	n.d. (work in progress)	frequent
Cardiomyopathy	≥ 20 months; DCM in female and HCM in male mice	detectable at 6 months via ECG	detectable [6]; sudden cardiac death due to mild stressors	evident at 16 years
Cognitive & CNS defects	mild	n.d.	n.d. (work in progress)	1/3 of DMD
Histopathology & Biomolecular Changes				
	mdx-Mice	**Dogs**	**Pigs**	**Humans**
At birth	minimal	minimal	severe	minimal
Acute necrosis of muscle fibers	2-6 weeks	none	1st week of life	none

Limb muscle fibrosis	minimum in adult	extensive and progressive	extensive and progressive	extensive and progressive
Skeletal muscle regeneration	robust	poor	poor	n.a.
Alterations in the gastrointestinal tract	increased concentration of collagen fibers in submucosal region[1]	Not reported	Colon: putative increase of Type I collagene fibers	Esophagus: marked fibrosis, loss of circular and longitud. Muscle[9]; stomach: loss of smooth muscle, marked fibrosis[10]

[1](Feder et al., 2018; Mulè et al., 2010), [2](Ambrosio et al., 2009), [3](DeVanna et al., 2014; Kornegay, 2017), [4](Spurney et al., 2009), [5] (Sharp et al., 1992), [6](Moretti et al., 2020), [7] (Burns et al., 2019), [8] (Kraus et al., 2016), [9] (Leon et al., 1986), [10] (Barohn et al., 1988)

Tabe 10 highlights the limitations of the *mdx*-mice, compared to dogs and pigs as model of DMD. There are several different mouse models of DMD. However, none of them appropriately mirrors the phenotype of DMD patients. Furthermore, the mouse as animal model imposes limitations on analysis, such as dose-finding in therapeutic trials of new treatments, due to its small body size. With regard to the body size, the dog model of DMD is a more appropriate animal model for DMD. It furthermore reflects most of the phenotypic characteristics of DMD (Brinkmeyer-Langford and N Kornegay, 2013). Nevertheless, the big disadvantage of all DMD dog models is the high phenotypic dog-to-dog diversity. Great individual variations result in difficulties of reaching the size of an experimental group and in showing clear statistically significant results (reviewed in Wells, 2018). In our DMD pig breeding herd, likewise a variation in phenotype was observed. Several newborn *DMD*$^{Y/-}$ piglets needed to be euthanized due to a severely reduced general condition. In part, these animals showed gross anatomic muscle alterations. Concerning histological findings, in the examined short-term surviving *DMD*$^{Y/-}$ piglets local calcium deposits were observed in the striated muscles, whereas no foci with calcifications were found in muscles of examined long-term surviving *DMD*$^{Y/-}$ piglets. Apart from this, some *DMD*$^{Y/-}$ piglets were observed with gastrointestinal impairment.

Similar to the DMD dog models there is also a variability in phenotype in the short-term surviving *DMD*$^{Y/-}$ cohort, which might potentially influence the results of studies. However, a stable phenotype can be ensured by selecting only the long-term surviving *DMD*$^{Y/-}$ animals as experimental cohort, as it was done for the therapeutic trial which is part of this work. Statistically relevant experimental group sizes could be obtained.

In human DMD patients the first clinical manifestations of the disease appear in the early childhood (average at 2.5 years) (Ciafaloni et al., 2009). Compared to human DMD patients, DMD pigs show an accelerated course of the disease. The weight at birth of affected piglets was already reduced in comparison to WT littermates. Body weight increase was delayed and always stayed below the mean body weight of male WT littermates. Severe histologic alterations consistent with the DMD phenotype were observable already in newborn *DMD*$^{Y/-}$ animals. In adolescent *DMD*$^{Y/-}$ pigs, histologic samples showed a severe DMD phenotype as well. An increase of connective tissue was highly apparent in newborn as well as in adolecent *DMD*$^{Y/-}$ pigs, whereas fatty infiltration, which was expected to be likewise increased in adolecent *DMD*$^{Y/-}$ animals, was putatively low. These observations are in line with previous reports about findings in human DMD patients: the intramuscular fat content in biceps and quadriceps femoris muscles of DMD patients ranged from 0.89±0.70% (Bettica et al., 2016) to 3.4±4.1%, whereas fibrosis (peri- and endomysial) exceeded 30% (Desguerre et al., 2009). The accelerated appearance of the phenotype can be beneficial with regards to therapeutic trials, as ameliorations of the phenotype due to a therapeutic agent can be validated prematurely, compared to other DMD animal models (see Table 10), reducing the total experimental duration.

Concerning the gastrointestinal impairment found in some *DMD*$^{Y/-}$ piglets, a more detailed examination of the abdominal symptoms and correlating pathologic alterations is in progress. However, impairment of the gastrointestinal function, mainly occuring in the form of constipation, is described as very frequent complication in DMD patients (Kraus et al., 2016). Therefore, the examination of the underlying cause of gastrointestinal impairment in DMD is of need. First investigations in *DMD*$^{Y/-}$ piglets showed an increased survival rate after therapeutic measures (treatment with laxatives and digestion-aiding nutritional supplements of all n = 7 *DMD*$^{Y/-}$ piglets of 2 litters, of which one or more animals showed gastrointestinal symptoms). This supports the in Birnkrant et al. (2018b) indicated importance of gastrointestinal and nutritional management. As possible reason for gastrointestinal problems in *DMD*$^{Y/-}$ piglets, hypomotility or atonia, caused by a reduced innervation, is discussed. As second hypothesis, an increase of fibrotic tissue in the intestinal wall might lead to strictures, disturbing the intestinal passage and leading to obstruction, as found in human patients with ulcerative colitis (Parray et al., 2012). As the DMD pig model seems to mirror DMD in regards to gastrointestinal impairment, investigations of this aspect in the DMD pig can promote the research in this area.

Identification of potential modifier genes in the *DMD*$^{Y/-}$ pig

The manifestation and severity of the DMD phenotype in human DMD patients can be strongly influenced by modifier genes. Several modifying loci have already been identified, but the overall knowledge in this field still is initial and incomplete. As individual differences in disease progression highly complicate the interpretation of results of clinical trials, a more detailed knowledge about modifier genes in DMD is of need (reviewed in Aartsma-Rus and Spitali, 2015). In human DMD patients, as well as in the *mdx* mouse, most studies investigating potential genetic modifiers rely on previously drawn up hypotheses. Thus, most of the discovered candidate genes are pre-specified genes of interest, which are already known to play a role in muscle health and with their pathways beeing already well understood.

Instead of investigating only putative mutations, genome-wide combined linkage disequilibrium and linkage analyses (cLDLA) scan the whole genome for common genetic variations. As hypothesis-free, unbiased approach, cLDLA is able to identify also unexpected associations in DMD. To investigate the origin of the variable survival time observed in our *DMD*$^{Y/-}$ pigs generated by breeding, cLDLA was applied for a selected subset of animals.

A scoring system, to accurately identify subgroups which share the same potential modifiers was developed. In human individuals with DMD, the the age at loss of ambulation (LoA) is used to determine subgroups with potential common genetic modifiers (Bello et al., 2016). As the *DMD*$^{Y/-}$ animals only show an activity decrease but no LoA, and all other detected phenotypic variations in *DMD*$^{Y/-}$ pigs were only imprecisely determinable, the survival time was chosen as a most reliable categorizing parameter. Color-coded partial pedigrees were created to illustrate the survival time of the individual animals at first sight. The SNP-genotypes were analysed using two different aspects of survival as criterion: PhContinous categorized "length of life in days"; and PhDiscrete, categorized phenotype 1 as short-term survivors (death within 2-9 days of life) and phenotype 2 as long-term survivors (death within ≥ 10 days of life). Using PhDiscrete, a splitting in these two subgroups of 1:1.7 (equivalent to n = 19 short-term survivors and n = 33 long-term survivors) was shown. The uneven distribution of the two subgroups is explainable by a lower number of short-term survivors due to an exlcusion of all short-term survivors which were crushed or possibly crushed by the sow or died due to an uncertain reason (e.g. infection).

Using PhContinous and PhDiscrete as criteria, so far no genome-wide significant quantitative trait loci (QTL) responsible for the variable phenotype in DMD$^{Y/-}$ pigs could be identified. However, with a continously increasing number of animals included in the study, the likelihood ratio test (LRT) curves became smoother and less peaked. On some chromosomes highly indicative values were observable. On other chromosomes indicative, but no marked peaks were found. On most chromosomes an evenly low, homogenous pattern of LRT-values was observed.

One of the most researched genetic modifieres in human DMD patients is *SPP1*, encoding SPP1 or Osteopontin. According to the *Sus scrofa* reference genome assembly Sscrofa11.1 (Genome - Assembly - NCBI) *SPP1* is located on pig chromosome 8 (131,077,787-131,085,264 bp). Here used cLDLA mapping procedure mapped an indicative QTL on pig chromosome 8 at 109.7 Mb (LRT = 12.6). However, this indicative QTL is far (21.4 Mb) from candidate modifier *SPP1*.

LTBP4, encoding latent TGFB binding protein 4, is another frequently researched genetic modifier in DMD. It is located at pig chromosome 6 (48,833,008-48,861,246). In our study pig chromosome 6 displayed an evenly low, homogenous pattern of LRT values. No significant LRT value was observable at the *LTBP4* locus.

For the less researched genetic modifiers *ACTN3* (encoding α-actinin-3), *CD40* (encoding CD40 or tumor necrosis factor receptor superfamily member 5, TNFRSF5) and *THBS1* (encoding thrombospondin-1, THBS1), likewise no significant LRT values were observable on the corresponding pig chromosomes.

Due to these results, the described known modifiers in human DMD patients are unlikely to be also responsible for a variable phenotype in our *DMD*$^{Y/-}$ pigs.

Supposing monogenic inheritance of underlying modifier, and according to previous experiences with cLDLA mapping applied to monogenic traits (Kunz et al., 2016), we would expect clear and significant mapping in the here presented design. The absence of such clear signal strengthens our presumption, that not only one, but several modifying loci reveal the observed phenotypic variation in *DMD*$^{Y/-}$ pigs. Therefore, a higher number of animals and, eventually, a more explicit classification system, are necesscary for further investigations. According to mapping results at this stage we decided not to perform any further candidate gene analyses at only indicative regions.

The *DMD*Δ52-pig is a suitable animal model for the establishment of new treatments

Animal models play a substantial role in the establishment of new treatments in clinical application (Aigner et al., 2010). In this therapeutic trial we showed that the DMD pig represents an ideal model for the establishment and validation of a new therapeutic approach aiming at somatic gene editing by sequence-specific nucleases.

In human DMD patients 60 - 72% of the disease causing mutations are exon deletions (Aartsma-Rus et al., 2006; Muntoni et al., 2003), located in two mutational hot spots: one minor hot spot spanning from exons 2 to 20 and one major hot spot between exons 47 and 53 (Den Dunnen et al., 1989; Koenig et al., 1987). Exon deletions can lead to a shift of the open reading frame resulting in unstable mRNA products, which are subsequently eliminated by nonsense-mediated mRNA decay. The consequence is a total loss of the muscle structure protein dystrophin, resulting in the typical DMD phenotype. The DMD pig established at our institute lacks exon 52 of the *DMD* gene (*DMD*Δ52) (Klymiuk et al., 2013). This mutation leads to the above described pathway, resulting in a total absence of dystrophin. As the deletion of exon 52 is one of the more frequent mutations in DMD patients, the generation of *DMD*Δ52 pigs was considered as appropriate in therapeutical research.

Somatic gene editing restores dystrophin expression and ameliorates muscle function in *DMD*$^{Y/-}$ pigs

The therapeutic approach used in this study is described in detail in Moretti et al. (2020). In brief, adeno-associated viral vectors, serotype 9, coated with PAMAM-G2 nanoparticles and carrying an intein-split Cas9 and a pair of guide RNAs, targeting exon 51 flanking sequences (G2-AAV9-Cas9-gE51), were used. G2-AAV9-Cas9-gE51 was aimed to restore the open reading frame, introducing the expession of an internally truncated (*DMD*Δ51-52), but partially functional, dystophin protein, thus converting Duchenne muscular dystrophy into the milder Becker muscular dystrophy.

This principle approach of exon skipping to reframe *DMD* transcripts has already been established using antisense-oligonucleotides (AONs) (Sharp et al., 2011) and has been successfully translated into clinical trials (Goemans et al., 2011; Van Deutekom et al., 2007). However, the AON-mediated exon skipping only shows a limited expression of dystrophin and has solely a temporary effect (Verhaart et al., 2014). In contrast, somatic gene editing by sequence specific nucleases is able to permanently correct the open reading frame and is already confirmed to be more effective, as demonstrated in the *mdx* mouse (Long et al., 2016; Xu et al., 2016).

The success of this approach was recently confirmed in a dog model of DMD, demonstrating a restored expression of a shortened dystrophin in several muscles after i.v. application of AAV9 delivering CRISPR-Cas9 components (Amoasii et al., 2018). However, as yet, data demonstrating an improved muscle function due to somatic gene editing is still missing.

Only long term surviving *DMD*$^{Y/-}$ animals were used for the therapeutic trial to avoid incorrect interpretation of the results due to phenotypic variations. The results show, that G2-AAV9-Cas9-gE51 is capable to restore the disrupted reading frame of *DMD*Δ52 pigs by skipping exon 51. In intramuscularly treated *DMD*$^{Y/-}$ pigs a robust expression of internally truncated but partially functional dystrophin was detectable in the injected muscle regions. Minimal editing of non-injected muscles (contralateral side, diaphragm, heart) due to leakage of the vector into blood-vessels, was observable. In high-dose systemically treated *DMD*$^{Y/-}$ pigs a broad transduction in muscles, including the vital organs such as diaphragm and heart, was achieved.

The expression of dystrophin was confirmed by immunofluorescence staining. Among other methods, selected reaction monitoring (SRM) was used to detect dystrophin. There are several advantages concerning this method. First, SRM allows the sensitive and targeted absolute quantification of proteins out of highly complex protein mixtures, such as cell lysates. Second, when compared to classical techniques like ELISA/RIA or Western Blot, antibodies, which often have a limited specificity and selectivity, are not needed for the SRM approach. Beside the high specificity and sensitivity of the technique, a large dynamic range of quantification of at least three orders of magnitude is a further benefit. SRM allowed the exact quantification of dystrophin, given as "% of normal". As even low levels of dystrophin (>4%) have been estimated to improve muscle function and prolong survival, and dystrophin levels approaching 20% were found to prevent the development of dystrophic symptoms (Godfrey et al., 2015), the detected dystrophin levels of up to 62% (of WT dystrophin level) in i.m. treated and up to 38% (of WT dystrophin level) in high-dose i.v. treated *DMD*$^{Y/-}$ pigs were counted as success of the therapeutic approach. The effective elimination of exon 51 was confirmed at the genomic and transcript level. To examine whether the dystrophin expression and the maintained muscle integrity are sustained, prolonged studies are of need. Likewise, as an irregular distribution of dystrophin expression was observable in different analyzed muscle specimens of systemically treated *DMD*$^{Y/-}$ pigs, there is still optimization-potential to achieve a more homogeny dystrophin coverage.

The results of the holistic proteome analysis of muscle specimens of high dose i.v. treated *DMD*$^{Y/-}$ pigs indicated a partial normalization of proteins, which are normally dysregulated in DMD. A principal component analysis revealed, that the global protein profile of G2-AAV9-Cas9-gE51-treated muscles resided closer to WT than to untreated *DMD*$^{Y/-}$ animals. These results likewise confirmed the therapeutic effect of G2-AAV9-Cas9-gE51-mediated somatic gene editing.

Furthermore, the muscle-damage indicating enzyme creatine kinase was measured in serum of all animals. However, only plausible values were used for interpretation, whereas implausible values (e.g. blood sample was taken several hours after death, or animal died under conditions of severe stress) were excluded from analysis. The creatine kinase (CK) levels in high-dose i.v. treated *DMD*$^{Y/-}$ pigs decreased in comparison to CK levels measured in untreated *DMD*$^{Y/-}$ pigs. The parameter was used as biomarker in evaluating the tested somatic gene editing

approach. The decrease of CK levels was interpreted as a reduction of muscle damage in high-dose i.v. treated *DMD*$^{Y/-}$ pigs. Elevated CK levels indicate a floride, i.e. active, state of the disease. As CK elevation is directly associated with muscle damage, the parameter is seen as useful biomarker the evaluation of new therapeutic approaches. However, it is discussed that a decline of CK can stand for both, a reduced CK-leakage and hence the success of a therapeutic approach or a further progressed muscle quality decrease (reviewed in Aartsma-Rus and Spitali, 2015; Jensen et al., 2017). As shown in chapter IV.3.2., CK levels measured in our *DMD*$^{Y/-}$ pigs did not decrease over time but stayed highly elevated above the threshold of 2000 U/l. Thus, in the case of our DMD pig model the use of CK as biomarker to validate the efficiency of the applied therapeutic approach was reasonable.

In human DMD patients the 6-minute walk test (6-MWT) is the one of the primary used outcome measures for the assessment of physical capacity and the validation of therapeutic interventions (Bushby et al., 2014; McDonald et al., 2010; Mendell et al., 2016). In DMD animal models treadmill tests are performed to evaluate functional muscle parameters, as they are thought to most precisely mirror the assessment criteria used in human DMD patients (Capogrosso et al., 2018; Xu et al., 2016). However, physical examinations in humans as well as in animals normally rely on the individual performance of the day and on an active cooperation. This highly limits their diagnostic validity in DMD patients as well as in DMD animal models. Nevertheless, the assessment of functional muscle parameters in our *DMD*$^{Y/-}$ pigs as biomarker for the clinical course of the disease was indispensible for the evaluation of the somatic gene editing approach achieved by G2-AAV9-Cas9-gE51. Since some *DMD*$^{Y/-}$ individuals died due to sudden arrhythmia-induced death following mild environmental stressors such as weighing, taking blood samples or transportation, performing treadmill tests to assess muscle strength and endurance was decided to be not feasible. Therefore, to overcome the obstacles of the above explained limited diagnostic validity of physical examinations and the possiblity of sudden cardiac death in *DMD*$^{Y/-}$ pigs, a video surveillance system was installed, allowing to observe the animals at any time of a day, on seven days a week (24/7). Video surveillance does not require interaction with the animals and thus facilitates random objective evaluation, preventing assessment errors due to interaction triggered behavioral changes. Furthermore, it allows repeated analysis, which avoids analysis errors. Thus, video surveillance was the most objective, stressfree and closest-to-reality method to assess physical capacity in WT, high-dose i.v. treated and untreated *DMD*$^{Y/-}$ pigs.

Analyses were performed with regards to activity- versus resting-phases and individual behavior. For all animals one whole day (24 hours) was viewed, analyzed and interpreted. On average day 64 of life was choosen for analysis, as at this timepoint the therapy was expected to already be fully effective and most animals included in the study were still alive. As i.m. injection of G2-AAV9-Cas9-gE51 was attributed exclusively to the muscles of one side of the body, and no behavioral changes or functional impairment was expected in these animals when compared to untreated *DMD*$^{Y/-}$ pigs, all i.m. treated *DMD*$^{Y/-}$ and untreated *DMD*$^{Y/-}$ animals were considered as one group, designated as *DMD*$^{Y/-}$ untreated. All *DMD*$^{Y/-}$ animals were analysed blinded for the treatment status, whenever possible.

Already during review of the videosurveillance material, several individuals showed obviously increased resting-phases. Analysing the total standing time in 24 hours, untreated *DMD*$^{Y/-}$ pigs showed a significantly decreased total standing time

when compared to male age matched WT littermates, whereas for high-dose i.v. treated *DMD*$^{Y/-}$ pigs a significant increase in total duration of standing events was observed. In addition, the average duration of standing events was as a tendency decreased in untreated *DMD*$^{Y/-}$ pigs. However, no significant difference could be shown here. Using instantaneous sampling, a randomized analytical method, the increased activity in high-dose i.v. treated *DMD*$^{Y/-}$ compared to untreated *DMD*$^{Y/-}$ pigs could be visualized. Interestingly, here a difference between untreated and i.m. treated *DMD*$^{Y/-}$ animals was observable, with a mild but obvious activity increase in i.m. treated compared to untreated *DMD*$^{Y/-}$ animals. However, as animal numbers of the individual treatment groups were low, no statistical analysis was possible. Increased resting-phases were interpreted as premature fatigue, most probable due to muscle weakness. This interpretation was supported by observed individual behaviors, consistent with signs of fatigue, such as pattering of the hind limbs, or eating in lying posture.

Concerning the detection of possible off-target effects triggered by the treatment with G2-AAV9-Cas9-gE51 two different approaches were used to ensure the generation of reliable results: targeted sequencing was used to detect the most likely predicted off-targets and whole genome sequencing was performed as holistic approach to detect further potential off-targets. Results showed, that even in highly transduced peripheral muscle tissue no intracellular off-targets were detected.

Just recently, vector-dose-dependent toxicity of AAV vectors in non-human primates and piglets was reported (Hinderer et al., 2018). To achieve a sufficiently effective muscle transduction, including transduction of vital organs such as diaphragm and heart, the utilized virus particles in our therapeutic approach were dendrimer coated with G2-PAMAMs. Thereby, the need of higher virus doses, potentially exceeding levels of toxicity, could be avoided. Concerning efficacy and safety of new drugs, the evaluation of therapeutic approaches in animal models is indispensable. The pig as animal model resembles in body size and several similarities in physiology, anatomy, metabolism and pathology in comparison to humans (Aigner et al., 2010). Concerning dose finding, this model allows a cautious approach towards non-toxic but effective doses.

Evaluation of MSOT, a new noninvasive *in vivo* molecular imaging technique to detect muscle degeneration, in the DMD pig

Several new treatments for DMD are in focus of intense research. However, there is an unmet need of fast and sensitive methods to accurately measure symptom progression and the success of pharmaceutical interventions (Hrach and Mangone, 2019). So far, manual (Brooke et al., 1983) and quantitative investigation of the muscles (Escolar et al., 2011) as well as timed function tests form the primary outcome measures in DMD. The 6-MWT to date presents the most frequently used primary endpoint to evaluate disease progression in DMD patients. This test and other muscular function tests do not require special equipment. However, they are dependent on the patients' understanding (especially important for young DMD patients with congnitive impairment), active compliance and the individual performance of the day (Geiger et al., 2007; McDonald et al., 2010). These parameters may vary substantially between different measurement dates and thus can influence the interpretation of results. Furthermore, these biomarkers for the evaluation of disease progression are only of use in ambulatory patients, thereby excluding very young (approximately 0-3 years of age) and wheelchairbound individuals (which build the majority of DMD patients (Straub et al., 2016)).

Objective monitoring techniques, such as ultrasound imaging and MRI, either necessitate long scan times or require immobilization, and in young pediatric patients, sedation. Thus, these procedures are typically avoided in early life periods, when they are not well tolerated (Birnkrant et al., 2018a). Additionally, MRI imaging protocols are limited regarding the detection of fibrosis, which however is a frequent finding in DMD and an informative biomarker for the progression of the disease. Due to sensitivity to edema, inflammation, fibrosis and necrosis, as well as the influence of glucocorticoid treatment, signals in T_2-weighted, water sensitive MRI images are non-specific in this case (Arpan et al., 2014).

To overcome this lack of noninvasive, age-independent, fast to apply, specific and sensitive biomarkers, we examined the feasability of a new noninvasive *in vivo* molecular imaging technique, called multispectral optoacoustic tomography (MSOT), in DMD. MSOT is based on a photoacoustic effect: using pulsed laser light, the system induces thermoelastic expansion of endogenous absorbers in the examined tissue, resulting in detectable acoustic pressure waves. By spectral unmixing, based on the specific absorption and reflection spectra of the emitted light of each chromophore, the different endogenous absorbers can be identified. This enables the visualization of endogenous molecular chromophores, such as hemoglobin (oxygenated or deoxygenated), oxygen saturation or melanin. The feasibility and clinical usability of this technique has already been demonstrated in breast cancer (Diot et al., 2017), skin cancer (Rey-Barroso et al., 2018), melanoma lymph nodes (Stoffels et al., 2015) and Crohn's disease (Knieling et al., 2017; Waldner et al., 2016). We could demonstrate, that the illumination in the near- and extended near-infrared range (exNIR, from 680 to 1.100 nm) enables the visualization and quantification of collagens in affected muscles of *DMD*$^{Y/-}$ pigs, as well as in human DMD patients (not shown). The complete results of this study are published in Regensburger et al. (2019). The increase of fibrotic proportions in muscles of DMD patients is an early aspect of the disease. The average proportion of connective tissue is already increased (16.5%) at young age (1-6 years of age), and rapidly peaks to 30% and more in subsequent years (Peverelli et al., 2015). Therefore, fibrosis is discussed as a useful imaging target in DMD. As *DMD*$^{Y/-}$ pigs show an accelerated disease progression, with histologic muscle alterations including a severe increase of fibrotic tissue already observable in newborn piglets, the animal was an optimal model for the detection of collagen by MSOT.

Before imaging, all animals were shaved at the regions to be examined. For MSOT imaging, sedation of most of the animals was not necessary, as the method is painless and requires only short acquisition times. Only at older ages (4 weeks of age), some highly active WT pigs received mild sedation via noninvasive mucosal (intranasal) application. During imaging, a reflective ultrasound computed tomography (RUCT) image helped to anatomically guide the investigator. At the time point of imaging, genotypes of all animals were already determined. The investigator and persons carrying out analysis, however, were blinded to the genotypes. Genotypes were correctly classified by the investigators after analyzing MSOT collagen signals. This allowed a first conclusion in respect to the sensitivity of MSOT.

In a first proof-of-principle study, newborn *DMD*$^{Y/-}$ piglets and WT littermates were scanned by MSOT at days 1-3 of life. In a subsequent approach, muscles of *DMD*$^{Y/-}$ and WT pigs at week 1, 2, 3 and 4 of life were imaged in a longitudinal study. Thereby, the quantitative visualization of disease progression at an early stage could be demonstrated by MSOT. In all individual muscle regions, the

visualization and quantification of collagen was feasible. Significant MSOT collagen$_{mean/max}$ signal differences between *DMD*$^{Y/-}$ and WT animals were observed for all individually imaged muscle regions. In the proof-of principle study, n = 9 animals (n = 6 WT and n = 3 *DMD*$^{Y/-}$) were euthanized after imaging. In the longitudinal study, n = 3 *DMD*$^{Y/-}$ piglets had to be euthanized after the first scanning session, due to deterioration of the general condition. n = 2 WT littermates were euthanized in parallel, serving as controls. The remaining n = 5 animals (n = 3 WT and n =2 *DMD*$^{Y/-}$) were euthanized after the last scanning session (week 4 of life). Of all these animals muscle samples of the previously imaged anatomical regions were harvested and subsequently examined.

Immunohistochemical staining was performed to representatively visualize the absolute loss of dystrophin in *DMD*$^{Y/-}$ pigs. Hematoxylin and Eosin (H.E.) staining was used to assess cellular and tissue structure. Muscle tissue of all examined *DMD*$^{Y/-}$ pigs showed the typical signs of severe dystrophy. With Masson Trichrome (MT) and Sirius Red (SR) staining intense fibrotic infiltrations in the muscle tissue of *DMD*$^{Y/-}$ animals was visualized. In the MT and SR stained tissue sections, quantitative analyzes of positive-stained areas revealed a significantly increased collagen content in the *DMD*$^{Y/-}$ compared to WT cohort. Performed assays for total collagen (hydroxyproline) and total protein quantification likewise confirmed the increase of collagens in *DMD*$^{Y/-}$ animals. In the longitudinal study the progressive increase of MSOT collagen$_{mean/max}$ signal in accordance with an actual increasing collagen amount in the muscle tissue was demonstrated using the described methods. A receiver operator characteristics (ROC) analysis was applied to determine the ability of MSOT derived collagen signals to distinguish between muscles of affected and healthy animals and an excellent capacity of the MSOT technique was revealed. Additional performance of a holistic proteome analysis likewise confirmed muscular fibrosis in *DMD*$^{Y/-}$ pigs as the potential origin of MSOT signals. When comparing the collagens in skeletal muscle tissue of both genotypes, collagen VI was found to be already enriched in 1-week-old *DMD*$^{Y/-}$ piglets, whereas in 4-week-old *DMD*$^{Y/-}$ piglets, besides the most abundant collagen VI, also the collagens III and XIV were increased. In a principal component analysis and an unsupervised hierarchical clustering of LFQ values the proteomes of examined muscle specimens separated exactly according to the genotype and the age.

Premature phenotypic characteristics of DMD and an accelerated disease progression in *DMD*$^{Y/-}$ animals allowed the detection of early-stage fibrotic muscular transformation and follow-up of the clinical course by MSOT. Thus, the DMD pig was highly appropriate for the evaluation of MSOT as new diagnostic biomarker in DMD. The ease of use of MSOT as noninvasive bedside imaging modality was highlighted by the fact, that sedation in most of the animals was not necessary, as the technique is painless and requires only short acquisition times. The exact scan times of the technique were evaluated in the MSOT study performed in pediatric DMD patients and healthy volunteers (not shown). The MSOT technique was shown to be suitable for the *in vivo* monitoring of muscle degeneration involving fibrotic processes. Especially for new therapeutic approaches which aim at an ultrastructural restoration of damaged muscle, such as the somatic gene editing approach also shown in this work (Moretti et al., 2020), direct visualization by MSOT might be a helpful tool to validate the therapeutic efficacy.

VI. SUMMARY

Evaluation of emerging diagnostic and therapeutic strategies in a tailored pig model for Duchenne muscular dystrophy

DMD is a severe and progressive neuromuscular disease, leading to premature death of affected patients. The reason lies in a loss of function of the muscle structure protein dystrophin. The most important therapeutic measures are treatment with glucocorticoids aiming to relieve the symptoms and to slow down disease progression, and multidisciplinary care. For the most frequent underlying genetic defects there is no cure. However, in the past few years considerable progress has been made concerning mutation-specific therapies intending to restore dystrophin expression. The most recent molecular therapy approaches under investigation aim to restore dystrophin expression permanently by editing the genome. Furthermore, diagnostic tools to accurately assess disease progression and, in particular, to reliably allow the validation of new therapeutic approaches, are of need. In a former work, a tailored DMD pig, mirroring one of the most frequent DMD causing mutations (lack of exon 52 of the *DMD* gene) has been generated by somatic cell nuclear transfer (SCNT) and characterized at our institute.

One aim of this work was to establish a stable DMD pig breeding herd, allowing to generate high numbers of affected DMD knockout animals to provide statistically relevant experimental group sizes. Moreover, phenotypic characteristics of the DMD knockout pigs generated by breeding were investigated. Over a period of approximately four years, altogether n = 97 DMD knockout pigs were produced. Within this DMD cohort, a high mortality rate was observed (about 50% within week 1 of life). However, by a steady improvement of the parameters influencing rearing, the survival rate was increased from 17% up to 70%. The enzyme creatine kinase (CK) was already severely elevated in 1-week-old affected DMD piglets. No decrease of CK levels in adolecent DMD knockout pigs could be observed. Moreover, DMD knockout pigs showed a reduced birth weight, a severe weight-loss within the fist 24 hours after birth, as well as a reduced body weight gain over time. Gross anatomical and histological findings of short- and long-term surviving DMD knockout animals revealed divergent findings between these two cohorts. Nearly exclusively in short-term surviving DMD piglets, macroscopically visible white bundels of muscles were observed, histologically, local calcium foci were prominent. Moreover, some DMD animals exhibited gastrointestinal impairment. As possible reason for the phenotypic variations genetic modifiers were discussed. Therefore, one further approach of this work was to identify potential genetic modifier loci in the DMD knockout pig. The application of a genome wide combined linkage disequilibrium and linkage analysis (cLDLA), using the survival time as objective study criteria for single nucleotide polymorphism (SNP) genotyping, was commenced. So far, three potential but not genome-wide significant quantitative trait loci (QTL) on chromosomes 1, 7, and 8 were identified. However, the results are still initial and might change with a higher number of animals. Thus, further investigations with a larger group size, and eventually an improved categorization system, are of need.

Another item of this work was the validation of a new therapeutic approach, using somatic gene editing to permanently restore an internally truncated but partially functional dystrophin protein, in the *DMD*Δ52 pig. The correction of the open

reading frame (*DMD*ΔE51-52) was achieved by Cas9-mediated excision of exon 51. The therapeutic agent was transmitted by adeno-associated viral (AAV) vectors. The successful restoration of dystrophin expression in skeletal muscle was demonstrated using different analytical methods. Furthermore, CK levels were observed to improve under treatment. As a further important aspect, functional improvement of the muscles was assessed by analysing video recordings of a 24-hour surveillance audit with regards to individual activity patterns. The main outcome was a significant increase of activity of systemically (high-dose) treated animals, indicating a decrease of muscle weakness. Summarizing, in this study, the therapeutic approach was shown to ameliorate skeletal and cardiac muscle failure in DMD knockout pigs.

The last aspect of this work was the validation of multispectral optoacoustic tomography (MSOT), a new noninvasive diagnostic imaging biomarker to assess the state of muscle degeneration in the DMD knockout pig. Illuminations in the near- and extended near-infrared ranges allowed the visualization and quantification of the endogenous absorber collagen in skeletal muscle. The feasibility of the approach to distinguish between healthy (WT) and diseased (DMD knockout) muscle was evaluated in a first proof-of-principle study. The ability of MSOT to also quantitatively visualize early-stage disease progression was confirmed in a second longitudinal study. A highly significant elevation of MSOT collagen signal was detected in skeletal muscle of DMD knockout piglets compared to WT littermates. A significant increase of MSOT collagen signal over time in affected DMD pigs could be shown. The increased collagen content was confirmed by the quantitation of positive-stained areas of Masson Trichrome and Sirius Red stained muscle slices, by total collagen and total protein quantification, and by a holistic proteome analysis. A study in pediatric DMD patients likewise confirmed an increased MSOT collagen signal in skeletal muscle of affected boys. Thus, MSOT was shown to be a feasible noninvasive imaging tool for the visualisation and quantification of collagens as biomarker in DMD.

Summarizing, in this work the applicability of the DMD pig as adequate animal model for DMD was demonstrated.

VII. ZUSAMMENFASSUNG

Evaluierung neuer Strategien zur Diagnostik und Therapie der Duchenne Muskeldystrophie anhand eines maßgeschneiderten Schweinemodells

Die Duchenne Muskeldystrophie (DMD) ist eine schwerwiegende, progressiv verlaufende und letztendlich letale neuromuskuläre Erkrankung. Ursächlich sind verschiedene Mutationen im *DMD* Gen, welche eine Synthesestörung des Muskelstrukturproteins Dystrophin bewirken. Dies führt nachfolgend zu einem Untergang von Muskelfasern. Die Behandlung der Erkrankung beschränkt sich bisher auf die multidisziplinäre Versorgung betroffener Patienten. Weiterhin kann mit Glukokortikoiden eine Linderung der Krankheitssymptome und eine geringgradige Verlangsamung des Krankheitsverlaufs bewirkt werden. Für die meisten zugrunde liegenden genetischen Defekte gibt es dennoch keine effektiven Heilungsmöglichkeiten. Allerdings wurde in den letzten Jahren ein erheblicher Fortschritt im Hinblick auf die Entwicklung mutationsspezifischer Therapien gemacht, welche darauf abzielen die Dystrophin-Synthese wiederherzustellen. Die neusten molekularen Therapieansätze sind zudem darauf ausgerichtet, durch Veränderungen auf Genom-Ebene eine dauerhafte Wiederherstellung der Dystrophin-Expression zu ermöglichen. Für die Erforschung und Beurteilung neuer Therapiemöglichkeiten ist die Entwicklung diagnostischer Hilfsmittel wichtig, welche die präzise Beurteilung des Krankheitsverlaufs ermöglichen. In einer vorhergehenden Arbeit an unserem Institut wurde mittels somatischem Zellkerntransfer ein maßgeschneidertes DMD Schweinemodell erstellt, welches eine der häufigsten zugrunde liegenden Mutationen (nämlich das Fehlen von Exon 52 im *DMD* Gen) widerspiegelt.

Ein Hauptziel dieser Arbeit war der Aufbau einer stabilen Zuchtherde des DMD Schweinemodells, um die Bereitstellung statistisch relevanter Tierzahlen für experimentelle Versuchsgruppen zu ermöglichen. Weiterhin wurden die phänotypischen Eigenschaften der durch Zucht erzeugten DMD-Knockout Tiere untersucht. Innerhalb eines Zeitraums von etwa 4 Jahren wurden insgesamt 97 DMD-Knockout Tiere erzeugt. Die DMD-Tiere zeigten insgesamt eine stark erhöhte Mortalitätsrate (ca. 50% innerhalb der ersten Lebenswoche). Durch eine stetige Verbesserung der Aufzuchtsbedingungen konnte jedoch eine Steigerung der Überlebensrate von anfänglichen 17% auf 70% erzielt werden. Erhöhte Kreatinkinase-Werte wurde bereits bei 1-Woche alten Ferkeln gemessen. Ein Absinken des CK-Wertes bei heranwachsenden DMD-Tieren wurde nicht beobachtet. Weiterhin wiesen DMD-Schweine ein reduziertes Geburtsgewicht auf, mit einer nachfolgend starken Gewichtsabnahme innerhalb der ersten 24 Stunden nach der Geburt. Die anschließende Gewichtszunahme überlebender Tiere lag stets unter der der Wildtyp-Wurfgeschwister. Bei der Sektion der DMD-Tiere wurden makroskopisch sowie histologisch unterschiedliche Befunde zwischen den Kurzzeit-Überlebern (≤ 1 Woche) und den Langzeit-Überlebern beobachtet. Unter anderem zeigten Kurzzeit-Überleber makroskopisch eine weiße Streifung der Muskulatur, histologisch wurden Kalkablagerungen in der Muskulatur nachgewiesen. Außerdem wiesen manche DMD-Tiere eine Beeinträchtigung der gastrointestinalen Funktion auf. Als mögliche Ursache für diese phänotypische Varianz wurden Modifier-Gene diskutiert. Deshalb wurde, mit Hilfe einer Kartierung per kombinierter Kopplungsungleichgewichts- und Kopplungsanalyse

(cLDLA), die Identifizierung möglicher modifizierender Genloci im DMD-Schweinemodell untersucht. Als weitestgehend objektives Kriterium, zur Erfassung möglicher genetischer Varianten (Einzelnukleotid-Polymorphismen (SNP)) innerhalb der DMD-Knockout-Tiere wurde die „Überlebensdauer“ verwendet. Bisher wurden somit insgesamt drei potenziell modifizierte Genloci auf den Chromosomen 1, 7 und 8 eruiert, welche jedoch nicht genomweit signifikant sind. Diese Ergebnisse könnten sich folglich, unter Einbeziehung weiterer Tiere, verändern. Eine Weiterführung des Projekts mit höheren Tierzahlen und möglicherweise ein verbessertes Kategorisierungs-System sind nötig.

Ein weiteres Thema der vorliegenden Arbeit war die Validierung einer neuen somatischen Gentherapie: Im DMD-Schwein (*DMD*Δ52) sollte die dauerhafte Wiederherstellung der Expression eines verkürzten aber funktionellen Dystrophin-Proteins durch Korrektur des DNA-Leserahmens mittels CRISPR/Cas9 bewirkt werden (*DMD*Δ51-52). Zum Transfer des CRISPR/Cas9-Systems in die Zellen wurden Adenoassozierte Virale Vektoren (AAV) verwendet. Die erfolgreiche Wiederherstellung der Dystrophin-Synthese in Skelettmuskel (u.a. Zwerchfell) und Herz konnte mittels verschiedener Analyseverfahren nachgewiesen werden. Zudem wurde eine Absinken der CK-Werte in systemisch therapierten DMD-Tieren beobachtet. Als weiterer wichtiger Aspekt der Validierung des Therapieerfolges wurde die Muskelfunktion beurteilt. Hierfür wurde Filmmaterial eines 24-Stunden Videoüberwachungssystems, hinsichtlich der Aktivitätsmuster der individuellen Tiere, ausgewertet. Ein signifikanter Anstieg der Aktivität bei systemisch behandelten Tieren (hohe Dosis) wurde beobachtet, vereinbar mit einem Rückgang der Muskelschwäche. Zusammenfassend konnten eine Verbesserung der Muskel- sowie Herzfunktion durch die angewandte Gentherapie im maßgeschneiderten DMD Schweinemodell gezeigt werden.

Als letzter Aspekt der vorliegenden Dissertation wurde im DMD Schweinemodell die multispektrale optoakustische Tomographie (MSOT), ein neues nicht-invasives bildgebendes Diagnoseverfahren zur Erfassung von Muskeldegeneration validiert. Bei dem Verfahren werden Pulse eines Nahinfrarot-Lasers in das zu untersuchende Muskelgewebe gesandt und die dabei entstehenden optoakustischen Druckwellen, welche spezifisch für jeweilige körpereigene Chromophore (Farbstoffe wie z.B. Kollagene im Skelettmuskel) sind, visualisiert und quantifiziert. Die Anwendbarkeit dieser Diagnostikmethode zur Unterscheidung zwischen gesundem (WT) und erkranktem (DMD-Knockout) Muskel wurde in einer ersten Machbarkeitsstudie untersucht. In einer nachfolgenden Längsschnittstudie wurde auch die Fähigkeit von MSOT, das Fortschreiten der Erkrankung im Frühstadium quantitativ zu visualisieren, bestätigt. Im Skelettmuskel von DMD-Knockout-Ferkeln im Vergleich zu WT-Wurfgeschwistern wurde eine hoch signifikante Erhöhung des MSOT-Kollagensignals festgestellt. Weiterhin konnte ein signifikanter Anstieg des MSOT-Kollagensignals im Laufe der Zeit bei betroffenen DMD-Schweinen gezeigt werden. Der erhöhte Kollagengehalt wurde durch Anwendung verschiedener Methoden bestätigt. So wurden zum einen auf den mit Masson-Trichrom- und Siriusrot-Färbung angefärbten Muskelschnitten die positiv gefärbter Bereiche quantifiziert. Weiterhin wurden der Gesamtkollagengehalt in entsprechenden Muskelproben (Nachweis von Hydroxyprolin aus Kollagen) sowie der Gesamtproteingehalt ermittelt. Zudem wurde eine ganzheitliche Proteomanalyse durchgeführt. Eine Studie an pädiatrischen DMD-Patienten bestätigte ebenfalls ein erhöhtes MSOT-Kollagensignal im Skelettmuskel betroffener Jungen. Die MSOT-Methode wurde also als praktikables, nicht-invasives Bildgebungsverfahren zur Visualisierung und Quantifizierung von

Kollagen als Biomarker bei der DMD vorgestellt.

Zusammenfassend wurde in der vorliegenden Dissertation die Anwendung des DMD-Schweins als adäquates Tiermodell für die Duchenne Muskeldystrophie demonstiert.

VIII. INDEX OF FIGURES

IX. INDEX OF TABLES

X. REFERENCES

(2001). Biomarkers and surrogate endpoints: preferred definitions and conceptual framework. Clin Pharmacol Ther *69*, 89-95.

(2002). ATS statement: guidelines for the six-minute walk test. Am J Respir Crit Care Med *166*, 111-117.

Aartsma-Rus, A., Ginjaar, I.B., and Bushby, K. (2016). The importance of genetic diagnosis for Duchenne muscular dystrophy. J Med Genet *53*, 145-151.

Aartsma-Rus, A., and Spitali, P. (2015). Circulating Biomarkers for Duchenne Muscular Dystrophy. J Neuromuscul Dis *2*, S49-s58.

Aartsma-Rus, A., Fokkema, I., Verschuuren, J., Ginjaar, I., Van Deutekom, J., van Ommen, G.J., and Den Dunnen, J.T. (2009). Theoretic applicability of antisense-mediated exon skipping for Duchenne muscular dystrophy mutations. Human mutation *30*, 293-299.

Aartsma-Rus, A., Van Deutekom, J.C., Fokkema, I.F., Van Ommen, G.J.B., and Den Dunnen, J.T. (2006). Entries in the Leiden Duchenne muscular dystrophy mutation database: an overview of mutation types and paradoxical cases that confirm the reading-frame rule. Muscle & Nerve: Official Journal of the American Association of Electrodiagnostic Medicine *34*, 135-144.

Abbs, S., and Bobrow, M. (1992). Analysis of quantitative PCR for the diagnosis of deletion and duplication carriers in the dystrophin gene. J Med Genet *29*, 191-196.

Abdallah, C., Dumas-Gaudot, E., Renaut, J., and Sergeant, K. (2012). Gel-based and gel-free quantitative proteomics approaches at a glance. Int J Plant Genomics *2012*, 494572.

Aigner, B., Renner, S., Kessler, B., Klymiuk, N., Kurome, M., Wünsch, A., and Wolf, E. (2010). Transgenic pigs as models for translational biomedical research. Journal of molecular medicine *88*, 653-664.

Alagaratnam, S., Mertens, B.J., Dalebout, J.C., Deelder, A.M., van Ommen, G.J., den Dunnen, J.T., and t Hoen, P.A. (2008). Serum protein profiling in mice: identification of Factor XIIIa as a potential biomarker for muscular dystrophy. Proteomics *8*, 1552-1563.

Ambrosio, C.E., Fadel, L., Gaiad, T.P., Martins, D.S., Araujo, K.P., Zucconi, E.,

Brolio, M.P., Giglio, R.F., Morini, A.C., Jazedje, T., *et al.* (2009). Identification of three distinguishable phenotypes in golden retriever muscular dystrophy. Genet Mol Res *8*, 389-396.

Amoasii, L., Hildyard, J.C., Li, H., Sanchez-Ortiz, E., Mireault, A., Caballero, D., Harron, R., Stathopoulou, T.-R., Massey, C., and Shelton, J.M. (2018). Gene editing restores dystrophin expression in a canine model of Duchenne muscular dystrophy. Science *362*, 86-91.

Aoki, Y., Yokota, T., Nagata, T., Nakamura, A., Tanihata, J., Saito, T., Duguez, S.M., Nagaraju, K., Hoffman, E.P., and Partridge, T. (2012). Bodywide skipping of exons 45–55 in dystrophic mdx52 mice by systemic antisense delivery. Proceedings of the National Academy of Sciences *109*, 13763-13768.

Arahata, K., Ishihara, T., Kamakura, K., Tsukahara, T., Ishiura, S., Baba, C., Matsumoto, T., Nonaka, I., and Sugita, H. (1989). Mosaic expression of dystrophin in symptomatic carriers of Duchenne's muscular dystrophy. New England Journal of Medicine *320*, 138-142.

Araki, E., Nakamura, K., Nakao, K., Kameya, S., Kobayashi, O., Nonaka, I., Kobayashi, T., and Katsuki, M. (1997). Targeted disruption of exon 52 in the mouse dystrophin gene induced muscle degeneration similar to that observed in Duchenne muscular dystrophy. Biochemical and biophysical research communications *238*, 492-497.

Arikawa-Hirasawa, E., Koga, R., Tsukahara, T., Nonaka, I., Mitsudome, A., Goto, K., Beggs, A.H., and Arahata, K. (1995). A severe muscular dystrophy patient with an internally deleted very short (110 kD) dystrophin: presence of the binding site for dystrophin-associated glycoprotein (DAG) may not be enough for physiological function of dystrophin. Neuromuscul Disord *5*, 429-438.

Arpan, I., Willcocks, R.J., Forbes, S.C., Finkel, R.S., Lott, D.J., Rooney, W.D., Triplett, W.T., Senesac, C.R., Daniels, M.J., and Byrne, B.J. (2014). Examination of effects of corticosteroids on skeletal muscles of boys with DMD using MRI and MRS. Neurology *83*, 974-980.

Asadi, S. (2017). Assessment of Genetic Mutations DMD, DYSF, EMD, LMNA, DUX4, DMPK, ZNF9, PABPN1 Genes Induction Duchenne Muscular Dystrophy. SOJ Immunol *5*, 1-8.

Athanasopoulos, T., Fabb, S., and Dickson, G. (2000). Gene therapy vectors based on adeno-associated virus: characteristics and applications to acquired and inherited diseases (review). Int J Mol Med *6*, 363-375.

Athanasopoulos, T., Graham, I., Foster, H., and Dickson, G. (2004). Recombinant

adeno-associated viral (rAAV) vectors as therapeutic tools for Duchenne muscular dystrophy (DMD). Gene therapy *11*, S109-121.

Austin, R.C., Howard, P.L., D'Souza, V.N., Klamut, H.J., and Ray, P.N. (1995). Cloning and characterization of alternatively spliced isoforms of Dp71. Hum Mol Genet *4*, 1475-1483.

Bajek, A., Porowinska, D., Kloskowski, T., Brzoska, E., Ciemerych, M.A., and Drewa, T. (2015). Cell therapy in Duchenne muscular dystrophy treatment: clinical trials overview. Crit Rev Eukaryot Gene Expr *25*, 1-11.

Bakay, M., Zhao, P., Chen, J., and Hoffman, E.P. (2002). A web-accessible complete transcriptome of normal human and DMD muscle. Neuromuscul Disord *12 Suppl 1*, S125-141.

Barison, A., Aquaro, G.D., Passino, C., Falorni, M., Balbarini, A., Lombardi, M., Pasquali, L., Emdin, M., and Siciliano, G. (2009). Cardiac magnetic resonance imaging and management of dilated cardiomyopathy in a Duchenne muscular dystrophy manifesting carrier. J Neurol *256*, 283-284.

Barnard, A.M., Willcocks, R.J., Finanger, E.L., Daniels, M.J., Triplett, W.T., Rooney, W.D., Lott, D.J., Forbes, S.C., Wang, D.J., Senesac, C.R., *et al.* (2018). Skeletal muscle magnetic resonance biomarkers correlate with function and sentinel events in Duchenne muscular dystrophy. PLoS One *13*, e0194283.

Barohn, R.J., Levine, E.J., Olson, J.O., and Mendell, J.R. (1988). Gastric hypomotility in Duchenne's muscular dystrophy. N Engl J Med *319*, 15-18.

Becker, S., Florian, A., Patrascu, A., Rosch, S., Waltenberger, J., Sechtem, U., Schwab, M., Schaeffeler, E., and Yilmaz, A. (2016). Identification of cardiomyopathy associated circulating miRNA biomarkers in patients with muscular dystrophy using a complementary cardiovascular magnetic resonance and plasma profiling approach. J Cardiovasc Magn Reson *18*, 25.

Beggs, A.H., Hoffman, E.P., Snyder, J.R., Arahata, K., Specht, L., Shapiro, F., Angelini, C., Sugita, H., and Kunkel, L.M. (1991). Exploring the molecular basis for variability among patients with Becker muscular dystrophy: dystrophin gene and protein studies. Am J Hum Genet *49*, 54-67.

Beggs, A.H., Koenig, M., Boyce, F.M., and Kunkel, L.M. (1990). Detection of 98% of DMD/BMD gene deletions by polymerase chain reaction. Hum Genet *86*, 45-48.

Bell, C.D., and Conen, P.E. (1968). Histopathological changes in Duchenne muscular dystrophy. J Neurol Sci *7*, 529-544.

Bell, J.D., and Jones, J. T1 weighted image.

Bello, L., Flanigan, K.M., Weiss, R.B., Spitali, P., Aartsma-Rus, A., Muntoni, F., Zaharieva, I., Ferlini, A., Mercuri, E., Tuffery-Giraud, S., *et al.* (2016). Association Study of Exon Variants in the NF-kappaB and TGFbeta Pathways Identifies CD40 as a Modifier of Duchenne Muscular Dystrophy. Am J Hum Genet *99*, 1163-1171.

Bello, L., Gordish-Dressman, H., Morgenroth, L.P., Henricson, E.K., Duong, T., Hoffman, E.P., Cnaan, A., and McDonald, C.M. (2015a). Prednisone/prednisolone and deflazacort regimens in the CINRG Duchenne Natural History Study. Neurology *85*, 1048-1055.

Bello, L., Kesari, A., Gordish-Dressman, H., Cnaan, A., Morgenroth, L.P., Punetha, J., Duong, T., Henricson, E.K., Pegoraro, E., and McDonald, C.M. (2015b). Genetic modifiers of ambulation in the cooperative international Neuromuscular research group Duchenne natural history study. Annals of neurology *77*, 684-696.

Bello, L., and Pegoraro, E. (2019). The "Usual Suspects": Genes for Inflammation, Fibrosis, Regeneration, and Muscle Strength Modify Duchenne Muscular Dystrophy. J Clin Med *8*, E649.

Berard, C., Payan, C., Hodgkinson, I., and Fermanian, J. (2005). A motor function measure for neuromuscular diseases. Construction and validation study. Neuromuscul Disord *15*, 463-470.

Bettica, P., Petrini, S., D'Oria, V., D'Amico, A., Catteruccia, M., Pane, M., Sivo, S., Magri, F., Brajkovic, S., Messina, S., *et al.* (2016). Histological effects of givinostat in boys with Duchenne muscular dystrophy. Neuromuscul Disord *26*, 643-649.

Birnkrant, D.J., Bushby, K., Bann, C.M., Alman, B.A., Apkon, S.D., Blackwell, A., Case, L.E., Cripe, L., Hadjiyannakis, S., and Olson, A.K. (2018a). Diagnosis and management of Duchenne muscular dystrophy, part 2: respiratory, cardiac, bone health, and orthopaedic management. The Lancet Neurology *17*, 347-361.

Birnkrant, D.J., Bushby, K., Bann, C.M., Apkon, S.D., Blackwell, A., Brumbaugh, D., Case, L.E., Clemens, P.R., Hadjiyannakis, S., and Pandya, S. (2018b). Diagnosis and management of Duchenne muscular dystrophy, part 1: diagnosis, and neuromuscular, rehabilitation, endocrine, and gastrointestinal and nutritional management. The Lancet Neurology *17*, 251-267.

Bladen, C.L., Salgado, D., Monges, S., Foncuberta, M.E., Kekou, K., Kosma, K., Dawkins, H., Lamont, L., Roy, A.J., and Chamova, T. (2015). The TREAT-NMD DMD Global Database: analysis of more than 7,000 Duchenne muscular dystrophy mutations. Human mutation *36*, 395-402.

Blake, D.J., and Kroger, S. (2000). The neurobiology of duchenne muscular dystrophy: learning lessons from muscle? Trends Neurosci *23*, 92-99.

Blake, D.J., Weir, A., Newey, S.E., and Davies, K.E. (2002). Function and genetics of dystrophin and dystrophin-related proteins in muscle. Physiol Rev *82*, 291-329.

Bodensteiner, J.B., and Engel, A.G. (1978). Intracellular calcium accumulation in Duchenne dystrophy and other myopathies: a study of 567,000 muscle fibers in 114 biopsies. Neurology *28*, 439-446.

Bottomley, P.A., Foster, T.H., Argersinger, R.E., and Pfeifer, L.M. (1984). A review of normal tissue hydrogen NMR relaxation times and relaxation mechanisms from 1-100 MHz: dependence on tissue type, NMR frequency, temperature, species, excision, and age. Med Phys *11*, 425-448.

Bradley, W.G., Hudgson, P., Larson, P.F., Papapetropoulos, T.A., and Jenkison, M. (1972). Structural changes in the early stages of Duchenne muscular dystrophy. J Neurol Neurosurg Psychiatry *35*, 451-455.

Brinkmeyer-Langford, C., and N Kornegay, J. (2013). Comparative genomics of X-linked muscular dystrophies: the golden retriever model. Current genomics *14*, 330-342.

Brooke, M.H., Fenichel, G.M., Griggs, R.C., Mendell, J.R., Moxley, R., Miller, J.P., and Province, M.A. (1983). Clinical investigation in Duchenne dystrophy: 2. Determination of the "power" of therapeutic trials based on the natural history. Muscle & Nerve: Official Journal of the American Association of Electrodiagnostic Medicine *6*, 91-103.

Brooke, M.H., Griggs, R.C., Mendell, J.R., Fenichel, G.M., Shumate, J.B., and Pellegrino, R.J. (1981). Clinical trial in Duchenne dystrophy. I. The design of the protocol. Muscle Nerve *4*, 186-197.

Browning, B.L., Zhou, Y., and Browning, S.R. (2018). A One-Penny Imputed Genome from Next-Generation Reference Panels. Am J Hum Genet *103*, 338-348.

Buddhe, S., Lewin, M., Olson, A., Ferguson, M., and Soriano, B.D. (2016). Comparison of left ventricular function assessment between echocardiography and MRI in Duchenne muscular dystrophy. Pediatr Radiol *46*, 1399-1408.

Bulfield, G., Siller, W.G., Wight, P.A., and Moore, K.J. (1984). X chromosome-linked muscular dystrophy (mdx) in the mouse. Proc Natl Acad Sci U S A *81*, 1189-1192.

Burns, D.P., Murphy, K.H., Lucking, E.F., and O'Halloran, K.D. (2019). Inspiratory pressure-generating capacity is preserved during ventilatory and non-ventilatory behaviours in young dystrophic mdx mice despite profound diaphragm muscle weakness. J Physiol *597*, 831-848.

Bushby, K., Finkel, R., Wong, B., Barohn, R., Campbell, C., Comi, G.P., Connolly, A.M., Day, J.W., Flanigan, K.M., and Goemans, N. (2014). Ataluren treatment of patients with nonsense mutation dystrophinopathy. Muscle & nerve *50*, 477-487.

Bushby, K., Goodship, J., Nicholson, L., Johnson, M., Haggerty, I., and Gardner-Medwin, D. (1993). Variability in clinical, genetic and protein abnormalities in manifesting carriers of Duchenne and Becker muscular dystrophy. Neuromuscular Disorders *3*, 57-64.

Cacchiarelli, D., Legnini, I., Martone, J., Cazzella, V., d'Amico, A., Bertini, E., and Bozzoni, I. (2011). miRNAs as serum biomarkers for Duchenne muscular dystrophy. EMBO molecular medicine *3*, 258-265.

Campbell, K.P., and Kahl, S.D. (1989). Association of dystrophin and an integral membrane glycoprotein. Nature *338*, 259-262.

Capogrosso, R.F., Mantuano, P., Uaesoontrachoon, K., Cozzoli, A., Giustino, A., Dow, T., Srinivassane, S., Filipovic, M., Bell, C., Vandermeulen, J., *et al.* (2018). Ryanodine channel complex stabilizer compound S48168/ARM210 as a disease modifier in dystrophin-deficient mdx mice: proof-of-concept study and independent validation of efficacy. Faseb j *32*, 1025-1043.

Carberry, S., Brinkmeier, H., Zhang, Y., Winkler, C.K., and Ohlendieck, K. (2013). Comparative proteomic profiling of soleus, extensor digitorum longus, flexor digitorum brevis and interosseus muscles from the mdx mouse model of Duchenne muscular dystrophy. Int J Mol Med *32*, 544-556.

Carberry, S., Zweyer, M., Swandulla, D., and Ohlendieck, K. (2012a). Profiling of age-related changes in the tibialis anterior muscle proteome of the mdx mouse model of dystrophinopathy. J Biomed Biotechnol *2012*, 691641.

Carberry, S., Zweyer, M., Swandulla, D., and Ohlendieck, K. (2012b). Proteomics reveals drastic increase of extracellular matrix proteins collagen and dermatopontin in the aged mdx diaphragm model of Duchenne muscular dystrophy. Int J Mol Med *30*, 229-234.

Carpenter, J.L., Hoffman, E.P., Romanul, F.C., Kunkel, L.M., Rosales, R.K., Ma, N.S., Dasbach, J.J., Rae, J.F., Moore, F.M., McAfee, M.B., *et al.* (1989). Feline muscular dystrophy with dystrophin deficiency. Am J Pathol *135*, 909-919.

Carr, S.J., Zahedi, R.P., Lochmüller, H., and Roos, A. (2017). Mass-Spectrometry based protein analytics to unravel the tissue pathophysiology in Duchenne Muscular Dystrophy. Proteomics Clin Appl *12*, Epub, doi: 10.1002/prca.201700071.

Catapano, F., Domingos, J., Perry, M., Ricotti, V., Phillips, L., Servais, L., Seferian, A., Groot, I., Krom, Y.D., Niks, E.H., *et al.* (2018). Downregulation of miRNA-29, -23 and -21 in urine of Duchenne muscular dystrophy patients. Epigenomics *10*, 875-889.

Ceco, E., Bogdanovich, S., Gardner, B., Miller, T., DeJesus, A., Earley, J.U., Hadhazy, M., Smith, L.R., Barton, E.R., Molkentin, J.D., *et al.* (2014). Targeting latent TGFbeta release in muscular dystrophy. Sci Transl Med *6*, 259ra144.

Chamberlain, J.S., Gibbs, R.A., Ranier, J.E., Nguyen, P.N., and Caskey, C.T. (1988). Deletion screening of the Duchenne muscular dystrophy locus via multiplex DNA amplification. Nucleic Acids Res *16*, 11141-11156.

Chamberlain, J.S., Metzger, J., Reyes, M., Townsend, D., and Faulkner, J.A. (2007). Dystrophin-deficient mdx mice display a reduced life span and are susceptible to spontaneous rhabdomyosarcoma. Faseb j *21*, 2195-2204.

Cheeran, D., Khan, S., Khera, R., Bhatt, A., Garg, S., Grodin, J.L., Morlend, R., Araj, F.G., Amin, A.A., Thibodeau, J.T., *et al.* (2017). Predictors of Death in Adults With Duchenne Muscular Dystrophy-Associated Cardiomyopathy. J Am Heart Assoc *6*, e006340.

Chen, Y., Zheng, Y., Kang, Y., Yang, W., Niu, Y., Guo, X., Tu, Z., Si, C., Wang, H., Xing, R., *et al.* (2015). Functional disruption of the dystrophin gene in rhesus monkey using CRISPR/Cas9. Hum Mol Genet *24*, 3764-3774.

Chrzanowski, S.M., Baligand, C., Willcocks, R.J., Deol, J., Schmalfuss, I., Lott, D.J., Daniels, M.J., Senesac, C., Walter, G.A., and Vandenborne, K. (2017). Multi-slice MRI reveals heterogeneity in disease distribution along the length of muscle in Duchenne muscular dystrophy. Acta Myologica *36*, 151-162.

Ciafaloni, E., Fox, D.J., Pandya, S., Westfield, C.P., Puzhankara, S., Romitti, P.A., Mathews, K.D., Miller, T.M., Matthews, D.J., and Miller, L.A. (2009). Delayed diagnosis in duchenne muscular dystrophy: data from the Muscular Dystrophy Surveillance, Tracking, and Research Network (MD STARnet). The Journal of pediatrics *155*, 380-385.

Clarkson, P.M., Devaney, J.M., Gordish-Dressman, H., Thompson, P.D., Hubal, M.J., Urso, M., Price, T.B., Angelopoulos, T.J., Gordon, P.M., Moyna, N.M., *et al.* (2005). ACTN3 genotype is associated with increases in muscle strength in

response to resistance training in women. J Appl Physiol (1985) *99*, 154-163.

Collins, C.A., Olsen, I., Zammit, P.S., Heslop, L., Petrie, A., Partridge, T.A., and Morgan, J.E. (2005). Stem cell function, self-renewal, and behavioral heterogeneity of cells from the adult muscle satellite cell niche. Cell *122*, 289-301.

Colussi, C., Banfi, C., Brioschi, M., Tremoli, E., Straino, S., Spallotta, F., Mai, A., Rotili, D., Capogrossi, M.C., and Gaetano, C. (2010). Proteomic profile of differentially expressed plasma proteins from dystrophic mice and following suberoylanilide hydroxamic acid treatment. Proteomics Clin Appl *4*, 71-83.

Connolly, A.M., Florence, J.M., Cradock, M.M., Malkus, E.C., Schierbecker, J.R., Siener, C.A., Wulf, C.O., Anand, P., Golumbek, P.T., Zaidman, C.M., *et al.* (2013). Motor and cognitive assessment of infants and young boys with Duchenne Muscular Dystrophy: results from the Muscular Dystrophy Association DMD Clinical Research Network. Neuromuscul Disord *23*, 529-539.

Cynthia Martin, F., Hiller, M., Spitali, P., Oonk, S., Dalebout, H., Palmblad, M., Chaouch, A., Guglieri, M., Straub, V., Lochmuller, H., *et al.* (2014). Fibronectin is a serum biomarker for Duchenne muscular dystrophy. Proteomics Clin Appl *8*, 269-278.

Davis, D.B., Delmonte, A.J., Ly, C.T., and McNally, E.M. (2000). Myoferlin, a candidate gene and potential modifier of muscular dystrophy. Hum Mol Genet *9*, 217-226.

De Sanctis, R., Pane, M., Sivo, S., Ricotti, V., Baranello, G., Frosini, S., Mazzone, E., Bianco, F., Fanelli, L., Main, M., *et al.* (2015). Suitability of North Star Ambulatory Assessment in young boys with Duchenne muscular dystrophy. Neuromuscul Disord *25*, 14-18.

Declerck, I., Dewulf, J., Sarrazin, S., and Maes, D. (2016). Long-term effects of colostrum intake in piglet mortality and performance. J Anim Sci *94*, 1633-1643.

Deconinck, A.E., Rafael, J.A., Skinner, J.A., Brown, S.C., Potter, A.C., Metzinger, L., Watt, D.J., Dickson, J.G., Tinsley, J.M., and Davies, K.E. (1997). Utrophin-dystrophin-deficient mice as a model for Duchenne muscular dystrophy. Cell *90*, 717-727.

Deconinck, N., and Dan, B. (2007). Pathophysiology of duchenne muscular dystrophy: current hypotheses. Pediatric neurology *36*, 1-7.

Den Dunnen, J.T., Grootscholten, P.M., Bakker, E., Blonden, L.A., Ginjaar, H.B., Wapenaar, M.C., van Paassen, H.M., van Broeckhoven, C., Pearson, P.L., and van

Ommen, G.J. (1989). Topography of the Duchenne muscular dystrophy (DMD) gene: FIGE and cDNA analysis of 194 cases reveals 115 deletions and 13 duplications. Am J Hum Genet *45*, 835-847.

Desguerre, I., Mayer, M., Leturcq, F., Barbet, J.P., Gherardi, R.K., and Christov, C. (2009). Endomysial fibrosis in Duchenne muscular dystrophy: a marker of poor outcome associated with macrophage alternative activation. J Neuropathol Exp Neurol *68*, 762-773.

Deutsche Duchenne Stiftung (2017). Es nimmt seinen Lauf (Aktion Benni & Co e.V., kleine GROßE Helden e.V.).

DeVanna, J.C., Kornegay, J.N., Bogan, D.J., Bogan, J.R., Dow, J.L., and Hawkins, E.C. (2014). Respiratory dysfunction in unsedated dogs with golden retriever muscular dystrophy. Neuromuscular Disorders *24*, 63-73.

Dezawa, M., Ishikawa, H., Itokazu, Y., Yoshihara, T., Hoshino, M., Takeda, S.-i., Ide, C., and Nabeshima, Y.-i. (2005). Bone marrow stromal cells generate muscle cells and repair muscle degeneration. Science *309*, 314-317.

Diot, G., Metz, S., Noske, A., Liapis, E., Schroeder, B., Ovsepian, S.V., Meier, R., Rummeny, E., and Ntziachristos, V. (2017). Multispectral optoacoustic tomography (MSOT) of human breast cancer. Clinical Cancer Research *23*, 6912-6922.

Dorn, T., Kornherr, J., Parrotta, E.I., Zawada, D., Ayetey, H., Santamaria, G., Iop, L., Mastantuono, E., Sinnecker, D., Goedel, A., *et al.* (2018). Interplay of cell-cell contacts and RhoA/MRTF-A signaling regulates cardiomyocyte identity. Embo j *37*, e98133.

Doudna, J.A., and Charpentier, E. (2014). The new frontier of genome engineering with CRISPR-Cas9. Science *346*, 1258096.

Dowling, P., Murphy, S., Zweyer, M., Raucamp, M., Swandulla, D., and Ohlendieck, K. (2019). Emerging proteomic biomarkers of X-linked muscular dystrophy. Expert Rev Mol Diagn *19*, 739-755.

Duan, D. (2015). Duchenne muscular dystrophy gene therapy in the canine model. Hum Gene Ther Clin Dev *26*, 57-69.

Duan, D. (2018). Micro-Dystrophin Gene Therapy Goes Systemic in Duchenne Muscular Dystrophy Patients. Hum Gene Ther *29*, 733-736.

Eagle, M., Baudouin, S.V., Chandler, C., Giddings, D.R., Bullock, R., and Bushby,

K. (2002). Survival in Duchenne muscular dystrophy: improvements in life expectancy since 1967 and the impact of home nocturnal ventilation. Neuromuscular disorders *12*, 926-929.

Eagle, M., Bourke, J., Bullock, R., Gibson, M., Mehta, J., Giddings, D., Straub, V., and Bushby, K. (2007). Managing Duchenne muscular dystrophy--the additive effect of spinal surgery and home nocturnal ventilation in improving survival. Neuromuscul Disord *17*, 470-475.

Ebashi, S., Toyokura, Y., Momoi, H., and Sugita, H. (1959). High creatine phosphokinase activity of sera of progressive muscular dystrophy. The Journal of Biochemistry *46*, 103-104.

Echigoya, Y., Trieu, N., Hosoki, K., Duddy, W., Partridge, T., Hoffman, E., Kornegay, J., Rogers, C., and Yokota, T. (2016). 623. Dystrophin Exon 52-Deleted Pigs as a New Animal Model of Duchenne Muscular Dystrophy: Its Characterization and Potential as a Tool for Developing Exon Skipping Therapy. Molecular Therapy *24*, S247.

Emery, A.E. (1991). Population frequencies of inherited neuromuscular diseases—a world survey. Neuromuscular disorders *1*, 19-29.

Ervasti, J.M., and Campbell, K.P. (1993). A role for the dystrophin-glycoprotein complex as a transmembrane linker between laminin and actin. J Cell Biol *122*, 809-823.

Escolar, D., Hache, L., Clemens, P., Cnaan, A., McDonald, C.M., Viswanathan, V., Kornberg, A., Bertorini, T., Nevo, Y., and Lotze, T. (2011). Randomized, blinded trial of weekend vs daily prednisone in Duchenne muscular dystrophy. Neurology *77*, 444-452.

Eynon, N., Hanson, E.D., Lucia, A., Houweling, P.J., Garton, F., North, K.N., and Bishop, D.J. (2013). Genes for elite power and sprint performance: ACTN3 leads the way. Sports Med *43*, 803-817.

Fanin, M., Freda, M.P., Vitiello, L., Danieli, G.A., Pegoraro, E., and Angelini, C. (1996). Duchenne phenotype with in-frame deletion removing major portion of dystrophin rod: threshold effect for deletion size? Muscle Nerve *19*, 1154-1160.

Farnir, F., Grisart, B., Coppieters, W., Riquet, J., Berzi, P., Cambisano, N., Karim, L., Mni, M., Moisio, S., Simon, P., *et al.* (2002). Simultaneous mining of linkage and linkage disequilibrium to fine map quantitative trait loci in outbred half-sib pedigrees: revisiting the location of a quantitative trait locus with major effect on milk production on bovine chromosome 14. Genetics *161*, 275-287.

Feder, D., Ierardi, M., Covre, A.L., Petri, G., Carvalho, A.A.S., Fonseca, F.L.A., and Bertassoli, B.M. (2018). Evaluation of the gastrointestinal tract in mdx mice: an experimental model of Duchenne muscular dystrophy. Apmis *126*, 693-699.

Feener, C.A., Koenig, M., and Kunkel, L.M. (1989). Alternative splicing of human dystrophin mRNA generates isoforms at the carboxy terminus. Nature *338*, 509-511.

Fisher, K.J., Jooss, K., Alston, J., Yang, Y., Haecker, S.E., High, K., Pathak, R., Raper, S.E., and Wilson, J.M. (1997). Recombinant adeno-associated virus for muscle directed gene therapy. Nat Med *3*, 306-312.

Flanigan, K.M., Ceco, E., Lamar, K.M., Kaminoh, Y., Dunn, D.M., Mendell, J.R., King, W.M., Pestronk, A., Florence, J.M., Mathews, K.D., *et al.* (2013). LTBP4 genotype predicts age of ambulatory loss in Duchenne muscular dystrophy. Ann Neurol *73*, 481-488.

Forbes, S.C., Walter, G.A., Rooney, W.D., Wang, D.J., DeVos, S., Pollaro, J., Triplett, W., Lott, D.J., Willcocks, R.J., Senesac, C., *et al.* (2013). Skeletal muscles of ambulant children with Duchenne muscular dystrophy: validation of multicenter study of evaluation with MR imaging and MR spectroscopy. Radiology *269*, 198-207.

Forbes, S.C., Willcocks, R.J., Triplett, W.T., Rooney, W.D., Lott, D.J., Wang, D.-J., Pollaro, J., Senesac, C.R., Daniels, M.J., and Finkel, R.S. (2014). Magnetic resonance imaging and spectroscopy assessment of lower extremity skeletal muscles in boys with Duchenne muscular dystrophy: a multicenter cross sectional study. PloS one *9*, e106435.

Frohlich, T., Kemter, E., Flenkenthaler, F., Klymiuk, N., Otte, K.A., Blutke, A., Krause, S., Walter, M.C., Wanke, R., Wolf, E., *et al.* (2016). Progressive muscle proteome changes in a clinically relevant pig model of Duchenne muscular dystrophy. Sci Rep *6*, 33362.

Fukada, S., Morikawa, D., Yamamoto, Y., Yoshida, T., Sumie, N., Yamaguchi, M., Ito, T., Miyagoe-Suzuki, Y., Takeda, S., Tsujikawa, K., *et al.* (2010). Genetic background affects properties of satellite cells and mdx phenotypes. Am J Pathol *176*, 2414-2424.

Gaj, T., Gersbach, C.A., and Barbas, C.F., 3rd (2013). ZFN, TALEN, and CRISPR/Cas-based methods for genome engineering. Trends Biotechnol *31*, 397-405.

Garcia, S.M., Tamaki, S., Lee, S., Wong, A., Jose, A., Dreux, J., Kouklis, G., Sbitany, H., Seth, R., Knott, P.D., *et al.* (2018). High-Yield Purification,

Preservation, and Serial Transplantation of Human Satellite Cells. Stem Cell Reports *10*, 1160-1174.

Gaschen, L., Lang, J., Lin, S., Ade-Damilano, M., Busato, A., Lombard, C.W., and Gaschen, F.P. (1999). Cardiomyopathy in dystrophin-deficient hypertrophic feline muscular dystrophy. J Vet Intern Med *13*, 346-356.

Ge, Y., Molloy, M.P., Chamberlain, J.S., and Andrews, P.C. (2003). Proteomic analysis of mdx skeletal muscle: Great reduction of adenylate kinase 1 expression and enzymatic activity. Proteomics *3*, 1895-1903.

Ge, Y., Molloy, M.P., Chamberlain, J.S., and Andrews, P.C. (2004). Differential expression of the skeletal muscle proteome in mdx mice at different ages. Electrophoresis *25*, 2576-2585.

Gehrke, L.J., Capitan, A., Scheper, C., König, S., Upadhyay, M., Heidrich, K., Russ, I., Seichter, D., Tetens, J., and Medugorac, I. (2020). Are scurs in heterozygous polled (Pp) cattle a complex quantitative trait? Genetics Selection Evolution *52*, 1-13.

Geiger, R., Strasak, A., Treml, B., Gasser, K., Kleinsasser, A., Fischer, V., Geiger, H., Loeckinger, A., and Stein, J.I. (2007). Six-minute walk test in children and adolescents. J Pediatr *150*, 395-399, 399.e391-392.

Genome - Assembly - NCBI, International Swine Genome Sequencing Consortium Sscrofa11.1.

Gerhalter, T., Gast, L.V., Marty, B., Martin, J., Trollmann, R., Schussler, S., Roemer, F., Laun, F.B., Uder, M., Schroder, R., *et al.* (2019). (23) Na MRI depicts early changes in ion homeostasis in skeletal muscle tissue of patients with duchenne muscular dystrophy. J Magn Reson Imaging *50*, 1103-1113.

Giacopelli, F., Marciano, R., Pistorio, A., Catarsi, P., Canini, S., Karsenty, G., and Ravazzolo, R. (2004). Polymorphisms in the osteopontin promoter affect its transcriptional activity. Physiol Genomics *20*, 87-96.

Giltay, R., Kostka, G., and Timpl, R. (1997). Sequence and expression of a novel member (LTBP-4) of the family of latent transforming growth factor-beta binding proteins. FEBS Lett *411*, 164-168.

Glemser, P.A., Jaeger, H., Nagel, A.M., Ziegler, A.E., Simons, D., Schlemmer, H.P., Lehmann-Horn, F., Jurkat-Rott, K., and Weber, M.A. (2017). (23)Na MRI and myometry to compare eplerenone vs. glucocorticoid treatment in Duchenne dystrophy. Acta Myol *36*, 2-13.

Godfrey, C., Muses, S., McClorey, G., Wells, K.E., Coursindel, T., Terry, R.L., Betts, C., Hammond, S., O'Donovan, L., and Hildyard, J. (2015). How much dystrophin is enough: the physiological consequences of different levels of dystrophin in the mdx mouse. Human molecular genetics *24*, 4225-4237.

Goemans, N.M., Tulinius, M., van den Akker, J.T., Burm, B.E., Ekhart, P.F., Heuvelmans, N., Holling, T., Janson, A.A., Platenburg, G.J., Sipkens, J.A., *et al.* (2011). Systemic administration of PRO051 in Duchenne's muscular dystrophy. N Engl J Med *364*, 1513-1522.

Gowers, W.R. (1879). Pseudo-hypertrophic muscular paralysis: a clinical lecture (J. & A. Churchill).

Goyenvalle, A., Seto, J.T., Davies, K.E., and Chamberlain, J. (2011). Therapeutic approaches to muscular dystrophy. Human molecular genetics *20*, R69-R78.

Guevel, L., Lavoie, J.R., Perez-Iratxeta, C., Rouger, K., Dubreil, L., Feron, M., Talon, S., Brand, M., and Megeney, L.A. (2011). Quantitative proteomic analysis of dystrophic dog muscle. J Proteome Res *10*, 2465-2478.

Guiraud, S., and Davies, K.E. (2017). Pharmacological advances for treatment in Duchenne muscular dystrophy. Current opinion in pharmacology *34*, 36-48.

Guiraud, S., Squire, S.E., Edwards, B., Chen, H., Burns, D.T., Shah, N., Babbs, A., Davies, S.G., Wynne, G.M., Russell, A.J., *et al.* (2015). Second-generation compound for the modulation of utrophin in the therapy of DMD. Hum Mol Genet *24*, 4212-4224.

Hakim, C.H., Wasala, N.B., Pan, X., Kodippili, K., Yue, Y., Zhang, K., Yao, G., Haffner, B., Duan, S.X., Ramos, J., *et al.* (2017). A Five-Repeat Micro-Dystrophin Gene Ameliorated Dystrophic Phenotype in the Severe DBA/2J-mdx Model of Duchenne Muscular Dystrophy. Mol Ther Methods Clin Dev *6*, 216-230.

Haslett, J.N., Sanoudou, D., Kho, A.T., Han, M., Bennett, R.R., Kohane, I.S., Beggs, A.H., and Kunkel, L.M. (2003). Gene expression profiling of Duchenne muscular dystrophy skeletal muscle. Neurogenetics *4*, 163-171.

Hathout, Y., Liang, C., Ogundele, M., Xu, G., Tawalbeh, S.M., Dang, U.J., Hoffman, E.P., Gordish-Dressman, H., Conklin, L.S., van den Anker, J.N., *et al.* (2019). Disease-specific and glucocorticoid-responsive serum biomarkers for Duchenne Muscular Dystrophy. Sci Rep *9*, 12167.

Hathout, Y., Marathi, R.L., Rayavarapu, S., Zhang, A., Brown, K.J., Seol, H., Gordish-Dressman, H., Cirak, S., Bello, L., Nagaraju, K., *et al.* (2014). Discovery

of serum protein biomarkers in the mdx mouse model and cross-species comparison to Duchenne muscular dystrophy patients. Hum Mol Genet *23*, 6458-6469.

Hayes, J., Veyckemans, F., and Bissonnette, B. (2008). Duchenne muscular dystrophy: an old anesthesia problem revisited. Paediatr Anaesth *18*, 100-106.

Heckmatt, J., Leeman, S., and Dubowitz, V. (1982). Ultrasound imaging in the diagnosis of muscle disease. The Journal of pediatrics *101*, 656-660.

Heydemann, A., Ceco, E., Lim, J.E., Hadhazy, M., Ryder, P., Moran, J.L., Beier, D.R., Palmer, A.A., and McNally, E.M. (2009). Latent TGF-beta-binding protein 4 modifies muscular dystrophy in mice. J Clin Invest *119*, 3703-3712.

Hinderer, C., Katz, N., Buza, E.L., Dyer, C., Goode, T., Bell, P., Richman, L.K., and Wilson, J.M. (2018). Severe Toxicity in Nonhuman Primates and Piglets Following High-Dose Intravenous Administration of an Adeno-Associated Virus Vector Expressing Human SMN. Hum Gene Ther *29*, 285-298.

Hinton, V.J., Fee, R.J., Goldstein, E.M., and De Vivo, D.C. (2007). Verbal and memory skills in males with Duchenne muscular dystrophy. Dev Med Child Neurol *49*, 123-128.

Hoffman, E.P., Schwartz, B.D., Mengle-Gaw, L.J., Smith, E.C., Castro, D., Mah, J.K., McDonald, C.M., Kuntz, N.L., Finkel, R.S., Guglieri, M., *et al.* (2019). Vamorolone trial in Duchenne muscular dystrophy shows dose-related improvement of muscle function. Neurology *93*, e1312-e1323.

Hogarth, M.W., Houweling, P.J., Thomas, K.C., Gordish-Dressman, H., Bello, L., Pegoraro, E., Hoffman, E.P., Head, S.I., and North, K.N. (2017). Evidence for ACTN3 as a genetic modifier of Duchenne muscular dystrophy. Nat Commun *8*, 14143.

Hoogerwaard, E., Bakker, E., Ippel, P., Oosterwijk, J., Majoor-Krakauer, D., Leschot, N., Van, A.E., Brunner, H., and Wilde, A. (1999). Signs and symptoms of Duchenne muscular dystrophy and Becker muscular dystrophy among carriers in The Netherlands: a cohort study. Lancet (London, England) *353*, 2116-2119.

Hooijmans, M.T., Niks, E.H., Burakiewicz, J., Anastasopoulos, C., van den Berg, S.I., van Zwet, E., Webb, A.G., Verschuuren, J., and Kan, H.E. (2017). Non-uniform muscle fat replacement along the proximodistal axis in Duchenne muscular dystrophy. Neuromuscul Disord *27*, 458-464.

Horster, I., Weigt-Usinger, K., Carmann, C., Chobanyan-Jurgens, K., Kohler, C., Schara, U., Kayacelebi, A.A., Beckmann, B., Tsikas, D., and Lucke, T. (2015). The

L-arginine/NO pathway and homoarginine are altered in Duchenne muscular dystrophy and improved by glucocorticoids. Amino Acids *47*, 1853-1863.

Hrach, H.C., and Mangone, M. (2019). miRNA Profiling for Early Detection and Treatment of Duchenne Muscular Dystrophy. Int J Mol Sci *20*, E4638.

Huard, J., Bouchard, J., Roy, R., Malouin, F., Dansereau, G., Labrecque, C., Albert, N., Richards, C., Lemieux, B., and Tremblay, J. (1992). Human myoblast transplantation: preliminary results of 4 cases. Muscle & Nerve: Official Journal of the American Association of Electrodiagnostic Medicine *15*, 550-560.

Ikemoto, M., Fukada, S.-i., Uezumi, A., Masuda, S., Miyoshi, H., Yamamoto, H., Wada, M.R., Masubuchi, N., Miyagoe-Suzuki, Y., and Takeda, S.i. (2007). Autologous transplantation of SM/C-2.6+ satellite cells transduced with micro-dystrophin CS1 cDNA by lentiviral vector into mdx mice. Molecular Therapy *15*, 2178-2185.

Jensen, L., Petersson, S.J., Illum, N.O., Laugaard-Jacobsen, H.C., Thelle, T., Jorgensen, L.H., and Schroder, H.D. (2017). Muscular response to the first three months of deflazacort treatment in boys with Duchenne muscular dystrophy. J Musculoskelet Neuronal Interact *17*, 8-18.

Jinek, M., Chylinski, K., Fonfara, I., Hauer, M., Doudna, J.A., and Charpentier, E. (2012). A programmable dual-RNA–guided DNA endonuclease in adaptive bacterial immunity. science *337*, 816-821.

Kamdar, F., and Garry, D.J. (2016). Dystrophin-Deficient Cardiomyopathy. J Am Coll Cardiol *67*, 2533-2546.

Karpati, G. (1991). Myoblast transfer in Duchenne muscular dystrophy. A perspective. Muscular Dystrophy Research: From Molecular Diagnosis Towards Therapy, 101-108.

Kemper, A.R., and Wake, M.A. (2007). Duchenne muscular dystrophy: issues in expanding newborn screening. Curr Opin Pediatr *19*, 700-704.

Kim, J., Jung, I.Y., Kim, S.J., Lee, J.Y., Park, S.K., Shin, H.I., and Bang, M.S. (2018). A New Functional Scale and Ambulatory Functional Classification of Duchenne Muscular Dystrophy: Scale Development and Preliminary Analyses of Reliability and Validity. Ann Rehabil Med *42*, 690-701.

Klingler, W., Jurkat-Rott, K., Lehmann-Horn, F., and Schleip, R. (2012). The role of fibrosis in Duchenne muscular dystrophy. Acta Myologica *31*, 184.

Klymiuk, N., Blutke, A., Graf, A., Krause, S., Burkhardt, K., Wuensch, A., Krebs, S., Kessler, B., Zakhartchenko, V., Kurome, M., *et al.* (2013). Dystrophin-deficient pigs provide new insights into the hierarchy of physiological derangements of dystrophic muscle. Human Molecular Genetics *22*, 4368-4382.

Klymiuk, N., Seeliger, F., Bohlooly-Y, M., Blutke, A., Rudmann, D.G., and Wolf, E. (2016). Tailored pig models for preclinical efficacy and safety testing of targeted therapies. Toxicologic pathology *44*, 346-357.

Knieling, F., Hartmann, A., Uter, W., Urich, A., Claussen, J., Atreya, R., Rascher, W., and Waldner, M. (2017). Multispectral Optoacoustic Tomography in Crohn's disease-A First-in-human Diagnostic Clinical Trial. Journal of Nuclear Medicine *58*, 379-379.

Koch, A.J., Pereira, R., and Machado, M. (2014). The creatine kinase response to resistance exercise. J Musculoskelet Neuronal Interact *14*, 68-77.

Koenig, M., Beggs, A.H., Moyer, M., Scherpf, S., Heindrich, K., Bettecken, T., Meng, G., Muller, C.R., Lindlof, M., Kaariainen, H., *et al.* (1989). The molecular basis for Duchenne versus Becker muscular dystrophy: correlation of severity with type of deletion. Am J Hum Genet *45*, 498-506.

Koenig, M., Hoffman, E.P., Bertelson, C.J., Monaco, A.P., Feener, C., and Kunkel, L.M. (1987). Complete cloning of the Duchenne muscular dystrophy (DMD) cDNA and preliminary genomic organization of the DMD gene in normal and affected individuals. Cell *50*, 509-517.

Koenig, M., Monaco, A.P., and Kunkel, L.M. (1988). The complete sequence of dystrophin predicts a rod-shaped cytoskeletal protein. Cell *53*, 219-228.

Koppanati, B.M., Li, J., Reay, D.P., Wang, B., Daood, M., Zheng, H., Xiao, X., Watchko, J.F., and Clemens, P.R. (2010). Improvement of the mdx mouse dystrophic phenotype by systemic in utero AAV8 delivery of a minidystrophin gene. Gene therapy *17*, 1355.

Kornegay, J.N. (2017). The golden retriever model of Duchenne muscular dystrophy. Skelet Muscle *7*, 9.

Kraus, D., Wong, B., Hu, S., and Kaul, A. (2018). Gut Transit in Duchenne Muscular Dystrophy Is Not Impaired: A Study Utilizing Wireless Motility Capsules. J Pediatr *194*, 238-240.

Kraus, D., Wong, B.L., Horn, P.S., and Kaul, A. (2016). Constipation in Duchenne muscular dystrophy: prevalence, diagnosis, and treatment. The Journal of pediatrics

171, 183-188.

Krosschell, K.J., Maczulski, J.A., Crawford, T.O., Scott, C., and Swoboda, K.J. (2006). A modified Hammersmith functional motor scale for use in multi-center research on spinal muscular atrophy. Neuromuscul Disord *16*, 417-426.

Krosschell, K.J., Scott, C.B., Maczulski, J.A., Lewelt, A.J., Reyna, S.P., and Swoboda, K.J. (2011). Reliability of the Modified Hammersmith Functional Motor Scale in young children with spinal muscular atrophy. Muscle Nerve *44*, 246-251.

Kunz, E., Rothammer, S., Pausch, H., Schwarzenbacher, H., Seefried, F.R., Matiasek, K., Seichter, D., Russ, I., Fries, R., and Medugorac, I. (2016). Confirmation of a non-synonymous SNP in PNPLA8 as a candidate causal mutation for Weaver syndrome in Brown Swiss cattle. Genetics Selection Evolution *48*, 21.

Labun, K., Montague, T.G., Krause, M., Torres Cleuren, Y.N., Tjeldnes, H., and Valen, E. (2019). CHOPCHOP v3: expanding the CRISPR web toolbox beyond genome editing. Nucleic Acids Res *47*, W171-w174.

Lalic, T., Vossen, R.H., Coffa, J., Schouten, J.P., Guc-Scekic, M., Radivojevic, D., Djurisic, M., Breuning, M.H., White, S.J., and den Dunnen, J.T. (2005). Deletion and duplication screening in the DMD gene using MLPA. Eur J Hum Genet *13*, 1231-1234.

Lamar, K.M., Bogdanovich, S., Gardner, B.B., Gao, Q.Q., Miller, T., Earley, J.U., Hadhazy, M., Vo, A.H., Wren, L., Molkentin, J.D., *et al.* (2016). Overexpression of Latent TGFbeta Binding Protein 4 in Muscle Ameliorates Muscular Dystrophy through Myostatin and TGFbeta. PLoS Genet *12*, e1006019.

Larcher, T., Lafoux, A., Tesson, L., Remy, S., Thepenier, V., Francois, V., Le Guiner, C., Goubin, H., Dutilleul, M., Guigand, L., *et al.* (2014). Characterization of dystrophin deficient rats: a new model for Duchenne muscular dystrophy. PLoS One *9*, e110371.

Le Guiner, C., Servais, L., Montus, M., Larcher, T., Fraysse, B., Moullec, S., Allais, M., François, V., Dutilleul, M., and Malerba, A. (2017). Long-term microdystrophin gene therapy is effective in a canine model of Duchenne muscular dystrophy. Nature Communications *8*, 16105.

Lederfein, D., Levy, Z., Augier, N., Mornet, D., Morris, G., Fuchs, O., Yaffe, D., and Nudel, U. (1992). A 71-kilodalton protein is a major product of the Duchenne muscular dystrophy gene in brain and other nonmuscle tissues. Proc Natl Acad Sci U S A *89*, 5346-5350.

Lee, S.H., and Van der Werf, J.H. (2006). Using dominance relationship coefficients based on linkage disequilibrium and linkage with a general complex pedigree to increase mapping resolution. Genetics *174*, 1009-1016.

Leon, S.H., Schuffler, M.D., Kettler, M., and Rohrmann, C.A. (1986). Chronic intestinal pseudoobstruction as a complication of Duchenne's muscular dystrophy. Gastroenterology *90*, 455-459.

Linde, L., and Kerem, B. (2008). Introducing sense into nonsense in treatments of human genetic diseases. Trends in genetics *24*, 552-563.

Lindsay, H., Burger, A., Biyong, B., Felker, A., Hess, C., Zaugg, J., Chiavacci, E., Anders, C., Jinek, M., and Mosimann, C. (2016). CrispRVariants charts the mutation spectrum of genome engineering experiments. Nature biotechnology *34*, 701-702.

Llano-Diez, M., Ortez, C.I., Gay, J.A., Alvarez-Cabado, L., Jou, C., Medina, J., Nascimento, A., and Jimenez-Mallebrera, C. (2017). Digital PCR quantification of miR-30c and miR-181a as serum biomarkers for Duchenne muscular dystrophy. Neuromuscul Disord *27*, 15-23.

Lo Cascio, C.M., Goetze, O., Latshang, T.D., Bluemel, S., Frauenfelder, T., and Bloch, K.E. (2016). Gastrointestinal Dysfunction in Patients with Duchenne Muscular Dystrophy. PLoS One *11*, e0163779.

Long, C., Amoasii, L., Mireault, A.A., McAnally, J.R., Li, H., Sanchez-Ortiz, E., Bhattacharyya, S., Shelton, J.M., Bassel-Duby, R., and Olson, E.N. (2016). Postnatal genome editing partially restores dystrophin expression in a mouse model of muscular dystrophy. Science *351*, 400-403.

Lu, Q.L., Mann, C.J., Lou, F., Bou-Gharios, G., Morris, G.E., Xue, S.-a., Fletcher, S., Partridge, T.A., and Wilton, S.D. (2003). Functional amounts of dystrophin produced by skipping the mutated exon in the mdx dystrophic mouse. Nature medicine *9*, 1009.

Magrath, P., Maforo, N., Renella, P., Nelson, S.F., Halnon, N., and Ennis, D.B. (2018). Cardiac MRI biomarkers for Duchenne muscular dystrophy. Biomark Med *12*, 1271-1289.

Main, M., Kairon, H., Mercuri, E., and Muntoni, F. (2003). The Hammersmith functional motor scale for children with spinal muscular atrophy: a scale to test ability and monitor progress in children with limited ambulation. Eur J Paediatr Neurol *7*, 155-159.

Martin, P., Bateson, P.P.G., and Bateson, P. (1993). Measuring behaviour: an introductory guide (Cambridge University Press).

Mathur, S., Lott, D.J., Senesac, C., Germain, S.A., Vohra, R.S., Sweeney, H.L., Walter, G.A., and Vandenborne, K. (2010). Age-related differences in lower-limb muscle cross-sectional area and torque production in boys with Duchenne muscular dystrophy. Arch Phys Med Rehabil *91*, 1051-1058.

Matsunari, H., Watanabe, M., Nakano, K., Enosawa, S., Umeyama, K., Uchikura, A., Yashima, S., Fukuda, T., Klymiuk, N., Kurome, M., *et al.* (2018). Modeling lethal X-linked genetic disorders in pigs with ensured fertility. Proc Natl Acad Sci U S A *115*, 708-713.

Matsuo, M., Awano, H., Maruyama, N., and Nishio, H. (2019). Titin fragment in urine: A noninvasive biomarker of muscle degradation. Adv Clin Chem *90*, 1-23.

Mazzone, E., Martinelli, D., Berardinelli, A., Messina, S., D'Amico, A., Vasco, G., Main, M., Doglio, L., Politano, L., and Cavallaro, F. (2010). North Star Ambulatory Assessment, 6-minute walk test and timed items in ambulant boys with Duchenne muscular dystrophy. Neuromuscular Disorders *20*, 712-716.

Mcclorey, G., Moulton, H., Iversen, P., Fletcher, S., and Wilton, S. (2006). Antisense oligonucleotide-induced exon skipping restores dystrophin expression in vitro in a canine model of DMD. Gene therapy *13*, 1373.

McDonald, C.M., Campbell, C., Torricelli, R.E., Finkel, R.S., Flanigan, K.M., Goemans, N., Heydemann, P., Kaminska, A., Kirschner, J., and Muntoni, F. (2017). Ataluren in patients with nonsense mutation Duchenne muscular dystrophy (ACT DMD): a multicentre, randomised, double-blind, placebo-controlled, phase 3 trial. The Lancet *390*, 1489-1498.

McDonald, C.M., Henricson, E.K., Han, J.J., Abresch, R.T., Nicorici, A., Elfring, G.L., Atkinson, L., Reha, A., Hirawat, S., and Miller, L.L. (2010). The 6-minute walk test as a new outcome measure in Duchenne muscular dystrophy. Muscle Nerve *41*, 500-510.

McGreevy, J.W., Hakim, C.H., McIntosh, M.A., and Duan, D. (2015). Animal models of Duchenne muscular dystrophy: from basic mechanisms to gene therapy. Disease models & mechanisms *8*, 195-213.

McKusick, V.A. (2002). DYSTROPHIN; DMD * 300377

McLeish, M.J., and Kenyon, G.L. (2005). Relating structure to mechanism in creatine kinase. Crit Rev Biochem Mol Biol *40*, 1-20.

Medugorac, I., Graf, A., Grohs, C., Rothammer, S., Zagdsuren, Y., Gladyr, E., Zinovieva, N., Barbieri, J., Seichter, D., Russ, I., *et al.* (2017). Whole-genome analysis of introgressive hybridization and characterization of the bovine legacy of Mongolian yaks. Nat Genet *49*, 470-475.

Mendell, J.R., Goemans, N., Lowes, L.P., Alfano, L.N., Berry, K., Shao, J., Kaye, E.M., Mercuri, E., Group, E.S., Network, T.F.D.I., *et al.* (2016). Longitudinal effect of eteplirsen versus historical control on ambulation in D uchenne muscular dystrophy. Annals of neurology *79*, 257-271.

Mendell, J.R., Kissel, J.T., Amato, A.A., King, W., Signore, L., Prior, T.W., Sahenk, Z., Benson, S., McAndrew, P.E., and Rice, R. (1995). Myoblast transfer in the treatment of Duchenne's muscular dystrophy. New England Journal of Medicine *333*, 832-838.

Mendell, J.R., and Lloyd-Puryear, M. (2013). Report of MDA muscle disease symposium on newborn screening for Duchenne muscular dystrophy. Muscle & nerve *48*, 21-26.

Merlini, L., Gennari, M., Malaspina, E., Cecconi, I., Armaroli, A., Gnudi, S., Talim, B., Ferlini, A., Cicognani, A., and Franzoni, E. (2012). Early corticosteroid treatment in 4 Duchenne muscular dystrophy patients: 14-year follow-up. Muscle & nerve *45*, 796-802.

Messroghli, D.R., Moon, J.C., Ferreira, V.M., Grosse-Wortmann, L., He, T., Kellman, P., Mascherbauer, J., Nezafat, R., Salerno, M., Schelbert, E.B., *et al.* (2017). Clinical recommendations for cardiovascular magnetic resonance mapping of T1, T2, T2* and extracellular volume: A consensus statement by the Society for Cardiovascular Magnetic Resonance (SCMR) endorsed by the European Association for Cardiovascular Imaging (EACVI). J Cardiovasc Magn Reson *19*, 75.

Meuwissen, T.H., and Goddard, M.E. (2001). Prediction of identity by descent probabilities from marker-haplotypes. Genet Sel Evol *33*, 605-634.

Meuwissen, T.H., Karlsen, A., Lien, S., Olsaker, I., and Goddard, M.E. (2002). Fine mapping of a quantitative trait locus for twinning rate using combined linkage and linkage disequilibrium mapping. Genetics *161*, 373-379.

Mitchell, P.S., Parkin, R.K., Kroh, E.M., Fritz, B.R., Wyman, S.K., Pogosova-Agadjanyan, E.L., Peterson, A., Noteboom, J., O'Briant, K.C., Allen, A., *et al.* (2008). Circulating microRNAs as stable blood-based markers for cancer detection. Proc Natl Acad Sci U S A *105*, 10513-10518.

Monaco, A.P., Bertelson, C.J., Liechti-Gallati, S., Moser, H., and Kunkel, L.M.

(1988). An explanation for the phenotypic differences between patients bearing partial deletions of the DMD locus. Genomics *2*, 90-95.

Monaco, A.P., Neve, R.L., Colletti-Feener, C., Bertelson, C.J., Kurnit, D.M., and Kunkel, L.M. (1986). Isolation of candidate cDNAs for portions of the Duchenne muscular dystrophy gene. Nature *323*, 646-650.

Moore, C.J., Caughey, M.C., Meyer, D.O., Emmett, R., Jacobs, C., Chopra, M., Howard, J.F., Jr., and Gallippi, C.M. (2018). In Vivo Viscoelastic Response (VisR) Ultrasound for Characterizing Mechanical Anisotropy in Lower-Limb Skeletal Muscles of Boys with and without Duchenne Muscular Dystrophy. Ultrasound Med Biol *44*, 2519-2530.

Moorwood, C., Lozynska, O., Suri, N., Napper, A.D., Diamond, S.L., and Khurana, T.S. (2011). Drug discovery for Duchenne muscular dystrophy via utrophin promoter activation screening. PloS one *6*, e26169.

Moran, C.N., Yang, N., Bailey, M.E., Tsiokanos, A., Jamurtas, A., MacArthur, D.G., North, K., Pitsiladis, Y.P., and Wilson, R.H. (2007). Association analysis of the ACTN3 R577X polymorphism and complex quantitative body composition and performance phenotypes in adolescent Greeks. Eur J Hum Genet *15*, 88-93.

Moretti, A., Fonteyne, L., Giesert, F., Hoppmann, P., Meier, A.B., Bozoglu, T., Baehr, A., Schneider, C.M., Sinnecker, D., Klett, K., *et al.* (2020). Somatic gene editing ameliorates skeletal and cardiac muscle failure in pig and human models of Duchenne muscular dystrophy. Nature Medicine *26*, 207-214.

Moser, H.v., and Emery, A. (1974). The manifesting carrier in Duchenne muscular dystrophy. Clinical genetics *5*, 271-284.

Mulè, F., Amato, A., and Serio, R. (2010). Gastric emptying, small intestinal transit and fecal output in dystrophic (mdx) mice. The Journal of Physiological Sciences *60*, 75-79.

Muller, M.P., Rothammer, S., Seichter, D., Russ, I., Hinrichs, D., Tetens, J., Thaller, G., and Medugorac, I. (2017). Genome-wide mapping of 10 calving and fertility traits in Holstein dairy cattle with special regard to chromosome 18. J Dairy Sci *100*, 1987-2006.

Muntoni, F., Torelli, S., and Ferlini, A. (2003). Dystrophin and mutations: one gene, several proteins, multiple phenotypes. The Lancet Neurology *2*, 731-740.

Muntoni, F., and Wood, M.J. (2011). Targeting RNA to treat neuromuscular disease. Nature reviews Drug discovery *10*, 621.

Nadarajah, V., Mertens, B., Dalebout, H., Bladergroen, M., Alagaratnam, S., and Bushby, K. (2012). Serum peptide profiles of Duchenne Muscular Dystrophy (DMD) patients evaluated by data handling strategies for high resolution content. J Proteomics Bioinf *5*, 96-103.

Nadarajah, V.D., van Putten, M., Chaouch, A., Garrood, P., Straub, V., Lochmuller, H., Ginjaar, H.B., Aartsma-Rus, A.M., van Ommen, G.J., den Dunnen, J.T., *et al.* (2011). Serum matrix metalloproteinase-9 (MMP-9) as a biomarker for monitoring disease progression in Duchenne muscular dystrophy (DMD). Neuromuscul Disord *21*, 569-578.

Nakagawa, T., Takeuchi, A., Kakiuchi, R., Lee, T., Yagi, M., Awano, H., Iijima, K., Takeshima, Y., Urade, Y., and Matsuo, M. (2013). A prostaglandin D2 metabolite is elevated in the urine of Duchenne muscular dystrophy patients and increases further from 8 years old. Clin Chim Acta *423*, 10-14.

Nakamura, A., and Takeda, S.i. (2009). Exon-skipping therapy for Duchenne muscular dystrophy. Neuropathology *29*, 494-501.

Nakamura, A., and Takeda, S.i. (2011). Mammalian models of Duchenne Muscular Dystrophy: pathological characteristics and therapeutic applications. BioMed Research International *2011*, 184393.

Nakamura, K., Fujii, W., Tsuboi, M., Tanihata, J., Teramoto, N., Takeuchi, S., Naito, K., Yamanouchi, K., and Nishihara, M. (2014). Generation of muscular dystrophy model rats with a CRISPR/Cas system. Sci Rep *4*, 5635.

National Library of Medicine (2019) (National Institutes of Health (NIH)).

Nicholson, G., Morgan, G., Meerkin, M., Strauss, E., and McLeod, J. (1985). The creatine kinase reference interval: An assessment of intra-and inter-individual Variation. Journal of the neurological sciences *71*, 225-231.

Nigro, G., Comi, L., Politano, L., and Bain, R. (1990). The incidence and evolution of cardiomyopathy in Duchenne muscular dystrophy. International journal of cardiology *26*, 271-277.

Nigro, G., Comi, L.I., Politano, L., and Nigro, V. (1995). Dilated cardiomyopathy of muscular dystrophy: a multifaceted approach to management. Seminars in neurology *15*, 90-92.

Nowak, K.J., and Davies, K.E. (2004). Duchenne muscular dystrophy and dystrophin: pathogenesis and opportunities for treatment. EMBO reports *5*, 872-876.

O'Hagen, J.M., Glanzman, A.M., McDermott, M.P., Ryan, P.A., Flickinger, J., Quigley, J., Riley, S., Sanborn, E., Irvine, C., Martens, W.B., *et al.* (2007). An expanded version of the Hammersmith Functional Motor Scale for SMA II and III patients. Neuromuscul Disord *17*, 693-697.

Okizuka, Y., Takeshima, Y., Awano, H., Zhang, Z., Yagi, M., and Matsuo, M. (2009). Small mutations detected by multiplex ligation-dependent probe amplification of the dystrophin gene. Genet Test Mol Biomarkers *13*, 427-431.

Okubo, M., Minami, N., Goto, K., Goto, Y., Noguchi, S., Mitsuhashi, S., and Nishino, I. (2016). Genetic diagnosis of Duchenne/Becker muscular dystrophy using next-generation sequencing: validation analysis of DMD mutations. J Hum Genet *61*, 483-489.

Pane, M., Mazzone, E.S., Sivo, S., Sormani, M.P., Messina, S., D'Amico, A., Carlesi, A., Vita, G., Fanelli, L., Berardinelli, A., *et al.* (2014). Long term natural history data in ambulant boys with Duchenne muscular dystrophy: 36-month changes. PLoS One *9*, e108205.

Parray, F.Q., Wani, M.L., Malik, A.A., Wani, S.N., Bijli, A.H., and Irshad, I. (2012). Ulcerative colitis: a challenge to surgeons. International journal of preventive medicine *3*, 749-763.

Partridge, T.A., Morgan, J., Coulton, G., Hoffman, E., and Kunkel, L. (1989). Conversion of mdx myofibres from dystrophin-negative to-positive by injection of normal myoblasts. Nature *337*, 176-179.

Passamano, L., Taglia, A., Palladino, A., Viggiano, E., D'Ambrosio, P., Scutifero, M., Rosaria Cecio, M., Torre, V., F, D.E.L., Picillo, E., *et al.* (2012). Improvement of survival in Duchenne Muscular Dystrophy: retrospective analysis of 835 patients. Acta Myol *31*, 121-125.

Pegoraro, E., Hoffman, E.P., Piva, L., Gavassini, B.F., Cagnin, S., Ermani, M., Bello, L., Soraru, G., Pacchioni, B., Bonifati, M.D., *et al.* (2011). SPP1 genotype is a determinant of disease severity in Duchenne muscular dystrophy. Neurology *76*, 219-226.

Percy, M.E., Andrews, D.F., and Thompson, M.W. (1982). Serum creatine kinase in the detection of Duchenne muscular dystrophy carriers: effects of season and multiple testing. Muscle Nerve *5*, 58-64.

Perkins, K.J., and Davies, K.E. (2002). The role of utrophin in the potential therapy of Duchenne muscular dystrophy. Neuromuscul Disord *12 Suppl 1*, S78-89.

Perovic, A., and Dolcic, M. (2019). Influence of hemolysis on clinical chemistry parameters determined with Beckman Coulter tests - detection of clinically significant interference. Scand J Clin Lab Invest *79*, 154-159.

Petrof, B.J., Shrager, J.B., Stedman, H.H., Kelly, A.M., and Sweeney, H.L. (1993). Dystrophin protects the sarcolemma from stresses developed during muscle contraction. Proceedings of the National Academy of Sciences *90*, 3710-3714.

Peverelli, L., Testolin, S., Villa, L., D'Amico, A., Petrini, S., Favero, C., Magri, F., Morandi, L., Mora, M., Mongini, T., *et al.* (2015). Histologic muscular history in steroid-treated and untreated patients with Duchenne dystrophy. Neurology *85*, 1886-1893.

Pillen, S., Tak, R.O., Zwarts, M.J., Lammens, M.M., Verrijp, K.N., Arts, I.M., van der Laak, J.A., Hoogerbrugge, P.M., van Engelen, B.G., and Verrips, A. (2009). Skeletal muscle ultrasound: correlation between fibrous tissue and echo intensity. Ultrasound Med Biol *35*, 443-446.

Powell, J.E., Visscher, P.M., and Goddard, M.E. (2010). Reconciling the analysis of IBD and IBS in complex trait studies. Nat Rev Genet *11*, 800-805.

Prior, T.W., and Bridgeman, S.J. (2005). Experience and strategy for the molecular testing of Duchenne muscular dystrophy. J Mol Diagn *7*, 317-326.

Rando, T.A. (2001). The dystrophin-glycoprotein complex, cellular signaling, and the regulation of cell survival in the muscular dystrophies. Muscle Nerve *24*, 1575-1594.

Regensburger, A.P., Fonteyne, L.M., Jungert, J., Wagner, A.L., Gerhalter, T., Nagel, A.M., Heiss, R., Flenkenthaler, F., Qurashi, M., Neurath, M.F., *et al.* (2019). Detection of collagens by multispectral optoacoustic tomography as an imaging biomarker for Duchenne muscular dystrophy. Nat Med *25*, 1905-1915.

Reimers, K., Reimers, C.D., Wagner, S., Paetzke, I., and Pongratz, D.E. (1993). Skeletal muscle sonography: a correlative study of echogenicity and morphology. J Ultrasound Med *12*, 73-77.

Rey-Barroso, L., Burgos-Fernández, F.J., Delpueyo, X., Ares, M., Royo, S., Malvehy, J., Puig, S., and Vilaseca, M. (2018). Visible and extended near-infrared multispectral imaging for skin cancer diagnosis. Sensors *18*, 1441.

Richter, A., Kurome, M., Kessler, B., Zakhartchenko, V., Klymiuk, N., Nagashima, H., Wolf, E., and Wuensch, A. (2012). Potential of primary kidney cells for somatic cell nuclear transfer mediated transgenesis in pig. BMC Biotechnol *12*, 84.

Ricotti, V., Spinty, S., Roper, H., Hughes, I., Tejura, B., Robinson, N., Layton, G., Davies, K., Muntoni, F., and Tinsley, J. (2016). Safety, Tolerability, and Pharmacokinetics of SMT C1100, a 2-Arylbenzoxazole Utrophin Modulator, following Single- and Multiple-Dose Administration to Pediatric Patients with Duchenne Muscular Dystrophy. PLoS One *11*, e0152840.

Roberts, R.G., Coffey, A.J., Bobrow, M., and Bentley, D.R. (1993). Exon structure of the human dystrophin gene. Genomics *16*, 536-538.

Roberts, R.G., Gardner, R.J., and Bobrow, M. (1994). Searching for the 1 in 2,400,000: a review of dystrophin gene point mutations. Hum Mutat *4*, 1-11.

Rouillon, J., Lefebvre, T., Denard, J., Puy, V., Daher, R., Ausseil, J., Zocevic, A., Fogel, P., Peoc'h, K., Wong, B., *et al.* (2018). High urinary ferritin reflects myoglobin iron evacuation in DMD patients. Neuromuscul Disord *28*, 564-571.

Rouillon, J., Zocevic, A., Leger, T., Garcia, C., Camadro, J.M., Udd, B., Wong, B., Servais, L., Voit, T., and Svinartchouk, F. (2014). Proteomics profiling of urine reveals specific titin fragments as biomarkers of Duchenne muscular dystrophy. Neuromuscul Disord *24*, 563-573.

Russell, D.J., Rosenbaum, P.L., Cadman, D.T., Gowland, C., Hardy, S., and Jarvis, S. (1989). The gross motor function measure: a means to evaluate the effects of physical therapy. Dev Med Child Neurol *31*, 341-352.

Rutkove, S.B. (2009). Electrical impedance myography: Background, current state, and future directions. Muscle Nerve *40*, 936-946.

Rutkove, S.B., Geisbush, T.R., Mijailovic, A., Shklyar, I., Pasternak, A., Visyak, N., Wu, J.S., Zaidman, C., and Darras, B.T. (2014). Cross-sectional evaluation of electrical impedance myography and quantitative ultrasound for the assessment of Duchenne muscular dystrophy in a clinical trial setting. Pediatr Neurol *51*, 88-92.

Ryan, N.J. (2014). Ataluren: first global approval. Drugs *74*, 1709-1714.

Rybakova, I.N., Patel, J.R., and Ervasti, J.M. (2000). The dystrophin complex forms a mechanically strong link between the sarcolemma and costameric actin. J Cell Biol *150*, 1209-1214.

Ryder, S., Leadley, R., Armstrong, N., Westwood, M., De Kock, S., Butt, T., Jain, M., and Kleijnen, J. (2017). The burden, epidemiology, costs and treatment for Duchenne muscular dystrophy: an evidence review. Orphanet journal of rare diseases *12*, 79.

Sacco, A., Doyonnas, R., Kraft, P., Vitorovic, S., and Blau, H.M. (2008). Self-renewal and expansion of single transplanted muscle stem cells. Nature *456*, 502-506.

Sakamoto, M., Yuasa, K., Yoshimura, M., Yokota, T., Ikemoto, T., Suzuki, M., Dickson, G., Miyagoe-Suzuki, Y., and Takeda, S. (2002). Micro-dystrophin cDNA ameliorates dystrophic phenotypes when introduced into mdx mice as a transgene. Biochem Biophys Res Commun *293*, 1265-1272.

Sansovic, I., Barisic, I., and Dumic, K. (2013). Improved detection of deletions and duplications in the DMD gene using the multiplex ligation-dependent probe amplification (MLPA) method. Biochem Genet *51*, 189-201.

Sarig, R., Mezger-Lallemand, V., Gitelman, I., Davis, C., Fuchs, O., Yaffe, D., and Nudel, U. (1999). Targeted inactivation of Dp71, the major non-muscle product of the DMD gene: differential activity of the Dp71 promoter during development. Human molecular genetics *8*, 1-10.

Schlattner, U., Tokarska-Schlattner, M., and Wallimann, T. (2006). Mitochondrial creatine kinase in human health and disease. Biochim Biophys Acta *1762*, 164-180.

Schmalbruch, H. (1984). Regenerated muscle fibers in Duchenne muscular dystrophy: a serial section study. Neurology *34*, 60-65.

Scott, E., Eagle, M., Mayhew, A., Freeman, J., Main, M., Sheehan, J., Manzur, A., and Muntoni, F. (2012). Development of a functional assessment scale for ambulatory boys with Duchenne muscular dystrophy. Physiother Res Int *17*, 101-109.

Scott, O., Hyde, S., Goddard, C., and Dubowitz, V. (1982). Quantitation of muscle function in children: a prospective study in Duchenne muscular dystrophy. Muscle & Nerve: Official Journal of the American Association of Electrodiagnostic Medicine *5*, 291-301.

Sharp, N., Kornegay, J., Van Camp, S., Herbstreith, M., Secore, S., Kettle, S.a., Hung, W.-Y., Constantinou, C., Dykstra, M., and Roses, A. (1992). An error in dystrophin mRNA processing in golden retriever muscular dystrophy, an animal homologue of Duchenne muscular dystrophy. Genomics *13*, 115-121.

Sharp, P.S., Bye-a-Jee, H., and Wells, D.J. (2011). Physiological characterization of muscle strength with variable levels of dystrophin restoration in mdx mice following local antisense therapy. Molecular Therapy *19*, 165-171.

Shimatsu, Y., Yoshimura, M., Yuasa, K., Urasawa, N., Tomohiro, M., Nakura, M.,

Tanigawa, M., Nakamura, A., and Takeda, S. (2005). Major clinical and histopathological characteristics of canine X-linked muscular dystrophy in Japan, CXMDJ. Acta Myol *24*, 145-154.

Shklyar, I., Geisbush, T.R., Mijialovic, A.S., Pasternak, A., Darras, B.T., Wu, J.S., Rutkove, S.B., and Zaidman, C.M. (2015). Quantitative muscle ultrasound in Duchenne muscular dystrophy: a comparison of techniques. Muscle Nerve *51*, 207-213.

Sicinski, P., Geng, Y., Ryder-Cook, A.S., Barnard, E.A., Darlison, M.G., and Barnard, P.J. (1989). The molecular basis of muscular dystrophy in the mdx mouse: a point mutation. Science *244*, 1578-1580.

Silva, M.C., Magalhaes, T.A., Meira, Z.M., Rassi, C.H., Andrade, A.C., Gutierrez, P.S., Azevedo, C.F., Gurgel-Giannetti, J., Vainzof, M., Zatz, M., *et al.* (2017). Myocardial Fibrosis Progression in Duchenne and Becker Muscular Dystrophy: A Randomized Clinical Trial. JAMA Cardiol *2*, 190-199.

Silva, M.C., Meira, Z.M., Gurgel Giannetti, J., da Silva, M.M., Campos, A.F., Barbosa Mde, M., Starling Filho, G.M., Ferreira Rde, A., Zatz, M., and Rochitte, C.E. (2007). Myocardial delayed enhancement by magnetic resonance imaging in patients with muscular dystrophy. J Am Coll Cardiol *49*, 1874-1879.

Skuk, D., Goulet, M., Roy, B., Piette, V., Côté, C.H., Chapdelaine, P., Hogrel, J.-Y., Paradis, M., Bouchard, J.-P., and Sylvain, M. (2007). First test of a "high-density injection" protocol for myogenic cell transplantation throughout large volumes of muscles in a Duchenne muscular dystrophy patient: eighteen months follow-up. Neuromuscular Disorders *17*, 38-46.

Soltanzadeh, P., Friez, M.J., Dunn, D., von Niederhausern, A., Gurvich, O.L., Swoboda, K.J., Sampson, J.B., Pestronk, A., Connolly, A.M., and Florence, J.M. (2010). Clinical and genetic characterization of manifesting carriers of DMD mutations. Neuromuscular Disorders *20*, 499-504.

Song, Y., Morales, L., Malik, A.S., Mead, A.F., Greer, C.D., Mitchell, M.A., Petrov, M.T., Su, L.T., Choi, M.E., Rosenblum, S.T., *et al.* (2019). Non-immunogenic utrophin gene therapy for the treatment of muscular dystrophy animal models. Nat Med *25*, 1505-1511.

Spurney, C.F., Gordish-Dressman, H., Guerron, A.D., Sali, A., Pandey, G.S., Rawat, R., Van Der Meulen, J.H., Cha, H.J., Pistilli, E.E., Partridge, T.A., *et al.* (2009). Preclinical drug trials in the mdx mouse: assessment of reliable and sensitive outcome measures. Muscle Nerve *39*, 591-602.

Srivastava, N.K., Pradhan, S., Mittal, B., and Gowda, G.A. (2010). High resolution

NMR based analysis of serum lipids in Duchenne muscular dystrophy patients and its possible diagnostic significance. NMR Biomed *23*, 13-22.

Stoffels, I., Morscher, S., Helfrich, I., Hillen, U., Leyh, J., Burton, N.C., Sardella, T.C., Claussen, J., Poeppel, T.D., and Bachmann, H.S. (2015). Metastatic status of sentinel lymph nodes in melanoma determined noninvasively with multispectral optoacoustic imaging. Science translational medicine *7*, 317ra199-317ra199.

Straub, V., Balabanov, P., Bushby, K., Ensini, M., Goemans, N., De Luca, A., Pereda, A., Hemmings, R., Campion, G., Kaye, E., *et al.* (2016). Stakeholder cooperation to overcome challenges in orphan medicine development: the example of Duchenne muscular dystrophy. Lancet Neurol *15*, 882-890.

Straub, V., Bittner, R.E., Leger, J.J., and Voit, T. (1992). Direct visualization of the dystrophin network on skeletal muscle fiber membrane. J Cell Biol *119*, 1183-1191.

Straub, V., and Campbell, K.P. (1997). Muscular dystrophies and the dystrophin-glycoprotein complex. Current opinion in neurology *10*, 168-175.

Stuberg, W.A., and Metcalf, W.K. (1988). Reliability of quantitative muscle testing in healthy children and in children with Duchenne muscular dystrophy using a hand-held dynamometer. Phys Ther *68*, 977-982.

Sui, T., Lau, Y.S., Liu, D., Liu, T., Xu, L., Gao, Y., Lai, L., Li, Z., and Han, R. (2018). A novel rabbit model of Duchenne muscular dystrophy generated by CRISPR/Cas9. Disease models & mechanisms *11*, dmm032201.

Sun, C., Serra, C., Lee, G., and Wagner, K.R. (2019). Stem cell-based therapies for Duchenne muscular dystrophy. Exp Neurol *323*, 113086.

Syed, Y.Y. (2016). Eteplirsen: first global approval. Drugs *76*, 1699-1704.

Taipale, J., Miyazono, K., Heldin, C.H., and Keski-Oja, J. (1994). Latent transforming growth factor-beta 1 associates to fibroblast extracellular matrix via latent TGF-beta binding protein. J Cell Biol *124*, 171-181.

Takeshita, E., Komaki, H., Tachimori, H., Miyoshi, K., Yamamiya, I., Shimizu-Motohashi, Y., Ishiyama, A., Saito, T., Nakagawa, E., Sugai, K., *et al.* (2018). Urinary prostaglandin metabolites as Duchenne muscular dystrophy progression markers. Brain Dev *40*, 918-925.

Taylor, M., Jefferies, J., Byrne, B., Lima, J., Ambale-Venkatesh, B., Ostovaneh, M.R., Makkar, R., Goldstein, B., Smith, R.R., Fudge, J., *et al.* (2019). Cardiac and skeletal muscle effects in the randomized HOPE-Duchenne trial. Neurology *92*,

e866-e878.

Thangarajh, M., Zhang, A., Gill, K., Ressom, H.W., Li, Z., Varghese, R.S., Hoffman, E.P., Nagaraju, K., Hathout, Y., and Boca, S.M. (2019). Discovery of potential urine-accessible metabolite biomarkers associated with muscle disease and corticosteroid response in the mdx mouse model for Duchenne. PLoS One *14*, e0219507.

Urban, Z., Hucthagowder, V., Schurmann, N., Todorovic, V., Zilberberg, L., Choi, J., Sens, C., Brown, C.W., Clark, R.D., Holland, K.E., *et al.* (2009). Mutations in LTBP4 cause a syndrome of impaired pulmonary, gastrointestinal, genitourinary, musculoskeletal, and dermal development. Am J Hum Genet *85*, 593-605.

Valentine, B.A., Cooper, B.J., de Lahunta, A., O'Quinn, R., and Blue, J.T. (1988). Canine X-linked muscular dystrophy. An animal model of Duchenne muscular dystrophy: clinical studies. J Neurol Sci *88*, 69-81.

van den Bergen, J.C., Hiller, M., Bohringer, S., Vijfhuizen, L., Ginjaar, H.B., Chaouch, A., Bushby, K., Straub, V., Scoto, M., Cirak, S., *et al.* (2015). Validation of genetic modifiers for Duchenne muscular dystrophy: a multicentre study assessing SPP1 and LTBP4 variants. J Neurol Neurosurg Psychiatry *86*, 1060-1065.

Van der Auwera, G.A., Carneiro, M.O., Hartl, C., Poplin, R., Del Angel, G., Levy-Moonshine, A., Jordan, T., Shakir, K., Roazen, D., Thibault, J., *et al.* (2013). From FastQ data to high confidence variant calls: the Genome Analysis Toolkit best practices pipeline. Curr Protoc Bioinformatics *43*, 11.10.11-11.10.33.

Van Deutekom, J.C., Janson, A.A., Ginjaar, I.B., Frankhuizen, W.S., Aartsma-Rus, A., Bremmer-Bout, M., den Dunnen, J.T., Koop, K., van der Kooi, A.J., and Goemans, N.M. (2007). Local dystrophin restoration with antisense oligonucleotide PRO051. New England Journal of Medicine *357*, 2677-2686.

Van Ruiten, H., Bushby, K., and Guglieri, M. (2017). State of the art advances in Duchenne muscular dystrophy. EMJ *2*, 90-99.

Verhaart, I.E., van Vliet-van den Dool, L., Sipkens, J.A., de Kimpe, S.J., Kolfschoten, I.G., van Deutekom, J.C., Liefaard, L., Ridings, J.E., Hood, S.R., and Aartsma-Rus, A. (2014). The Dynamics of Compound, Transcript, and Protein Effects After Treatment With 2OMePS Antisense Oligonucleotides in mdx Mice. Mol Ther Nucleic Acids *3*, e148.

Verhaart, I.E.C., Johnson, A., Thakrar, S., Vroom, E., De Angelis, F., Muntoni, F., Aartsma-Rus, A.M., and Niks, E.H. (2019). Muscle biopsies in clinical trials for Duchenne muscular dystrophy - Patients' and caregivers' perspective. Neuromuscul Disord *29*, 576-584.

Verma, S., Anziska, Y., and Cracco, J. (2010). Review of Duchenne muscular dystrophy (DMD) for the pediatricians in the community. Clinical pediatrics *49*, 1011-1017.

Vetrone, S.A., Montecino-Rodriguez, E., Kudryashova, E., Kramerova, I., Hoffman, E.P., Liu, S.D., Miceli, M.C., and Spencer, M.J. (2009). Osteopontin promotes fibrosis in dystrophic mouse muscle by modulating immune cell subsets and intramuscular TGF-beta. J Clin Invest *119*, 1583-1594.

Vidal, B., Serrano, A.L., Tjwa, M., Suelves, M., Ardite, E., De Mori, R., Baeza-Raja, B., Martinez de Lagran, M., Lafuste, P., Ruiz-Bonilla, V., *et al.* (2008). Fibrinogen drives dystrophic muscle fibrosis via a TGFbeta/alternative macrophage activation pathway. Genes Dev *22*, 1747-1752.

Vieira, N.M., Spinazzola, J.M., Alexander, M.S., Moreira, Y.B., Kawahara, G., Gibbs, D.E., Mead, L.C., Verjovski-Almeida, S., Zatz, M., and Kunkel, L.M. (2017). Repression of phosphatidylinositol transfer protein alpha ameliorates the pathology of Duchenne muscular dystrophy. Proc Natl Acad Sci U S A *114*, 6080-6085.

Vo, A.H., and McNally, E.M. (2015). Modifier genes and their effect on Duchenne muscular dystrophy. Current opinion in neurology *28*, 528.

Waldner, M.J., Knieling, F., Egger, C., Morscher, S., Claussen, J., Vetter, M., Kielisch, C., Fischer, S., Pfeifer, L., and Hagel, A. (2016). Multispectral optoacoustic tomography in Crohn’s disease: noninvasive imaging of disease activity. Gastroenterology *151*, 238-240.

Wallace, G., and Newton, R. (1989). Gowers' sign revisited. Archives of disease in childhood *64*, 1317-1319.

Wallimann, T., Wyss, M., Brdiczka, D., Nicolay, K., and Eppenberger, H.M. (1992). Intracellular compartmentation, structure and function of creatine kinase isoenzymes in tissues with high and fluctuating energy demands: the 'phosphocreatine circuit' for cellular energy homeostasis. Biochem J *281 (Pt 1)*, 21-40.

Walmsley, G.L., Arechavala-Gomeza, V., Fernandez-Fuente, M., Burke, M.M., Nagel, N., Holder, A., Stanley, R., Chandler, K., Marks, S.L., and Muntoni, F. (2010). A duchenne muscular dystrophy gene hot spot mutation in dystrophin-deficient cavalier king charles spaniels is amenable to exon 51 skipping. PloS one *5*, e8647.

Wang, Y., Yang, Y., Liu, J., Chen, X.C., Liu, X., Wang, C.Z., and He, X.Y. (2014). Whole dystrophin gene analysis by next-generation sequencing: a comprehensive

genetic diagnosis of Duchenne and Becker muscular dystrophy. Mol Genet Genomics *289*, 1013-1021.

Wei, X., Dai, Y., Yu, P., Qu, N., Lan, Z., Hong, X., Sun, Y., Yang, G., Xie, S., Shi, Q., *et al.* (2014). Targeted next-generation sequencing as a comprehensive test for patients with and female carriers of DMD/BMD: a multi-population diagnostic study. Eur J Hum Genet *22*, 110-118.

Weiss, R.B., Vieland, V.J., Dunn, D.M., Kaminoh, Y., and Flanigan, K.M. (2018). Long-range genomic regulators of THBS1 and LTBP4 modify disease severity in duchenne muscular dystrophy. Ann Neurol *84*, 234-245.

Wells, D.J. (2018). Tracking progress: an update on animal models for Duchenne muscular dystrophy. Dis Model Mech *11*, dmm035774.

Willcocks, R.J., Rooney, W.D., Triplett, W.T., Forbes, S.C., Lott, D.J., Senesac, C.R., Daniels, M.J., Wang, D.J., Harrington, A.T., Tennekoon, G.I., *et al.* (2016). Multicenter prospective longitudinal study of magnetic resonance biomarkers in a large duchenne muscular dystrophy cohort. Ann Neurol *79*, 535-547.

Willmann, R., Possekel, S., Dubach-Powell, J., Meier, T., and Ruegg, M.A. (2009). Mammalian animal models for Duchenne muscular dystrophy. Neuromuscul Disord *19*, 241-249.

Wokke, B., Van Den Bergen, J., Versluis, M., Niks, E., Milles, J., Webb, A., van Zwet, E., Aartsma-Rus, A., Verschuuren, J., and Kan, H. (2014). Quantitative MRI and strength measurements in the assessment of muscle quality in Duchenne muscular dystrophy. Neuromuscular Disorders *24*, 409-416.

Xu, L., Park, K.H., Zhao, L., Xu, J., El Refaey, M., Gao, Y., Zhu, H., Ma, J., and Han, R. (2016). CRISPR-mediated Genome Editing Restores Dystrophin Expression and Function in mdx Mice. Mol Ther *24*, 564-569.

Yeung, E.W., Whitehead, N.P., Suchyna, T.M., Gottlieb, P.A., Sachs, F., and Allen, D.G. (2005). Effects of stretch-activated channel blockers on [Ca2+]i and muscle damage in the mdx mouse. J Physiol *562*, 367-380.

Yiu, E.M., and Kornberg, A.J. (2015). Duchenne muscular dystrophy. J Paediatr Child Health *51*, 759-764.

Yokota, T., Lu, Q.l., Partridge, T., Kobayashi, M., Nakamura, A., Takeda, S., and Hoffman, E. (2009). Efficacy of systemic morpholino exon-skipping in Duchenne dystrophy dogs. Annals of Neurology: Official Journal of the American Neurological Association and the Child Neurology Society *65*, 667-676.

Yoshimura, M., Sakamoto, M., Ikemoto, M., Mochizuki, Y., Yuasa, K., Miyagoe-Suzuki, Y., and Takeda, S. (2004). AAV vector-mediated microdystrophin expression in a relatively small percentage of mdx myofibers improved the mdx phenotype. Mol Ther *10*, 821-828.

Zaharieva, I.T., Calissano, M., Scoto, M., Preston, M., Cirak, S., Feng, L., Collins, J., Kole, R., Guglieri, M., Straub, V., *et al.* (2013). Dystromirs as serum biomarkers for monitoring the disease severity in Duchenne muscular Dystrophy. PLoS One *8*, e80263.

Zaidman, C.M., Wu, J.S., Kapur, K., Pasternak, A., Madabusi, L., Yim, S., Pacheck, A., Szelag, H., Harrington, T., Darras, B.T., *et al.* (2017). Quantitative muscle ultrasound detects disease progression in Duchenne muscular dystrophy. Ann Neurol *81*, 633-640.

Zatz, M., Rapaport, D., Vainzof, M., Passos-Bueno, M.R., Bortolini, E.R., Pavanello Rde, C., and Peres, C.A. (1991). Serum creatine-kinase (CK) and pyruvate-kinase (PK) activities in Duchenne (DMD) as compared with Becker (BMD) muscular dystrophy. J Neurol Sci *102*, 190-196.

Zellweger, H., and Antonik, A. (1975). Newborn screening for Duchenne muscular dystrophy. Pediatrics *55*, 30-34.

Zocevic, A., Rouillon, J., Wong, B., Servais, L., Voit, T., and Svinartchouk, F. (2015). Evaluation of the serum matrix metalloproteinase-9 as a biomarker for monitoring disease progression in Duchenne muscular dystrophy. Neuromuscular Disorders *25*, 444-446.

XI. ACKNOWLEDGEMENTS

I would like to start by thanking Prof. Dr. Eckhard Wolf for giving me this great opportunity to do my doctoral thesis at the Chair for Molecular Animal Breeding and Biotechnology, LMU Munich. Thank you very much for your trust in my work and ideas, your honesty and understanding and your continuous support. I really appreciate the work on my topic, and sincerely hope to support the progress on fighting Duchenne muscular dystrophy.

I am thankful to all my colleagues at the Moorversuchsgut, who helped and supported me at many different situations. Particularly, I want to thank to my mentor Dr. Barbara Kessler for assisting me at every time, wherever possible. Special thanks also to Dr. Elisabeth Kemter for giving me important advices, and Christina Blechinger for keeping my back free whenever necessary. I would also like to acknowledge the work of all animal caretakers, especially Harald Paul and Sylvia Hering.

My special thanks and appreciation go to the team of the Department of Pediatrics and Adolescent Medicine, University Hospital Erlangen, FAU Erlangen Nuremberg, Erlangen. Dr, Ferdinand Knieling, thank you very much for your advice and support in every respect. Special thanks also to Dr. Adrian Regensburger and Alexandra Wagner, I really appreciated working with you. My special thanks also go to Dr. Jing Claussen from iThera Medical GmbH.

I would like to acknowledge our collaboration with the team of the Clinic and Policlinic for Internal Medicine I, Klinikum Rechts der Isar, TU Munich, and the team of the Institute of Developmental Genetics, Helmholtz-Centre and Munich School of Life Sciences Weihenstephan, TU Munich, Freising. Particularly, I would like to thank Prof. Dr. Christian Kupatt for his trust and recognition of my work and Dr. Andrea Bähr for her support. Many thanks also to Dr. Florian Giesert for his help and supporting ideas.

Thank you to our colleagues of the Gene Center Munich, Institute for Molecular Animal Breeding and Biotechnology, LMU Munich. Especially I would like to thank Dr. Maik Dahlhoff for preparing me for a doctoral thesis during my practical course, Dr. Thomas Fröhlich and his team for their collaboration, constant support and advices, and Dr. Stefan Krebs, for his detailed explanations.

I show my gratitude also to Priv.-Doz. Dr. habil. Ivica Međugorac and his team of the Population Genomics Group, Department of Veterinary Science, Faculty of Veterinary Medicine, LMU Munich, Martinsried.

Special thanks to the members of the Chair for Veterinary Pathology, especially to Dr. Christian Loch, for his interest in the subject and cooperation.

I would also like to thank the team of the Friedrich Baur Institute, especially Priv.-Doz. Dr. Dr. Sabine Krause, Tina Donandt and Maria Schmuck for their personal advice.

Particularly I thank all sacrificed and alive animals used for this work, especially my first DMD knockout Kaspar, may God rest his soul, and founder sow #3040 who donated 11 litters. Without animals, research on this level would not be possible.

Finally, I want to thank my boyfriend Michael Saller, whom I got to know working on my doctoral thesis. You give me strength, humor and patiently support me throughout all my work. Special thanks also to my beloved family for always keeping their faith in me.

Moreover, I would like to acknowledge the Else Kröner-Fresenius Foundation for supporting my work financially.